"Spectroscopic and Crystallographic Characterization of Enantiopure Planar Chiral N-Oxazolidinoyl Diene Iron(0) Tricarbonyl Complexes For Use in Diastereoselective Synthesis"

Nathan W. Dow
Senior Honors Thesis
Advisor: Robert S. Paley
Honors Examiner: Dr. Sarah Wengryniuk, Temple University
Department of Chemistry & Biochemistry
Swarthmore College
Submitted May 24, 2018

Table of Contents

Acknowledgements

First, I would like to thank Professor Robert Paley for his guidance and support while serving as the advisor for my laboratory projects. His dedication to thorough, ambitious undergraduate science is matched only by his passion for instruction. There is no doubt that his mentorship will decisively impact both this thesis work and my future endeavors in synthetic chemistry. Beyond the science, his undeniably impeccable taste in sports (go Yankees!) and music only served to make my time in the group more enjoyable. I am proud to call him my advisor and delighted to call him my friend as well.

I also have to thank the members of the Department of Chemistry & Biochemistry at Swarthmore, both faculty and students alike, for everything that they have taught me over the last four years. In particular, I want to thank my coworker in the Paley group, Ben Hejna, for his friendship and support over the last year and a half. Having someone as diligent, collaborative and intelligent in the group as Ben was a pleasure, and I greatly valued every discussion, scientific or not, that we had in the lab. Additionally, my predecessors, in particular Sooyun Choi, Raundi Quevedo and Mason Yu, were instrumental in the conceiving and execution of the projects that I eventually lead and that are detailed in this work. Lastly, I must thank several collaborators for their assistance with characterization, as this work could not be accomplished without their generosity: Barrett Powell and the Yatsunyk laboratory (for their assistance with circular dichroism spectroscopy) and the Pike group at the College of William and Mary (for their assistance with X-ray crystallography).

Lastly, I want to thank my family and friends, especially Liz, for their unwavering support, through both the good times and the bad, that made this thesis possible.

Abstract

Iron(0) tricarbonyl-diene complexes have emerged from the field of organometallics as motifs of particular importance due to their robust synthetic applications. As a result of their planar chiral configurations, these removable iron units have been effectively used as diene protecting groups, stereodirecting groups and dienyl cation stabilizers to facilitate the total synthesis of architecturally complex structures, such as pharmaceutically-relevant natural products. However, to further optimize iron(0) tricarbonyl utilization in diastereoselective synthesis, methods must be developed to direct iron-diene complexation reactions in a facially selective manner and to characterize these optical outcomes. Additionally, the established number of reactions tolerant to iron(0) tricarbonyl mediation must be expanded to facilitate the use of such methodologies on a widespread or industrial level.

Herein we report the synthesis and characterization of N-oxazolidinoyl diene iron(0) tricarbonyl complexes as model platforms to address both of these existing challenges. The use of enantiopure N-oxazolidinoyl chiral auxiliaries as directing groups has now been shown to efficiently and predictably direct facially-selective complexation reactions. Furthermore, the planar chirality of these species was ascertained via crystallographic and circular dichroism spectroscopy, the latter being a novel technique for such complexes. Efforts to utilize an N-oxazolidinoyl complex in the first intramolecular Pictet-Spengler cyclization directed by planar chirality were also undertaken, ultimately producing the most structurally demanding N-oxazolidinoyl complex synthesized to date. Lastly, projects involving novel auxiliaries, such as cyclic ureas and sulfonamides, to better direct complexation reactions are also detailed.

List of Common Abbreviations

Ar = aryl

Bn = benzyl

Boc = tert-butoxycarbonyl

CD = circular dichroism

DIAD = diisopropyl azodicarboxylate

DMF = dimethylformamide

d.r. = diastereomeric ratio

e.e. = enantiomeric excess

Ms = methanesulfonyl ("mesyl")

Ns = 2-nitrobenzenesulfonyl ("nosyl")

OAc = acetate

Ph = phenyl

TBAF = tetrabutylammonium fluoride

TBS (or TBDMS) = tert-butyldimethylsilyl

TBDPS = tert-butyldiphenylsilyl

TEOC = trimethylsilyl ethoxycarbonyl

TFA = trifluoroacetic acid

THF = tetrahydrofuran

TIPS = triisopropylsilyl

TMS = trimethylsilyl

Ts = *p*-toluenesulfonyl ("tosyl")

Introduction

Iron-diene compounds and the early days of organometallic chemistry

The field of organometallic chemistry plays an integral role in the modern scientific world by expanding the methods available to researchers with such broad-ranging interests as synthesis, catalysis, materials science, and biological chemistry. Applications of this field have monumentally transformed common industrial and biomedical endeavors, changing the way scientists approach pharmaceutical development, semiconductor design, enzyme/protein studies and fuel generation.[1] Despite the current ubiquitous nature of organometallic compounds, these structures had been largely ignored in the early days of chemistry, and the majority of development for this topic has occurred over the last several decades. In particular, the year 1951 featured the landmark inadvertent discovery of the bis-η^5 "sandwich" compound ferrocene.[2] By the following year, the unique pentahapto structure of the organoiron complex had been deduced by both Ernst Otto Fischer and the team of Woodward and Wilkinson, sparking unprecedented interest in the budding field of transition metal organometallic chemistry.[3,4] The importance of such groundbreaking work into metallocene properties is further emphasized by the 1973 Nobel Prize in Chemistry, awarded to Fischer and Wilkinson for their contributions to the field.[5] Although certain organometallic compounds had been isolated more than a century prior to ferrocene's identification, this anomalous complex launched deeper investigations into inorganic structures, including organoiron species of varying hapticities.

The first documented synthesis of (butadiene)iron tricarbonyl (**1**) was executed by Reihlen in 1930, via thermally-induced complexation of iron(0) pentacarbonyl with

butadiene (structure presented in Fig. 1).[6] Largely ignored until the isolation of metallocenes, Pauson (responsible for the discovery of ferrocene) and Hallam revitalized the importance of the acyclic iron-diene complex by proposing the now-accepted η^4 structure of **1** in 1958.[7] Particularly notable were the empirical requirements of both π-system conjugation as well as an s-*cis* diene conformation to induce complexation; in circumstances preventing isomerization from the s-*trans* form, complexation was not observed (Fig. 1). The molecular orbital interactions between the metal center and the diene π-system needed to produce such a structure were verified several years later via X-ray crystallography, disproving previous notions of covalent σ-bond attachment and shining light on a wider range of organic substrates compatible with inorganic dative bonding.[8]

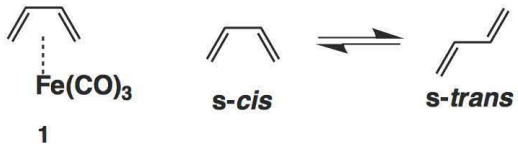

1

Fig. 1. Structure of s-*cis*-(butadiene)iron(0) tricarbonyl (1), resulting from the isomerization of butadiene between the two indicated conformations.

Naturally, the expansion of substrate scope for organoiron chemistry has led to the implementation of new complexation conditions that avoided difficulties such as thermal instability, rearrangement/isomerization and dimerization observed for preliminary pentacarbonyliron(0) systems.[9] Nonacarbonyldiiron(0), dodecacarbonyltriiron(0), enneacarbonyldiiron(0) and (benzylideneacetone)iron tricarbonyl have all been employed as iron fragment transfer reagents, as well as modified pentacarbonyliron(0) conditions featuring trimethylamine N-oxide as a stoichiometric decarbonylation reagent.[9] Photochemical conditions also exist to induce

complexation, although the tendency to produce an undesired bis-diene organoiron limit the potential for this approach. Removal of the iron(0) tricarbonyl fragment from stable diene complexes has become an equally ubiquitous procedure, making complexation a highly reversible process. The most common method for demetallation is oxidation of the metal center, and numerous metallic and non-metallic oxidizing agents seen frequently in synthetic work are applicable for this style of deprotection.[9,10]

With the identification of numerous facile approaches for iron-diene complexation came a greater understanding of the applications of iron(0) tricarbonyl moieties to organic synthesis when coordinated to acyclic dienes – examples of the unit as a protecting group, a stereodirecting group and a stabilizer of adjacent reactive dienyl cations serve as particular highlights in the synthesis of natural products and other structures of interest.

Iron(0) tricarbonyl units as protecting/stabilizing groups for acyclic s-cis dienes

Given the prevalence of conjugated olefin motifs in natural products and other privileged organic compounds, the retention of these reactive functionalities through reaction sequences is a critical, albeit challenging, task for synthetic researchers to accomplish. Thanks to the consistent stability observed for diene iron(0) tricarbonyl substrates, the iron(0) tricarbonyl unit has emerged as a notable candidate for diene protection, providing chemical inertness to a wide variety of conditions. For example, the Vogel and Schwarzenbach groups performed an asymmetric hydroboration of iron tricarbonyl-protected 5,6-dimethylidenebicyclo[2.2.2]oct-2-ene (**2**) using monoisopinocamphenylborane ($IpcBH_2$) and oxidative conditions, furnishing alcohol **3** in

62% yield with perfect diastereoselectivity (Scheme 1).[11] Notably, complete chemo- and regiocontrol was possible, leaving the protected exocyclic diene intact.

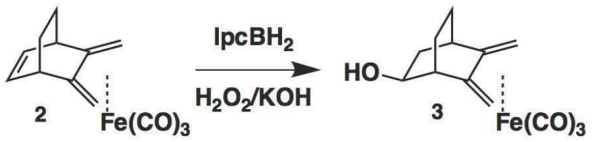

Scheme 1. Asymmetric hydroboration of a protected dimethylidenebicyclooctene, reported by the Vogel and Schwarzenbach groups.

Diene protection was also successfully employed by Donaldson and coworkers during the oxidative Lemieux-Johnson cleavage of terminal olefin **3** (Scheme 2).[12] Dihydroxylation in excess osmium tetraoxide afforded vicinal diol **4**, which was cleaved by high-valent sodium periodate to deliver conjugated aldehyde **5** in 45% total yield from **3**. This oxidation was a major step in validating the potential of iron(0) fragments as diene protecting groups, as previous ozonolysis attempts had resulted in complete decomposition of triene **3**.

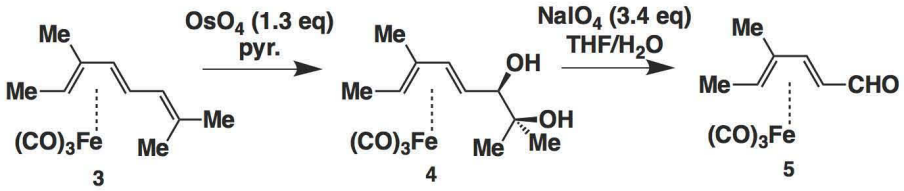

Scheme 2. Lemieux-Johnson oxidative cleavage of a protected triene executed by Donaldson *et al.*

To verify the stability of iron-diene complexes throughout transformations which chemoselectively target labile dienes, Gree and team completed several variations of cycloadditions on protected triene **7**, generated under Wittig conditions from phosphorene **6** (Scheme 3).[13] The vinyl diester unit of **7** was found to behave as the lone Diels-Alder dienophile of the system, generating adducts **8a** and **8b** from 2,3-dimethyl butadiene, and pyrrolidines **9a** and **9b** were synthesized via a 1,3-dipolar addition with an appropriate azomethine ylide reagent. Although diastereoselectivity remained an issue (dr

70:30 for best case), yields from the cycloadditions were high (93-96%), and, more importantly, the protected diene (a possible diene or dienophile for the Diels-Alder reaction) remained inert throughout both processes.

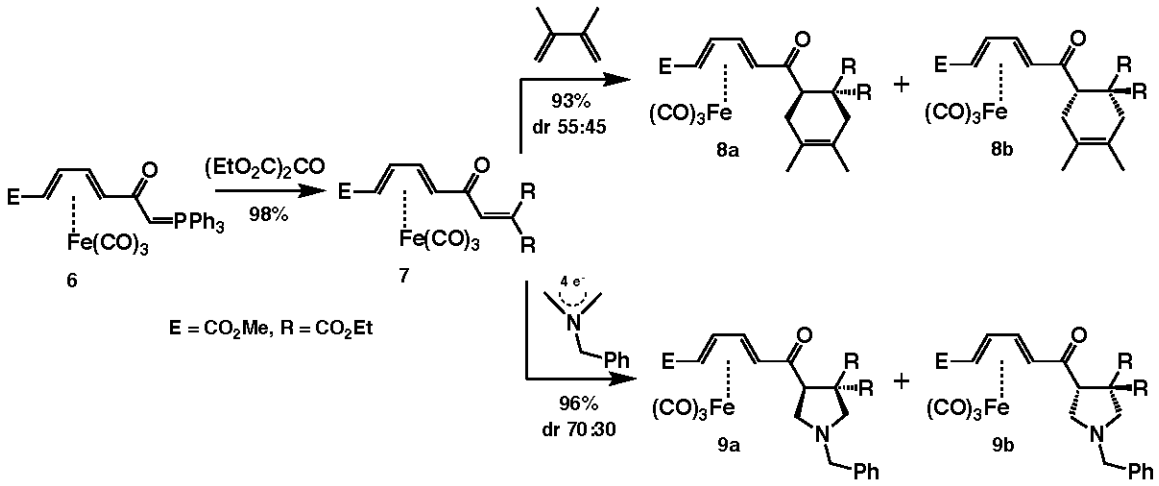

Scheme 3. Diastereoselective cycloadditions of protected trienes reported by Gree *et al.*

Iron(0) tricarbonyl stabilization has also enabled previously challenging reactions to take place by limiting the production of unwanted byproducts that originate from the diene fragment. One example is the Friedel-Crafts acylation reported by Geoffroy and coworkers, seen in Scheme 4.[14] Although modification of the diene does occur to generate the key η^3 π-allyl intermediate in this process (formally removing the "protecting group" status of the iron moiety), the retention of the diene through the electrophilic acylation was unprecedented, as prior attempts had produced polymerized butadiene derivatives as the major product. In comparison to these failures, the use of complexes **10a** and **10b** as acylation substrates generated the cis-isomers of dienal **11a** and dienone **11b** exclusively. This is a result of increased acidity α to the carbonyl, induced by Lewis acid-base interactions of the carbonyl with the iron center of the π-allyl fragment, which leads to facile α-deprotonation that regenerates the η^4 iron-diene framework. Via organometallic stabilization and newfound Lewis acidity, this previously

challenging Friedel-Crafts reaction could be performed in straightforward fashion that leaves the diene substructure uncompromised.

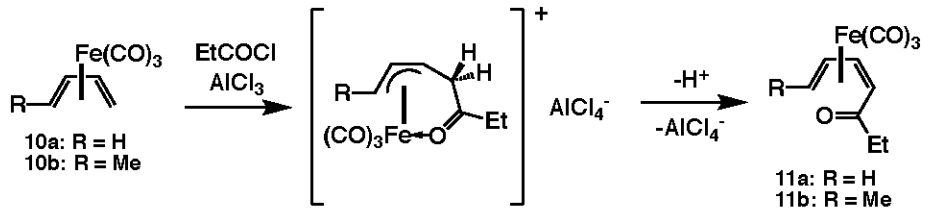

Scheme 4. Novel Friedel-Crafts acylation of a protected 1,3-butadiene system executed by Geoffroy *et al.*

Beyond the demonstration of iron(0)-based diene protection in these cases, numerous reactions employed daily in industry and academic research have been reported as being compatible with iron(0) tricarbonyl-diene complexation. Asymmetric variants of allylations, aldol condensations, reductions, Grignard additions and alkene metatheses, as well as other common addition reactions, have been performed on protected dienes, consistently in a highly regioselective manner that leaves the diene fragment unaltered.[15,16,17,18,19]

Iron(0) tricarbonyl units as directing groups for diastereoselective synthesis

The η^4 coordination of iron(0) tricarbonyl to acyclic dienes, and the complete retention of planar sp^2 character throughout the diene system following complexation, leads to unique stereochemical properties for iron-diene compounds that can be exploited for subsequent asymmetric transformations. Due to the planar character of π-conjugated substrates, an η^4 iron(0) tricarbonyl diene possesses chirality without requiring the presence of an additional stereogenic center.[9,20] This stereochemistry is called "planar chirality," and two possible isomers exist, depending on the "facial" coordination of the iron fragment relative to the diene plane – an example of planar chiral stereoisomers for model substrate s-*cis*-2,4-pentadiene-1-ol is presented in Figure 2.

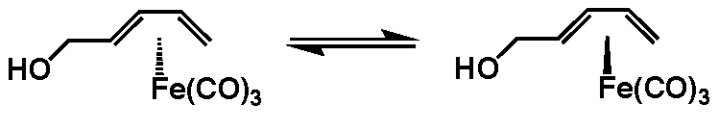

Figure 2. Planar chiral stereoisomers formed by the coordination of $Fe(CO)_3$ to s-*cis*-2,4-pentadiene-1-ol.

As seen in previous cases, reactions performed on planar chiral iron-diene substrates have the potential to be diastereoselective. In particular, transformations performed adjacent to a protected diene substrate can be directed via facial steric hindrance, requiring reagents to approach *anti* to the bulky iron fragment (with a trajectory toward the opposite diene face) and thereby inducing high degrees of diastereoselective control.[21] This methodology has become a useful technique in asymmetric synthesis, allowing researchers to access highly enantioenriched dienyl products following demetallation.

One example of a directed stereogenerating process involving planar chiral iron(0) tricarbonyl moieties is the diastereoselective hetero-Diels-Alder reported by Donaldson and coworkers (Scheme 5).[22] Under Lewis acidic conditions, cycloaddition between s-*cis* dienal **12** and Danishefsky's diene was found to proceed with both high regioselectivity and modest diastereoselectivity (dr 3:1). The rationale for the reaction's stereoselectivity is presented in the concerted mechanism shown, where repulsion with a carbonyl ligand on the large iron unit prevents a *Si*-face approach to the aldehyde. Directed approach from the bottom *Re*-face predominantly yields the major silyl enol ether isomer shown, which, following elimination under acidic conditions, affords dihydropyrone **13a** as the major diastereomer. Interestingly, replacement of the borane with an inorganic Lewis acid such as titanium tetrachloride can reverse the diastereoselectivity of this reaction (dr 1:3.8), possibly via coordination of both reactive substrates that overcomes the kinetic barrier associated with a top-face process.

Additionally, this outcome relies on the tendency of protected dienals to adopt an enal-based s-*cis* conformation at room temperature (indicated in Scheme 5) – a conformational shift to the s-*trans* enal isomer would also reverse the observed stereoselectivity.

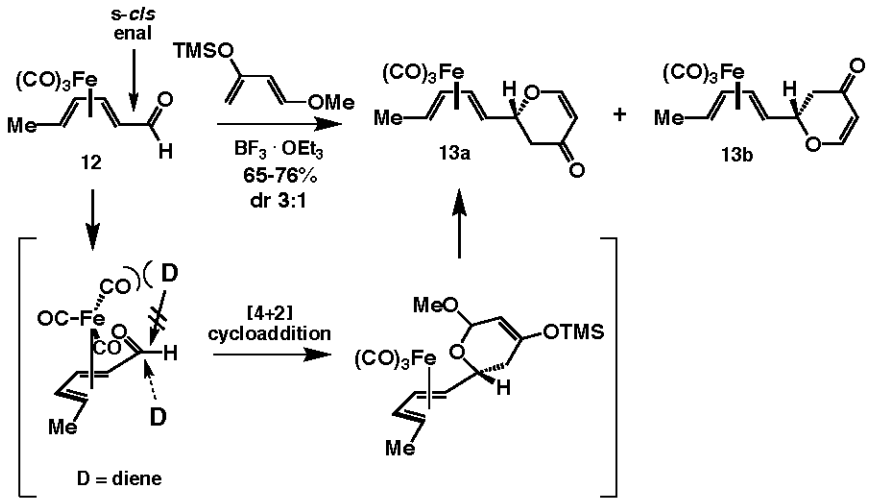

Scheme 5. Diastereoselective hetero-Diels-Alder reported by Donaldson et al., with mechanistic representation of stereoselective origins.

Intramolecular reactions directed by iron-diene units also have the potential to be highly stereoselective, and in some cases are even better controlled than intermolecular variants. One example is the intramolecular Claisen rearrangement of allylic acetate complexes, a transformation reported by the Roush group. In this work, the [3,3]-sigmatropic reaction proceeded with perfect diastereoselectivity to solely produce (*S*)-configured homoallylic acid **15**, regardless of the E/Z isomerism of the starting acetate reagent (Scheme 6).[23] The selectivity of this process relies on several factors, with one being the requirement of an *anti* approach by each intermediate silyl ketene acetal functionality relative to the iron fragment. In addition, stereocontrol is enforced by the relative stability of the reacting alkene (E or Z) when in an s-*trans* relationship to the protected diene – the s-*cis* transition state is energetically unfavorable for both acetate reagents, which is particularly exemplified by the 1,5-conformational strain for the s-*cis*

transition state derived from **14b**. Because of the strain necessarily induced in this intramolecular process, diastereoselectivity for the Claisen rearrangement can be optimized when directed in an *anti* fashion by an iron-diene unit.

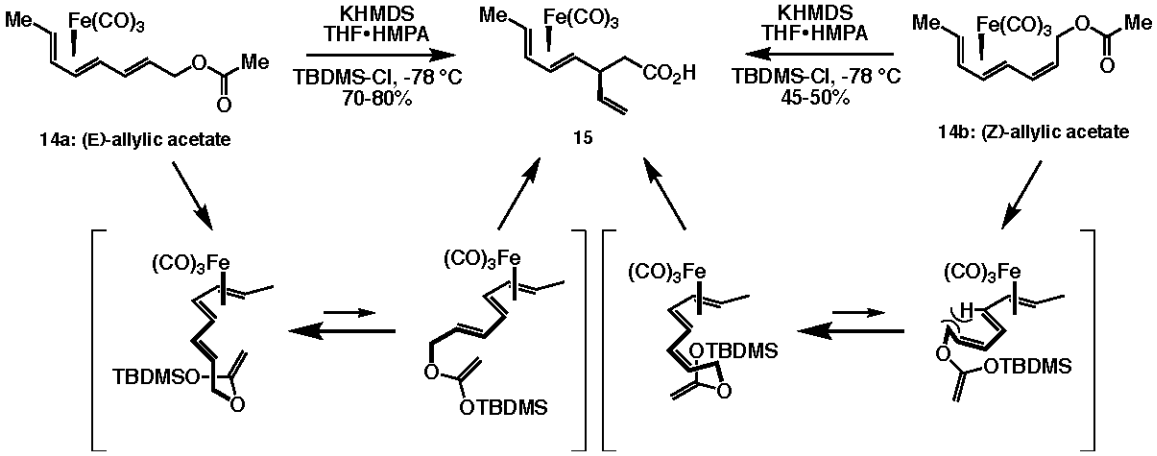

Scheme 6. Diastereoselective Claisen rearrangements reported by Roush et al. to produce a single optically active iron-diene product.

In addition to control through steric repulsion, the planar chiral iron(0) tricarbonyl group can also dictate stereochemical outcomes via coordinative participation in reaction mechanisms. Pearson and coworkers have identified a useful [6+2] spirocyclization that relies on this mode of activation, furnishing single diastereomers of bicyclic γ-lactones and γ-lactams from pendant olefin cyclohexadiene derivatives under a carbon monoxide atmosphere (Scheme 7).[24,25] Such a process generates two new stereocenters in a highly specific manner, and a mechanistic pathway has been proposed to rationalize this outcome. Thermal or photochemically-induced loss of a carbonyl ligand from the iron moiety, followed by coordination of the pendant alkene, enables the formation of an unusual spirometallacyclic π-allyl intermediate via a formal oxidative addition. Although this directed cyclization establishes the stereoconfiguration of the spirocyclic center in a facile manner via typical steric control, the chirality of the second stereocenter is determined by the relative stability of two possible metallacyclic conformations shown

below. Based on the strain induced in the intermediate that would furnish an (*R*)-configured chiral center, the alternate conformation is instead the only structure formed.

Following hydrogen migration to establish a rearranged diene from the π-allyl system (a formal hydrogen atom transfer) and subsequent reductive elimination/coordination of a free carbonyl ligand, bicyclic (*S*)-4-methyl heterocycles such as lactone **17a** and lactam **17b** are delivered as the lone diastereomers (although this absolute chirality requires pre-established "top-face" iron-diene complexation). This example indicates that, thanks to both inherent steric bulkiness and participation via classic transition metal catalytic behavior, the planar chiral iron(0) tricarbonyl moiety can successfully be employed for a diverse range of highly stereoselective transformations that take place along the periphery of coordinated dienes.

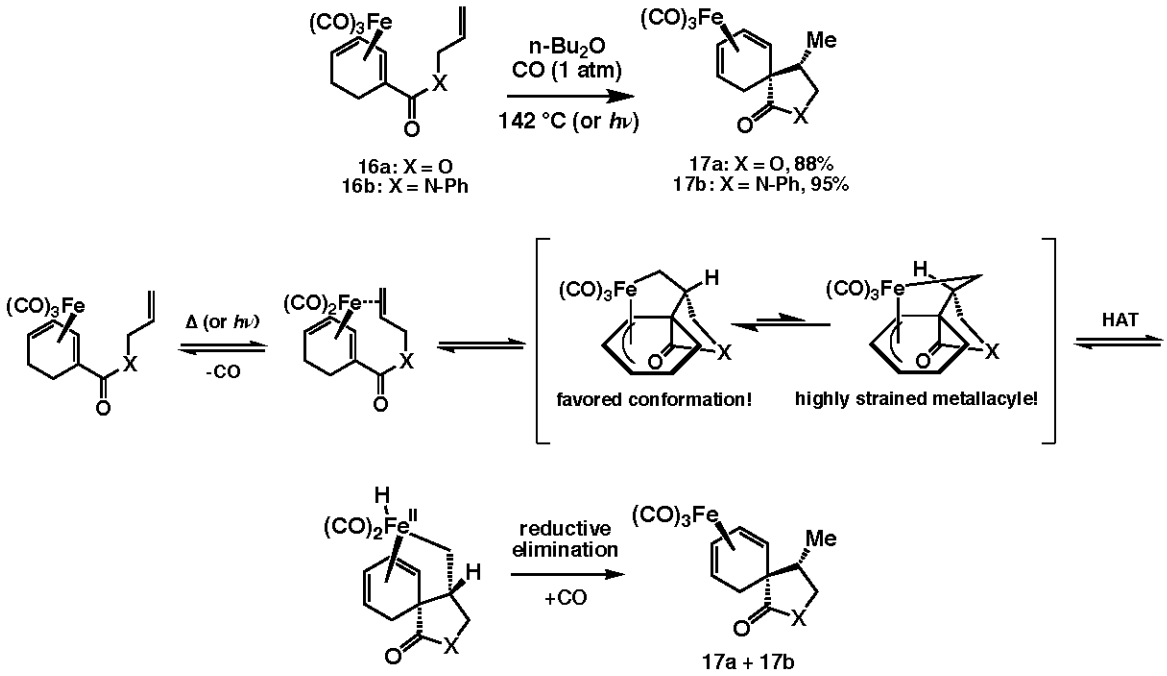

Scheme 7. Diastereoselective spirocyclizations reported by Pearson et al. along with proposed mechanism detailing both steric and metallacyclic origins of stereocontrol.

Iron(0) tricarbonyl units as stabilizers of reactive dienyl cations

As a relatively electron-rich d^8 metal, iron(0) tricarbonyl units (despite possessing Lewis acid character) can also stabilize highly electrophilic dienyl cations, so long as the positive charge is localized in a region adjacent to the coordinated diene.[26,27] This behavior can be exploited for new forms of highly controlled reactivity that further optimizes important classes of selective transformations. The intermediates in these reactions are predicted to possess various isomers, mainly the η^4-dienyl or η^5-pentadienyl structures shown in Figure 3 – the inherent delocalization provided by iron(0) complexation affords stability that allows these cations to serve as useful reaction intermediates.

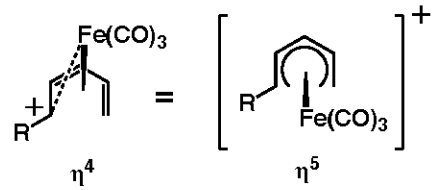

Fig. 3. η^4-dienyl and η^5-pentadienyl isomers of iron(0) tricarbonyl-dienyl cations.

In one particular application of complexed dienyl cations, the Donaldson group identified a protocol for the chemoselective oxidation of complexed secondary 2,4-diene-1-ol units in the presence of a heterocyclic oxidizing agent, N-methylmorpholine N-oxide (NMO) (Scheme 8)[28]. Although two mechanisms for this procedure have been proposed, both rely on the nucleophilic properties of NMO to deliver the carbonyl heteroatom as well as the stabilization of pentadienyl cations to ensure the completion of the oxidation reaction. This proved to be considerably important, as the reaction relies on the ejection of a hydroxyl leaving group, which is generally unfavorable due to the strong basic properties of hydroxyl substituents. The coordination to the subvalent carbon α to the diene, and the stability this affords to intermediates along each pathway, is also the

source of chemoselectivity in this procedure. Such selectivity is not only dependent on the incorporation of an iron(0) moiety, but is also particularly impressive given that a primary alcohol is the functionality remaining unaffected - this degree of substitution is usually labile to all oxidation conditions given the limited steric bulk present near the site of reactivity.

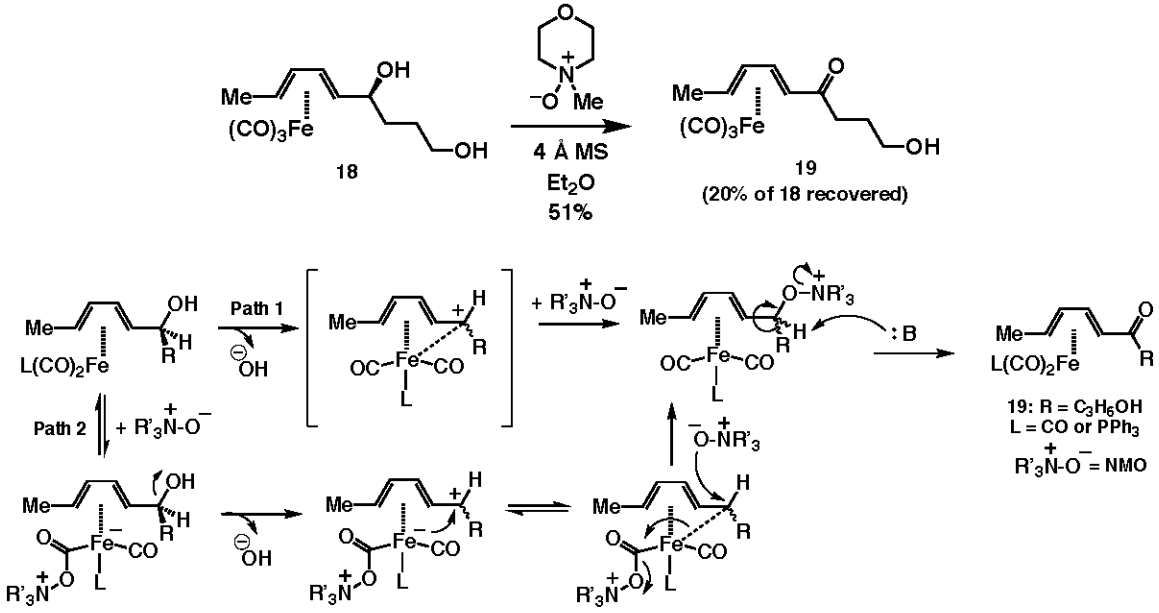

Scheme 8. Chemoselective iron(0) tricarbonyl-mediated oxidation of secondary alcohols reported by Donaldson et al., with two proposed cationic mechanisms.

Cox and coworkers also reported a highly stereoselective synthesis of N-heterocycles such as pyrrolidines (**21**) and piperidines (**22**) that relied on intermediate cation stabilization (Scheme 9).[29] Following regioselective reductive amination at the α-ketone with a borohydride to generate the corresponding imine, nucleophilic attack of the δ-ketone produced an endocyclic iminium ion intermediate that initiates heterocycle formation. Based on resonance, the iron moiety can stabilize the subvalent electrophilic carbon of the iminium unit, providing the intermediate sufficient lifetime to undergo reduction by another equivalent of borohydride reagent. Beyond promoting intermediate stability, steric repulsion between the bulky iron fragment and the iminium alkyl

substituent originating from the primary amine reagent dictates the stereochemistry of the reaction, favoring placement of the new hydrogen atom *syn* to the coordinated iron(0) tricarbonyl. By varying the chain length between ketone substituents, multiple heterocycles derived from iron-stabilized endocyclic iminium ions are easily accessible in high yield and with perfect diastereoselectivity.

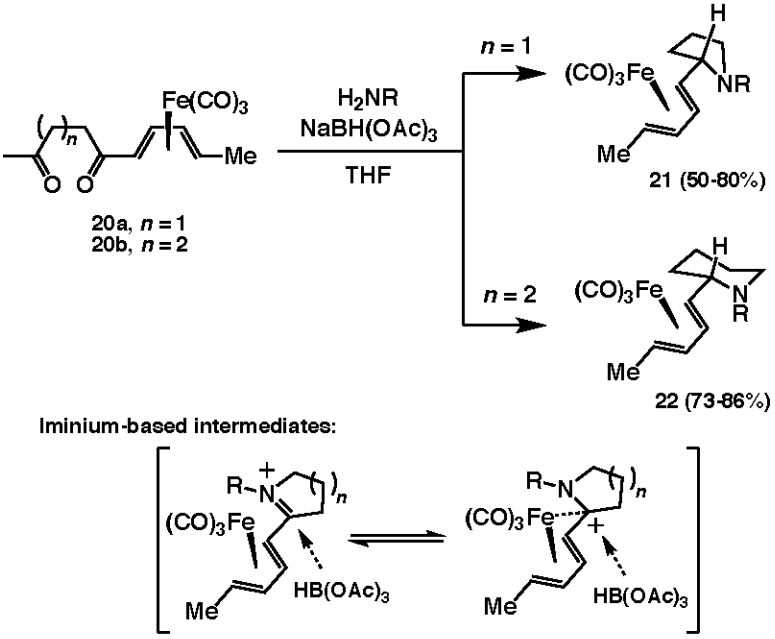

Scheme 9. Directed synthesis of dienyl pyrrolidines (21) and piperidines (22) via reductive amination, including proposed intermediate iminium stabilization via resonance.

A third example of iron(0) cation coordination as a mode of accessing unique reactivity is the Lewis acid-catalyzed 1,3-dipolar addition of dienylcyclopropanes to aldehydes reported by the Dawson group.[30] Generation of the 1,3-ylide from spontaneous fragmentation of the strained cyclopropane system would likely be impossible without further stabilization of both localized charges; in this case, the selection of a β-diester (acidic at the α position) as part of the cyclopropane ring allowed facile formation of the anionic center, whereas the cationic region, encompassed in the pentadienyl system by being α to the diene, was stabilized by iron(0) coordination. The ability to form this intermediate provided simple access to dienyl tetrahydrofurans via a simple dipolar

addition, a transformation that would be challenging to accomplish in one step without the iron unit. Although the unconventional reactivity reported here is remarkable, it is worth noting that the diastereoselectivity is less than ideal, in particular due to the lack of control over the *Re* vs. *Si* facial approach relative to the aldehyde.

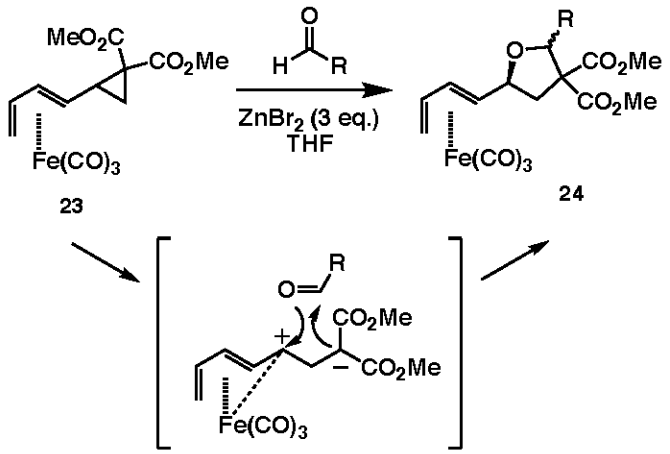

Scheme 10. Dipolar addition of 1,3-ylides derived from cyclopropenyl dienes for the synthesis of dienyl tetrahydrofurans, as reported by Dawson et al.

Iron(0) tricarbonyl dienes in synthetic pathways for natural product derivatives

To further demonstrate the importance iron(0) tricarbonyl-diene behavior in organic synthesis, several examples of natural products or portions of their architecture synthesized from pathways influenced by iron(0) tricarbonyl-diene complexes will be discussed. First, the concise total synthesis of (11*Z*)-retinal, a vitamin A chromophore that enables vision in humans via photoinduced *Z*/*E* isomerization, was completed by the Ito group using an iron(0) tricarbonyl-diene scaffold.[31] As a pentaene compound, the selective protection of unsaturated segments of the molecule is critical to avoid unwanted functionalization during transformations, making iron(0) tricarbonyl an obvious candidate as a protecting group. However, the bulkiness of the iron unit also serves a second, more critical role by directing the stereochemistry of the key Peterson olefination

step, selectively producing the desired *cis*-alkene after the failure of modified Horner-Wadsworth-Emmons conditions to accomplish the same task.

The rationale for the selectivity is presented below; from the two competing s-*trans* (aldehyde to diene) synclinal transition states, the approach of the ester enolate that produces the *Z*-isomer is the only trajectory that avoids steric repulsion between the iron unit and the relatively large α-silane substituent on the enolate. Having accomplished a regioselectively challenging *cis*-olefination on a polyalkene substrate by utilizing an iron(0) protecting group, Ito and team were able to then finish the synthesis of (11*Z*)-retinal in four additional steps (41% total yield), delivering the key chromophore through a short, novel approach.

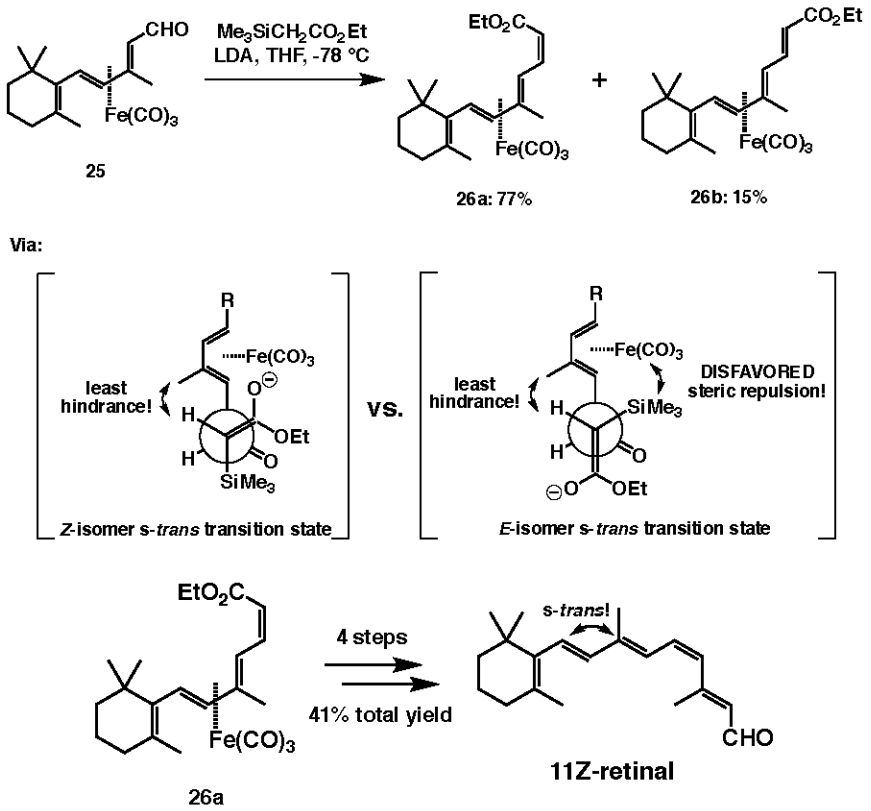

Scheme 11. Stereodirected Peterson olefination reported by Ito et al. for the total synthesis of 11Z-retinal.

The Takemoto group also reported a racemic total synthesis of the C1-C15 framework of macrolactin A, a natural macrocylic product shown below in Figure 4:[32]

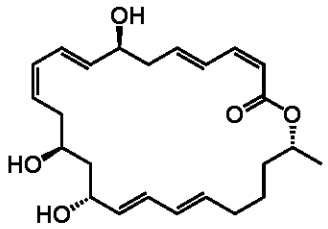

Fig. 4. Structure of macrolactin A.

The scalable synthesis of this macrocyclic species is of great importance, largely due to the well-documented antibacterial and anticancer properties and potential AIDS-combatting applications of the compound.[33] A number of steps in this sequence depend on the directing and stabilizing properties of the iron-diene framework to proceed. After furnishing cyanophosphate **29** from the major ester diastereomer **28a**, 1,2-migration enabled by hydride treatment of the phosphonate ester delivered pentadienyl cationic intermediate **30**, which was subsequently trapped by nucleophilic thiophenol (in a stereoselective fashion, as dictated by *anti* addition relative to the planar chiral iron unit) to afford rearranged complex **31**. Following DIBAL reduction and acylation, silyl ether **34** was delivered as a mixture of diastereomers. Pinacol borane-initiated hydroboration of major diastereomer **34a** and tandem desilylation using an *in situ*-modified Rh(I) catalyst (reminiscent of Wilkinson's classic hydrogenation catalyst), followed by Suzuki cross-coupling, furnished ester **36**. The group eventually generated **37**, a modified C1-C15 fragment of macrolactin A, after further deprotection. As displayed by the Takemoto synthesis, architecturally complex molecules featuring numerous motifs can be synthesized from iron-diene precursors in straightforward reaction sequences, offering

new insight into natural product generation and asymmetric methodology as related to total synthesis.

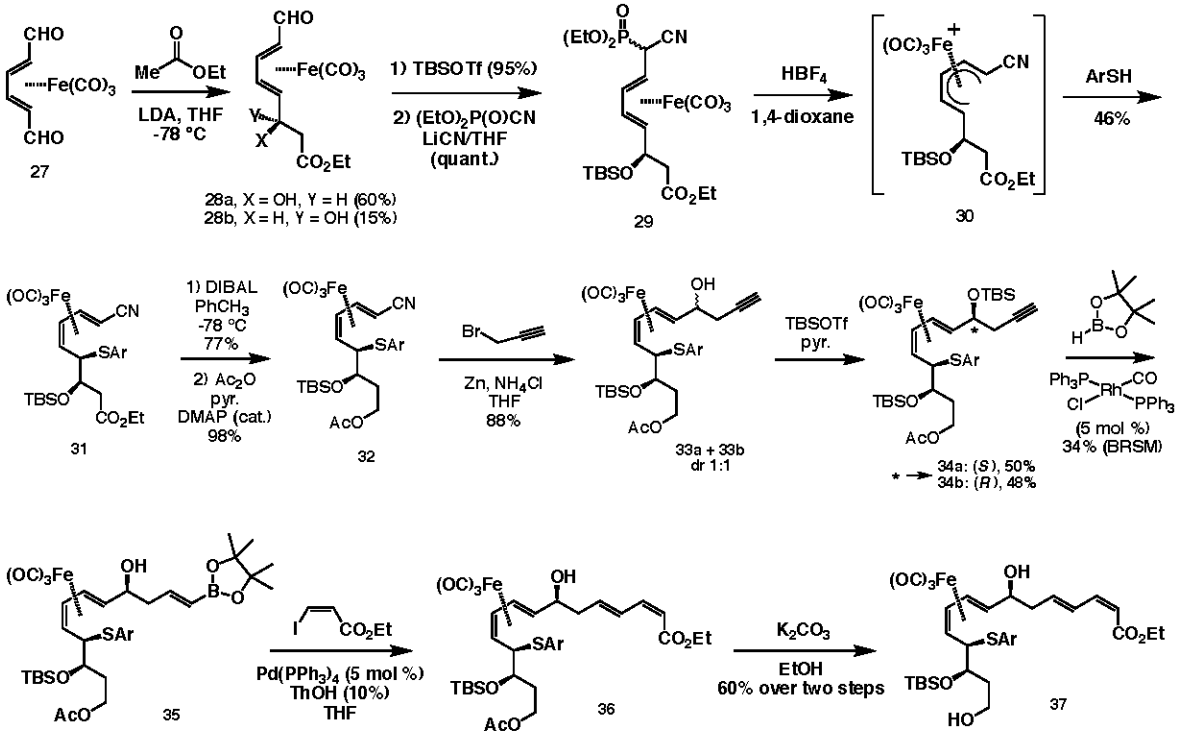

Scheme 12. Synthesis of C1-C15 fragment of macrolactin A directed by a planar chiral iron-diene complex, as reported by Takemoto et al.

Iron(0) tricarbonyl dienes and the Paley group

Research in the Paley group is conducted with the goal of broadening knowledge surrounding applications of iron(0) tricarbonyl-diene complexes in directed asymmetric synthesis. This typically involves developing new methodologies for synthesizing enantioenriched planar chiral iron(0) tricarbonyl-diene complexes which are later used in novel, highly diastereoselective transformations that expand the known capabilities of these systems in synthetic contexts. Specifically, many asymmetric transformations referenced above that utilize planar chiral iron(0) directing groups do not offer protocols for effectively furnishing complexes with a single planar chirality, which is critical for

ensuring high diastereomeric ratios in future products. To alleviate this issue, we incorporate enantiopure chiral auxiliaries, such as sulfoxides or N-oxazolidinones, into diene frameworks so as to direct iron coordination preferentially to a particular face, often delivering high diastereoselectivities for complexation reactions (>15:1 in some cases).[34] We are frequently looking for new auxiliaries which may direct facial selectivity with even greater control, and we also look to incorporate new characterization techniques to ascertain planar chiral features. Additionally, these auxiliary-mediated complexes are then used in common reactions that have yet to be asymmetrically directed by planar chirality in order to broaden the known set of reaction types that can be influenced in such a manner. Several examples, including highly stereoselective spiroketalizations and ring-closing metatheses, are shown in Scheme 13 (select data not published).[35]

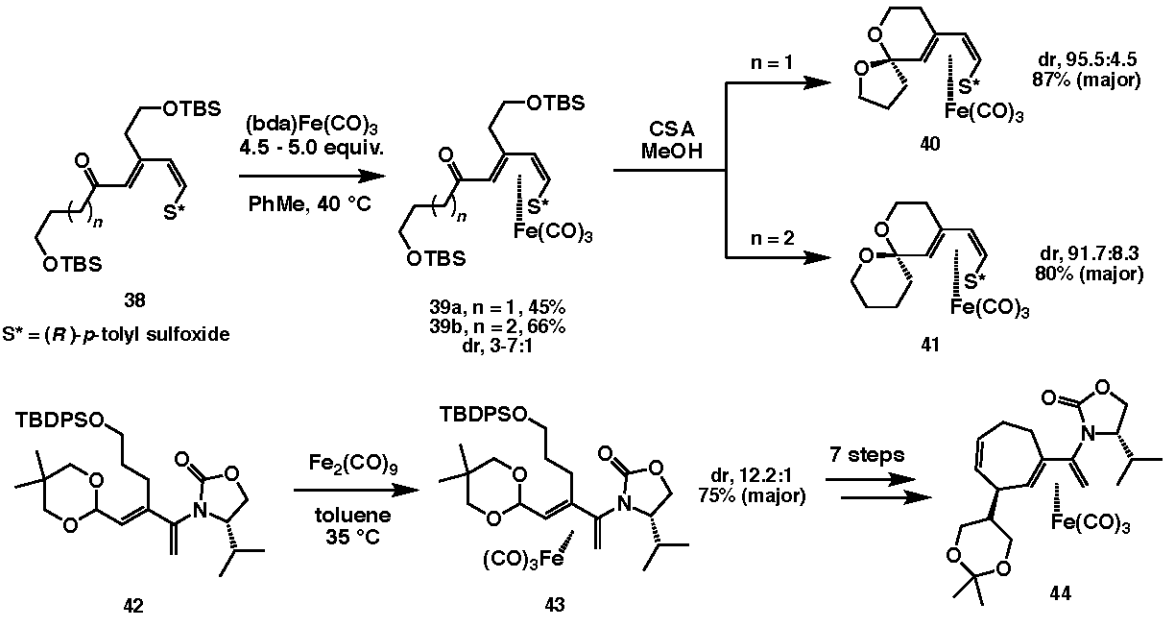

Scheme 13. Examples of several highly diastereoselective iron-diene complexations mediated by chiral auxiliaries, as well as subsequent stereospecific transformations, reported by the Paley group.

Results and Discussion

Assignment of absolute planar stereochemistry for N-oxazolidinoyl diene-iron(0) tricarbonyl complexes via crystallography and circular dichroism spectroscopy

The use of an enantiopure chiral auxiliary as a stereodirecting group for the complexation of iron(0) tricarbonyl units to diene substrates should allow for facile control regarding the planar chirality of the coordinated iron moiety.[36,37] The isolation of a single facial stereoisomer following complexation allows synthetic chemists greater control for subsequent asymmetric reactions that employ the organoiron substrate, and absolute planar chirality is therefore a physical property of great significance. However, the number of techniques available for characterizing absolute planar chirality are limited, and a specific dearth of literature exists for characterizing auxiliary-controlled complexation outcomes. In order to ensure the efficacy of iron-diene substrates in directing asymmetric processes, robust methods must be developed to monitor the absolute planar stereochemistry obtained during complexations, particularly those mediated by enantiopure chiral auxiliaries.

The most obvious technique for ascertaining the planar selectivity of complexation reactions is X-ray crystallography. For solid complexation products that can be crystallized from a predominantly nonpolar solvent mixture, an X-ray crystal structure can routinely determine the spatial orientation of each functional group within an organic structure.[38] The Paley group had previously utilized crystallographic approaches to determine the absolute planar stereochemistry achieved when mediating the complexation reaction with the (*S*)-(-)-4-isopropyl-2-oxazolidinone auxiliary (Figure

5, data not published). This crystal structure had indicated the expected *anti* complexation of the iron(0) tricarbonyl unit relative to the isopropyl group of the auxiliary. In addition, the most stable positioning of the N-oxazolidinone, which is free to rotate around the C-N bond attaching the auxiliary to the diene, could be reliably predicted by accounting for the minimization of nonbonding interactions between adjacent substituents at the 2 and 3 positions of the 1,3-diene periphery. With the auxiliary occupying one of these positions, it was apparent that the conformation producing the greatest distance between the oxazolidinone isopropyl unit and the adjacent vinylic methyl group was lowest in energy, and thus preferred. It was also noted that the selective placement of the iron(0) moiety, *anti* to the isopropyl unit but notably aligned with the N-oxazolidinoyl carbonyl group, could also be reinforced by an electrostatic interaction between the heteroatomic carbonyl and the Lewis acidic iron(0) unit, although this hypothesis remains unverified without further computational analysis.

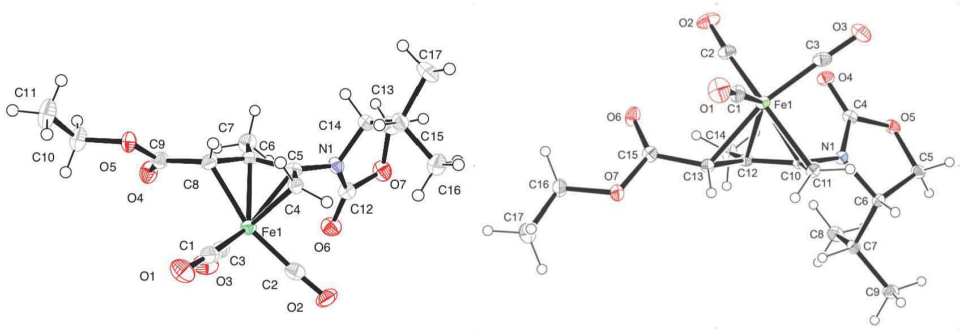

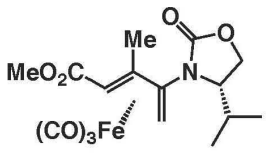

45

Fig. 5. ORTEP X-ray diagrams obtained from crystallographic analysis of (*S*)-isopropyl diene complex 45.

These crystallographic results allowed us to hypothesize that, because of the restrictions for determining a stable positioning for the auxiliary, the use of an auxiliary

with opposite chiral configuration (i.e. (*R*) instead of (*S*) chirality at the 4-position) should allow for the selective complexation of an iron(0) carbonyl unit to afford the opposite absolute planar stereochemistry as what was observed for the (*S*)-isopropyl-mediated dienyl substrate. Furthermore, we expected that these results could easily be verified by an analogous x-ray diffraction procedure to what was conducted previously. To test these expectations, as well as verify that (4*S*)-configured auxiliaries would consistently produce the same absolute stereofacial outcomes as seen previously, we decided to construct a library of enantiopure iron(0) tricarbonyl-diene complexes using various N-oxazolidinoyl auxiliaries, namely the (4*R*, 5*S*)-(+)-4-methyl-5-phenyl and (*S*)-4-benzyl variants.

We envisioned the delivery of N-oxazolidinoyl complexes via iron(0) tricarbonyl coordination to dienes furnished as products of Stille couplings, a class of Pd-catalyzed sp^2 C-C bond-forming coupling reactions that can tolerate vinyl halides and vinyl stannanes as coupling partners. Previous unpublished work in the group has identified the efficiency of this coupling when the oxazolidinoyl fragment is incorporated within the stannane partner, and we decided to continue this approach.

To start, each auxiliary was functionalized with a vinyl stannane unit, afforded through a two-step sequence as shown in Scheme 14. First, Pd-catalyzed N-vinylation of each auxiliary was achieved using vinyl butyl ether as the olefination partner. This was followed by the addition of the tributyl stannyl fragment to each general vinyl auxiliary **47** using tributyltin chloride, added regiospecifically through the selective lithiation of the geminal vinyl position using lithium tetramethylpiperidide (LiTMP) as a base to generate Stille partners **48a** and **48b**.[39,40]

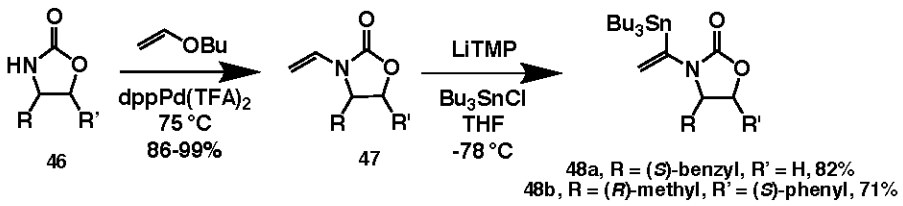

Scheme 14. Generation of N-oxazolidinoyl Stille partners.

In designing a vinyl iodide coupling partner, we looked to incorporate protected privileged functionalities, such as alcohols and aldehydes, within the substrate for future revealing; with this in mind, we decided on a concise four-step procedure to generate a Stille partner featuring both an acetal α to the diene and a silyl ether tether. Silylation of commercially-available 4-pentyn-1-ol (**49**) followed by Lewis acid-catalyzed installation of a diethyl acetal delivered alkyne **50**, which was promptly converted to the more robust pinacol acetal **51**. Regioselective stannylcupration, followed by iodination of the vinyl stannane intermediate using N-iodosuccinimide (NIS), afforded desired Stille partner **52** in high yield.

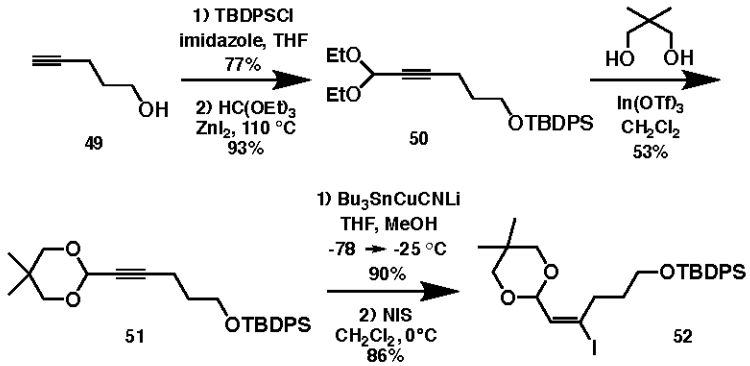

Scheme 15. Synthesis of vinyl iodide coupling partners.

Vinyl iodide **52** was then coupled to each auxiliary using a Fürstner-modified Stille protocol to furnish the corresponding dienes.[41] These compounds were subjected to complexation, utilizing diiron(0) nonacarbonyl to deliver the desired iron(0) tricarbonyl moiety, found in products **54** (dr, 3.6:1) and **56**. Disappointingly, the planar chiral

diastereomers of **56** were inseparable by chromatography, but we intended to purify this compound prior to crystallization by converting to a separable diastereomeric analog.

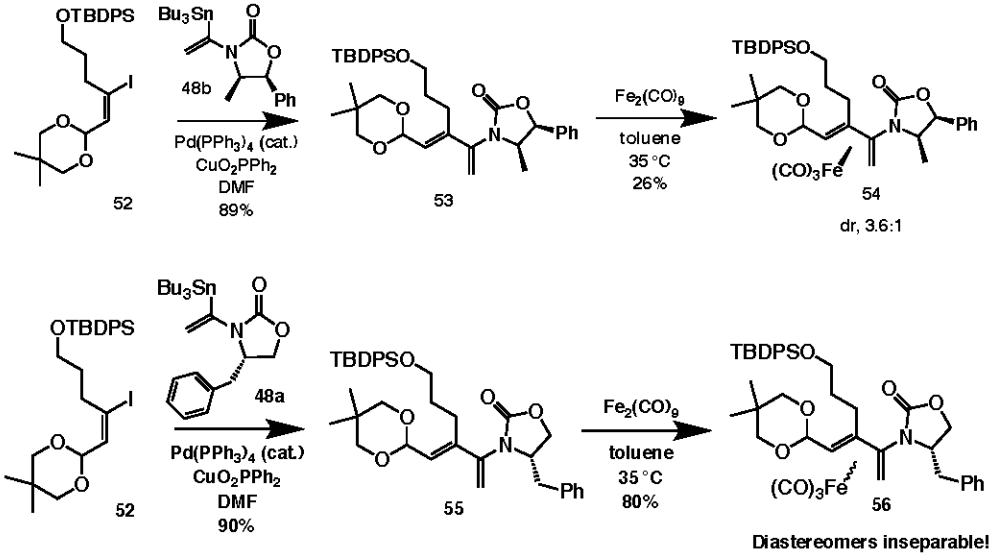

Scheme 17. Synthesis of N-oxazolidinoyl complexes for X-ray crystallography studies.

Having synthesized complexation products that were non-crystallizable oils, we then considered the execution of simple transformations that could potentially furnish solid products, eventually deciding to desilylate each complex using TBAF to deliver alcohols **57** and **58** (Scheme 18). Although desilylation was performed only on the major diastereomer of **57**, both diastereomers of **58** were subjected to deprotection and then separated, where the major diastereomer was obtained with approximate dr 17.5:1.This procedure resulted in two powdery solid products, which were both subjected to milligram-scale crystallization. Alcohol **57**, recrystallized in a facile manner from a mixture of excess hexane and chloroform, was subjected to X-ray analysis, resulting in the crystal structure depicted in Figure 6.

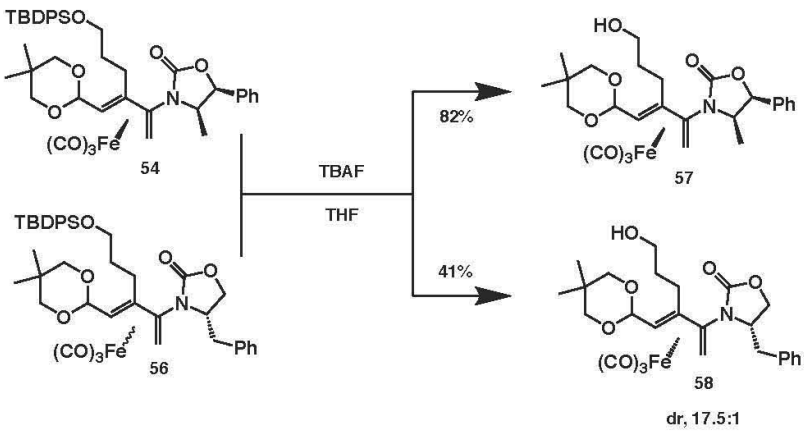

Scheme 18. Desilylation protocol to reveal alcohols for crystallization.

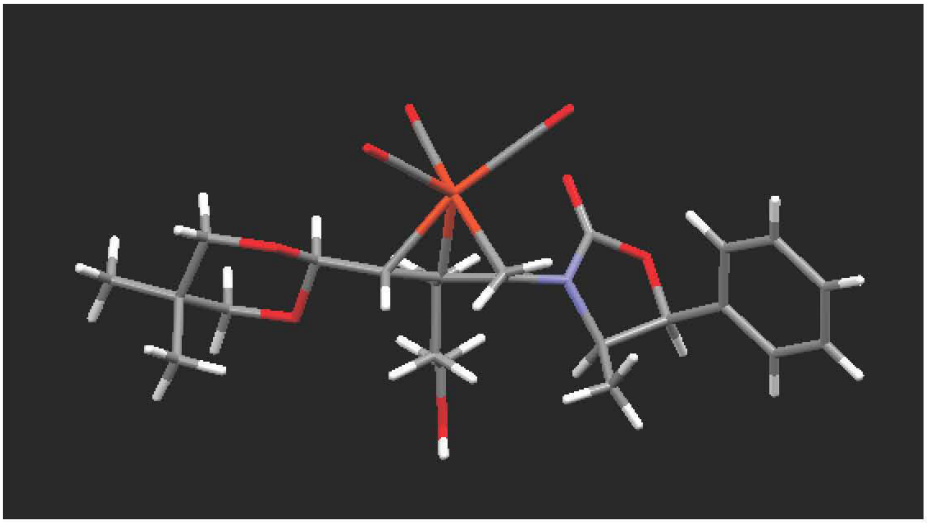

Fig. 6. Crystal structure of complex 57, diffracted to 2.0 Å. Atomic key: white = H, gray = C, red = O, blue = N, orange = Fe.

The spatial depictions indicated by this structure verified our expectations for the dominant absolute stereofacial preference that could be afforded by complexations mediated by an N-oxazolidinone auxiliary containing a (4*R*)-configured substituent. As expected, the orientation of the auxiliary appears to be primarily impacted by the possible nonbonding interactions between the chiral alkyl groups and the alkyl chain of the silyl ether tether originating adjacent to the auxiliary on the diene periphery. These interactions result in C-N bond rotation that places the auxiliary's chiral alkyl substituents farther away from the diene scaffold, and the subsequent iron(0) tricarbonyl coordination

occurs in an *anti* fashion to the new positions of these auxiliary substituents. Additionally, the alignment of the iron(0) unit and the oxazolidinone carbonyl suggests electrostatic favorability for the observed stereofacial selectivity, similar in nature to the Paley lab's previous crystal structure for an (*S*)-configured auxiliary.

Most importantly, this crystal structure indicated that the use of the (4*R*, 5*S*)-4-methyl-5-phenyl auxiliary to direct the coordination of the iron(0) unit resulted in the opposite facial selectivity of the coordination outcome observed in the (*S*)-isopropyl crystal structure. This result matched our expectation that the absolute planar chirality of iron(0) tricarbonyl moieties coordinated to N-oxazolidinoyl dienes should be controllable, notably with excellent selectivity, through proper selection of the optical configuration of the auxiliary.

To further confirm these stereofacial trends, we envisioned designing crystallization procedures for other analogous complexes, starting with alcohol **58**. However, this compound proved to be non-crystallizable, as the compound precipitated out of each solvent combination investigated (these combinations included varying amounts of hexanes, toluene, chloroform, THF and dichloromethane). Benzyl ester analogs formed via 4-dimethylaminopyridine-catalyzed acylation, expected to furnish crystallizable solids, also delivered products that precipitated out of solution.[42] Realizing the inconsistent nature of X-ray crystallography as our predominant method for stereochemical characterization, we started shifting our focus toward other spectroscopic techniques for optical differentiation that could be employed for a wider range of compounds, namely oils and other non-solid products.

Circular dichroism (CD) spectroscopy has been considered a useful method for the determination of transition metal coordination environments since the early days of organometallic research.[43] The unique use of circularly polarized light as a primary radiation source has been of particular interest. This stems from the observation that certain optically active substituents within substrates of interest will absorb each circular polarization of incident rays (termed "left" or "right-handed" light) to a different extent, and the difference in directional absorbance allows for the direct characterization of chirality for specific functional groups present in the compound's structure.[44] The first studies regarding this area focused on the characterization of optically active metallocenes (namely ferrocene) and proved the validity of this approach for polycoordinate transition metal centers.[45] These investigations eventually expanded to include the stereofacial characterization of dienes protected by iron(0) tricarbonyl units by taking advantage of the impact the planar chiral metal center can have on neighboring carbonyl groups within the diene substructure.[46,47]

Many spectroscopic techniques, including CD, primarily use radiation in the UV-Vis portion of the electromagnetic spectrum to probe chemical environments. Based on this technical design, the usefulness of collected spectra are dependent upon the presence of functional groups that possess energetically-accessible electrons, as these can easily undergo photoinduced promotion to generate a measureable absorption event.[44] Early work in transition metal characterization therefore noted that carbonyl-based substituents, even simple units like aldehydes, ketones and esters, could have spectroscopic use within metal-diene complexes due to the characteristic $n \rightarrow \pi^*$ electronic transition that occurs for these groups after stimulation with UV-Vis radiation. Experiments conducted with

substrates of this nature indicated that the carbonyl n→ π^* transition displayed optical activity that was dependent on the absolute planar stereochemistry of the iron(0) moiety.[45] Through comparison with X-ray structures, it was confirmed that the desired asymmetric carbonyl transition could produce either a positive or negative ellipticity value (consistently at a characteristic wavelength for the electronic transition studied) and that this optical behavior was solely impacted by the face of the diene to which the metal center was coordinated. In essence, the presence of an enantiomeric planar chiral iron unit was able to convert an sp^2-hybridized heteroatomic substituent into an optically active region of the compound, so long as the carbonyl was furnished α to the diene backbone – at greater distances, the induced chiral effect was often insufficient for stereochemical characterization.[46]

Naturally, we sought to isolate enantiopure α-carbonyl derivatives of representative iron(0)-diene complexes synthesized in our lab in order to validate the usefulness of CD spectroscopy for identifying absolute planar chirality within our compounds. In particular, α-carbonyl analogs of the major diastereomers that delivered the two crystal structures, namely the (*S*)-isopropyl and (4*R*, 5*S*)-4-methyl-5-phenyl N-oxazolidinoyl variants, were mandatory inclusions within this new CD spectral library, as the correlation between a particular ellipticity sign (positive or negative) and the absolute stereochemistry of the iron(0) tricarbonyl unit needed to be established; without correlating the crystal structures with the corresponding CD signals, only relative stereochemistry (whether two compounds had the similar planar chirality) could be evaluated, rendering this technique inadequate for comprehensive optical characterization.

Conveniently, many of our retrosynthetic approaches for making complexes included steps for the furnishing of an acetal unit at a terminal position of the diene substructure – this choice was made because the facile deprotection of the acetal leaves behind an exceedingly electrophilic aldehyde group, a valuable unit to possess for subsequent diastereoselective transformations once the complex has been formed. For the purposes of our project, the simple unmasking of the aldehyde could deliver a reactive center, but, more importantly, could furnish a useful carbonyl substituent, adjacent to the diene scaffold, that could be probed spectroscopically.

For complexes possessing the acetal unit (of which examples utilizing each of the three N-oxazolidinone auxiliaries exist), acidic hydrolysis, conducted in relatively mild conditions of acetic acid (HOAc), water and THF, could deliver derivatives fully prepared for CD analysis (Scheme 19). Three major diastereomers (**60**-**62**), as well as one minor diastereomer (**63**, synthesized by Prof. Paley) of α-aldehyde complexes were prepared (acetal **59** had been prepared by previous Paley group researchers and stored at 2-8 °C until this procedure). Samples of each complex for CD analysis were prepared by dissolving the compound in methanol (chosen for its low UV-cutoff wavelength, 205 nm, to avoid interference with the aldehyde n→ π^* band) within a vial and mixing via vortex until homogenized.[48]

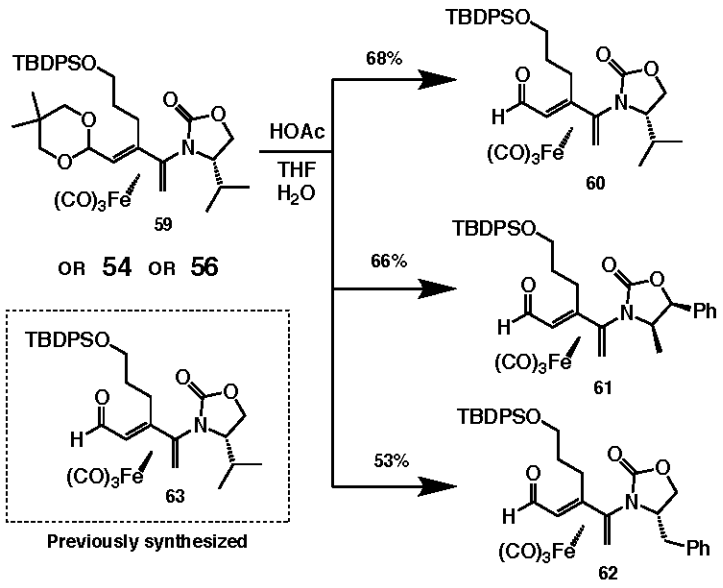

Scheme 19. Hydrolysis procedure to synthesize dienal complexes for CD analysis (63 previously synthesized by Prof. Paley as minor diastereomer).

CD results for the four complexes presented in Scheme 19 are summarized in Figure 7. All four samples displayed the anticipated iron(0)-influenced carbonyl $n \rightarrow \pi^*$ electronic transition between 388-390 nm, with sufficiently high molar ellipticity values (proportional to intensity) for analysis. Dienals containing (*S*)-configured auxiliaries (**60** and **62**) were found to produce this transition with a positive ellipticity measurement, whereas the (*R*)-configured analogs (**61** and **63**) exhibited the opposite behavior, producing negative ellipticity peaks. This CD experiment represents the first comprehensive, multi-sample analysis relating the chirality of an N-oxazolidinoyl auxiliary to the planar chirality of an intramolecular iron(0) tricarbonyl-diene complex (via measurement of α-aldehyde behavior). These results also comprehensively verify our expectation that changing the auxiliary chirality will necessarily change the face to which the iron fragment is coordinated. Notably, all complexes display roughly equivalent absolute values for maximum ellipticity except for **61**, which is considerably less; from our qualitative observations of CD behavior, we predict that this indicates an

impure sample for **61** that likely contains considerable amounts of the positive ellipticity-producing minor diastereomer.

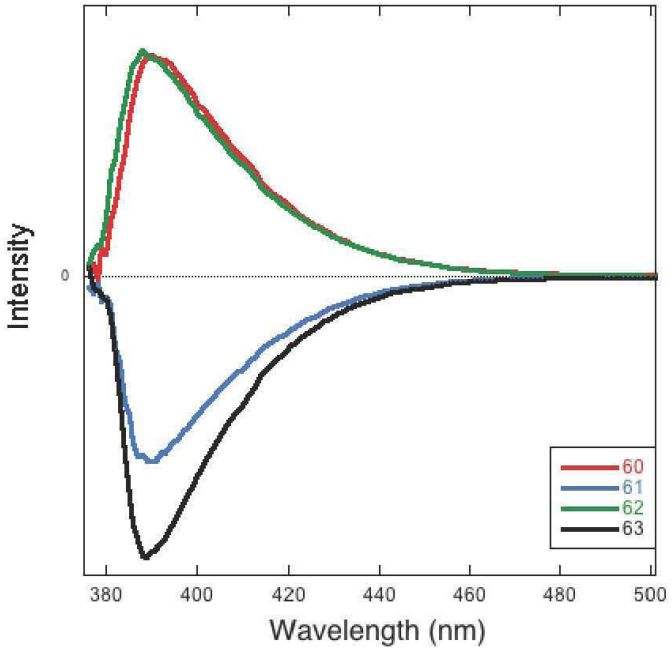

Fig. 7. CD spectra for complexes 60-63, collected for 6.7 mg/mL samples in methanol.

Although this data only indicates the change in *relative* planar chirality when the auxiliary's stereocenter is reconfigured, the combination of CD and X-ray results, which have now been obtained for both (*R*) and (*S*)-oriented oxazolidinonyl diene complexes, means that CD results can also be correlated to predict *absolute* planar stereochemistry. Specifically, all complexes producing positive-intensity CD results are observed to have facial complexation analogous spatially to **45**, while compounds with negative intensities will display facial behavior analogous to **57**. Although this was assumed to be the case, this correlation, officially proving our predictions experimentally, allows for precise future knowledge of all optical features for N-oxazolidinoyl iron(0)-dienal complexes.

We have therefore identified the precise absolute planar stereochemistry of complexes synthesized for all three N-oxazolidinoyl auxiliary types, a novel

determination and one that verifies the usefulness of our auxiliary-directed complexation model for producing enantiopure planar chiral complexes for use in asymmetric synthesis. Additionally, we have proven the usefulness of CD spectroscopy as an analytical tool for the characterization of non-solid acetal-containing complexes, allowing us to optically characterize a far greater number of samples going forward, as the requirement of synthesizing solid complexes is no longer enforced.

Development of substituted cyclic ureas and cyclic sulfonamides as new chiral auxiliaries for facially-selective iron(0) tricarbonyl-diene complexations

Given the pressing need for stereocontrol to ensure the efficacy of iron(0) tricarbonyl units as directing groups for asymmetric synthesis, the Paley lab is constantly looking to expand its library of viable chiral auxiliaries in order to achieve the highest planar diastereoselectivity possible during complexations. The bulk of previous work in the lab has involved the preparation of enantiopure sulfinyl dienes, via analogous Stille cross-coupling chemistry, that enables the use of chiral sulfoxide units to direct the preferred facial approach of the iron-delivering reagents (Scheme 13); diastereomeric ratios as high as 16:1 can be achieved using terminal sulfoxides, taking advantage of the steric limitations assigned to one face as conformationally-induced allylic strain is relieved for the sulfoxide unit.[34,49]

More recently, our endeavors have focused on Evans' classic enantiopure N-oxazolidinoyl auxiliaries, which are used most often in synthesis to mediate stereoselective aldol reactions (Scheme 13).[50] The best results achieved with

oxazolidionyl directing groups have been obtained using the valine-derived (*S*)-isopropyl oxazolidinoyl analog, where diastereomeric ratios for complexation reactions are as high as 15:1; a mechanistic analysis for facial selectivity during complexation is presented in the discussion of X-ray and CD spectroscopy results in the previous section (data not published).

However, in order to screen for optimized complexation conditions, a more thorough investigation of analogous but chemically distinct auxiliaries must be embarked upon, as the potential for increased facial selectivity, and therefore greater synthetic applicability of pendant iron moieties, remains relatively unexplored. In order to replicate our previous retrosynthetic approaches with only subtle chemical variation, we decided to employ a new class of auxiliaries that were both structural compliments to the oxazolidinones and could also be generated in short sequences from the "chiral pool" of amino acid templates.

The most logical starting point based on structural and electronic similarity was the design of substituted 2-imidazolidinones, or cyclic ureas, easily obtained in quick fashion from commercially available chiral valinol reagents (Scheme 20). In accordance with procedures reported by Lee and coworkers, condensation of (*L*)-valinol (**64**) with benzyl isocyanate, followed by tosylation and alkoxide-mediated regioselective cyclization, delivered our first urea auxiliary, the (*S*)-isopropyl benzyl-protected variant **66**.[51] Analogous to oxazolidinone functionalization, we anticipated that Pd-catalyzed N-olefination of the urea's unprotected substituent to produce **67**, followed by directed lithiation and stannyl chloride substitution, would afford a vinyl stannane fully prepared for the key diene-furnishing Stille coupling. However, olefination did not take place;

although surprising, this result has been rationalized by noting an anticipated decrease in lability (i.e. higher pKa) of the targeted urea N-H bond compared to the oxazolidinone variant.[52]

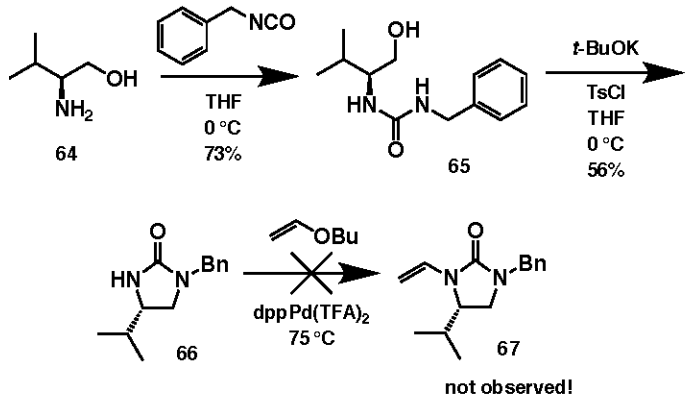

Scheme 20. Attempted synthesis of enantiopure (*S*)-isopropyl N-olefin cyclic urea via Pd-catalyzed olefination.

Realizing that direct delivery of the vinyl stannane unit may not be so straightforward, we set our sights on alkynylation of the urea, as Pd-catalyzed hydrostannylation would be expected to afford the vinyl stannane in relatively few additional steps. Adapting protocols reported by Danheiser and coworkers, direct coupling of urea **66** with TIPS bromoacetylene via copper sulfate catalysis was acheieved to afford **68**, albeit in a modest 20% yield (Scheme 21).[53] The variation of conditions such as catalyst equivalents, phenanthroline ligand equivalents, base selection and temperature did not result in yields higher than 23%. Deciding to carry on, desilylation of **68** followed by hydrostannylation successfully produced vinyl stannane **70** in 68% yield, preparing our first urea auxiliary for incorporation into a diene scaffold.

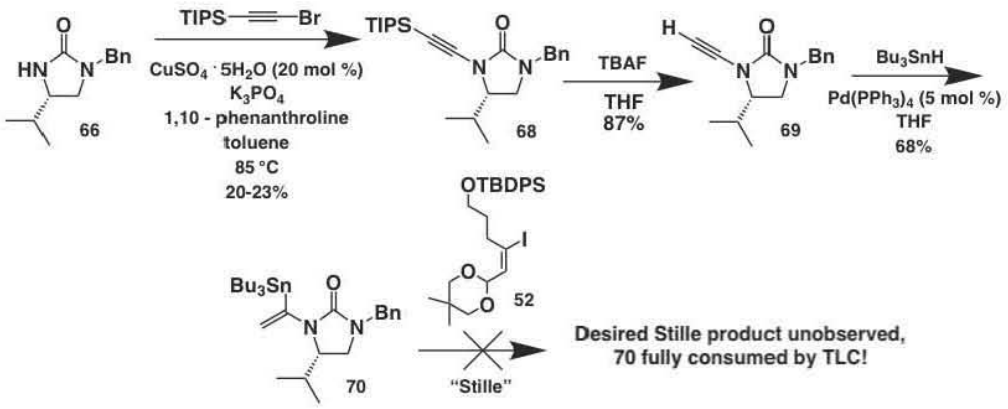

Scheme 21. Attempted synthesis of the vinyl stannane derivative of an (*S*)-isopropyl cyclic urea auxiliary, via alkynyl C-N coupling route.

As with all dienes furnished in the Paley lab, Stille coupling of urea **70** with functionalized vinyl iodide **52** was attempted using Fürstner-modified conditions. However, no diene product was detected by TLC, and, despite the presence of unused vinyl iodide starting material, no trace of urea **70** reagent was observed. The loss of this material led us to believe that, in avoiding the typically labile vinyl iodide moiety, the Pd(0) catalyst for the coupling underwent oxidative addition into the benzyl C-N bond of the urea coupling partner to generate the Pd(II) intermediate shown in Figure 8. This type of reactivity would be unexpected but not entirely unprecedented, as several groups have indicated the reactivity of labile amines in transition metal catalytic cycles.[54,55] Unfortunately, this explanation indicated that the selection of our benzyl protecting group, naturally incorporated into the original isocyanate reagent used before urea cyclization, prevented the possibility of diene formation. To remedy this situation, we chose to repeat this synthetic sequence using a variation of sp^3 alkyl-functionalized isocyanate reagents to ensure the incorporation of robust protecting groups, ones that would allow Stille couplings to eventually take place without reagent decomposition.

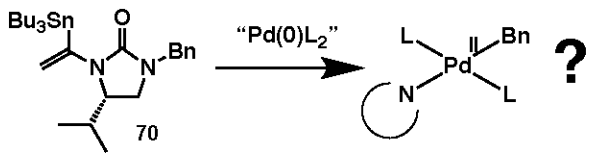

Fig. 8. Hypothesized intermediate generated during failed Stille coupling, assuming oxidative addition of the urea substrate.

By varying the substituent on each commercially available isocyanate, (*S*)-configured cyclized ureas protected by ethyl, butyl and tert-butyl alkyl chains (**72a-c**) were obtained, each in two steps (Scheme 22). Proceeding forward with the butyl-protected variant, N-alkynylation via copper(II)-catalyzed cross-coupling was attempted in an analogous fashion to the prior benzyl urea sequence, but failed to produce the desired alkynyl urea product under any set of conditions attempted.

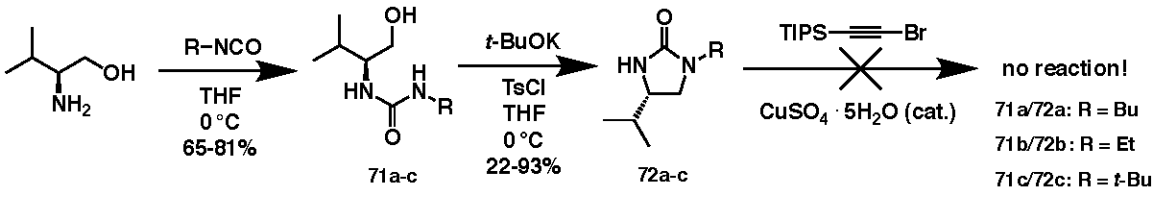

Scheme 22. Failed alkynylation sequence for alkyl-protected cyclic urea auxiliaries.

Akin to the poor reactivity of the benzyl urea seen previously, we hypothesize that, again, the reduced acidity and lability of the targeted N-H urea bond prevents the use of valinol-derived ureas in cross-coupling reactions. In principle, urea should behave as the stronger base (and weaker acid) relative to the corresponding amide, due to the prevalence of the iminium-based amide resonance form that prevents the amide N lone pair from acid-base interactions; for the analogous urea compound, lone pair participation from each atom in resonance forms is reduced, since both N-substituents participate in resonance behavior. The amide, displaying greater acidity, is assumed to possess an N-H bond more labile to oxidative addition, and therefore participates more readily in transition metal-catalyzed reactions.[56]

Deciding to abandon this cross-coupling synthetic approach, we sought to deliver the alkynyl unit in an elaborated sequence that would avoid the use of transition metal catalysts. Adopting a strategy first reported by Anderson and coworkers, we envisioned a two-step sequence to deliver the alkynyl derivative of the butyl-protected urea, via formation of a dichloroenyl analog (**73**) using trichloroethylene in basic conditions followed by a phenyllithium-induced elimination to the alkyne (Scheme 23).[57] Although generation of the dichloroenyl derivative proceeded as anticipated in 76% yield, all efforts to perform the subsequent elimination resulted in nucleophilic addition of the basic carbanion to the chlorinated olefin, furnishing what was hypothesized as a diphenylalkene product that was unsuitable for hydrostannylation.

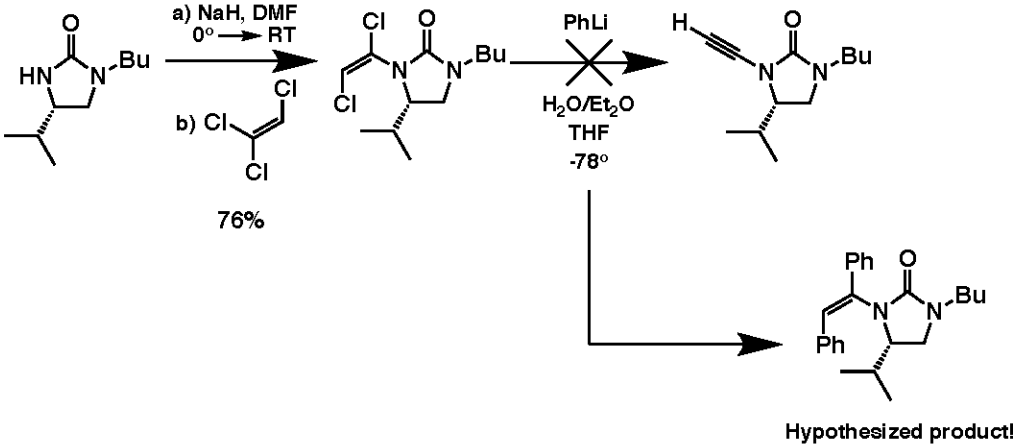

Scheme 23. Attempted alkynylation procedure for butyl-protected ureas based on dichloroalkene elimination.

A number of different olefination/elimination conditions were attempted, all with similar undesired results. Realizing the mounting difficulty in generating a vinyl stannane derivative of an enantiopure cyclic urea auxiliary, we decided to postpone efforts to incorporate chiral urea units into functionalized dienes and to instead pursue an alternative class of auxiliaries, with structures still analogous to the optimized N-

oxazolidinone template. To date, no further work on the urea project has been attempted by the Paley group.

Still focused on designing auxiliaries in short sequences originating from abundantly available natural substances (such as amino acid variants), we considered the generation of a chiral cyclic sulfonamide from the same L-valinol reagent implemented in the urea pathways. Unlike the ureas, for which the protecting group was determined by the isocyanate architecture and therefore subject to variation, the reagent chosen to deliver the necessary sulfone fragment was limited to mesylate frameworks such as mesyl chloride, as the methyl substituent within the sulfonamide could be deprotonated and utilized as a nucleophile in the cyclization procedure to generate the auxiliary.[58] Conversion of L-valinol to the mesylate/sulfonamide derivate, followed by selective substitution of the mesylate for chloride and subsequent dianion cyclization of **75**, was expected to produce the (*S*)-isopropyl cyclic sulfonamide auxiliary **76** in a concise three-step sequence that, according to literature, would not require chromatographic purification between steps (Scheme 24).

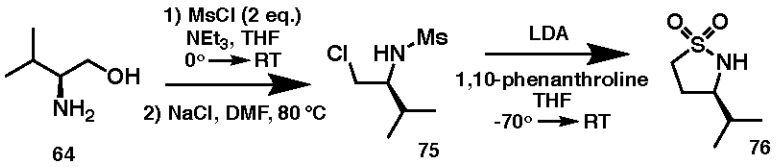

Scheme 24. Expected synthetic pathway to produce (*S*)-isopropyl cyclic sulfonamide auxiliary.

One-pot generation of the expected cyclic sulfonamide was, however, not achieved, as indicated by ^{1}H NMR of the obtained product. Instead, this three-step pathway exclusively generated aziridine **77** in quantitative yields. Replacement of the *in situ*-generated base, lithium diisopropylamide (LDA), with commercially-available LDA solution (in a solvent mixture of THF/heptanes/ethylbenzene) caused no change in the

reaction outcome. To determine which step in the sequence resulted in undesired aziridine production, purification and characterization by ^{1}H NMR was carried out following each step. Mesylation was found to proceed in near-perfect yield, but the following chlorination, despite generating the expected chlorosulfonamide, could only be carried out at 46% conversion even at elevated temperatures and lengthened reaction times. Although these yields were below expectations, NMR verified the identity of the desired chlorosulfonamide **75** (which had not been purified or characterized previously), leading us to hypothesize the mechanism indicated in Scheme 25 used for aziridine formation. With this mechanistic knowledge in hand, we were optimistic that the LDA-initiated dianion cyclization step could be optimized to deliver the expected cyclic sulfonamide auxiliary.

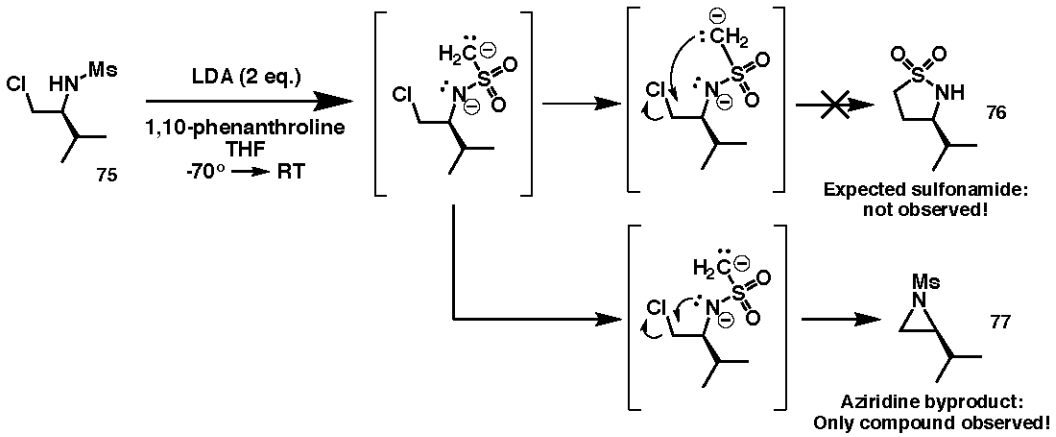

Scheme 25. Possible cyclization mechanism leading to formation of aziridine during attempted cyclic sulfonamide synthesis.

However, production of the sulfonamide could not be detected under any set of conditions screened, and exclusive formation of the unwanted aziridine was continually observed. Variations in reaction time and equivalents of LDA base were unsuccessful in altering the chemoselectivity for this process. Unable to monitor any evidence of desired sulfonamide cyclization, we ultimately decided to postpone further work with this

auxiliary and, ultimately, with the new auxiliary project entirely. Despite successfully generating one example of a novel Stille-functionalized auxiliary for directing complexations (the benzyl-protected 2-imidazolidinone), we were unable to incorporate new auxiliaries into diene frameworks to determine their efficacy in influencing selective generation of additional chirality. Future work in this area should address the task of improving urea auxiliary reactivity during cross-coupling processes (which other urea substrates are known to engage in, typically in robust fashion) and focus on the identification of new N-oxazolidinone analogs for implementation as novel chiral auxiliaries.

Elaboration of indole derivatives for use in diastereoselective Pictet-Spengler condensation reactions mediated intramolecularly by planar chiral iron(0) tricarbonyl-diene frameworks

Beyond designing new organometallic complexes featuring novel chiral auxiliaries, the Paley lab is also broadly interested in the use of enantiopure planar chiral iron(0) tricarbonyl-diene complexes as unconventional directing groups, chiefly for the selective introduction of new stereogenic centers within potentially useful substrates such as natural product derivatives. In particular, functionalized indole substrates have long been investigated as compounds of anticipated biological or medicinal application, and aromatic indole substructures are themselves considered "privileged" scaffolds.[59,60] As such, reactions that modify indole cores, especially in stereospecific ways, are of great importance within biocompatible synthetic strategies to design pharmacophores and other

alkaloids. Of even greater intrigue are reactions of this type that also generate unique and typically inaccessible architectural features, such as polycyclic or polyfunctionalized indole frameworks that are wholly produced in a single step. An example of such a process is the Pictet-Spengler condensation.[61]

A variation of the ubiquitous Mannich reaction, this is an unconventional cyclization that, in the traditional process, simultaneously generates a new stereocenter (provided by the identity of the aldehyde reagent) from a tryptamine (β-arylethylamine) template using an acid-activated aldehyde as an iminium ion source. Two proposed mechanistic pathways for the Pictet-Spengler cyclization are provided below in Scheme 26, varied only by the regioselectivity of one C-C bond-forming step. In the most plausible mechanism, reactivity at the typically nucleophilic C3 position of the aromatic indole framework is expected and should generate a second endocyclic iminium ion, which indicates that a ring-expanding alkyl shift is required to rearomatize the system and complete the process.[62]

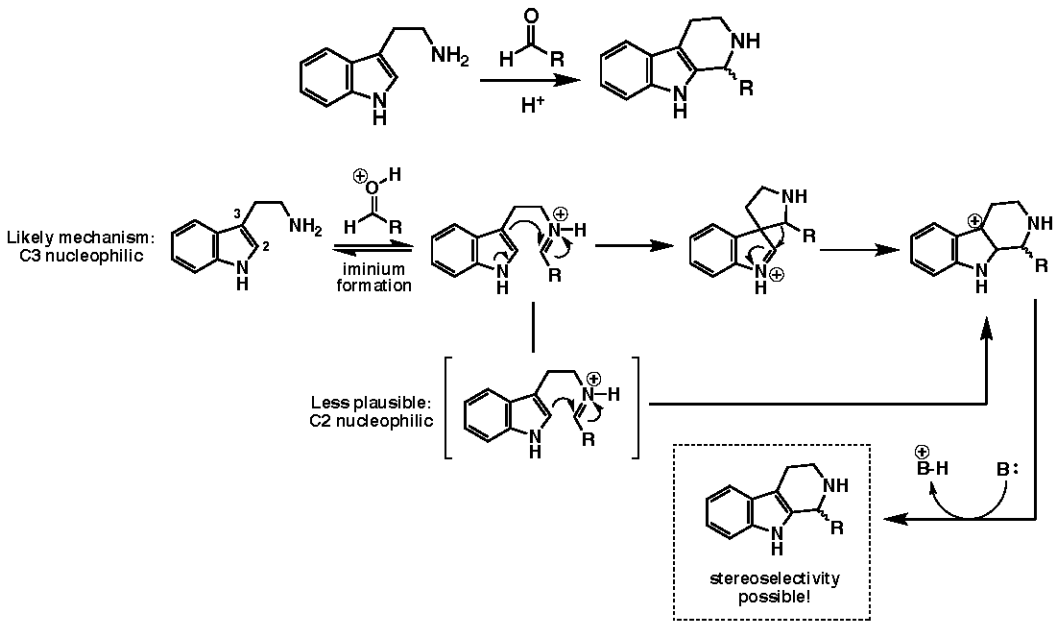

Scheme 26. Proposed mechanisms for the Pictet-Spengler cyclization to generate tricyclic indoleamines.

As presented, there is no specificity to the way in which the new chiral center is oriented (without further definition of substituent R in Scheme 26, it can be assumed that the product mixture may be racemic). To direct the chirality of that position, existing chirality must already be present in the reaction system. To this end, we envisioned that the furnishing of a planar chiral iron(0) tricarbonyl-diene complex as a substituent on the aldehyde (replacing substitutent R in Scheme 26) would allow for diastereoselective control over the cyclization reaction. Specifically, this would enable facile production of a single chiral configuration for the complex indole structure (77) via formation of the key C-C bond *anti* to the iron unit. Further, we anticipated that through careful retrosynthetic planning, we could tether the necessary protected indole framework to an internal position of the s-*cis* diene, produced from a Stille coupling of the vinyl iodide analog **79** with (*S*)-isopropyl oxazolidinoyl auxiliary **80**, via an aminoalkyl chain. Following tandem acid catalysis/deprotection, this approach would both allow the ultimate Pictet-Spengler reaction to take place intramolecularly (ensuring better

diastereoselective control) and would modify the reaction conditions to stimulate a novel indole bis-annulation process mediated by planar chirality (Scheme 27).

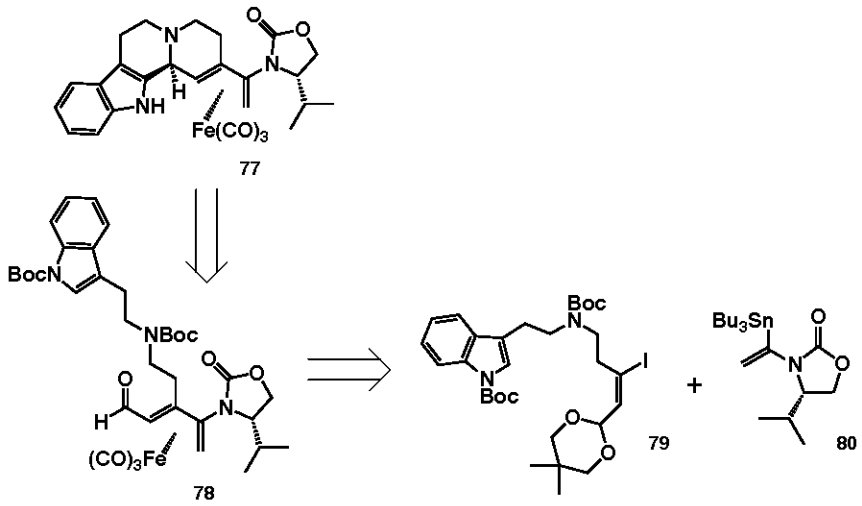

Scheme 27. Envisioned retrosynthetic approach for the planar chirality-mediated Pictet-Spengler cyclization.

In planning such a sequence, we were optimistic that the incorporation of the amino indole unit could be accomplished by modification of appropriate acetal-functionalized alkynyl alcohols, a substrate class that the lab has worked with numerous times during previous syntheses of N-oxazolidionyl complexes. In pursuing a straightforward procedure to link the two units together, we settled upon the Mitsunobu reaction, a robust procedure for the generation of heteroatomic products, such as amines, that for such a product would utilize both an alcohol and a primary or secondary amine in the traditional setup.[63] Upon exposure of both heteroatomic reagents to a dialkyl azodicarboxylate derivate (often diisopropyl azodicarboxylate, or DIAD) and triphenylphospine, N-alkylation of the amine substrate is achieved through a simple S_N2 reaction featuring the deprotonated amine as the nucleophile, with generation of a stable byproduct, triphenylphosphine oxide, providing thermodynamic favorability to drive the

reaction forward.[64] For amine and alcohol reagents, the mechanism for the Mitsunobu reaction follows the general pattern in Scheme 28:

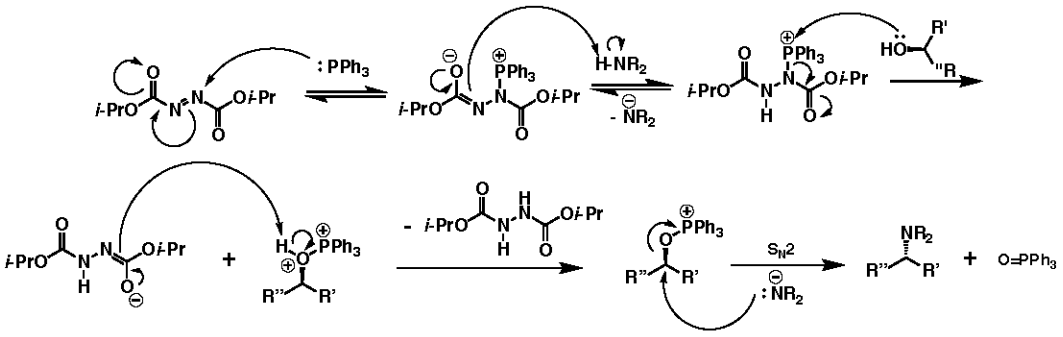

Scheme 28. General mechanism for the Mitsunobu reaction using secondary amine and alcohol substrates to generate an enantiopure tertiary amine product.

In the simplest case, we envisioned that the Mitsunobu condensation of an alkynyl alcohol (furnished using our previous methodology) with an appropriately-protected tryptamine (potentially obtained in one step from commercially-available materials) would deliver the ligated alkynyl tryptamine needed to pursue an asymmetric Pictet-Spengler process; following steps such as regioselective stannylcupration, halogenation of the vinyl stannane product, and Stille coupling/complexation, the iron(0)-diene complex could be afforded from a relatively concise pathway. However, a serious obstacle was identified before attempts were made to perform these conversions. Literature has indicated that, in previous work optimizing Mitsunobu conditions, the presence of a sulfonamide protecting group on the amine greatly improves reaction performance (specifically, these conditions comprise the eventual protocol for the Fukuyama amine synthesis).[65,66] This is presumably due to a lowering of the pKa associated with the remaining amino proton, which must be removed to generate the required nucleophile. Unfortunately, the presence of this sulfonamide, most often the 2-nitrobenzenesulfonyl (Ns) protecting group, can interfere with the efficient execution of organometallic chemistry; in particular, previous unpublished work by the Paley group

indicated the halting of iron(0) tricarbonyl-diene complexation on sulfonamide substrates, resulting from unwanted reduction of the sulfonamide (in this case, iron most likely acts as a two-electron oxidant) to generate a substituted aniline. Based on these setbacks, we identified the need to either switch protecting groups after Mitsunobu execution to something more robust to complexation (for example, t-butylcarbamate, or BOC), or to attempt the Mistunobu with a seldom tested amine protecting group (such as BOC) attached instead.

Aside from this need for protecting group screening arising from our previous work, several issues still existed. Although we believed that Mitsunobu conversion could deliver our desired amine-tether alkynyl indole substrate, it was unclear whether the presence of the nucleophilic amine on the indole or alkyne fragment would affect the performance of the reaction, or whether it would be necessary to place the amine on a specific reaction partner to obtain quantitative yields. Accordingly, we were prepared to modify our pathways to change which partner contained the necessary amine, most likely by performing additional Mistunobu reactions to interconvert between alcohol and amine groups. Additionally, it was unclear when the key stannylcupration step should take place in the sequence; most notably, we were unsure whether the central Mitsunobu step could be performed on the vinyl stannane or vinyl iodide derivative of the acetal-functionalized alcohol fragment (i.e. after stannylcupration/halogen of the original alkyne). Having identified each of these potential obstacles to correct during experimentation, we proceeded forward with our first attempts to synthesize partners for the key Mitsunobu step.

Original efforts to screen for appropriate Mitsunobu conditions delivered a number of setbacks; some of these attempts are summarized below in Figure 9. Protected tryptamine derivatives such as **82** were found to be incompatible with certain Mitsunobu conditions, furnishing modest-yield adducts like **83** from alkynyl alcohols reagents (**81**) that could not be chromatographically separated from starting materials. This situation was remedied for Mitsunobu reactions in which the alcohol partner contained a vinyl stannane (**84**) rather than an alkyne (indicating the previously questioned tolerance of the Mitunsobu reaction to these substrates), allowing for facile conversion to vinyl iodide **87**. However, attempts to place BOC protecting groups onto both nitrogenated regions of the aminoindole fragment (necessary to avoid unwanted Ns reduction in the presence of iron) were ultimately unsuccessful in affording target compound **88**. 4-dimethylaminopyridine (DMAP)-catalyzed acylation returned a product distinct from unprotected starting material **87** as evidenced by TLC, but only one BOC group could be identified by ^{1}H NMR. We posited that the presence of the potentially reactive vinyl halide may have interfered with the efficient furnishing of both BOC groups, leading us to conclude that our pathway should be designed around complete functionalization of the alkynyl indole (including protecting group installation) prior to hydrostannylation/halogenation.

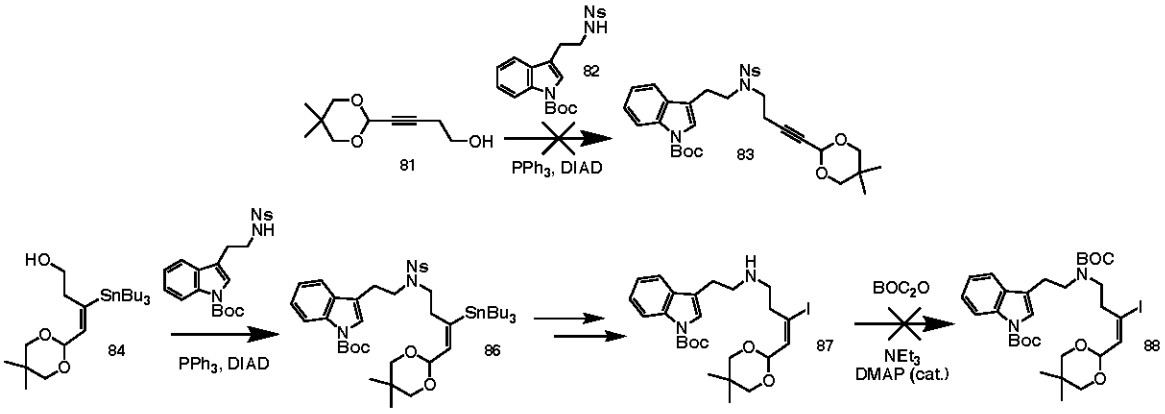

Fig. 9. Observed patterns of reactivity during screening for optimized Mitsunobu/BOC acylation conditions.

These collective observations led us to focus on conversion of the alknyl alcohol to an amine substrate (via an initial Mitsunobu reaction using a simple bis-protected secondary amine) to be condensed later with tryptophol in a second, more elaborate Mitsunobu process. As shown in Scheme 29, acetal-functionalized homopropargylic alcohol **90** was synthesized through a concise four-step sequence beginning with commercially available 3-butyn-1-ol (**89**). Conversion of the alcohol to sulfonamide **92** via Mitsunobu coupling was achieved in 87% yield, using secondary amine **91** protected by both Ns and 2-(trimethylsilyl)ethoxycarbonyl (TEOC) groups that had been generated in house (see SI for details). Deprotection of the TEOC group using TBAF (resulting in decarboxylation followed by irreversible evolution of ethylene gas as a byproduct) prepared the aminoalkyne for condensation with tryptophol through a second Mistunobu procedure, which ultimately afforded Ns-protected indolamine **93** in 73% yield over the two steps. Unlike other Mistunobu reactions attempted, this procedure required a unique dicarboxylate reagent, di-(4-chlorobenzyl)azodicarboxylate (DCAD), due to challenges with chromatographic separations when using the conventional DIAD reagent.[67]

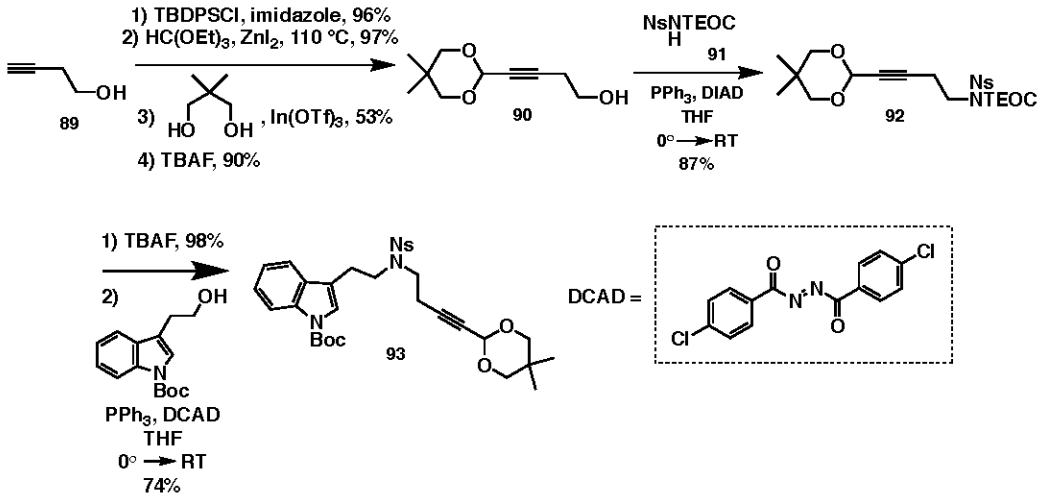

Scheme 29. Synthesis of sulfonamide-protected alkynyl indole via sequential Mistunobu reactions.

Having successfully designed the alkynyl indolamine necessary to proceed toward a Pictet-Spengler precursor complex, we focused our attention toward optimizing a sequence for swapping the sulfonamide protecting group with the BOC variant. Initial work with thioglycolic acid in tandem with weakly basic potassium carbonate failed to provide the desired amine in quantitative yields, likely due to unexpected reactive character from the acid fragment of the thiol reagent. To correct these issues, we replaced this system with one comprised of thiophenol (a more traditional thiol used for sulfonamide deprotection via nucleophilic aromatic substitution) and cesium carbonate as a weak base (Scheme 30).[68] This improved system afforded amine **94** in 71% yield, which was then successfully acylated to the corresponding bis-BOC protected tryptamine product **95**, again in 71% yield.

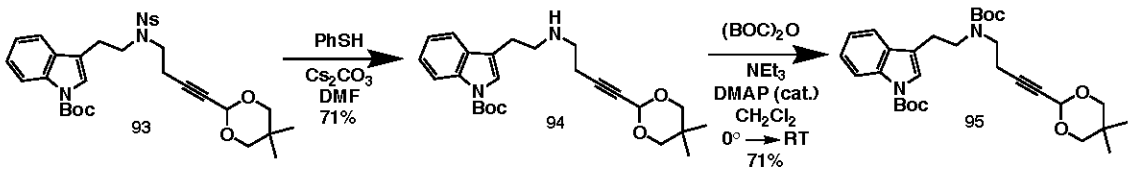

Scheme 30. Synthesis of BOC-protected alkynyl tryptamine.

With the appropriate BOC-protected alkynyl substrate **95** in hand, we turned toward the execution of the stannylcupration/iodination sequence that would deliver the vinyl iodide needed for diene-furnishing Stille cross-coupling (Scheme 31). Using an *in situ*-generated higher order cuprate, a species that generally perform insertions in a highly regioselective manner, no reactivity was seen. Typically, the nature of this reaction's regioselective nature stems from steric repulsion between the bulky stannane group and the larger alkynyl substituent.[69] In this particular case, we believe that steric hindrance between the cuprate and the architecturally complex alkynyl substrate (specifically the sizeable indole fragment) prevents the cuprate from accessing the site of reactivity.

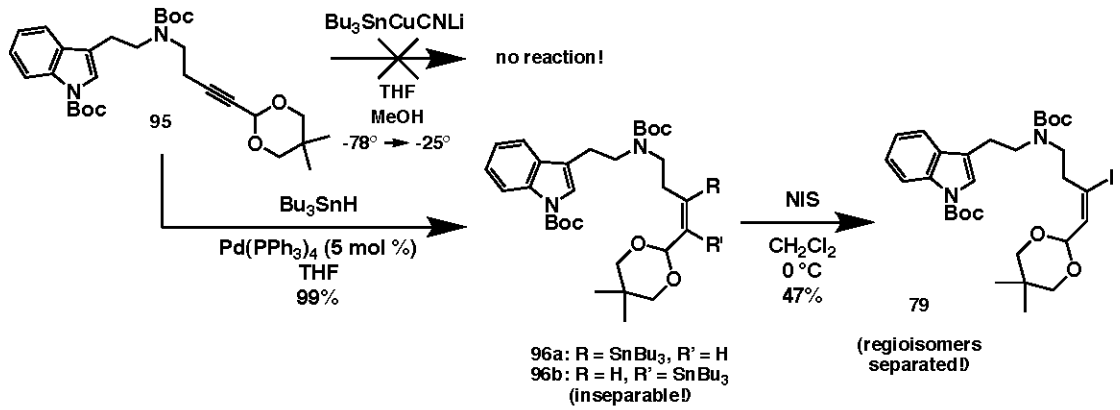

Scheme 31. Failed stannylcupration procedure, along with alternate hydrostannylation route, used for synthesis of vinyl iodide-functionalized aminoindole Stille partner.

Disappointed, we could not envision a sufficiently optimized path forward using this particular aminoindole substrate. However, in order to probe the viability of this general approach for the design of iron(0)-diene complexes, we proposed the use of an alternative procedure, a palladium-catalyzed hydrostannylation, as a non-specific method to access the necessary vinyl stannane analog. Surprisingly, this reaction was successful in generating the desired vinylic species, presumably due to a different Pd(0) catalytic mechanism that does not undergo the same steric hindrance as the analogous stannylcupration method. As expected, the *syn* addition performed was not regioselective, and, with no simple procedure available to interconvert the isomers **96a** and **96b**, we acknowledged the inability of this route to be optimized. However, to obtain proof-of-concept results for the Pictet-Spengler procedure, both regiomers were combined and subjected to halogenation using N-iodosuccinimide (NIS) (Scheme 31). During flash chromatography purification, the two now-halogenated regiomers became separable, delivering desired vinyl iodide **79** in 47% yield (relative to both regioisomeric starting materials).

With one Stille partner in hand, we attempted the cross-coupling using the (*S*)-isopropyl N-oxazolidinoyl vinyl stannane **80** as the other partner, due to high

diastereomeric ratios obtained during complexations mediated by this auxiliary (Scheme 32). Diene **97** was obtained in 92% yield (although the homocoupled byproduct, inseparable by chromatography, was found by H^1 NMR as a contaminant), and subsequent complexation using excess diiron nonacarbonyl furnished iron(0) tricarbonyl-diene complex **98** in 66% yield, with a major/minor diastereomeric ratio of 12.6:1. To prepare the substrate for the intramolecular cyclization reaction, the key aldehyde was revealed by acidic hydrolysis, furnishing the immediate Pictet-Spengler precursor **78** in 91% yield. This organometallic complex, a novel and essential precursor to a planar chiral-mediated asymmetric Pictet-Spengler cyclization, remains the most architecturally elaborate iron complex synthesized in the Paley lab to date.

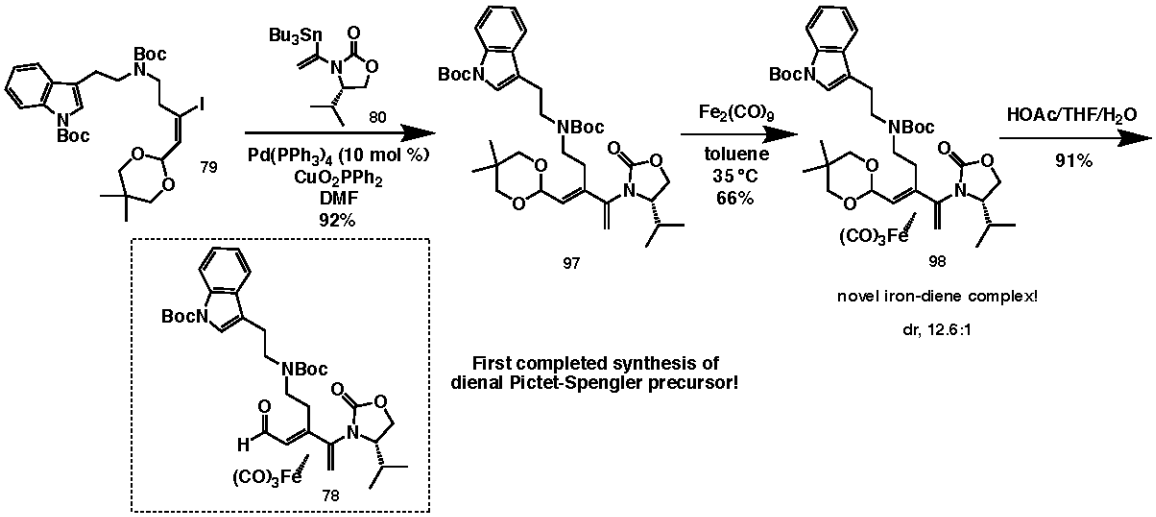

Scheme 32. Synthesis of novel iron(0) tricarbonyl-dienal complex 78 for use in the asymmetric Pictet-Spengler reaction.

At this point, we were prepared to attempt the lab's first Pictet-Spengler reaction, initiated by an excess of trifluoroacetic acid to both deprotect both BOC carbamates and to provide Lewis acid activation of the aldehyde involved in cyclization. After stirring at room temperature overnight, the reaction mixture contained a variety of distinguishable compounds as evidenced by TLC. NMR studies of each compound, isolated via flash

chromatography, failed to indicate the presence of any structure as architecturally complex as the desired polycyclic Pictet-Spengler product **77**; as such, it was concluded that the reaction did not proceed in any observable capacity (Figure 10). Based on the presence of both aromatic and aliphatic byproducts obtained from the reaction mixture, we hypothesize that exposure to excess acid caused fragmentation/decomposition of the Pictet-Spengler precursor, although a rationale for the alternate pathway observed (or what occurs during this pathway) has not been established. Retrospectively, the purity of the precursor substrate, as well as the ability to accurately execute the cyclization reaction on a small (< 20 mg) scale, have emerged as possible factors for the failure of the reaction, although these claims are unverified by the experimental results.

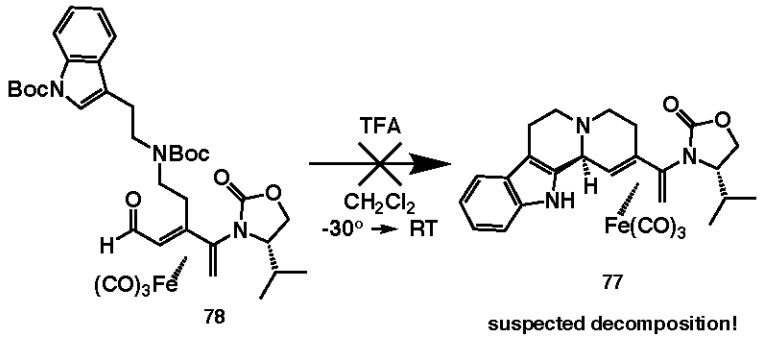

Figure 10. Anticipated but unobserved cyclization product from planar chiral-mediated asymmetric Pictet-Spengler reaction.

After failing to obtain new insight into the viability of a planar chirality-directed Pictet-Spengler reaction from our first attempt, we pursued the generation of the same precursor through an alternative sequence, one that provides greater optimization potential than the previous pathway that relies on the non-regioselective hydrostannylation to proceed. We envisioned the delivery of Stille partner **79** from the reductive amination of aldehyde **100** with BOC-protected amino vinyl iodide **99**, afforded under mild and typically robust conditions (Scheme 33).[70] Although this procedure was attempted several times with the indicated substrates, the desired adduct was not obtained

under any set of screened conditions. When performing the reaction as reported in literature using excess sodium triacetoxyborohydride as the reducing agent, the major product afforded was BOC-protected tryptophol, the reduction product of the aldehyde reagent. Upon rescaling to a stoichiometric amount of borohydride reagent, no reaction was observed to proceed, and quantitative amounts of each starting material were isolated.

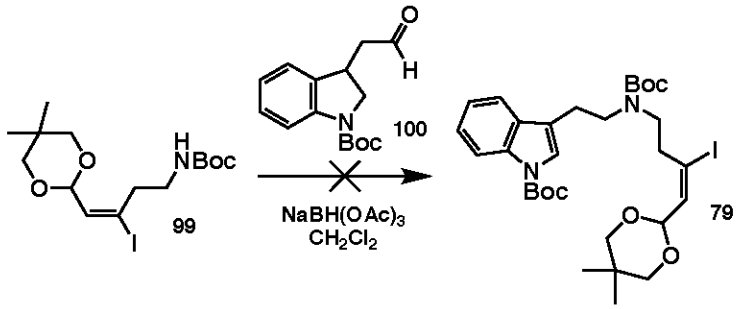

Scheme 33. Attempted synthesis of indole Stille partner via reductive amination.

No further work has been conducted for furnishing Pictet-Spengler prescursor complexes. Given the challenges seen in furnishing complex indolamines via reductive amination sequences, future work would include the identification of new procedures to afford secondary tryptophan derivatives compatible with a Pictet-Spengler pathway. One option may be the late-stage generation of the indole fragment via Fischer indole synthesis using phenylhydrazine and the appropriate alkynal; a classic transformation, the general mechanism is depicted below (Scheme 34, although transition metal-catalyzed variants have been proposed by Buchwald and coworkers):[71,72]

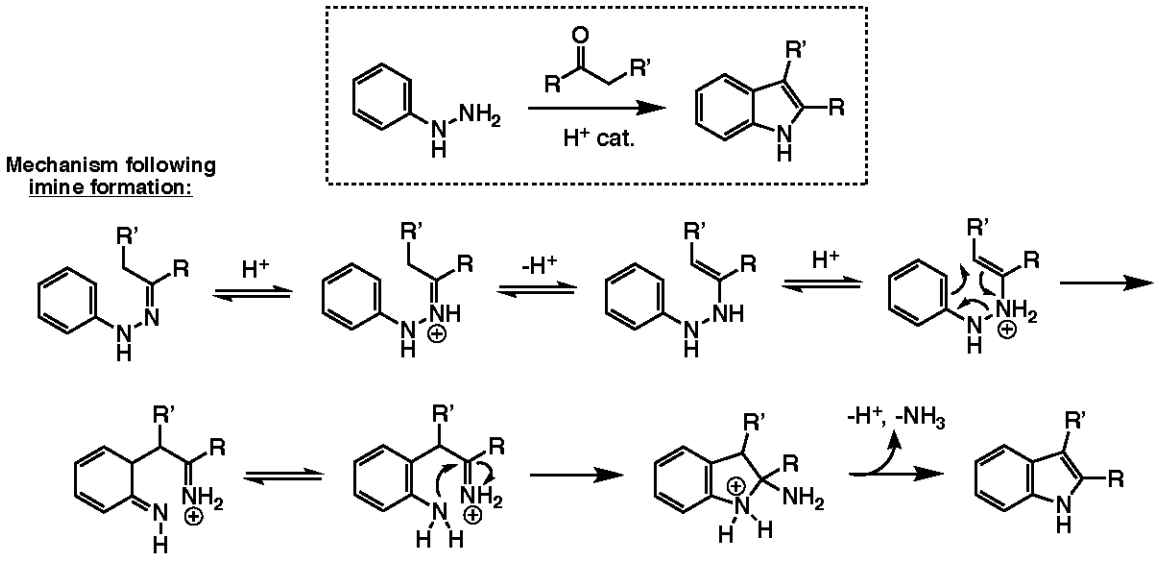

Scheme 34. General mechanism of the Fischer indole synthesis.

Additionally, the reductive amination procedure could be repeated by switching the reactive functional groups on each partner (incorporating indolamine and alkynal partners), although concerns exist about the stability of the hypothetical alkynal partner prior to amination – one-pot conditions may be necessary to execute such a protocol.

Closing Remarks

Although several obstacles have yet to be resolved regarding the use of new chiral auxiliaries to direct asymmetric iron-diene complexation reactions, as well as the execution of a planar chiral-directed Pictet-Spengler reaction, numerous contributions to the understanding of iron(0) tricarbonyl-diene synthesis and applications have still been accomplished. In particular, the validation of CD spectroscopy as an alternative to X-ray crystallography for the stereochemical characterization of dienal N-oxazolidinoyl complexes is a major breakthrough in establishing techniques for monitoring absolute planar chirality. Going forward, this approach should be sufficient for determining the absolute stereochemistry of a wide variety of iron-diene compounds, which will greatly

advance the potential of the iron(0) tricarbonyl moiety for effective mediation of asymmetric synthesis. Additionally, once a number of comparable chiral auxiliaries have had their dienal complex analogs characterized by CD spectroscopy, libraries can be quickly compiled to identify the most effective auxiliaries for obtaining highly enantioenriched iron-diene complexes. This advancement has the potential to make incorporation of iron-diene fragments into reaction pathways a relatively simple process, again paving the way for ubiquitous use of the iron unit as an effective synthetic tool.

Clearly, future work must focus on the discovery of new auxiliaries for directing complexation reactions and the broadening on known transformations tolerant to stereocontrol induced by coordinated iron fragments. Generation of the Pictet-Spengler precursor complex, the most structurally demanding iron-diene compound synthesized by the Paley group, inspires optimism that challenging synthetic targets can eventually be accessed through pathways involving iron-diene coordination. Undoubtedly, the breadth of this field will increase in the future as complexation reactions become more facially selective and as the number of reported reactions compatible with iron(0) tricarbonyl units rises. Hopefully, this burgeoning will lead to a widespread use of these functionalities for accessing key pharmacophores and natural products whose syntheses would be challenging without diene stabilization or planar chiral control, and will advance medicinal and pharmaceutical innovation as a result.

References

(1) Crabtree, R. H. Applications of Organometallic Chemistry. In *The Organometallic Chemistry of the Transition Metals*; Wiley-Blackwell, 2005; pp 343–377.

(2) Kealy, T. J.; Pauson, P. L. *Nature* **1951**, *168*, 1039–1040.

(3) Woodward, R. B.; Rosenblum, M.; Whiting, M. C. *J. Am. Chem. Soc.* **1952**, *74*, 2125–2126.

(4) Fischer, E. O.; Pfab, W. *Z Naturforsch B* **1952**, *7*, 377–379.

(5) Werner, H. *Angew. Chem. Int. Ed.* **2012**, *51*, 6052–6058.

(6) Reihlen, H.; Gruhl, A.; Hesslein, G. v.; Pfrengle, O. *Leibigs Ann Chem* **1930**, *482*, 161.

(7) Hallam, B. F.; Pauson, P. L. Jr9580000642.Pdf. *J Chem Soc* **1958**, *0*, 642–645.

(8) Mills, O. S.; Robinson, G. *Acta Crystallogr* **1963**, *16*, 758.

(9) Donaldson, W. A. Stoichiometric Applications of Acyclic π-Organoiron Complexes to Organic Synthesis. *Curr. Org. Chem.* **2000**, *4*, 837–868.

(10) Bauer Ingmar; Knölker Hans-Joachim. The Chemistry of Diene–Iron and Dienyl–Iron Complexes. *PATAIS Chem. Funct. Groups* **2009**.

(11) Carrupt, P.-A.; Berchier, F.; Vogel, P.; Pinkerton, A. A.; Schwarzenbach, D. Synthesis of Optically Pure Tricarbonyliron Complexes of 5,6-Dimethylidenebicyclo[2.2.2.]Oct-2-yl Derivatives. Crystal Structure and Absolute Configuration of (+)-tricarbonyl(1S,2S,4R,5R,6S)-C,5,6,C,-η-(5,6-dimethylidenebicyclo[2.2.2]Oct-2-yl P-bromobenzoate)Iron. *Helv. Chim. Acta* **1988**, *71* (5), 1349–1353.

(12) Donaldson, W. A.; Shang, L. 1-S2.0-0040403995022031-Main.Pdf. *Tetrahedron Lett.* **1996**, *37* (4), 423–424.

(13) Marchand, N. J.; Grée, D. M.; Martelli, J. T.; Grée, R. L.; Toupet, L. J. Synthesis and Reactivity of Cross-Conjugated Polyenones with a Planar Chirality. *J. Org. Chem.* **1996**, *61* (15), 5063–5072.

(14) Franck-Neumann, M.; Bissinger, P.; Geoffroy, P. One-Carbon Friedel-Crafts Functionalizations of Acyclic Diene Iron Tricarbonyl Complexes. *Tetrahedron Lett.* **1993**, *34* (29), 4643–4646.

(15) Paley, R. S.; Estroff, L. A.; McCulley, D. J.; Martínez-Cruz, L. A.; Jiménez Sánchez, A.; Cano, F. H. Diastereoselective Allylations of Enantiopure 3- and 4-Substituted η^4 -(1 *Z*)-(Sulfinyldienal)Iron(0) Tricarbonyl Complexes. *Organometallics* **1998**, *17* (9), 1841–1849.

(16) Franck-Neumann, M.; Colson, P.-J.; Geoffroy, P.; l'aba, K. M. The Aldol Condensation Reaction of Diene (Tricarbonyl) Iron Complexes. From Metal Coordinated Trimethylsilyl Enol Ethers to Polyols of Known Configuration. *Tetrahedron Lett.* **1992**, 33 (14), 1903-1906.

(17) Chang, S.; White, P. S.; Brookhart, M. Hydride Reduction of (Diene)Iron Tricarbonyl Complexes as a Route to Substituted (Allyl)Iron Tricarbonyl Anions. Detection of a Formyl Intermediate in the Hydride Reduction of (1,3-Butadiene)Iron Tricarbonyl by Et3BH-. *Organometallics* **1993**, *12* (9), 3636–3644.

(18) Thomas, S. E. Nucleophilic Addition to Iron Tricarbonyl Complexes of α,β-Unsaturated Ketones. *J. Chem. Soc., Chem. Commun.* **1987**, 1, 226-227.

(19) Paley, R. S.; Estroff, L. A.; Gauguet, J.-M.; Hunt, D. K.; Newlin, R. C. Enantiopure η^4 -(1-Sulfinyldiene)Iron(0) Tricarbonyl Complexes as Templates for Carbocycle Construction via Ring-Closing Metathesis. *Org. Lett.* **2000**, *2* (3), 365–368.

(20) Pettit, R.; Emerson, G.; Mahler, J. Chemistry of the Diene-Iron Tricarbonyl Complexes. *J. Chem. Educ.* **1963**, *40* (4), 175.

(21) Benvegnu, T.; Martelli, J.; Grée, R. Diels-Aler Reactions On Linear Polyenes, Selectively Protected As Their Tricarbonyl-Iron Complexes. *Tetrahedron Lett.* **1990**, 31 (22), 3145-3148.

(22) Donaldson, W. A.; Tao, C.; Bennett, D. W.; Grubisha, D. S. Model Studies toward the Synthesis of Leukotrienes: Hetero-Diels-Alder Reactivity of Tricarbonyl(Diene)Iron Complexes. *J. Org. Chem.* **1991**, *56* (14), 4563–4566.

(23) Roush, W. R. Diastereofacially Selective Enolate Claisen Rearrangements of [4-7-η^4-(1-Acyloxy-2,4,6-Octatrienyl)]Tricarbonyliron Complexes. *Tetrahedron Lett.* **1997**, 38 (3), 351-354.

(24) Pearson, A. J.; Zettler, M. W. Intramolecular Coupling between Tricarbonyl(Diene)Iron Complexes and Pendant Alkenes. *J. Am. Chem. Soc.* **1989**, *111* (11), 3908–3918.

(25) Pearson, A. J.; Wang, X.; Dorange, I. B. Intramolecular Iron-Mediated Diene/Olefin Cyclocoupling: Formation of Carbon Spirocycles. *Org. Lett.* **2004**, *6* (15), 2535–2538.

(26) Pearson, A. J.; Alimardanov, A.; Pinkerton, A. A.; Fouchard, D. M.; Kirschbaum, K. Stereocontrolled Cyclization of Unactivated Alkene onto Cationic Dienyl Iron Tricarbonyl Systems. *Tetrahedron Lett.* **1998**, *39* (33), 5919–5922.

(27) Donaldson, W. A.; Chaudhury, S. Recent Applications of Acyclic (Diene)Iron Complexes and (Dienyl)Iron Cations in Organic Synthesis. *Eur. J. Org. Chem.* **2009**, *2009* (23), 3831–3843.

(28) Dasgupta, B.; Donaldson, W. A. Chemoselective, Metal-Mediated Oxidation of (Dienol)Iron Complexes with N-Methylmorpholine N-Oxide. *Tetrahedron Lett.* **1998**, *39* (5), 343–346.

(29) Williams, I.; Reeves, K.; Kariuki, B. M.; Cox, L. R. Stereoselective Synthesis of 2-Dienyl-Substituted Piperidines Using an H4-Dienetricarbonyliron Complex as the Stereocontrolling Element in a Double Reductive Amination Cascade. *Org. Biomol. Chem.* **2007**, *5* (20), 3325.

(30) Christie, S. D. R.; Cummins, J.; Elsegood, M. R. J.; Dawson, G. *Synlett.* **2009**, *2*, 257–259.

(31) Wada, A.; Fujioka, N.; Tanaka, Y.; Ito, M. A Highly Stereoselective Synthesis of 11 *Z* -Retinal Using Tricarbonyliron Complex †. *J. Org. Chem.* **2000**, *65* (8), 2438–2443.

(32) Fukuda, A.; Kobayashi, Y.; Kimachi, T.; Takemoto, Y. Synthetic Studies on Macrolactin A by Using a (Diene)Fe(CO)3 Complex. *ChemInform* **2004**, *35* (11).

(33) Smith, A. B. Total Synthesis of (−)-Macrolactin A. *J. Am. Chem. Soc.* **1996**, 118, 13095-13096.

(34) Paley, R. S.; de Dios, A.; Estroff, L. A.; Lafontaine, J. A.; Montero, C.; McCulley, D. J.; Rubio, M. B.; Ventura, M. P.; Weers, H. L.; Fernández de la Pradilla, R.; et al. Synthesis and Diastereoselective Complexation of Enantiopure Sulfinyl Dienes:

The Preparation of Sulfinyl Iron(0) Dienes. *J. Org. Chem.* **1997**, *62* (18), 6326–6343.

(35) Paley, R. S.; Laupheimer, M. C.; Erskine, N. A. K.; Rablen, P. R.; Pike, R. D.; Jones, J. S. Diastereoselective Spiroketalization: Stereocontrol Using An Iron(0) Tricarbonyl Diene Complex. *Org. Lett.* **2011**, *13* (1), 58–61.

(36) *Asymmetric Synthesis: The Essentials*; Christmann, M., Bräse, S., Eds.; Wiley-VCH: Weinheim, 2007.

(37) Chang, S.; Halperin, S. D.; Moore, J.; Britton, R. Chiral Auxiliaries in Drug Synthesis. In *Stereoselective Synthesis of Drugs and Natural Products*; American Cancer Society, 2013; pp 1–24.

(38) Mauro, A. E.; Casagrande, O. L.; Nogueira, V. M.; Santos, R. H. A.; Gambardella, M. T. P.; Lechat, J. R.; Filho, M. F. J. Reaction of Pentacarbonyliron with a Nitrogen Heterocycle. X-Ray Crystal Structure of Bis[(Carbonyl)(Quinoline-2-Thiolate-N,S)]Iron(II). *Polyhedron* **1993**, *12* (3), 297–301.

(39) Lander, P. A.; Hegedus, L. S. Asymmetric Synthesis of Alpha.-Amino Acids by Copper-Catalyzed Conjugate Addition of Grignard Reagents to Optically Active Carbamatoacrylates. *J. Am. Chem. Soc.* **1994**, *116* (18), 8126–8132.

(40) Brice, J. L.; Meerdink, J. E.; Stahl, S. S. Formation of Enamides via Palladium(II)-Catalyzed Vinyl Transfer from Vinyl Ethers to Nitrogen Nucleophiles. *Org. Lett.* **2004**, *6* (11), 1845–1848.

(41) Fürstner, A.; Funel, J.-A.; Tremblay, M.; Bouchez, L. C.; Nevado, C.; Waser, M.; Ackerstaff, J.; Stimson, C. C. A Versatile Protocol for Stille–Migita Cross Coupling Reactions. *Chem. Commun.* **2008**, No. 25, 2873.

(42) Furukawa, D.; Matsumoto, A. Reaction Mechanism Based on X-Ray Crystal Structure Analysis during the Solid-State Polymerization of Muconic Esters. *Macromolecules* **2007**, *40* (17), 6048–6056.

(43) Hidaka, J.; Douglas, B. E. Circular Dichroism of Coordination Compounds. II. Some Metal Complexes of 2,2'-Dipyridyl and 1,10-Phenanthroline. *Inorg. Chem.* **1964**, *3* (8), 1180–1184.

(44) Urbach, A. R. Circular Dichroism Spectroscopy in the Undergraduate Curriculum. *J. Chem. Educ.* **2010**, *87* (9), 891–893.

(45) Falk, H.; Hofer, O. Stereochemistry of Metallocenes. XXVIII. Ferrocenes. 49. Optically Active [3] and [3][3]Ferrocenophanes. 2. Studies on the Optical Activity (Circular Dichroism) of the [3]Ferrocenophane System. *Monatsh Chem* **1969**, *100* (Copyright (C) 2018 American Chemical Society (ACS). All Rights Reserved.), 1540–1551.

(46) Gabioud, R.; Vogel, P.; Pinkerton, A. A.; Schwarzenbach, D. Circular Dichroism of Tricarbonyl(Diene)Iron Complexes. The Octant Rule Applied to Ketones Perturbed by Remote Fe(CO)3 Groups. Crystal Structure of (±)-Tricarbonyl[(1RS,4RS,5RS,6SR)-C5,6,C-η-(5,6,7,8-Tetramethylidene-2-Bicyclo[2.2.2]Octanone)]Iron. *Helv. Chim. Acta* **1986**, *69* (2), 271–282.

(47) Stephenson, G. R.; Howard, P. W.; Taylor, S. C. Assignment of Absolute Configurations from the Circular Dichroism Spectra of Cyclic H4-Diene Complexes of Fe(CO)3. *J. Chem. Soc. Chem. Commun.* **1991**, *0* (2), 127–129.

(48) Dhole, S. M.; Khedekar, P. B.; Amnerkar, N. D. Comparison of UV Spectrophotometry and High Performance Liquid Chromatography Methods for the Determination of Repaglinide in Tablets. *Pharm. Methods* **2012**, *3* (2), 68–72.

(49) Paley, R. S.; Rubio, M. B.; Ferna, R.; Hundal, G. Diastereoselective Formation of an [H4-(1Z)-Sulfinyl Diene]Iron(0) Tricarbonyl Complex. Diastereoselective Allylation of the Derived Iron Dienal. *Organometallics* **1996**, 15, 4672-4674.

(50) Heravi, M. M.; Zadsirjan, V.; Farajpour, B. Applications of Oxazolidinones as Chiral Auxiliaries in the Asymmetric Alkylation Reaction Applied to Total Synthesis. *RSC Adv.* **2016**, *6* (36), 30498–30551.

(51) Kim, T. H.; Lee, G.-J. Regiocontrolled Cyclization Reaction of *N* -(2-Hydroxyethyl)Ureas by Transfer of Activation: One-Pot Synthesis of 2-Imidazolidinones. *J. Org. Chem.* **1999**, *64* (8), 2941–2943.

(52) Fraser, R. R.; Mansour, T. S.; Savard, S. Acidity Measurements in THF. V. Heteroaromatic Compounds Containing 5-Membered Rings. *Can. J. Chem.* **1985**, *63* (12), 3505–3509.

(53) Dunetz, J. R.; Danheiser, R. L. Copper-Mediated N-Alkynylation of Carbamates, Ureas, and Sulfonamides. A General Method for the Synthesis of Ynamides. *Org. Lett.* **2003**, *5* (21), 4011–4014.

(54) Liao, G.; Yin, X.-S.; Chen, K.; Zhang, Q.; Zhang, S.-Q.; Shi, B.-F. Stereoselective Alkoxycarbonylation of Unactivated C(Sp^3)–H Bonds with Alkyl Chloroformates via Pd(II)/Pd(IV) Catalysis. *Nat. Commun.* **2016**, *7*, 12901.

(55) Wong, S. Palladium-Catalyzed Buchwald-Hartwig Amination and Suzuki-Miyaura Cross-Coupling Reaction of Aryl Mesylates. *Org. Synth.* **2015**, *92*, 195–212.

(56) Böhm, S.; Exner, O. Acidity of Hydroxamic Acids and Amides. *Org. Biomol. Chem.* **2003**, *1* (7), 1176–1180.

(57) Mansfield, S. J.; Campbell, C. D.; Jones, M. W.; Anderson, E. A. A Robust and Modular Synthesis of Ynamides. *Chem Commun* **2015**, *51* (16), 3316–3319.

(58) Okada, T.; Morimoto, T.; Achiwa, K. Asymmetric Hydrosilylation of Cyclopentadiene and Styrene with Chlorosilanes Catalyzed by Palladium Complexes of Chiral (β-N-Sulfonylaminoalkyl)Phosphines. *Chem. Lett.* **1990**, *19* (6), 999–1002.

(59) Corsello, M. A.; Kim, J.; Garg, N. K. Indole Diterpenoid Natural Products as the Inspiration for New Synthetic Methods and Strategies. *Chem. Sci.* **2017**, *8* (9), 5836–5844.

(60) Stempel, E.; Gaich, T. Cyclohepta[b]Indoles: A Privileged Structure Motif in Natural Products and Drug Design. *Acc. Chem. Res.* **2016**, *49* (11), 2390–2402.

(61) Pictet, A.; Spengler, T. Über Die Bildung von Isochinolin-derivaten Durch Einwirkung von Methylal Auf Phenyl-äthylamin, Phenyl-alanin Und Tyrosin. *Berichte Dtsch. Chem. Ges.* **1911**, *44* (3), 2030–2036.

(62) Larghi, E. L.; Amongero, M.; Bracca, A. B. J.; Kaufman, T. S. The Intermolecular Pictet-Spengler Condensation with Chiral Carbonyl Derivatives in the Stereoselective Syntheses of Optically-Active Isoquinoline and Indole Alkaloids. *Arkivoc* **2005**, *2005* (12), 98.

(63) Fletcher, S. The Mitsunobu Reaction in the 21 St Century. *Org. Chem. Front.* **2015**, *2* (6), 739–752.

(64) Camp, C.; von Itzstein, M.; Jenkins, I. D. The Mechanism of the First Step of the Mitsunobu Reaction. *Tetrahedron* **2015**, *71* (30), 4946–4948.

(65) Li, J. J. Fukuyama Amine Synthesis. In *Name Reactions*; Springer, Berlin, Heidelberg, 2003; pp 153–154.

(66) Huang, H.; Kang, J. Y. Mitsunobu Reaction Using Basic Amines as Pronucleophiles. *J. Org. Chem.* **2017**, 82 (13), 6604-6614.

(67) Lipshutz, B. H.; Chung, D. W.; Rich, B.; Corral, R. Simplification of the Mitsunobu Reaction. Di-p-Chlorobenzyl Azodicarboxylate: A New Azodicarboxylate. *Org. Lett.* **2006**, *8* (22), 5069–5072.

(68) Michaelidou, S. S.; Koutentis, P. A. Detosylation of 3-Amino-1-Tosylindole-2-Carbonitriles Using DBU and Thiophenol. *Tetrahedron* **2010**, *66* (16), 3016–3023.

(69) Barbero, A.; Pulido, F. J. Allylstannanes and Vinylstannanes from Stannylcupration of C–C Multiple Bonds. Recent Advances and Applications in Organic Synthesis. *Chem. Soc. Rev.* **2005**, *34* (11), 913.

(70) Abdel-Magid, A. F.; Maryanoff, C. A.; Carson, K. G. Reductive Amination of Aldehydes and Ketones by Using Sodium Triacetoxyborohydride. *Tetrahedron Lett.* **1990**, *31* (39), 5595–5598.

(71) Robinson, B. The Fischer Indole Synthesis. **1962**, 29, 374-398.

(72) Wagaw, S.; Yang, B. H.; Buchwald, S. L. A Palladium-Catalyzed Method for the Preparation of Indoles via the Fischer Indole Synthesis. *J. Am. Chem. Soc.* **1999**, *121* (44), 10251–10263.

Experimental Section

General Experimental Protocol

All reactions conducted using air- and moisture-sensitive reagents or solvents were performed in inert atmosphere conditions, in flame-dried Schlenk glassware, either on a Schlenk manifold (argon atmosphere) or in the glove box (nitrogen atmosphere). Anhydrous toluene, THF and CH_2Cl_2 solvents were purchased from J.T. Baker Inc. and dispensed from an Innovative Technology solvent still, subjected to drying via an alumina/copper(II) oxide column while dispensing under Ar flow. Anhydrous ether was purchased from Sigma-Aldrich and used as acquired. Select amine bases and solvents were distilled and stored under Ar in Schlenk tubes until further use. DMSO and DMF solvents, as well as all air- and moisture-sensitive reagents, were stored and handled exclusively in the glove box under a nitrogen atmosphere. All liquids and solutions were transferred using gas-tight syringes or via cannula.

Column chromatography was performed in glass columns using nitrogen-flushed silica gel from Acros Organics possessing a mean diameter of 60 Å. Eluents for chromatography were primarily mixtures of hexane and EtOAc, and in instances where crude samples were not soluble in these eluents, toluene or chloroform were used for column loading. TLC experiments for monitoring reaction or column progress were carried out on Analtech Uniplate™ pre-coated glass slides (250 μm) and visualized under UV light. In instances where compounds of interest were not UV-active, these TLC plates were visualized in vanillin or permanganate dips, in addition to iodine chambers.

All NMR spectra were collected on a Bruker Ascend 400 MHz spectrometer using samples prepared in anhydrous deuterated chloroform purchased from Sigma-

Aldrich (stored over 4 Å molecular sieves, containing 0.03% internal TMS reference). Fourier transform infrared (FT-IR) spectroscopy was conducted on a Thermo Fisher Nicolet iS5 spectrometer. Solid samples were analyzed neat using an iD5 ATR apparatus, while oil samples were prepared on salt plates (sodium chloride) and analyzed using an iD1 Transmission apparatus. Optical rotation analysis was performed on a JASCO P-2000 polarimeter using chloroform solutions of known concentration. Circular dichroism (CD) spectroscopy was performed on an Aviv Model 435 spectrometer using the following collection parameters: bandwidth = 2.00 nm, temperature = 25.00 °C, averaging time = 1.00 seconds, number of scans = 3 per sample. All samples for CD analysis were prepared in methanol in separate quartz cuvettes, and the resulting data for each sample is an average of the three scans corrected for an external methanol baseline obtained for each cuvette. X-ray crystallography data was collected and reported to us by our collaborators in the Pike group at the College of William and Mary, Williamsburg, VA.

Stannane 48a

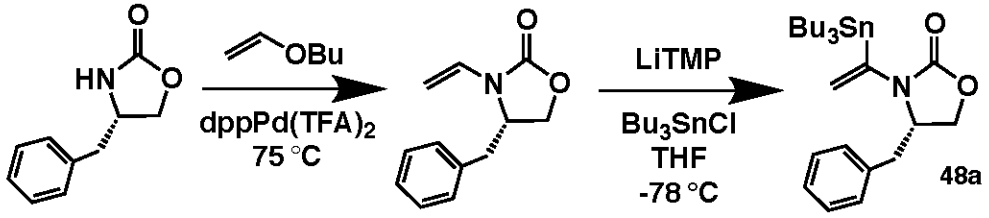

Vinylation catalyst **dppPd(TFA)$_2$** and the intermediate vinyl oxazolidinone were synthesized in 58% and 86% yield, respectively, according to procedures reported by Brice et al. (*Org. Lett.,* **2004**, 6, 1845-1848) using commercially-available (*S*)-4-benzyl-2-oxazolidinone. Stannane **48a** was subsequently synthesized in 82% yield according to procedures reported by Lander et al. (*JACS*, **1994**, 116, 8126-8132).

^{1}H NMR (400 MHz, Chloroform-*d*) δ 7.39 – 7.29 (m, 2H), 7.33 – 7.25 (m, 1H), 7.22 – 7.14 (m, 2H), 6.85 (dd, *J* = 16.0, 9.4 Hz, 1H), 4.62 – 4.53 (m, 2H), 4.35 – 4.23 (m, 2H), 4.27 (m, 1H), 3.26 (dd, *J* = 14.0, 3.0 Hz, 1H), 2.79 (dd, *J* = 13.9, 8.6 Hz, 1H), 2.05 (s, 1H).

Stannane 48b

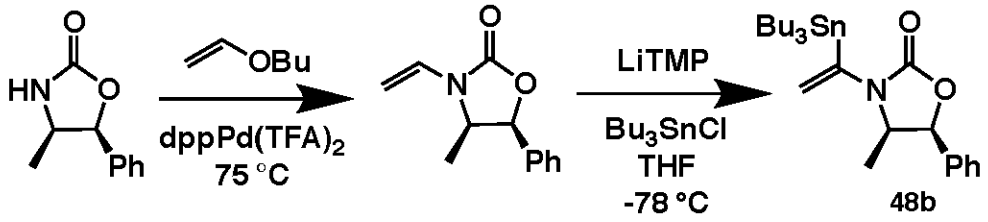

Vinylation catalyst **dppPd(TFA)$_2$** and the intermediate vinyl oxazolidinone were synthesized in 58% and 99% yield, respectively, according to procedures reported by Brice et al. (*Org. Lett.,* **2004**, 6, 1845-1848) using commercially-available (4*R*, 5*S*)-(+)-4-methyl-5-phenyl-2-oxazolidinone. Stannane **48a** was subsequently synthesized in 71% yield according to procedures reported by Lander et al. (*JACS*, **1994**, 116, 8126-8132).

^{1}H NMR (400 MHz, Chloroform-*d*) δ 7.46 – 7.33 (m, 3H), 7.37 – 7.26 (m, 2H), 6.83 (ddd, *J* = 16.2, 9.2, 0.5 Hz, 1H), 5.73 – 5.67 (m, 1H), 4.50 (dd, *J* = 9.3, 1.3 Hz, 1H), 4.46 – 4.32 (m, 1H), 0.86 (d, *J* = 6.6 Hz, 3H).

Acetal 50

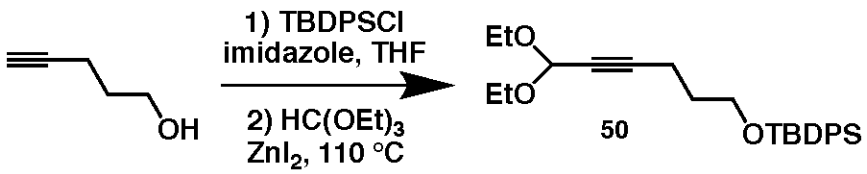

4-pentyn-1-ol (0.837 mL, 9.00 mmol) was dissolved in THF (30 mL) under Ar. Imidazole (1.53 g, 22.5 mmol, 2.5 eq) and *tert*-butyldiphenylsilyl chloride (2.76 mL, 10.8 mmol, 1.2 eq) were added in that order. The reaction was stirred overnight at room temperature. The reaction mixture was then dissolved in Et_2O, washed with NH_4Cl and brine, dried over $MgSO_4$, filtered and concentrated *in vacuo*. The resulting crude product was purified via flash chromatography (silica gel, 40:1 Hex/EtOAc) to afford the intermediate silyl ether as a clear oil in 77% yield. ^{1}H NMR (400 MHz, Chloroform-*d*) δ 7.71 – 7.63 (m, 4H), 7.47 – 7.38 (m, 2H), 7.42 – 7.33 (m, 4H), 3.74 (t, *J* = 6.0 Hz, 2H), 2.35 (td, *J* = 7.2, 2.7 Hz, 2H), 1.92 (t, *J* = 2.7 Hz, 1H), 1.77 (tt, *J* = 7.2, 5.9 Hz, 2H), 1.05 (s, 9H).

The intermediate silyl ether (2.23 g, 6.92 mmol) was dissolved in triethyl orthoformate (40 mL) under Ar. Zinc iodide (2.21 g, 6.92 mmol, 1 eq) was added all at once. The reaction flask was placed into an oil bath at 110 °C and stirred for 43 hours. The reaction mixture was then separated by distillation, and the resulting crude product was purified via flash chromatography (silica gel, 40:1 Hex/EtOAc) to afford **50** in 93% yield. ^{1}H NMR (400 MHz, Chloroform-*d*) δ 7.69 – 7.61 (m, 4H), 7.46 – 7.33 (m, 6H), 5.23 (t, *J* = 1.6 Hz, 1H), 3.77 – 3.70 (m, 2H), 3.74 – 3.65 (m, 2H), 3.55 (dq, *J* = 9.5, 7.1 Hz, 2H), 2.40 (td, *J* = 7.2, 1.7 Hz, 2H), 1.78 (tt, *J* = 7.3, 6.0 Hz, 2H), 1.21 (t, *J* = 7.1 Hz, 6H), 1.04 (s, 9H).

Acetal 51

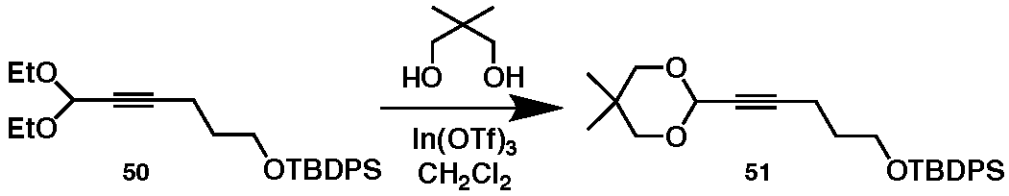

Acetal **50** (2.72 g, 6.40 mmol) was dissolved in CH_2Cl_2 (8 mL) under Ar. 2,2-dimethyl-1,3-propanediol (3.33 g, 32.01 mmol, 5 eq) and indium(III) triflate (144 mg 0.256 mmol, 4 mol %) were added in that order. The reaction was stirred overnight at room temperature. The crude mixture was then purified via flash chromatography (basic aluminum oxide, 19:1 Hex/EtOAc, loaded neatly) to afford acetal **51** in 53% yield.

^{1}H NMR (400 MHz, Chloroform-*d*) δ 7.69 – 7.61 (m, 4H), 7.46 – 7.37 (m, 2H), 7.41 – 7.32 (m, 4H), 5.24 (t, *J* = 1.7 Hz, 1H), 3.76 – 3.69 (m, 4H), 3.47 – 3.39 (m, 2H), 2.41 (td, *J* = 7.3, 1.6 Hz, 2H), 1.79 (tt, *J* = 7.3, 5.9 Hz, 2H), 1.08 (s, 3H), 1.04 (s, 9H), 0.86 (s, 3H).

Iodide 52

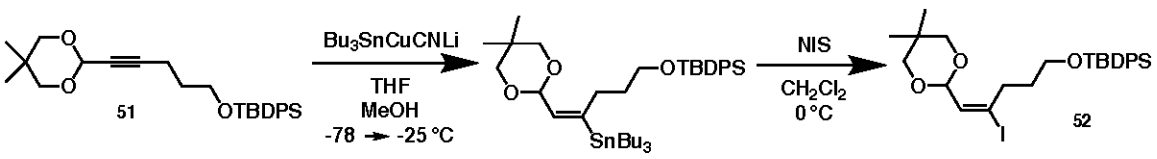

Bis(tributyltin) (3.32 mL, 7.50 mmol, 2.2 eq) was dissolved in THF (30 mL) under Ar and cooled to -78 °C. A 1.6 M solution of n-BuLi (4.48 mL, 7.16 mmol, 2.1 eq) was added dropwise, and the reaction was warmed to -40 °C and stirred for 30 minutes before being recooled to -78 °C. Copper(I) cyanide (611 mg, 6.82 mmol, 2.0 eq) was added, the temperature was raised back to -40 °C and the reaction was stirred for 45 minutes. After 45 minutes, the flask was recooled to -78 °C. Anhydrous methanol (207 μL, 5.11 mmol, 1.5 eq) was added, followed by a solution of alkyne **51** (1.49 g, 3.41 mmol, 1 eq.) in THF (10 mL) under Ar. The reaction was stirred and allowed to warm to -25 °C over 2.5 hours. The reaction was then quenched with a 9:1 solution of saturated NH_4Cl and NaOH. The resulting mixture was then diluted and back extracted with EtOAc, and this organic layer was subsequently washed with brine, dried over $MgSO_4$, filtered and concentrated *in vacuo*. The resulting crude product was purified via flash chromatography (silica gel, hexanes with 3% NEt_3) to afford the intermediate vinyl stannane in 90% yield. ^{1}H NMR (400 MHz, Chloroform-*d*) δ 7.72 – 7.62 (m, 4H), 7.47 – 7.33 (m, 6H), 5.64 (dd, *J* = 6.0, 1.3 Hz, 1H), 5.18 (d, *J* = 6.0 Hz, 1H), 3.77 – 3.64 (m, 2H), 3.60 (dt, *J* = 11.2, 1.3 Hz, 2H), 3.49 – 3.38 (m, 2H), 2.58 – 2.36 (m, 2H), 1.66 – 1.46 (m, 2H), 1.49 – 1.42 (m, 2H), 1.46 – 1.28 (m, 3H), 1.32 – 1.23 (m, 6H), 1.21 (d, *J* = 0.9 Hz, 2H), 1.07 (s, 6H), 1.12 – 1.02 (m, 3H), 1.05 – 0.79 (m, 13H), 0.68 (s, 3H).

The intermediate vinyl stannane (2.24 g, 3.07 mmol) was dissolved in CH_2Cl_2 (30 mL) under Ar and the flask was cooled in an ice bath to 0 °C. N-iodo succinimide (830 mg, 3.69 mmol, 1.2 eq) was added all at once, and the reaction was stirred for 2 hours. The reaction was then quenched with a mixture of saturated $NaHCO_3$ and saturated $Na_2S_2O_3$. The reaction mixture was diluted with EtOAc and transferred to a separatory funnel; after separation, the organic layer was washed with brine, dried over $MgSO_4$, filtered and concentrated *in vacuo*. The crude product was subsequently purified via flash chromatography (silica gel, 40:1 Hex/EtOAc with 1% NEt_3) to afford vinyl iodide **52** in 86% yield. ^{1}H NMR (400 MHz, Chloroform-*d*) δ 7.70 – 7.61 (m, 4H), 7.47 – 7.34 (m, 6H), 6.31 (dt, *J* = 6.1, 0.8 Hz, 1H), 5.09 (d, *J* = 6.1 Hz, 1H), 3.70 (t, *J* = 5.8 Hz, 2H), 3.56 (dt, *J* = 11.1, 1.3 Hz, 2H), 3.40 – 3.32 (m, 2H), 2.69 – 2.60 (m, 2H), 1.82 – 1.71 (m, 2H), 1.27 (s, 1H), 1.17 (d, *J* = 0.9 Hz, 3H), 1.07 (s, 8H), 1.10 – 1.03 (m, 1H), 0.94 – 0.84 (m, 1H), 0.66 (s, 3H).

Diene 53 and Iron-Diene Complex 54

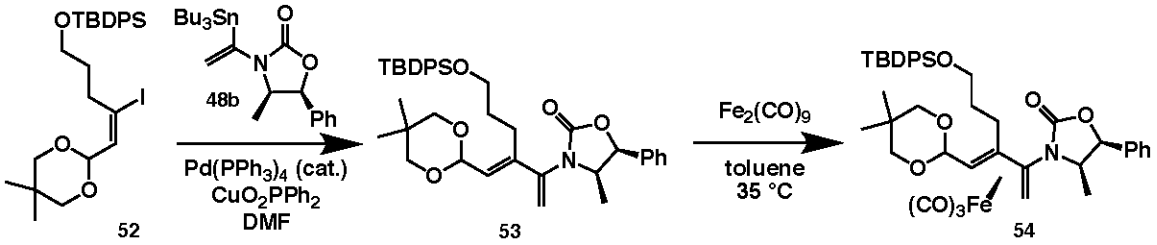

Vinyl iodide **52** (296 mg, 0.523 mmol, 0.97 eq) was dissolved in DMF (3 mL) in the glove box and transferred via pipette to a flask containing vinyl stannane **48b** (267 mg, 0.541 mmol, 1 eq). Tetrakis(triphenylphosphine)palladium(0) (62.4 mg, 54.0 μmol, 10 mol %) and copper(I) diphenylphosphinate (175 mg, 0.622 mmol, 1.15 eq) were added together, and the reaction was stirred in the glove box overnight. The reaction flask was removed from the glove box and the reaction mixture was filtered through a pad of silica on a glass-frit filter using EtOAc as an eluent. After concentration, the remaining residue was dissolved in Et_2O and the organic layer was washed with water and brine, dried over $MgSO_4$, filtered and concentrated *in vacuo*. The crude product was subsequently purified via flash chromatography (silica gel, 4:1 Hex/EtOAc) to afford diene **53** in 90% yield. ^{1}H NMR (400 MHz, Chloroform-*d*) δ 7.67 (dt, *J* = 8.0, 1.8 Hz, 4H), 7.47 – 7.36 (m, 6H), 7.40 – 7.33 (m, 3H), 7.36 – 7.27 (m, 2H), 3.69 (t, *J* = 5.8 Hz, 2H), 3.60 (ddd, *J* = 11.0, 8.2, 2.6 Hz, 2H), 3.44 (t, *J* = 12.1 Hz, 2H), 1.08 (s, 9H), 0.71 – 0.65 (m, 6H); ^{13}C NMR (101 MHz, $CDCl_3$) δ 155.68, 140.85, 140.80, 135.55, 135.53, 134.77, 133.85, 133.74, 129.67, 129.64, 128.53, 128.44, 127.68, 126.91, 125.91, 113.90, 98.37, 78.17, 63.25, 56.45, 31.81, 30.00, 26.96, 25.38, 23.02, 21.92, 19.30, 14.86.

Diiron(0) nonacarbonyl (602.1 mg, 1.66 mmol, 3.5 eq) was placed into a Schlenk flask in the glove box, after which the flask was removed from the glove box and placed under Ar on a Schlenk line. A solution of diene **53** (302.6 mg, 0.473 mmol, 1 eq) in

toluene (5 mL) was added to the flask via cannula transfer. The flask was placed in a 35 °C oil bath and the reaction was left to stir for 22 hours. The reaction flask was then removed from the oil bath and the reaction mixture was filtered through a pad of silica on a glass-frit filter using EtOAc with 2% NEt_3 as an eluent. After concentration *in vacuo*, the crude product was purified via flash chromatography (silica gel, 1:1 Hex/CH_2Cl_2 with 1% NEt_3, followed by a second column of silica gel, 6:1 Hex/EtOAc) to afford complex **54** in 26% yield. ^{1}H NMR (400 MHz, Chloroform-*d*) δ 7.73 – 7.65 (m, 4H), 7.47 – 7.29 (m, 8H), 7.22 – 7.14 (m, 2H), 5.46 (d, *J* = 7.8 Hz, 1H), 4.41 (d, *J* = 6.2 Hz, 1H), 4.33 – 4.21 (m, 1H), 3.77 (t, *J* = 6.2 Hz, 2H), 3.60 (dd, *J* = 11.1, 2.7 Hz, 1H), 3.49 (dd, *J* = 11.0, 2.8 Hz, 1H), 3.39 – 3.29 (m, 2H), 2.74 (ddd, *J* = 13.6, 11.6, 5.1 Hz, 1H), 2.34 (td, *J* = 13.5, 12.7, 4.7 Hz, 1H), 2.15 (tt, *J* = 11.9, 5.7 Hz, 1H), 1.84 (td, *J* = 12.1, 5.9 Hz, 1H), 1.60 (d, *J* = 3.5 Hz, 1H), 1.17 (s, 3H), 1.08 (s, 9H), 0.88 (d, *J* = 6.6 Hz, 3H), 0.65 (s, 3H), 0.51 (d, *J* = 6.3 Hz, 1H), 0.31 (d, *J* = 3.6 Hz, 1H); ^{13}C NMR (101 MHz, $CDCl_3$) δ 135.60, 135.55, 134.72, 133.85, 133.72, 129.72, 129.68, 128.70, 128.58, 127.75, 127.71, 126.21, 101.56, 100.69, 77.97, 64.06, 59.91, 56.76, 37.59, 33.99, 29.73, 26.94, 25.65, 23.06, 21.74, 19.27, 16.56.

Diene 55 and Iron-Diene Complex 56

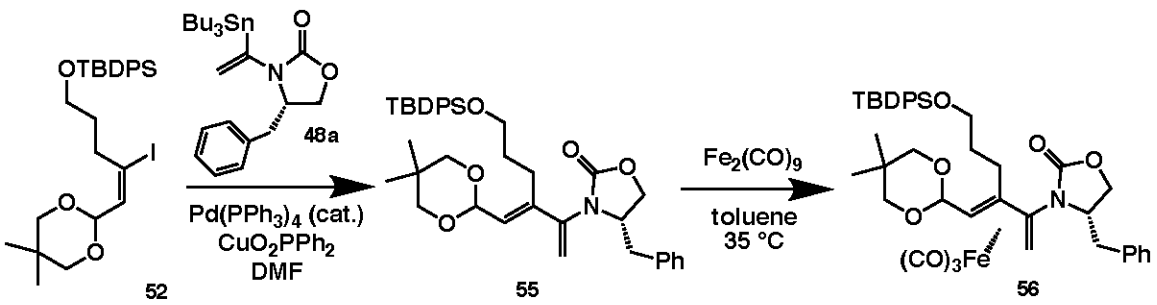

Vinyl iodide **52** (527 mg, 0.934 mmol, 1 eq) was dissolved in DMF (3 mL) in the glove box and transferred via pipette to a flask containing vinyl stannane **48a** (462 mg, 0.938 mmol, 1 eq). Tetrakis(triphenylphosphine)palladium(0) (109 mg, 93.4 μmol, 10 mol %) and copper(I) diphenylphosphinate (302 mg, 1.07 mmol, 1.15 eq) were added together, and the reaction was stirred in the glove box overnight. The reaction flask was removed from the glove box and the reaction mixture was filtered through a pad of silica on a glass-frit filter using EtOAc as an eluent. After concentration, the remaining residue was dissolved in Et_2O and the organic layer was washed with water and brine, dried over $MgSO_4$, filtered and concentrated *in vacuo*. The crude product was subsequently purified via flash chromatography (silica gel, 3:1 Hex/EtOAc) to afford diene **55** in 89% yield. ^1H NMR (400 MHz, Chloroform-*d*) δ 7.71 – 7.63 (m, 4H), 7.40 (dddd, *J* = 9.4, 8.0, 6.8, 3.8 Hz, 6H), 7.38 – 7.20 (m, 3H), 7.16 – 7.09 (m, 2H), 5.76 (d, *J* = 6.2 Hz, 1H), 5.45 (s, 1H), 5.33 (s, 1H), 5.21 (d, *J* = 6.2 Hz, 1H), 4.24 – 4.15 (m, 1H), 4.18 – 4.04 (m, 2H), 3.77 – 3.65 (m, 2H), 3.68 – 3.56 (m, 2H), 3.45 (dd, *J* = 17.4, 11.1 Hz, 2H), 3.07 (dd, *J* = 13.5, 3.2 Hz, 1H), 2.68 – 2.54 (m, 2H), 2.33 – 2.21 (m, 1H), 1.79 – 1.65 (m, 1H), 1.22 (s, 3H), 1.08 (s, 9H), 1.08 (d, *J* = 6.0 Hz, 1H), 0.69 (s, 3H); ^{13}C NMR (101 MHz, $CDCl_3$) δ 155.82, 141.20, 140.78, 135.55, 135.52, 135.49, 133.86, 133.75, 129.65, 129.62, 129.20,

128.84, 127.67, 127.09, 112.56, 98.27, 76.69, 66.35, 63.19, 57.53, 38.64, 31.73, 29.98, 26.96, 25.48, 22.99, 21.92, 19.29, 14.19.

Diiron(0) nonacarbonyl (1.06 mg, 2.92 mmol, 3.5 eq) was placed into a Schlenk flask in the glove box, after which the flask was removed from the glove box and placed under Ar on a Schlenk line. A solution of diene **55** (581 mg, 0.835 mmol, 1 eq) in toluene (10 mL) was added to the flask via cannula transfer. The flask was placed in a 35 °C oil bath and the reaction was left to stir for 21 hours. The reaction flask was then removed from the oil bath and the reaction mixture was filtered through a pad of silica on a glass-frit filter using EtOAc with 2% NEt_3 as an eluent. After concentration *in vacuo* (note: caution should be exhibited with the iron pentacarbonyl solution likely present in the collection reservoir of the rotary evaporator), the crude product was purified via flash chromatography (silica gel, 7:1 Hex/CH_2Cl_2 with 1% NEt_3, followed by a second column of silica gel, 6:1 Hex/EtOAc) to afford complex **56** in 80% yield. ^{1}H NMR (400 MHz, Chloroform-*d*) δ 7.73 – 7.62 (m, 4H), 7.47 – 7.22 (m, 7H), 7.15 – 7.04 (m, 2H), 4.42 (t, *J* = 6.3 Hz, 1H), 4.23 – 4.07 (m, 1H), 4.05 – 3.92 (m, 2H), 3.74 (dtd, *J* = 16.2, 10.1, 6.0 Hz, 2H), 3.61 (dd, *J* = 11.1, 2.8 Hz, 1H), 3.49 (ddd, *J* = 14.3, 12.0, 3.4 Hz, 2H), 3.43 – 3.28 (m, 2H), 2.76 – 2.62 (m, 2H), 2.32 (td, *J* = 12.9, 4.4 Hz, 1H), 2.15 (dt, *J* = 13.9, 7.2 Hz, 1H), 1.74 (d, *J* = 3.6 Hz, 1H), 1.58 (s, 1H), 1.18 (d, *J* = 3.3 Hz, 3H), 1.07 (d, *J* = 16.2 Hz, 2H), 1.06 (s, 6H), 0.65 (d, *J* = 6.3 Hz, 3H), 0.59 (t, *J* = 6.9 Hz, 1H), 0.45 (d, *J* = 3.6 Hz, 1H); ^{13}C NMR (101 MHz, $CDCl_3$) δ 154.79, 135.59, 135.55, 135.53, 135.15, 135.05, 133.85, 133.82, 133.60, 129.70, 129.65, 129.06, 129.03, 129.01, 128.80, 127.72, 127.69, 127.68, 127.37, 102.20, 101.72, 101.49, 101.34, 66.83, 65.98, 64.05, 61.73, 61.10, 60.41,

56.23, 40.18, 39.79, 36.64, 33.90, 33.47, 29.75, 29.71, 26.96, 26.92, 25.78, 25.44, 23.09, 23.05, 21.73, 21.07, 19.29, 19.25, 14.20.

Alcohol 57

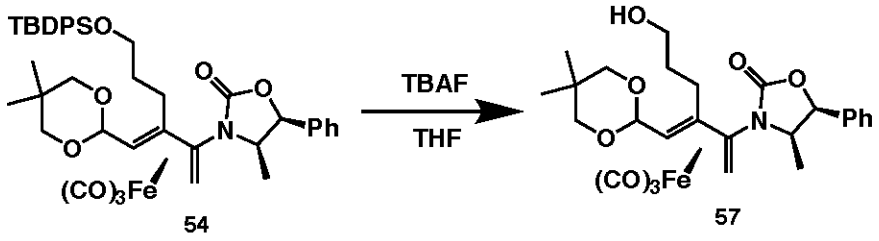

Silyl ether **54** (89.5 mg, 0.122 mmol) was dissolved in THF (1 mL) in a round bottom flask. A 1M solution of TBAF (150 μL, 0.147 mmol, 1.2 eq) was added via syringe to the flask. The flask was capped and the reaction was allowed to stir at room temperature for 49 hours. The reaction mixture was then diluted in EtOAc, washed with saturated $NaHCO_3$ and brine, dried over $MgSO_4$, filtered and concentrated *in vacuo*. The crude product was subsequently purified via flash chromatography (silica gel, 1.5:1 Hex/EtOAc) to afford alcohol **57** in 82% yield.

^{1}H NMR (400 MHz, Chloroform-*d*) δ 7.44 – 7.32 (m, 3H), 7.30 – 7.24 (m, 2H), 5.67 (d, J = 7.9 Hz, 1H), 4.48 – 4.36 (m, 2H), 3.75 (t, J = 5.8 Hz, 2H), 3.71 – 3.60 (m, 2H), 3.51 (d, J = 10.8 Hz, 1H), 3.45 (d, J = 11.0 Hz, 1H), 2.94 (ddd, J = 13.9, 8.5, 5.4 Hz, 1H), 2.33 (dt, J = 14.5, 8.0 Hz, 1H), 2.07 – 1.86 (m, 1H), 1.69 (d, J = 3.6 Hz, 1H), 1.59 (s, 1H), 1.26 (d, J = 1.9 Hz, 2H), 1.22 (s, 1H), 1.20 (s, 3H), 0.96 (d, J = 6.6 Hz, 3H), 0.73 (s, 3H), 0.52 (d, J = 6.7 Hz, 1H), 0.37 (d, J = 3.6 Hz, 1H); ^{13}C NMR (101 MHz, $CDCl_3$) δ 155.61, 134.72, 128.76, 128.64, 126.25, 104.00, 102.14, 100.98, 78.26, 77.61, 61.94, 60.04, 56.30, 38.00, 33.39, 29.85, 29.71, 24.98, 23.07, 21.78, 16.89; IR: ν_{max} 3485.6, 2925.7, 2872.1, 2051.4, 1990.7, 1971.7, 1737.1, 1498.9, 1456.1, 1421.8, 1394.1, 1386.8, 1379.4, 1373.1, 1312.9, 1294.0, 1220.2; $[\alpha]^{23}$ = -54.3 (c = 0.505 g/mL).

Alcohol 58

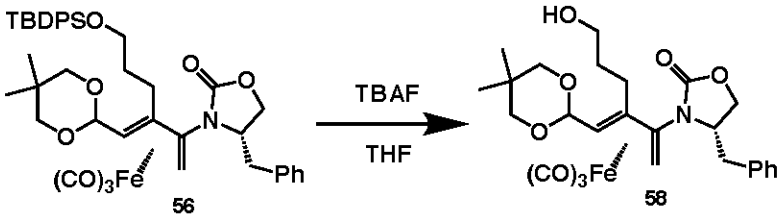

Silyl ether **56** (522 mg, 0.670 mmol) was dissolved in THF (7 mL) in a round bottom flask. A 1M solution of TBAF (820 μL, 0.804 mmol, 1.2 eq) was added via syringe to the flask. The flask was capped and the reaction was allowed to stir at room temperature for 26 hours. The reaction mixture was then diluted in EtOAc, washed with saturated $NaHCO_3$ and brine, dried over $MgSO_4$, filtered and concentrated *in vacuo*. The crude product was subsequently purified via flash chromatography (silica gel, 1:1 Hex/EtOAc) to afford alcohol **58** as a mixture of planar diastereomers in 41% yield.

^{1}H NMR (400 MHz, Chloroform-*d*) δ 7.38 – 7.28 (m, 2H), 7.32 – 7.24 (m, 1H), 7.20 – 7.12 (m, 2H), 4.46 (dd, *J* = 8.2, 6.7 Hz, 1H), 4.28 – 4.15 (m, 1H), 4.15 – 4.00 (m, 1H), 3.79 – 3.72 (m, 1H), 3.72 (s, 2H), 3.72 – 3.61 (m, 2H), 3.57 – 3.50 (m, 1H), 3.54 – 3.42 (m, 2H), 2.86 (ddd, *J* = 14.1, 8.8, 5.5 Hz, 1H), 2.74 (dd, *J* = 13.2, 10.6 Hz, 1H), 2.40 – 2.25 (m, 1H), 1.91 – 1.78 (m, 2H), 1.26 (s, 1H), 1.21 (s, 3H), 0.92 – 0.81 (m, 1H), 0.74 (s, 3H), 0.59 (d, *J* = 6.5 Hz, 1H), 0.48 (dd, *J* = 8.0, 3.7 Hz, 1H).

General procedure for acetal hydrolysis of complexes 54, 56 and 59

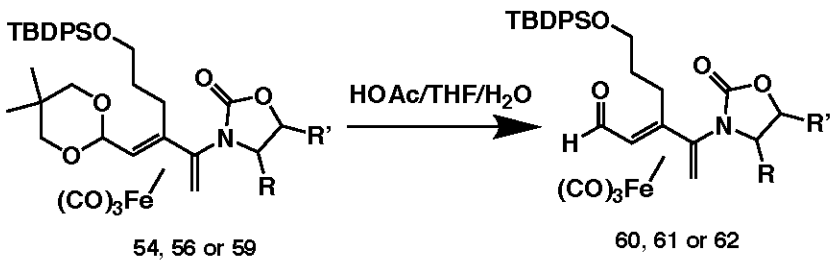

The acetal substrate (1 eq) was dissolved in THF (0.1 M relative to the acetal). Water and acetic acid were added in that order to the flask to produce an 8:5:2 mixture of acetic acid/THF/water by volume, and the reaction was stirred overnight. The reaction mixture was then diluted in EtOAc, washed with 1 M NaOH, water and brine, dried over $MgSO_4$, filtered and concentrated *in vacuo*. The crude product was subsequently purified via flash chromatography (silica gel) to afford the corresponding aldehyde product.

60: Aldehyde **60** (R = (*S*)-isopropyl, R' = H) was synthesized according to the general procedure using acetal **59** (65.3 mg, 89.3 μmol) and a mixture of acetic acid (1.6 mL), THF (1 ml) and water (0.4 mL). Following column chromatography (5:1 Hex/EtOAc as eluent), **60** was isolated in 68% yield and characterized by NMR and CD spectroscopy. ^{1}H NMR (400 MHz, Chloroform-*d*) δ 9.35 (d, *J* = 6.7 Hz, 1H), 7.64 (ddd, *J* = 8.0, 4.8, 1.6 Hz, 4H), 7.49 – 7.34 (m, 6H), 4.12 – 4.01 (m, 2H), 3.90 (ddd, *J* = 7.4, 5.6, 3.3 Hz, 1H), 3.73 (qt, *J* = 10.3, 6.0 Hz, 2H), 2.74 (tdd, *J* = 14.9, 11.7, 7.6 Hz, 2H), 2.33 (pd, *J* = 6.8, 3.2 Hz, 1H), 2.15 (d, *J* = 3.8 Hz, 1H), 2.05 (s, 0H), 1.86 – 1.74 (m, 1H), 1.57 (s, 2H), 1.34 – 1.22 (m, 7H), 1.06 (s, 8H), 1.06 (d, *J* = 5.9 Hz, 1H), 0.93 – 0.84 (m, 10H), 0.77 (d, *J* = 3.7 Hz, 1H), 0.70 (d, *J* = 6.7 Hz, 1H); ^{13}C NMR (101 MHz, $CDCl_3$) δ 195.22, 156.05, 135.52, 135.48, 133.44, 129.83, 127.81, 127.79, 105.31, 103.90, 64.09, 63.20, 61.50, 53.63, 38.21, 35.04, 31.60, 29.01, 26.88, 25.31, 22.66, 19.20, 17.97, 14.14, 13.67.

61: Aldehyde **61** (R = (*R*)-methyl, R' = (*S*)-phenyl) was synthesized according to the general procedure using acetal **54** (13.5 mg, 17.3 μmol) and a mixture of acetic acid (533 μL), THF (333 μl) and water (133 μL). Following column chromatography (5:1 Hex/EtOAc with 0.5% NEt_3 as eluent), **61** was isolated in 66% yield and characterized by NMR and CD spectroscopy. ^{1}H NMR (400 MHz, Chloroform-*d*) δ 9.37 (d, *J* = 6.6 Hz, 1H), 7.67 (ddt, *J* = 8.4, 6.4, 1.7 Hz, 4H), 7.48 – 7.32 (m, 9H), 7.12 (dd, *J* = 6.8, 2.9 Hz, 2H), 5.40 (d, *J* = 7.8 Hz, 1H), 4.32 (p, *J* = 6.7 Hz, 1H), 3.77 (td, *J* = 5.9, 3.1 Hz, 2H), 2.84 (t, *J* = 7.9 Hz, 2H), 2.03 (d, *J* = 3.7 Hz, 1H), 1.85 (ddt, *J* = 19.6, 14.0, 7.0 Hz, 1H), 1.25 (s, 2H), 1.08 (s, 9H), 0.90 (d, *J* = 6.6 Hz, 3H), 0.80 (d, *J* = 3.7 Hz, 1H), 0.72 (d, *J* = 6.6 Hz, 1H), 0.07 (s, 1H); ^{13}C NMR (101 MHz, $CDCl_3$) δ 195.18, 155.55, 135.55, 135.49, 134.26, 133.59, 133.48, 129.84, 128.91, 128.68, 127.85, 127.82, 126.15, 106.24, 103.05, 78.11, 63.08, 59.70, 53.62, 39.58, 35.40, 29.71, 26.92, 25.23, 19.24, 16.54, 1.02.

62: Aldehyde **62** (R = (*S*)-benzyl, R' = H) was synthesized according to the general procedure using acetal **56** (46.2 mg, 59.3 μmol) and a mixture of acetic acid (1.6 mL), THF (1 ml) and water (0.4 mL). Following column chromatography (6:1 Hex/EtOAc with 0.5% NEt_3 as eluent), **62** was obtained as a likely mixture of diastereomers in 53% yield and subsequently characterized by NMR and CD spectroscopy. ^{1}H NMR (400 MHz, Chloroform-*d*) δ 9.38 (d, *J* = 6.5 Hz, 1H), 7.62 (ddd, *J* = 8.0, 4.4, 1.6 Hz, 4H), 7.40 (dd, *J* = 5.6, 3.0 Hz, 1H), 7.41 – 7.31 (m, 4H), 7.35 – 7.27 (m, 3H), 7.15 – 7.08 (m, 2H), 4.22 (ddt, *J* = 11.3, 7.1, 3.6 Hz, 1H), 3.94 (d, *J* = 7.2 Hz, 2H), 3.82 – 3.66 (m, 2H), 3.46 (dd, *J* = 13.2, 4.3 Hz, 1H), 2.81 (dt, *J* = 16.8, 8.4 Hz, 1H), 2.78 – 2.67 (m, 2H), 2.19 (d, *J* = 3.7 Hz, 1H), 1.89 – 1.81 (m, 1H), 1.25 (s, 1H), 1.10 – 1.01 (m, 1H), 1.04 (s, 8H), 0.88 (d, *J* = 3.7 Hz, 1H), 0.75 (d, *J* = 6.6 Hz, 1H); ^{13}C NMR

(101 MHz, $CDCl_3$) δ 195.10, 155.92, 135.51, 135.47, 134.61, 133.43, 133.38, 129.81, 129.15, 128.95, 127.79, 127.77, 127.58, 106.54, 103.44, 66.06, 63.11, 60.85, 53.58, 39.96, 39.32, 35.52, 29.71, 26.88, 25.24, 19.18.

General procedure for the synthesis of ureas 65 and 71a-c

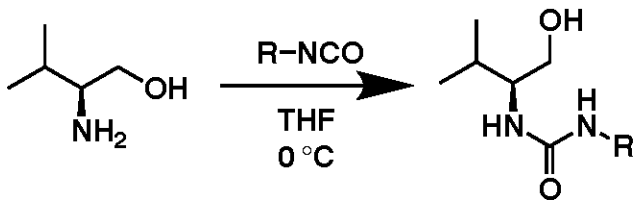

65 or 71a-c

L-valinol (1 eq) was dissolved in THF under Ar and the flask was cooled to 0 °C in an ice bath. The alkylated isocyanate reagent (1.1 eq) was added all at once to the flask, and the reaction mixture was left to stir and warm to room temperature overnight. The solvent was subsequently removed *in vacuo*, and the product was purified via recrystallization from a mixture of hexanes/EtOAc.

65: Urea **65** (R = Bn) was synthesized according to the general procedure using L-valinol (557 μL, 5.00 mmol), benzyl isocyanate (679 μL, 5.500 mmol, 1.1 eq) and THF (10 mL) Following recrystallization from 2:3 Hex/EtAOc, **65** was isolated in 73% yield. Characterization was completed following synthesis of **66**.

71a: Urea **71a** (R = Bu) was synthesized according to the general procedure using L-valinol (557 μL, 5.00 mmol), butyl isocyanate (520 μL, 5.500 mmol, 1.1 eq) and THF (10 mL) Following recrystallization from 1:1 Hex/EtAOc, **71a** was isolated in 81% yield. ^{1}H NMR (400 MHz, Chloroform-*d*) δ 4.91 (s, 1H), 4.84 (s, 1H), 3.71 (ddd, *J* = 10.0, 5.4, 2.8 Hz, 1H), 3.65 – 3.53 (m, 1H), 3.51 (qd, *J* = 6.8, 2.9 Hz, 1H), 3.15 (td, *J* = 7.1, 5.6 Hz, 2H), 1.84 (h, *J* = 6.8 Hz, 1H), 1.54 – 1.42 (m, 2H), 1.42 – 1.33 (m, 1H), 1.37 – 1.24 (m, 1H), 0.93 (dt, *J* = 10.3, 6.9 Hz, 9H); ^{13}C NMR (101 MHz, $CDCl_3$) δ 159.62, 65.16, 58.20, 40.40, 32.24, 29.61, 20.05, 19.54, 18.75, 13.81.

71b: Urea **71b** (R = Et) was synthesized according to the general procedure using L-valinol (557 μL, 5.00 mmol), ethyl isocyanate (435 μL, 5.500 mmol, 1.1 eq) and THF (10 mL) Following recrystallization from 1:1 Hex/EtAOc, **71b** was isolated in 65% yield. ^{1}H NMR (400 MHz, Chloroform-*d*) δ 4.36 (s, 2H), 3.74 (ddd, *J* = 10.3, 6.0, 2.6 Hz, 1H), 3.65 – 3.55 (m, 1H), 3.56 (s, 1H), 3.22 (qd, *J* = 7.2, 5.4 Hz, 2H), 3.06 (s, 1H), 1.85 (dq, *J* = 13.4, 6.7 Hz, 1H), 1.61 – 1.55 (m, 4H), 1.16 (t, *J* = 7.2 Hz, 3H), 0.96 (dd, *J* = 6.8, 6.0 Hz, 6H), 0.83 (s, 1H); ^{13}C NMR (101 MHz, $CDCl_3$) δ 65.44, 58.28, 35.61, 29.61, 19.53, 18.77, 15.35. IR: ν_{max} 3339.5, 2971.2, 2872.1, 1616.3, 1575.3, 1519.5, 1460.2, 1378.6, 1276.4, 1240.9, 1128.5, 1060.0, 972.0, 632.0; $[\alpha]^{23}$ = -44.5 (c = 0.500 g/mL).

71c: Urea **71c** (R = *t*-Bu) was synthesized according to the general procedure using L-valinol (557 μL, 5.00 mmol), *t*-butyl isocyanate (628 μL, 5.500 mmol, 1.1 eq) and THF (10 mL) Following recrystallization from 3:1 Hex/EtAOc, **71c** was isolated in 71% yield. ^{1}H NMR (400 MHz, Chloroform-*d*) δ 4.40 (s, 2H), 3.76 – 3.67 (m, 1H), 3.62 – 3.48 (m, 2H), 3.32 (s, 1H), 1.81 (dp, *J* = 13.5, 6.8 Hz, 1H), 1.69 – 1.61 (m, 1H), 1.34 (s, 9H), 0.94 (dd, *J* = 6.8, 4.3 Hz, 6H); ^{13}C NMR (101 MHz, $CDCl_3$) δ 158.66, 65.47, 57.95, 50.56, 29.70, 29.51, 19.50, 18.76. IR: ν_{max} 3235.8, 2963.1, 2185.5, 2025.8, 1653.6, 1559.7, 1511.8, 1453.1, 1388.0, 1361.0, 1310.5, 1257.3, 1215.4, 1143.7, 1120.8, 1077.6, 975.8, 663.0; $[\alpha]^{23}$ = -34.4 (c = 0.510 g/mL).

General procedure for the synthesis of cyclic ureas 66 and 72a-c

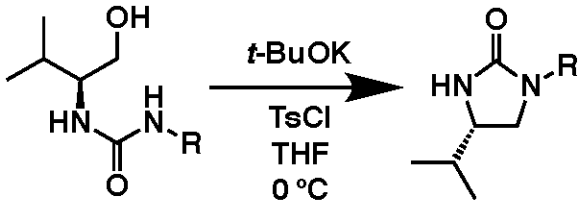

65 or 71a-c **66 or 72a-c**

The protected urea (1 eq) was dissolved in THF under Ar and the flask was cooled to 0 °C in an ice bath. A 1M solution of potassium *tert*-butoxide (2.40 eq) was added in portions to the flask, and the flask was allowed to warm to room temperature while stirring for 1.5 hours. After this time, the flask was cooled back to 0 °C, and a solution of *p*-toluenesulfonyl chloride (1.20 eq) in THF, added via cannula transfer. The reaction was left to stir in the ice bath overnight and was ultimately quenched by the addition of water. Following transfer to a separatory funnel, the aqueous layer was extracted from ether, and the combined organics were washed with brine, dried over $MgSO_4$, filtered and concentrated *in vacuo*. The crude product was subsequently purified via flash chromatography (silica gel) to afford the corresponding cyclic urea products.

66: Urea **66** (R = Bn) was synthesized according to the general procedure using urea **65** (860 mg, 3.64 mmol), potassium *tert*-butoxide (9.29 mL, 9.29 mmol, 2.40 eq), *p*-toluenesulfonyl chloride (832.9 mg, 4.37 mmol, 1.20 eq) in THF (17 mL total). Following column chromatography (99:1 CH_2Cl_2/MeOH as eluent), **66** was isolated in 56% yield. ^{1}H NMR (400 MHz, Chloroform-*d*) δ 7.39 – 7.29 (m, 2H), 7.32 – 7.23 (m, 3H), 5.53 (s, 1H), 4.47 – 4.33 (m, 2H), 2.40 – 2.34 (m, 1H), 2.17 (ddd, *J* = 7.5, 6.6, 4.1 Hz, 1H), 1.88 (d, *J* = 4.1 Hz, 1H), 1.42 (dq, *J* = 13.8, 6.8 Hz, 1H), 1.04 (d, *J* = 6.6 Hz, 3H), 0.96 (d, *J* = 6.8 Hz, 3H).

72a: Urea **72a** (R = Bu) was synthesized according to the general procedure using urea **71a** (108 mg, 0.531 mmol), potassium *tert*-butoxide (1.28 mL, 1.28 mmol, 2.40 eq), *p*-toluenesulfonyl chloride (122 mg, 0.638 mmol, 1.20 eq) in THF (2.5 mL total). Following column chromatography (2:1 Hex/EtOAc as eluent), **72a** was isolated in 62% yield. ^{1}H NMR (400 MHz, Chloroform-*d*) δ 5.23 (s, 1H), 3.20 (td, *J* = 7.0, 5.9 Hz, 2H), 2.33 (dd, *J* = 6.6, 0.5 Hz, 1H), 2.18 (s, 7H), 2.19 – 2.05 (m, 1H), 1.84 (d, *J* = 4.1 Hz, 1H), 1.54 – 1.28 (m, 5H), 1.05 (d, *J* = 6.7 Hz, 3H), 1.02 – 0.87 (m, 6H); ^{13}C NMR (101 MHz, $CDCl_3$) δ 207.03, 165.41, 45.26, 40.47, 31.88, 31.04, 30.96, 30.81, 20.02, 19.95, 19.16, 13.76.

72b: Urea **72b** (R = Et) was synthesized according to the general procedure using urea **71b** (563 mg, 3.23 mmol), potassium *tert*-butoxide (7.76 mL, 7.76 mmol, 2.40 eq), *p*-toluenesulfonyl chloride (740 mg, 3.88 mmol, 1.20 eq) in THF (15 mL total). Following column chromatography (3:1 Hex/EtOAc as eluent), **72b** was isolated in 22% yield. ^{1}H NMR (400 MHz, Chloroform-*d*) δ 5.21 (s, 1H), 3.31 – 3.16 (m, 2H), 2.32 (d, *J* = 6.6 Hz, 1H), 2.16 – 2.03 (m, 1H), 1.85 (d, *J* = 4.1 Hz, 1H), 1.64 (s, 1H), 1.63 – 1.56 (m, 1H), 1.40 (h, *J* = 6.9 Hz, 1H), 1.14 (td, *J* = 7.2, 0.9 Hz, 3H), 1.05 (dd, *J* = 6.6, 0.9 Hz, 3H), 1.00 – 0.84 (m, 3H).

72c: Urea **72c** (R = *t*-Bu) was synthesized according to the general procedure using urea **71c** (719 mg, 3.55 mmol), potassium *tert*-butoxide (8.53 mL, 8.53 mmol, 2.40 eq), *p*-toluenesulfonyl chloride (813 mg, 4.27 mmol, 1.20 eq) in THF (15 mL total). Following column chromatography (3:1 Hex/EtOAc as eluent), **72c** was isolated in 93% yield. ^{1}H NMR (400 MHz, Chloroform-*d*) δ 5.20 (s, 1H), 2.27 (d, *J* = 6.6 Hz, 1H), 2.12 –

2.03 (m, 1H), 1.80 (d, J = 4.1 Hz, 1H), 1.39 (dt, J = 13.8, 6.9 Hz, 1H), 1.32 (s, 9H), 1.04 (d, J = 6.7 Hz, 3H), 0.96 (d, J = 6.8 Hz, 3H).

Silane 68

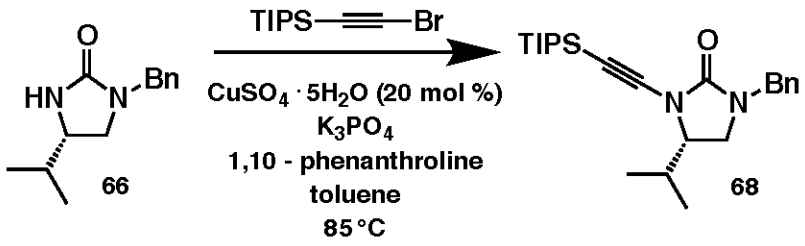

Silane **68** was synthesized in 22% yield according to procedures reported by Dunetz et al. (*Org. Lett.*, **2003**, 5, 4011-4014) using urea **66** as the substrate and an alkyne coupling partner synthesized previously by Professor Paley. ^{1}H NMR (400 MHz, Chloroform-*d*) δ 7.39 – 7.25 (m, 5H), 4.66 (s, 1H), 4.62 (d, *J* = 14.1 Hz, 1H), 2.49 – 2.40 (m, 1H), 2.28 (d, *J* = 6.3 Hz, 1H), 2.20 – 2.14 (m, 1H), 1.64 (dq, *J* = 13.1, 6.6 Hz, 1H), 1.25 (s, 2H), 1.16 (dd, *J* = 7.4, 3.0 Hz, 1H), 1.13 – 0.96 (m, 22H), 0.96 – 0.84 (m, 5H).

Alkynyl urea 69

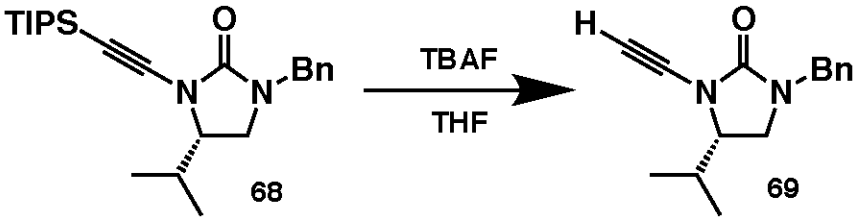

Silane **68** (36.3 mg, 91.1 μmol) was dissolved in THF (2 mL) in a round bottom flask. A 1M solution of TBAF (109 μL, 109 μmol, 1.2 eq) was added via syringe to the flask. The flask was capped and the reaction was allowed to stir at room temperature for 22.5 hours. The reaction mixture was then diluted in EtOAc, washed with saturated $NaHCO_3$ and brine, dried over $MgSO_4$, filtered and concentrated *in vacuo*. The crude product was subsequently purified via flash chromatography (silica gel, 7:1 Hex/EtOAc) to afford **69** in 87% yield. ^{1}H NMR (400 MHz, Chloroform-*d*) δ 7.38 – 7.27 (m, 5H), 4.65 (s, 2H), 2.97 (s, 1H), 2.44 (td, J = 6.5, 4.1 Hz, 1H), 2.33 (d, J = 6.4 Hz, 1H), 2.17 (d, J = 4.1 Hz, 1H), 1.69 (q, J = 6.8 Hz, 1H), 1.05-1.04 (m, 9H), 0.91-0.83 (m, 5H).

Vinyl stannane 70

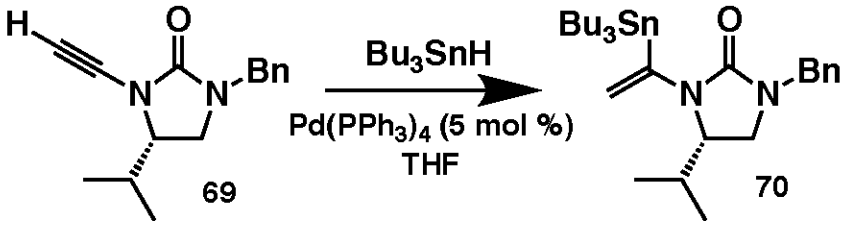

Alkyne **69** (21.2 mg, 79.0 μmol) was dissolved in THF (1 mL) under Ar. Tetrakis(triphenylphosphine)palladium(0) (4.6 mg, 5 mol %) was added all at once, followed by a dropwise addition of tributyltin hydride (23.0 μL, 86.9 μmol, 1.1 eq) via syringe. The reaction mixture was stirred at room temperature for 2 hours, after which the solvent was removed *in vacuo*. The crude product was subsequently purified via flash chromatography (silica gel, 15:1 Hex/EtOAc with 0.5% NEt_3) to afford **70** in 68% yield.

^{1}H NMR (400 MHz, Chloroform-*d*) δ 7.31 (t, *J* = 7.5 Hz, 2H), 7.22 (t, *J* = 7.2 Hz, 1H), 7.13 (d, *J* = 7.6 Hz, 2H), 5.20 (d, *J* = 17.3 Hz, 1H), 5.12 (d, *J* = 17.0 Hz, 1H), 4.97 (s, 1H), 4.53 (s, 1H), 2.30 (td, *J* = 6.3, 4.1 Hz, 1H), 2.11 (d, *J* = 6.5 Hz, 1H), 1.83 (d, *J* = 4.1 Hz, 1H), 1.53 – 1.45 (m, 2H), 1.50 – 1.37 (m, 2H), 1.40 – 1.19 (m, 11H), 1.09 – 0.97 (m, 5H), 1.00 – 0.82 (m, 21H), 0.82 – 0.72 (m, 2H).

Dichloroenyl urea 73 and attempted synthesis of alkyne 74

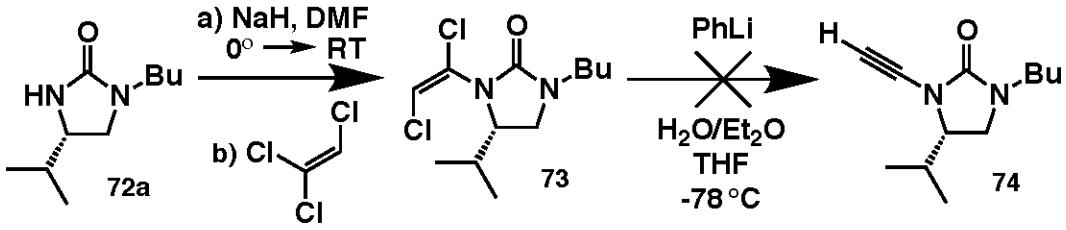

Sodium hydride (173 mg, 4.32 mmol, 2.2 eq) was placed in a Schlenk flask within the glove box and suspended in DMF (4 mL). The flask was capped, removed from the glove box and placed under Ar on the Schlenk line before being cooled to 0 °C in an ice bath. A solution of urea **72a** (362 mg, 1.96 mmol, 1 eq) in DMF (4 mL) was then added to the reaction flask. The ice bath was removed and the reaction was stirred at room temperature for 2 hours. After 2 hours, trichloroethylene (177 μL, 1.96 mmol, 1 eq) was added dropwise via syringe and the reaction was stirred overnight for 16 hours. The reaction was then quenched and diluted in Et_2O, washed with saturated $NaHCO_3$, water and brine, dried over $MgSO_4$, filtered and concentrated *in vacuo*. The crude product was subsequently purified via flash chromatography (silica gel, 15:1 Hex/EtOAc) to afford **73** in 76% yield. ^{1}H NMR (400 MHz, Chloroform-*d*) δ 6.29 (s, 1H), 3.53 – 3.43 (m, 2H), 2.48 – 2.26 (m, 2H), 1.99 (dd, J = 6.5, 4.0 Hz, 1H), 1.68 – 1.56 (m, 3H), 1.45 – 1.22 (m, 3H), 1.11 – 0.77 (m, 8H); ^{13}C NMR (101 MHz, $CDCl_3$) δ 116.05, 47.39, 45.55, 44.15, 31.58, 30.21, 29.70, 29.52, 22.65, 20.13, 19.92, 19.79, 19.66, 19.57, 17.99, 14.13, 13.79, 13.71; IR: ν_{max} 3085.3, 2960.1, 2873.7, 2248.3, 1694.0, 1631.0, 1467.9, 1402.9, 1366.0, 1301.6, 1228.3, 1188.5, 1113.2, 1066.5, 995.9, 973.4, 935.2, 895.9, 814.8, 733.7, 666.7, 643.7; $[\alpha]^{23}$ = 44.8 (c = 0.635 g/mL).

Dichloroenyl urea **73** (414 mg, 1.48 mmol) was dissolved in THF (15 mL) under Ar, and the flask was cooled to -78 °C in a dry ice/acetone bath. A 2M solution of

phenyllithium (1.63 mL, 3.26 mmol, 2.2 eq) was added dropwise via syringe, and the reaction mixture was stirred at -78 °C for 2 hours. After quenching of the reaction with water and transfer to a separatory funnel, the aqueous layer was extracted with Et_2O, and the combined organics were washed with brine, dried over $MgSO_4$, filtered and concentrated *in vacuo*. The crude product was subsequently purified via flash chromatography (silica gel, 12:1 Hex/EtOAc) to afford the product in 44% yield. **74** was not observed, and the hypothesized diphenylalkene derivative of **73** was instead isolated as the major product. ^{1}H NMR (400 MHz, Chloroform-*d*) δ 7.85 – 7.77 (m, 4H), 7.70 – 7.56 (m, 2H), 7.56 – 7.40 (m, 4H), 3.50 (td, *J* = 7.1, 2.1 Hz, 2H), 2.98 (s, 1H), 2.48 – 2.36 (m, 1H), 2.31 (d, *J* = 6.4 Hz, 1H), 2.15 (d, *J* = 4.1 Hz, 1H), 1.77 – 1.62 (m, 2H), 1.65 – 1.56 (m, 1H), 1.45 – 1.20 (m, 2H), 1.12 – 1.01 (m, 3H), 0.99 – 0.84 (m, 6H).

Sulfonamide 75 and aziridine 77

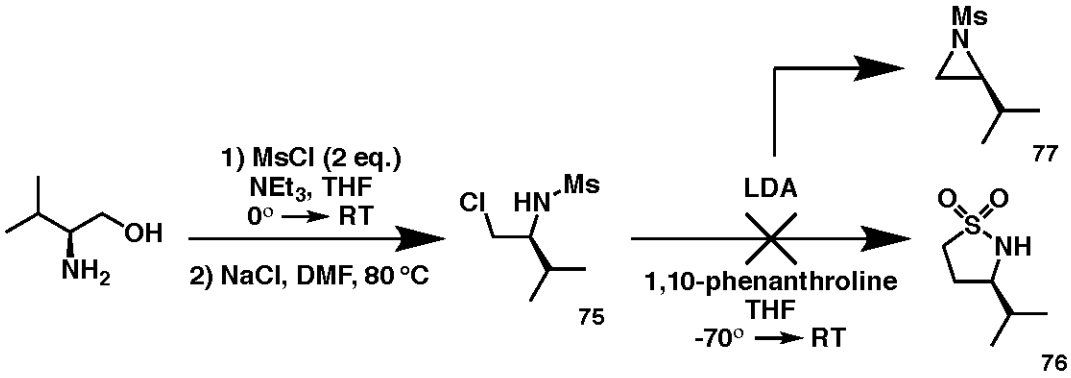

L-valinol (123 μL, 1.10 mmol) was dissolved in THF (1.5 mL) in a flame-dried Schlenk flask under Ar. Triethylamine (308 μL, 2.21 mmol, 2 eq) was added and the solution was cooled to 0 °C in an ice bath. Methanesulfonyl chloride (171 μL, 2.21 mmol, 2 eq) was added, the bath was removed, and the reaction was stirred overnight for 20.5 hours. Water was added to quench the reaction, and after transfer to a separatory funnel, the aqueous layer was extracted with EtOAc, and the combined organics were washed with brine, dried over $MgSO_4$, filtered and concentrated *in vacuo*. The crude bismesylate product was used as obtained for the next reaction.

The crude bismesylate (286 mg, 1.10 mmol) was dissolved in DMF under Ar. Sodium chloride (129 mg, 2.21 mmol, 2 eq) was added, and the flask was capped and placed into an 80 °C oil bath. The reaction was allowed to stir for 16 hours, after which the solvent was removed via distillation. Water was added to dilute the reaction, and after transfer to a separatory funnel, the aqueous layer was extracted with EtOAc, and the combined organics were washed with brine, dried over $MgSO_4$, filtered and concentrated *in vacuo* to afford **75**. The crude product **75** was used as obtained for the next reaction.

Sulfonamide **75** (32.8 mg, 164 μmol) was dissolved in THF (1 mL) under Ar and the flas was cooled to -70 °C. A 2M solution of lithium diisopropylamide in

THF/heptanes/ethylbenzene (370 μL, 739 μmol, 4.5 eq) was added dropwise via syringe, and the reaction mixture was allowed to warm to -30 °C while stirring for 2 hours. The reaction was subsequently quenched with 1M HCl and diluted in water. Following transfer to a separatory funnel, the aqueous layer was extracted with EtOAc, and the combined organics were washed with saturated $NaHCO_3$ and brine, dried over $MgSO_4$, filtered and concentrated *in vacuo*. The crude product was subsequently purified via flash chromatography (silica gel, 1:2 Hex/EtOAc) to afford aziridine **77** product in 21% yield. The expected sulfonamide **76** was not observed, as confirmed by NMR. ^{1}H NMR (400 MHz, Chloroform-*d*) δ 4.12 (qt, *J* = 7.1, 1.3 Hz, 1H), 3.06 (d, *J* = 1.3 Hz, 3H), 2.57 (s, 1H), 2.61 – 2.49 (m, 1H), 2.18 – 2.12 (m, 1H), 2.05 (t, *J* = 1.3 Hz, 1H), 1.61 – 1.45 (m, *J* = 6.7 Hz, 1H), 1.31 – 1.22 (m, 1H), 1.04 (ddt, *J* = 17.6, 6.8, 1.2 Hz, 6H).

Sequential Synthesis of Acetal 90:

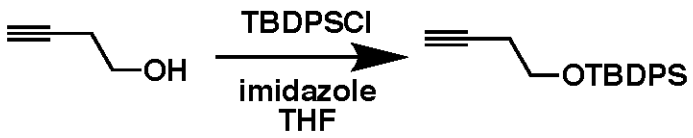

3-butyn-1-ol (1.00 mL, 13.2 mmol) was dissolved in THF (30 mL) under Ar. Imidazole (2.25 g, 33.0 mmol, 2.5 eq) and *tert*-butyldiphenylsilyl chloride (4.06 mL, 15.9 mmol, 1.2 eq) were added in that order. The reaction was stirred overnight at room temperature for 19 hours. The reaction mixture was then diluted in Et_2O, washed with saturated NH_4Cl and brine, dried over $MgSO_4$, filtered and concentrated *in vacuo*. The resulting crude product was purified via flash chromatography (silica gel, 40:1 Hex/EtOAc) to afford the intermediate silyl ether in 96% yield.

^{1}H NMR (400 MHz, Chloroform-*d*) δ 7.72 – 7.64 (m, 4H), 7.49 – 7.39 (m, 2H), 7.43 – 7.34 (m, 4H), 3.78 (t, J = 7.1 Hz, 2H), 2.45 (td, J = 7.1, 2.6 Hz, 2H), 1.95 (t, J = 2.7 Hz, 1H), 1.06 (s, 9H).

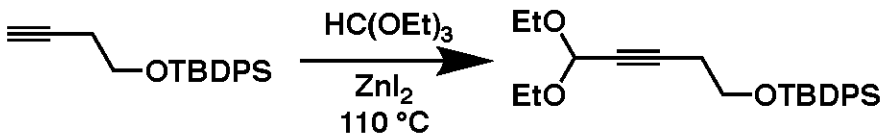

The intermediate silyl ether (3.96 g, 12.8 mmol) was dissolved in triethyl orthoformate (40 mL) under Ar. Zinc iodide (4.07 g, 12.8 mmol, 1 eq) was added all at once. The reaction flask was placed into an oil bath at 110 °C and stirred for 76 hours. The reaction mixture was filtered to remove unwanted precipitate, and the filtrate was subjected to distillation to remove excess triethyl orthoformate. The resulting crude product was purified via flash chromatography (silica gel, 40:1 Hex/EtOAc) to afford the intermediate diethyl acetal in 97% yield. ^{1}H NMR (400 MHz, Chloroform-*d*) δ 7.71 – 7.63 (m, 4H), 7.48 – 7.34 (m, 6H), 5.24 (t, *J* = 1.6 Hz, 1H), 3.77 (t, *J* = 7.1 Hz, 2H), 3.76 – 3.66 (m, 2H), 3.55 (dq, *J* = 9.4, 7.1 Hz, 2H), 2.52 (td, *J* = 7.1, 1.7 Hz, 2H), 1.30 – 1.17 (m, 6H), 1.05 (s, 9H).

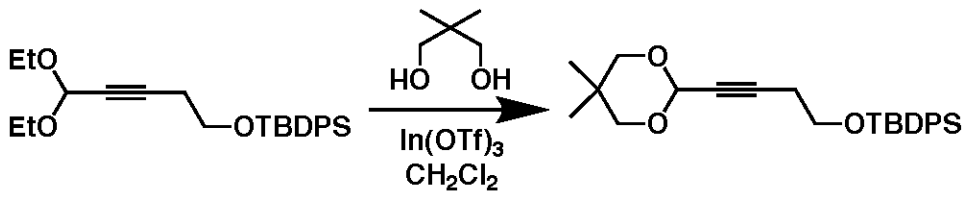

The intermediate diethyl acetal (5.06 g, 12.3 mmol) was dissolved in CH_2Cl_2 (15 mL) under Ar. 2,2-dimethyl-1,3-propanediol (6.38 g, 61.3 mmol, 5 eq) and indium(III) triflate (276 mg 0.491 mmol, 4 mol %) were added in that order. The reaction was stirred overnight at room temperature for 23 hours. The crude mixture was then purified via flash chromatography (basic aluminum oxide, 19:1 Hex/EtOAc, loaded neatly) to afford the intermediate cyclic acetal in 53% yield.

^{1}H NMR (400 MHz, Chloroform-*d*) δ 7.71 – 7.62 (m, 4H), 7.47 – 7.40 (m, 1H), 7.44 – 7.36 (m, 3H), 7.40 – 7.33 (m, 2H), 5.23 (t, *J* = 1.7 Hz, 1H), 3.79 (t, *J* = 7.3 Hz, 2H), 3.75 – 3.68 (m, 2H), 3.42 (d, *J* = 11.3 Hz, 2H), 2.54 (td, *J* = 7.3, 1.6 Hz, 2H), 1.34 – 1.22 (m, 3H), 1.06 (d, *J* = 12.3 Hz, 9H), 0.92 – 0.83 (m, 3H).

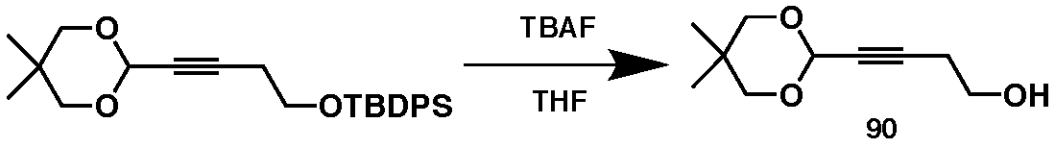

The intermediate cyclic acetal (954 mg, 2.26 mmol) was dissolved in THF (10 mL) in a round bottom flask. A 1M solution of TBAF (2.48 mL, 2.48 mmol, 1.2 eq) was added via syringe to the flask. The flask was capped and the reaction was allowed to stir at room temperature for 19.5 hours. The reaction mixture was then diluted in EtOAc, washed with saturated $NaHCO_3$ and brine, dried over $MgSO_4$, filtered and concentrated *in vacuo*. The crude product was subsequently purified via flash chromatography (silica gel, 1:1 Hex/EtOAc) to afford **90** in 85% yield.

^{1}H NMR (400 MHz, Chloroform-*d*) δ 5.25 (t, *J* = 1.7 Hz, 1H), 3.80 – 3.69 (m, 4H), 3.46 (d, *J* = 11.2 Hz, 2H), 2.54 (td, *J* = 6.4, 1.6 Hz, 2H), 2.15 (s, 1H), 1.13 (s, 3H), 0.85 (s, 3H); ^{13}C NMR (101 MHz, $CDCl_3$) δ 90.85, 83.13, 76.04, 60.71, 31.60, 30.34, 22.99, 22.76, 22.66, 22.09, 14.21, 14.14.

Carbamate 91

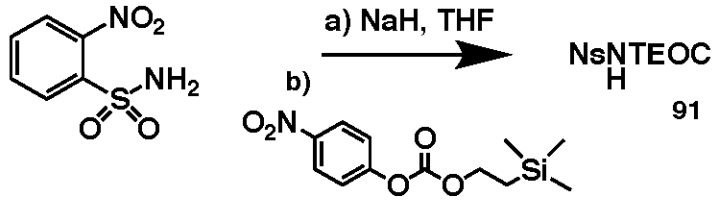

Sodium hydride (134 mg, 3.35 mmol, 1.2 eq) was placed in a Schlenk flask within the glove box. The flask was capped, removed from the glove box and placed under Ar on the Schlenk line, where the sodium hydride was suspended in THF (15 mL) and cooled to 0 °C in an ice bath. 2-nitrobenzenesulfonamide (677 mg, 3.35 mmol, 1.2 eq) was then added to the reaction flask, after which the ice bath was removed and the reaction was stirred at room temperature for 2 hours. After 2 hours, the reaction mixture was cooled back to 0 °C and 4-nitrophenyl 2-(trimethylsilyl)ethyl carbonate (791 mg, 2.79 mmol, 1 eq) was added. The ice bath was removed and the reaction stirred at room temperature for 21.5 hours. The reaction mixture was then partitioned in a 3:1 mixture of EtOAc and 3M NaOH in a separatory funnel. The layers were separated, and the organic layer was subsequently washed with 3M NaOH and brine, dried over $MgSO_4$, filtered and concentrated *in vacuo*. The crude product was subsequently purified via flash chromatography (silica gel, 3:1 Hex/EtOAc with 1% formic acid) to afford carbamate **91** in 67% yield.

^{1}H NMR (400 MHz, Chloroform-*d*) δ 8.43 – 8.34 (m, 1H), 7.92 – 7.83 (m, 1H), 7.87 – 7.76 (m, 2H), 7.76 (s, 1H), 4.26 – 4.17 (m, 2H), 1.05 – 0.95 (m, 2H), 0.01 (s, 9H).

Carbamate 92

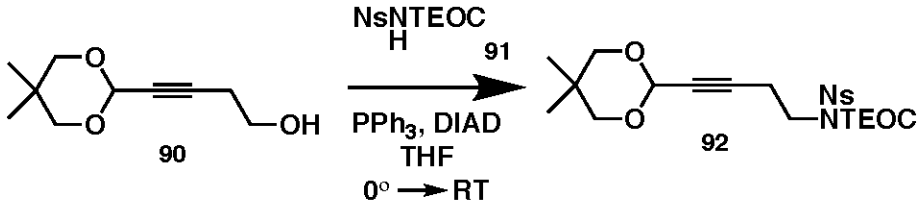

Alcohol **90** (300 mg, 1.63 mmol, 1 eq) was dissolved in THF (15 mL) under Ar. Sulfonamide **91** (563 mg, 1.63 mmol, 1 eq) and triphenylphosphine (427 mg, 1.63 mmol, 1 eq) were added in that order, and the flask was cooled to 0 °C in an ice bath. Diisopropyl azodicarboxylate (315 μL, 1.63 mmol, 1 eq) was then added dropwise, after which the ice bath was removed and the reaction was stirred at room temperature for 66 hours. The solvent was then removed *in vacuo*, and the crude product was subsequently purified via flash chromatography (silica gel, 4:1 Hex/EtOAc) to afford carbamate **92** in 88% yield.

^{1}H NMR (400 MHz, Chloroform-*d*) δ 8.41 – 8.33 (m, 1H), 7.81 – 7.69 (m, 3H), 5.31 (d, *J* = 1.7 Hz, 1H), 4.25 – 4.16 (m, 2H), 4.05 – 3.97 (m, 2H), 3.76 (d, *J* = 11.2 Hz, 2H), 3.44 (d, *J* = 11.2 Hz, 2H), 2.73 (ddd, *J* = 9.0, 6.2, 1.6 Hz, 2H), 1.08 (s, 3H), 1.03 – 0.90 (m, 2H), 0.88 (s, 3H); ^{13}C NMR (101 MHz, $CDCl_3$) δ 172.79, 153.42, 149.53, 136.30, 136.15, 134.33, 133.40, 126.11, 92.12, 83.75, 79.12, 79.05, 78.73, 68.40, 62.02, 47.41, 33.21, 32.02, 24.29, 23.85, 22.70, 21.88, 19.14, 15.84, 15.77; IR: ν_{max} 3020.8, 2958.6, 2870.0, 2359.7, 1732.8, 1545.5, 1470.1, 1388.3, 1365.9, 1333.1, 1271.2, 1252.1, 1216.7, 1173.3, 1143.9, 1091.9, 1032.4, 1015.4, 984.4, 960.8, 927.4, 853.9, 839.1, 755.7, 667.5; $[\alpha]^{23}$ = 2.27 (c = 0.620 g/mL).

Synthesis of sulfonamide 93

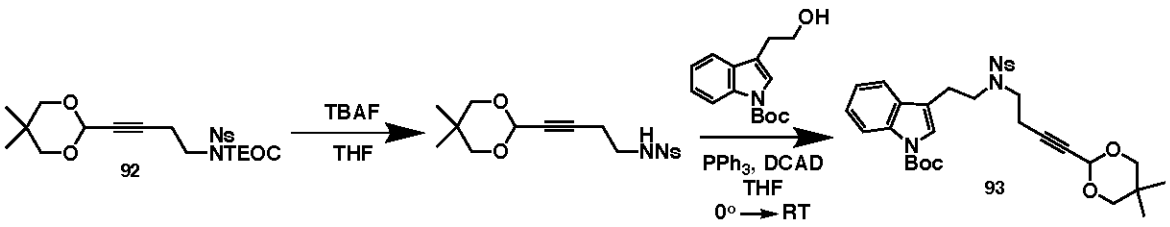

Carbamate **92** (733 mg, 1.43 mmol) was dissolved in THF (10 mL) in a round bottom flask. A 1M solution of TBAF (1.57 mL, 1.57 mmol, 1.1 eq) was added via syringe to the flask. The flask was capped and the reaction was allowed to stir at room temperature for 12 hours. The reaction mixture was then diluted in EtOAc, washed with saturated $NaHCO_3$ and brine, dried over $MgSO_4$, filtered and concentrated *in vacuo*. The crude product was subsequently purified via flash chromatography (silica gel, 1:1 Hex/EtOAc) to afford the intermediate protected amine in 98% yield. ^{1}H NMR (400 MHz, Chloroform-*d*) δ 8.19 – 8.10 (m, 1H), 7.95 – 7.84 (m, 1H), 7.82 – 7.71 (m, 2H), 5.74 (t, J = 6.2 Hz, 1H), 5.18 (d, J = 1.7 Hz, 1H), 3.68 (d, J = 11.4 Hz, 2H), 3.43 (d, J = 11.2 Hz, 2H), 3.30 (q, J = 6.6 Hz, 2H), 2.52 (td, J = 6.7, 1.6 Hz, 2H), 1.10 (s, 3H), 0.84 (s, 3H); ^{13}C NMR (101 MHz, $CDCl_3$) δ 147.98, 133.87, 133.67, 132.98, 130.88, 125.73, 90.54, 81.66, 77.89, 75.94, 60.41, 42.17, 30.32, 22.67, 22.06, 20.05; IR: ν_{max} 3345.7, 3097.1, 3020.5, 2958.2, 2260.1, 1732.6, 1594.0, 1540.1, 1411.0, 1232.2, 1166.6, 1089.7, 1013.7, 983.8, 927.5, 853.8, 742.5; $[\alpha]^{23}$ = 1.50 (c = 0.525 g/mL).

The intermediate amine (515 mg, 1.40 mmol, 1 eq) was dissolved in THF (8 mL) under Ar. Tryptophol (365 mg, 1.40 mmol, 1 eq), synthesized previously in the lab by Sooyun Choi, was dissolved in a separate flask in THF (3 mL), and the solution was transferred via cannula to the amine-containing flask. Triphenylphosphine (618 mg, 2.36 mmol, 1.69 eq) was added, after which the flask was cooled to 0 °C in an ice bath. Di-(4-

chlorobenzyl) azodicarboxylate (865 mg, 2.36 mmol, 1.69 eq) was then added, after which the ice bath was removed and the reaction was stirred at room temperature for 24 hours. The solvent was then removed *in vacuo*, and the crude product was subsequently purified via flash chromatography (silica gel, 4:1 Hex/EtOAc) to afford sulfonamide **93** in 74% yield. ^{1}H NMR (400 MHz, Chloroform-*d*) δ 8.05 (d, *J* = 8.1 Hz, 1H), 7.82 (d, *J* = 8.0 Hz, 1H), 7.60 – 7.51 (m, 2H), 7.45 (d, *J* = 7.7 Hz, 1H), 7.31 (s, 5H), 7.40 – 7.19 (m, 2H), 5.23 (s, 2H), 3.73 (d, *J* = 11.2 Hz, 2H), 3.67 (td, *J* = 7.6, 3.4 Hz, 4H), 3.44 (d, *J* = 11.2 Hz, 2H), 2.97 (t, *J* = 7.5 Hz, 2H), 2.64 (t, *J* = 7.3 Hz, 2H), 1.66 (s, 9H), 1.10 (s, 3H), 0.85 (s, 3H).

Amine 94

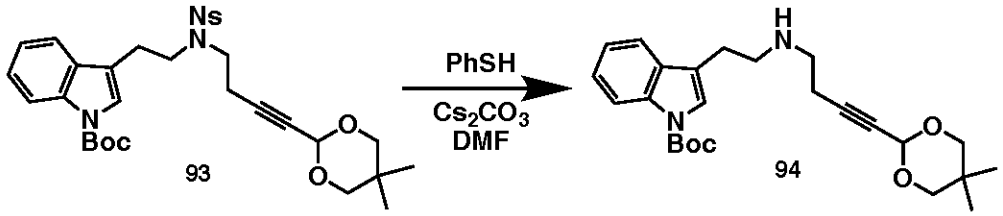

Sulfonamide **93** (323 mg, 0.529 mmol) was dissolved in DMF (9 mL) under Ar. Cesium carbonate (344 mg, 1.06 mmol, 2 eq) and thiophenol (81.4 μL, 0.793 mmol, 1.5 eq) were added to the flask in that order, and the reaction was left to stir for 16 hours. The solvent was then removed via distillation, and the resulting residue was partitioned between a 2:1 mixture of EtOAc and water in a separatory funnel. The layers were separated, and the aqueous layer was extracted several times with EtOAc. The combined organic layers were then washed with brine, dried over $MgSO_4$, filtered and concentrated *in vacuo*. The crude product was subsequently purified via flash chromatography (silica gel, 1:1 Hex/EtOAc with 1% NEt_3) to afford amine **94** in 71% yield.

^{1}H NMR (400 MHz, Chloroform-*d*) δ 8.12 (s, 1H), 7.54 (dd, *J* = 7.7, 1.2 Hz, 1H), 7.41 (s, 1H), 7.32 (td, *J* = 8.2, 7.7, 1.3 Hz, 1H), 7.28 – 7.20 (m, 1H), 5.17 (s, 1H), 3.74 – 3.66 (m, 2H), 3.43 (d, *J* = 11.2 Hz, 2H), 2.97 (td, *J* = 6.7, 1.5 Hz, 2H), 2.93 – 2.81 (m, 4H), 2.47 (td, *J* = 6.9, 1.6 Hz, 2H), 1.67-1.61 (s, 9H, two rotomers), 1.10 (s, 3H), 0.84 (s, 3H); ^{13}C NMR (101 MHz, $CDCl_3$) δ 124.36, 123.05, 122.42, 119.00, 48.64, 47.72, 30.33, 28.25, 25.71, 22.76, 22.15, 19.77; IR: ν_{max} 3332.2, 2955.4, 2850.2, 2359.5, 2249.5, 1727.9, 1609.6, 1537.0, 1453.4, 1383.6, 1256.4, 1226.0, 1162.2, 1092.2, 984.1, 960.4, 927.1, 857.6, 746.0; $[\alpha]^{23}$ = 0.403 (c = 0.505 g/mL).

Carbamate 95

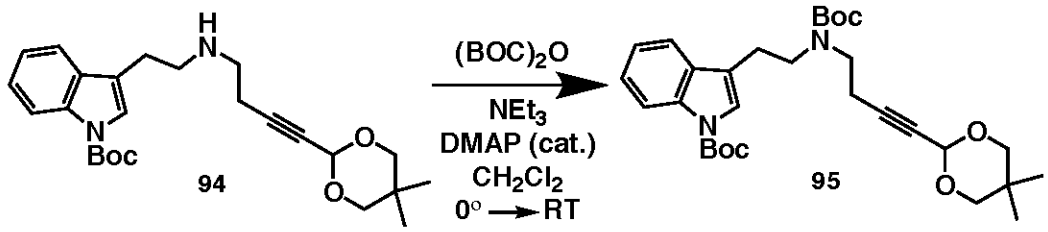

Amine **94** (154.9 mg, 0.363 mmol) was dissolved in CH_2Cl_2 (8 mL) and the flask was cooled to 0 °C in an ice bath. Anhydrous triethylamine (75.9 μL, 0.545 mmol, 1.5 eq) and a 1M solution of di-tert-butyl dicarbonate in THF (545 μL, 0.545 mmol, 1.5 eq) were added to the reaction in that order. The ice bath was removed and 4-dimethylaminopyridine (1.0 mg, 2.5 mol %) was added all at once. The reaction was stirred at room temperature for 16.5 hours, after which the reaction mixture was diluted in EtOAc, washed with saturated NH_4Cl, brine, dried over $MgSO_4$, filtered and concentrated *in vacuo*. The crude product was subsequently purified via flash chromatography (silica gel, 6:1 Hex/EtOAc) to afford carbamate **95** in 71% yield.

^{1}H NMR (400 MHz, Chloroform-*d*) δ 8.13 (s, 1H), 7.67 – 7.53 (m, 1H), 7.42 (d, *J* = 6.2 Hz, 1H), 7.32 (tdd, *J* = 8.3, 4.6, 1.3 Hz, 1H), 7.28 – 7.20 (m, 1H), 5.25 – 5.18 (m, 1H), 3.73 – 3.65 (m, 2H), 3.61 (ddd, *J* = 9.7, 5.7, 1.7 Hz, 2H), 3.49 – 3.35 (m, 4H), 3.07 – 2.94 (m, 2H), 2.60 (td, *J* = 6.9, 1.6 Hz, 1H), 2.52 (ddd, *J* = 8.3, 6.9, 1.5 Hz, 1H), 1.67 (d, *J* = 2.7 Hz, 9H), 1.55 (d, *J* = 7.1 Hz, 9H), 1.26 (t, *J* = 7.1 Hz, 1H), 1.08 (d, *J* = 13.7 Hz, 3H), 0.92 – 0.80 (m, 3H).

Vinyl stannanes 96a-b

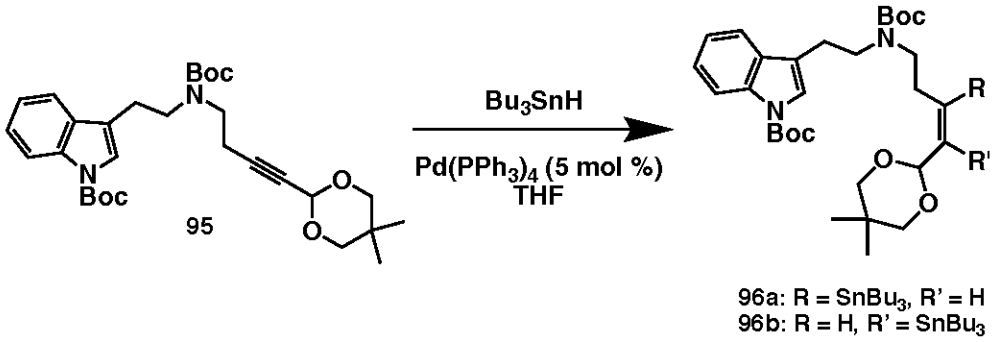

Carbamate **95** (49.8 mg, 94.6 μmol) was dissolved in THF (1 mL) under Ar. Tetrakis(triphenylphosphine)palladium(0) (5.5 mg, 5 mol %) was added all at once, followed by a dropwise addition of tributyltin hydride (28.0 μL, 104 μmol, 1.1 eq) via syringe. The reaction mixture was stirred at room temperature for 2.5 hours, after which the solvent was removed *in vacuo*. The crude product was subsequently purified via flash chromatography (silica gel, 9:1 Hex/EtOAc with 0.5% NEt_3) to afford a mixture of regioisomers **96a-b** in 99% total yield.

^{1}H NMR (400 MHz, Chloroform-*d*) δ 8.12 (s, 1H), 7.59 (s, 1H), 7.40 (s, 1H), 7.35 – 7.19 (m, 2H), 5.69 (d, *J* = 5.7 Hz, 1H), 5.19 (s, 1H), 5.12 (s, 1H), 3.60 (d, *J* = 10.8 Hz, 2H), 3.46 (s, 4H), 3.18 (s, 1H), 3.12 (s, 2H), 2.93 (s, 2H), 2.56 (s, 3H), 1.52 (s, 9H), 1.45 (dq, *J* = 18.0, 6.4, 5.7 Hz, 14H), 1.30 (dt, *J* = 14.7, 7.2 Hz, 7H), 1.22 (d, *J* = 16.2 Hz, 3H), 0.89 (dt, *J* = 14.5, 7.7 Hz, 15H), 0.67 (s, 3H).

Vinyl iodide 79

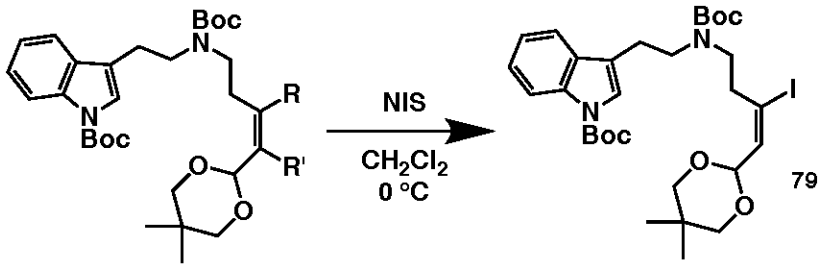

96a: R = $SnBu_3$, R' = H
96b: R = H, R' = $SnBu_3$

Vinyl stannane regioisomers **96a-b** (77.0 mg, 94.2 μmol) was dissolved in CH_2Cl_2 (1 mL) under Ar and the flask was cooled in an ice bath to 0 °C. N-iodo succinimide (25.4 mg, 113 μmol, 1.2 eq) was added all at once, and the reaction was stirred for 2 hours. The reaction was then quenched with a mixture of saturated $NaHCO_3$ and saturated $Na_2S_2O_3$. The reaction mixture was diluted with EtOAc and transferred to a separatory funnel; after separation, the organic layer was washed with brine, dried over $MgSO_4$, filtered and concentrated *in vacuo*. The crude product was subsequently purified via flash chromatography (silica gel, 7:1 Hex/EtOAc with 0.5% NEt_3) to afford vinyl iodide **79** as a contaminated major regioisomer in 47% yield (relative to both isomers as starting material).

^{1}H NMR (400 MHz, Chloroform-*d*) δ 8.13 (s, 1H), 7.60 – 7.50 (m, 1H), 7.42 – 7.19 (m, 3H), 6.42 (d, *J* = 9.7 Hz, 1H), 3.68 (d, *J* = 10.7 Hz, 2H), 3.61 – 3.48 (m, 2H), 3.42 (d, *J* = 13.6 Hz, 3H), 3.25 (s, 1H), 3.16 (s, 1H), 2.92 (s, 2H), 2.46 (s, 1H), 2.38 (d, *J* = 7.4 Hz, 1H), 1.66 (s, 10H), 1.44 (dd, *J* = 39.0, 9.5 Hz, 10H), 1.30 – 1.22 (m, 3H), 0.73 (s, 3H).

Diene 97

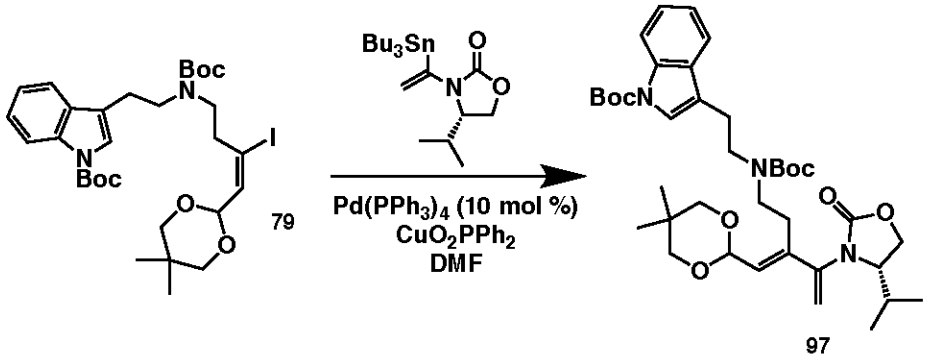

Vinyl iodide **79** (28.7 mg, 43.8 μmol, 1 eq) was dissolved in DMF (0.5 mL) in the glove box and transferred via pipette to a flask containing the (*S*)-isopropyl vinyl stannane auxiliary (19.5 mg, 43.8 μmol, 1 eq), synthesized previously in the lab by Ben Hejna. Tetrakis(triphenylphosphine)palladium(0) (5.1 mg, 10 mol %) and copper(I) diphenylphosphinate (14.2 mg, 50.4 μmol, 1.15 eq) were added together, and the reaction was stirred in the glove box overnight. The reaction flask was removed from the glove box and the reaction mixture was filtered through a pad of silica on a glass-frit filter using EtOAc as an eluent. After concentration, the remaining residue was dissolved in Et_2O and the organic layer was washed with water and brine, dried over $MgSO_4$, filtered and concentrated *in vacuo*. The crude product was subsequently purified via flash chromatography (silica gel, 2:1 Hex/EtOAc) to afford diene **97** as a contaminated product 92% yield (contaminant likely homocoupled bis-oxazolidinone byproduct as seen by NMR).

^{1}H NMR (400 MHz, Chloroform-*d*) δ 8.12 (s, 1H), 7.61 (d, *J* = 7.8 Hz, 1H), 7.55 (d, *J* = 7.6 Hz, 1H), 7.42 (s, 1H), 7.39 – 7.19 (m, 1H), 5.69 (t, *J* = 6.4 Hz, 1H), 5.55 (d, *J* = 5.7 Hz, 1H), 5.33 (s, 1H), 5.16 – 5.07 (dd, *J* = 5.8, 5.6 Hz, 1H), 4.31 (d, *J* = 8.0 Hz, 1H), 4.18 – 4.09 (m, 1H), 3.88 – 3.80 (m, 1H), 3.59 (d, *J* = 9.4 Hz, 2H), 3.48 (dt, *J* =

14.9, 7.8 Hz, 4H), 3.31 (q, J = 8.1 Hz, 1H), 3.22 (s, 1H), 2.93 (s, 1H), 2.88 (s, 1H), 2.40 (s, 1H), 1.88 (s, 1H), 1.66 (s, 9H), 1.52 (s, 4H), 1.39 (m, 5H), 1.19 (s, 3H), 0.88 (ddd, J = 15.8, 11.9, 8.2 Hz, 6H), 0.69 (d, J = 13.7 Hz, 3H); ^{13}C NMR (101 MHz, $CDCl_3$) δ 155.20, 130.54, 124.35, 123.11, 122.44, 117.90, 115.82, 63.10, 62.83, 59.70, 48.08, 29.99, 29.71, 28.84, 28.64, 28.34, 28.21, 27.83, 26.85, 22.99, 21.89, 17.84, 17.56, 14.53, 14.45, 13.62.

Iron-diene complex 98

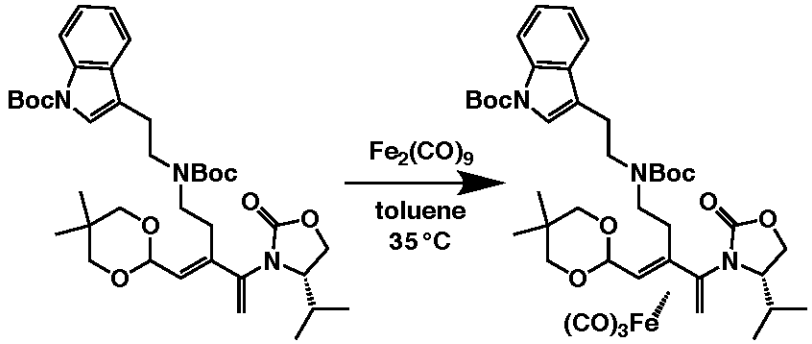

97 98

Diiron(0) nonacarbonyl (51.4 mg, 141 μmol, 3.5 eq) was placed into a Schlenk flask in the glove box, after which the flask was removed from the glove box, placed under Ar on a Schlenk line and dissolved in toluene (0.5 mL). A solution of diene **97** (27.5 mg, 40.3 μmol, 1 eq) in toluene (0.5 mL) was added to the reaction flask via cannula transfer. The flask was placed in a 35 °C oil bath and the reaction was left to stir for 20 hours. The reaction flask was then removed from the oil bath and the reaction mixture was filtered through a pad of silica on a glass-frit filter using EtOAc with 2% NEt_3 as an eluent. After concentration *in vacuo* (note: caution should be exhibited with the iron pentacarbonyl solution likely present in the collection reservoir of the rotary evaporator), the crude product was purified via flash chromatography (silica gel, 5:1 Hex/CH_2Cl_2 with 0.5% NEt_3) to afford complex **54** as a single diastereomer in 66% yield (dr 12.6:1).

^{1}H NMR (400 MHz, Chloroform-*d*) δ 8.11 (s, 1H), 7.54 (d, *J* = 7.8 Hz, 1H), 7.38 – 7.27 (m, 2H), 7.24 (t, *J* = 7.4 Hz, 1H), 4.68 (t, *J* = 8.3 Hz, 1H), 4.35 (d, *J* = 6.6 Hz, 1H), 4.09 (d, *J* = 8.5 Hz, 2H), 3.76 – 3.58 (m, 3H), 3.45 (d, *J* = 10.7 Hz, 1H), 3.41 – 3.19 (m, 4H), 2.90 (t, *J* = 7.4 Hz, 2H), 2.74 (t, *J* = 11.5 Hz, 1H), 2.35 (s, 2H), 1.74 (s, 1H), 1.66 (s,

9H), 1.50 (s, 2H), 1.39 (s, 7H), 1.16 (s, 3H), 0.92 (dd, J = 14.1, 6.8 Hz, 6H), 0.64 (s, 3H), 0.44 (d, J = 6.6 Hz, 1H), 0.30 (s, 1H).

Dienal complex 78 and attempted synthesis of Pictet-Spengler product 77

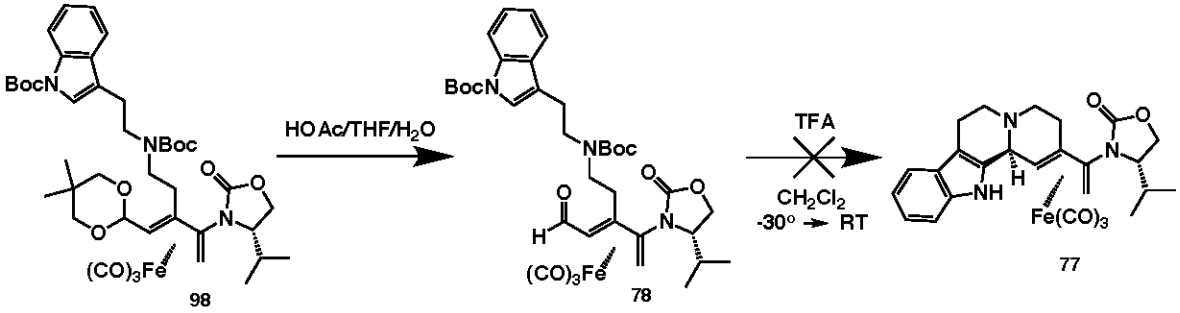

Iron-diene complex **98** (21.7 mg, 26.4 μmol, 1 eq) was dissolved in THF (0.33 mL). Water (0.13 mL) and acetic acid (0.53 mL) were added in that order to the flask to produce an 8:5:2 mixture of acetic acid/THF/water by volume, and the reaction was stirred overnight for 24.5 hours. The reaction mixture was then diluted in EtOAc, washed with 1 M NaOH, water and brine, dried over $MgSO_4$, filtered and concentrated *in vacuo.* The crude product was subsequently purified via flash chromatography (silica gel, 4:1 Hex/EtOAc) to afford the dienal **78** in 91% yield.

^{1}H NMR (400 MHz, Chloroform-*d*) δ 9.38 (d, *J* = 5.3 Hz, 1H), 8.12 (s, 1H), 7.52 (d, *J* = 7.6 Hz, 1H), 7.38 – 7.27 (m, 2H), 7.23 (dd, *J* = 7.3, 1.1 Hz, 1H), 4.51 (d, *J* = 8.9 Hz, 1H), 4.28 (s, 1H), 4.13 (s, 1H), 3.52 – 3.41 (m, 3H), 3.15 (d, *J* = 9.3 Hz, 2H), 2.88 (s, 2H), 2.79 – 2.68 (m, 1H), 2.36 (s, 1H), 2.15 – 2.07 (m, 1H), 1.67 (s, 9H), 1.46 (s, 2H), 1.37 (s, 7H), 1.26 (s, 3H), 0.98 (d, *J* = 6.8 Hz, 3H), 0.95 – 0.84 (m, 6H), 0.78 (d, *J* = 3.7 Hz, 1H), 0.62 (d, *J* = 5.2 Hz, 1H).

Dienal **78** (17.6 mg, 23.9 μmol) was dissolved in CH_2Cl_2 (0.5 mL) under Ar and the solution was cooled to -30 °C in a dry ice/acetone bath. Trifluoroacetic acid (34.7 μL, 467 μmol, 19.5 eq) was added at once, and the reaction was stirred for 4 hours. After 4 hours, the bath was removed, and the reaction was stirred at room temperature for 23 hours. The reaction was then quenched with saturated $NaHCO_3$, and the aqueous layer

was extracted several times with CH_2Cl_2. Following the washes, the combined organics were washed with brine, dried over $MgSO_4$, filtered and concentrated *in vacuo*. The crude product was subsequently purified via flash chromatography (silica gel, 4:1 Hex/EtOAc with 1% NEt_3). NMR results did not produce evidence of the expected product **77**, and instead revealed smaller fragments suggestive of sample decomposition.

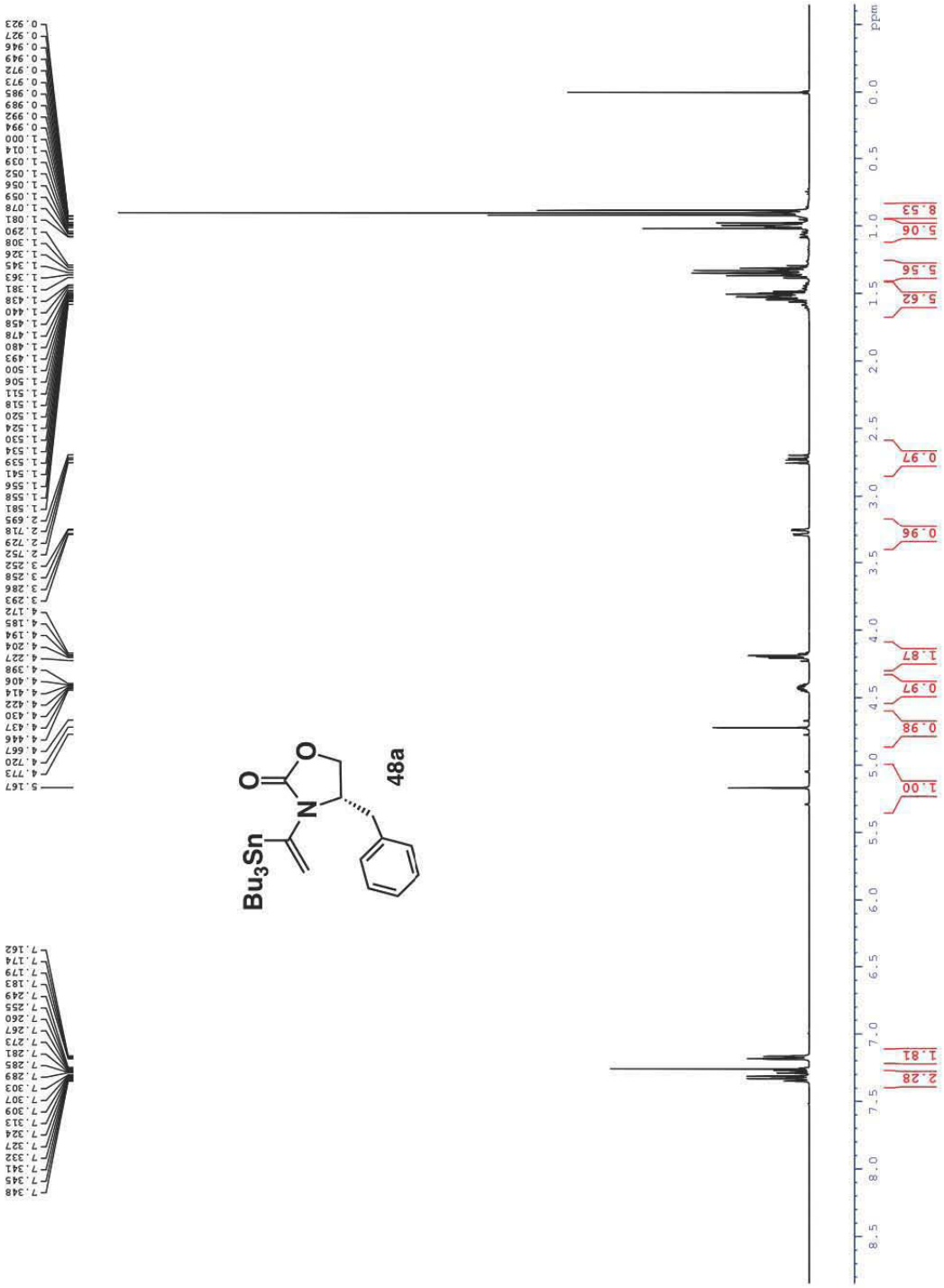
48a
Bu3Sn
O
N
O
8.53
5.06
5.56
5.62
0.97
0.96
1.87
0.97
0.98
1.00
1.81
2.28
ppm

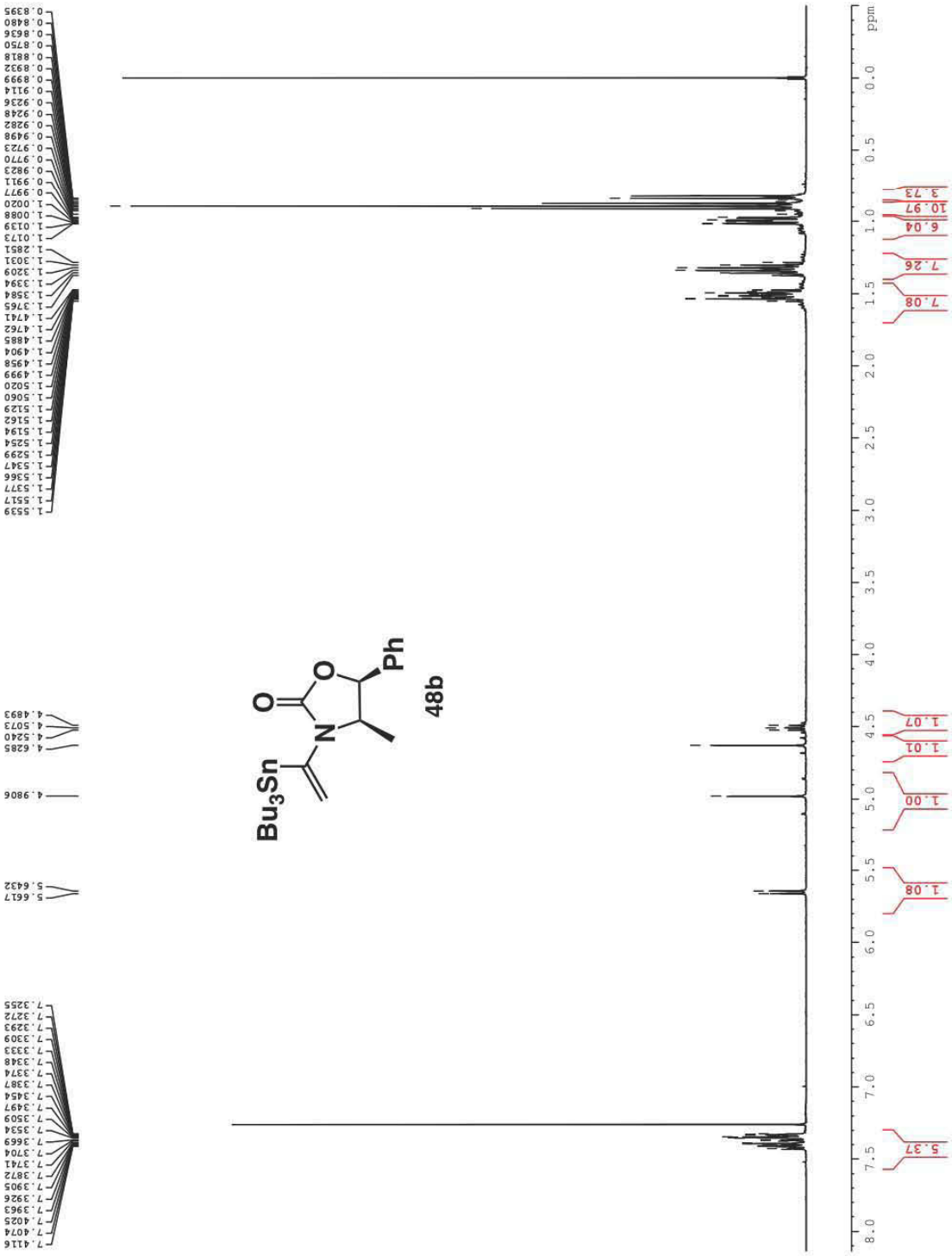
48b
Bu3Sn
O
O
N
Ph
ppm
0.0
0.5
1.0
1.5
2.0
2.5
3.0
3.5
4.0
4.5
5.0
5.5
6.0
6.5
7.0
7.5
8.0
3.73
10.97
6.04
7.26
7.08
1.07
1.01
1.00
1.08
5.37

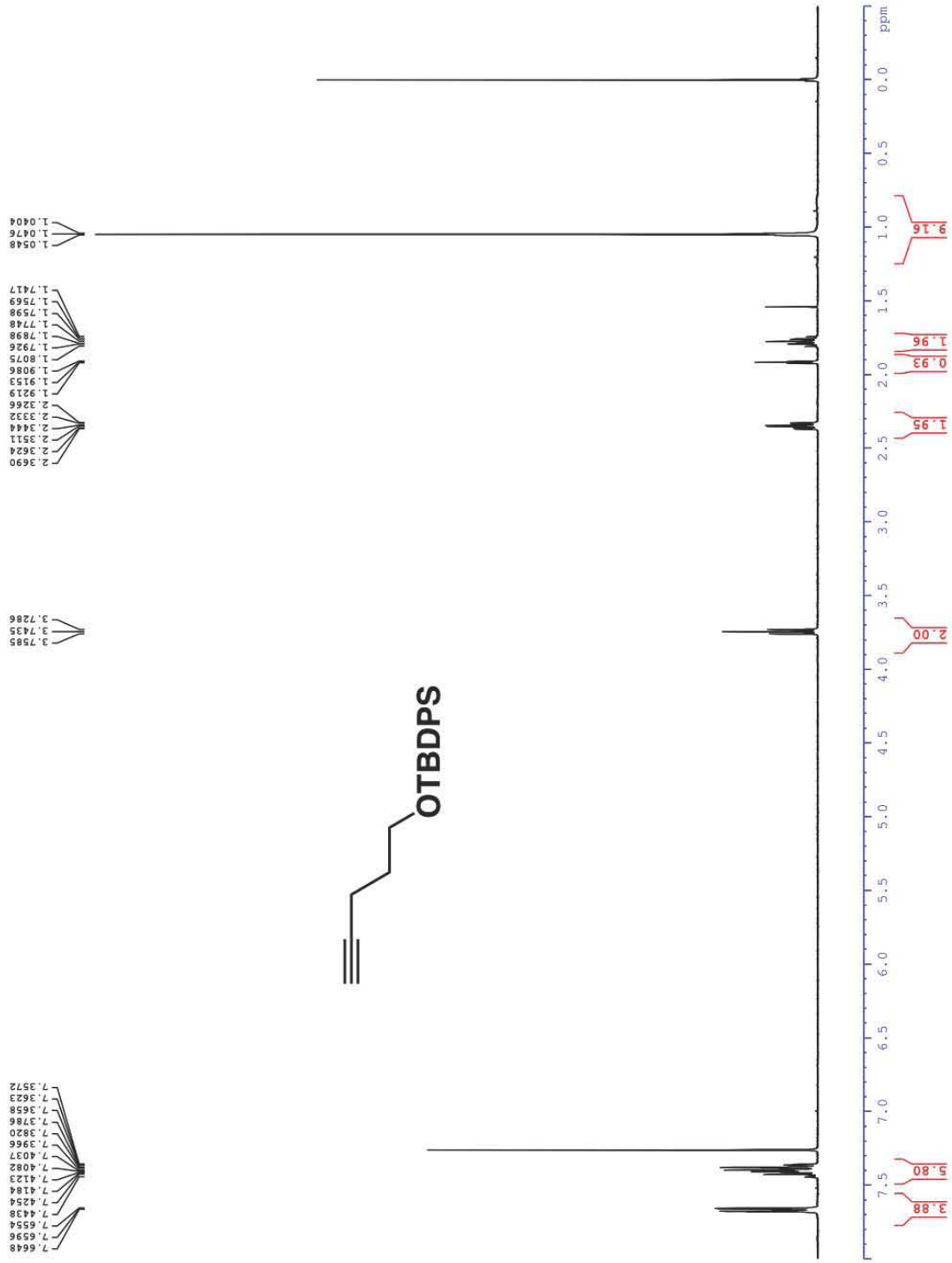
OTBDPS
1.0404
1.0476
1.0548
1.7417
1.7569
1.7598
1.7748
1.7898
1.7926
1.8075
1.9086
1.9153
1.9219
2.3266
2.3332
2.3444
2.3511
2.3624
2.3690
3.7285
3.7435
3.7586
7.3572
7.3623
7.3658
7.3786
7.3820
7.3966
7.4037
7.4082
7.4123
7.4184
7.4254
7.4438
7.6554
7.6596
7.6648
9.16
1.96
0.93
1.95
2.00
5.80
3.88
ppm

1.034
1.041
1.049
1.197
1.214
1.232
1.762
1.764
1.780
1.795
1.798
2.380
2.384
2.398
2.402
2.416
2.420
3.532
3.538
3.550
3.556
3.573
3.689
3.707
3.710
3.713
3.725
3.731
3.740
5.226
5.230
5.234
7.351
7.356
7.367
7.369
7.371
7.372
7.373
7.375
7.377
7.386
7.388
7.390
7.391
7.395
7.400
7.404
7.410
7.417
EtO
EtO
OTBDPS
50
ppm
9.24
6.10
2.01
2.03
2.05
4.03
1.00
5.98
4.05

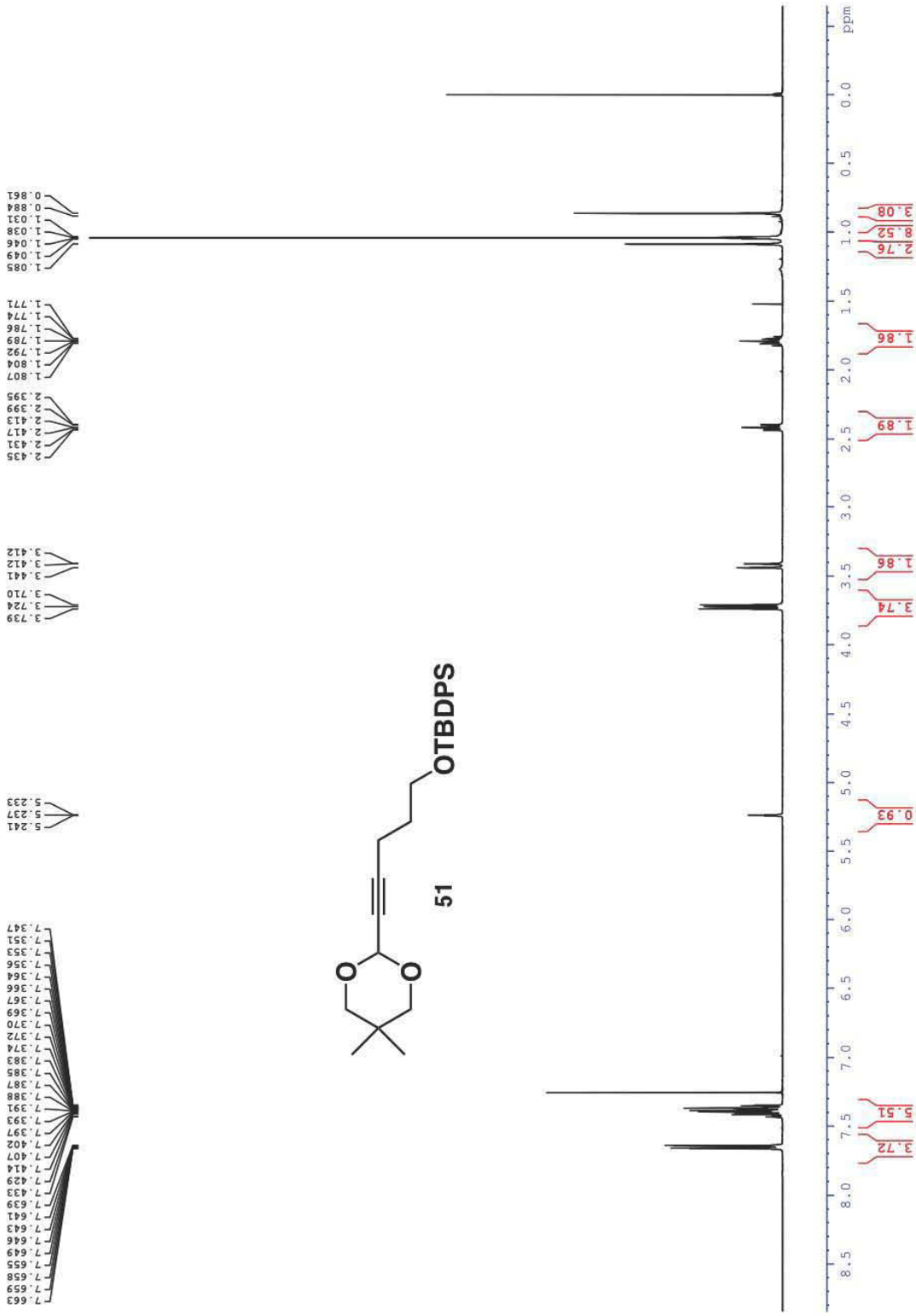
OTBDPS
51
ppm

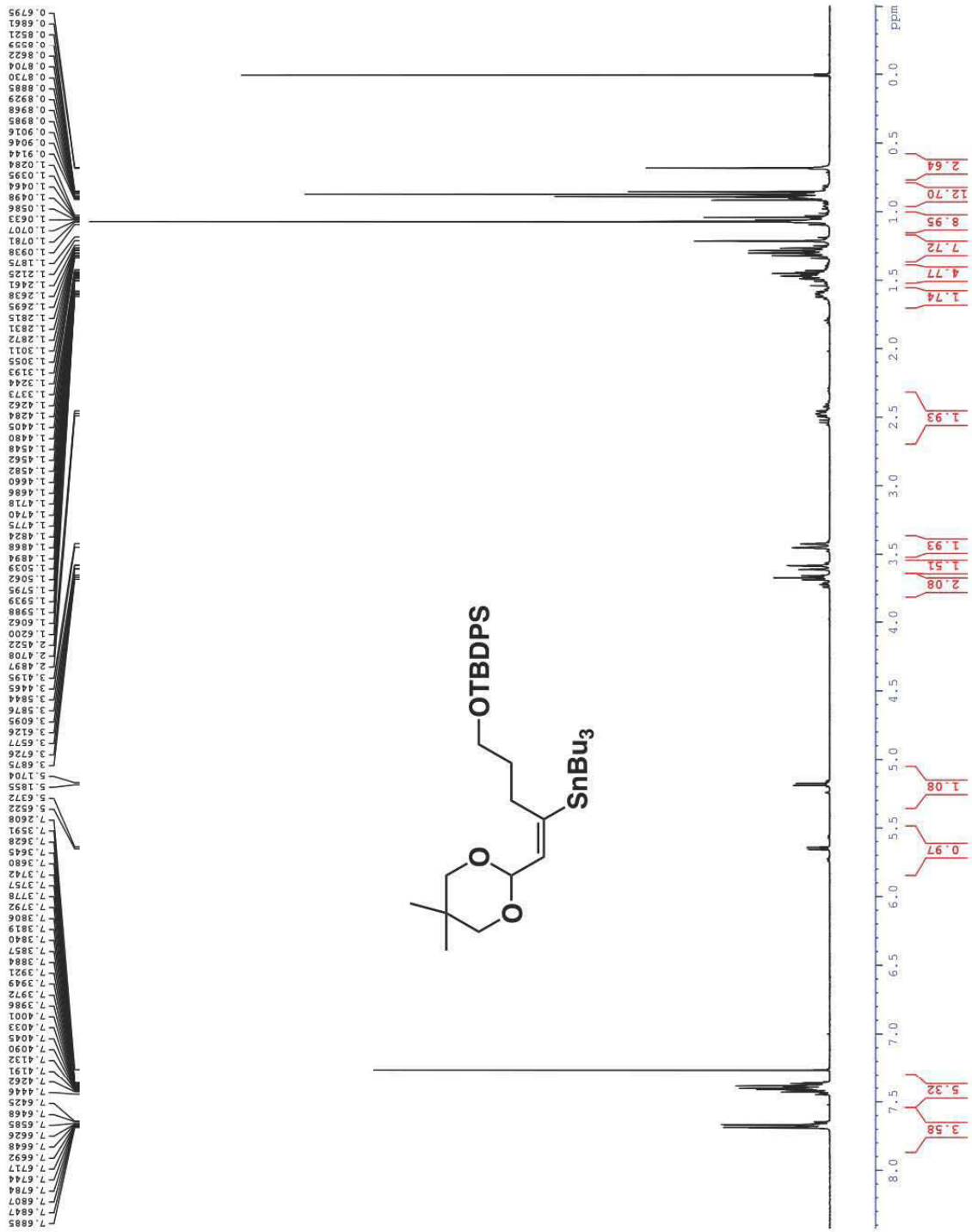
OTBDPS
SnBu3
ppm

OTBDPS
52
I
O
O
ppm

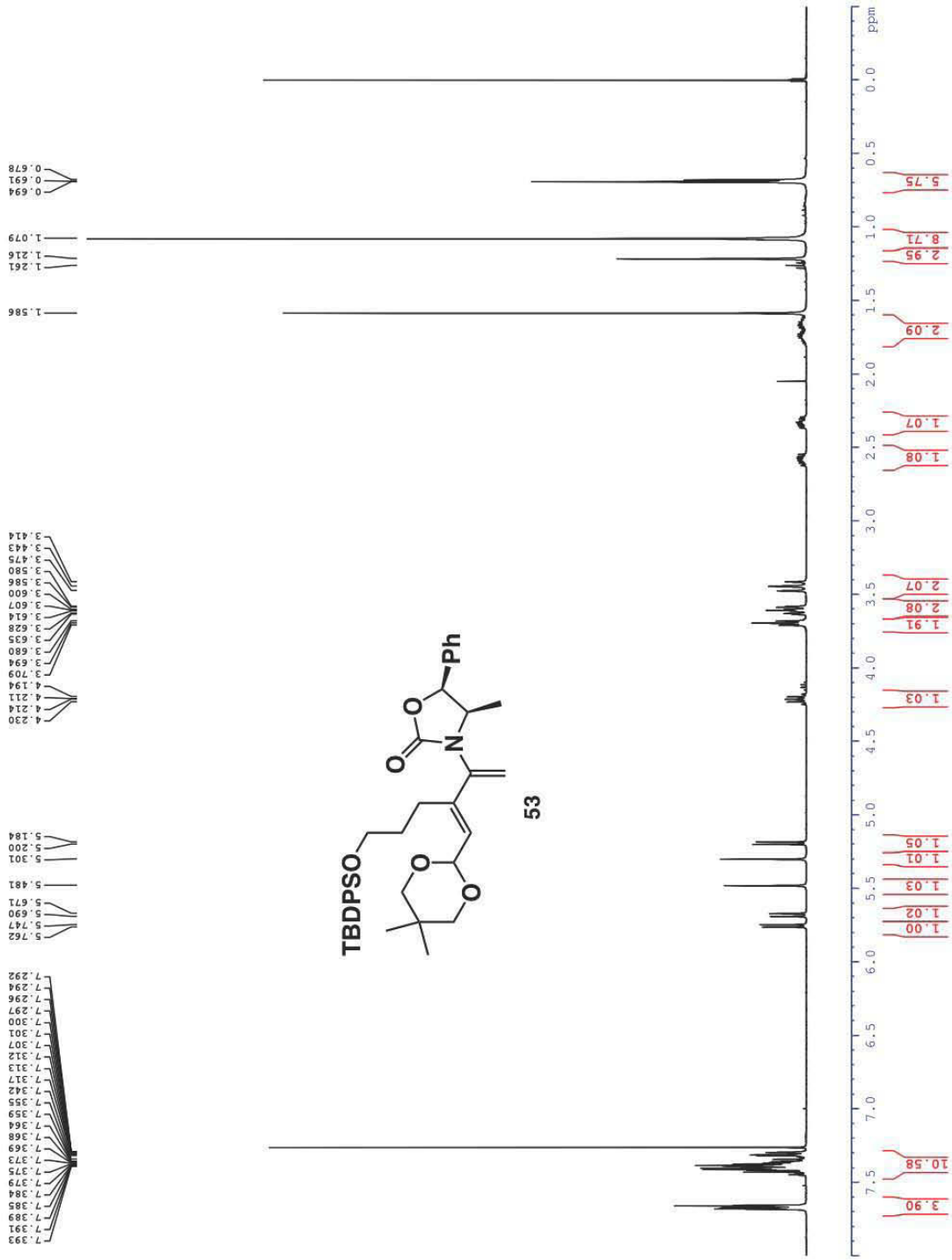
TBDPSO
Ph
O
N
O
O
O
53
ppm
0.0
0.5
1.0
1.5
2.0
2.5
3.0
3.5
4.0
4.5
5.0
5.5
6.0
6.5
7.0
7.5
5.75
8.71
2.95
2.09
1.07
1.08
2.07
2.08
1.91
1.03
1.05
1.01
1.03
1.02
1.00
10.58
3.90
0.678
0.691
0.694
1.079
1.216
1.261
1.586
3.414
3.443
3.475
3.580
3.586
3.600
3.607
3.614
3.628
3.635
3.680
3.694
3.709
4.194
4.211
4.214
4.230
5.184
5.200
5.301
5.481
5.671
5.690
5.747
5.762
7.292
7.294
7.296
7.297
7.300
7.301
7.307
7.312
7.313
7.317
7.342
7.355
7.359
7.364
7.368
7.369
7.373
7.375
7.379
7.384
7.385
7.389
7.391
7.393

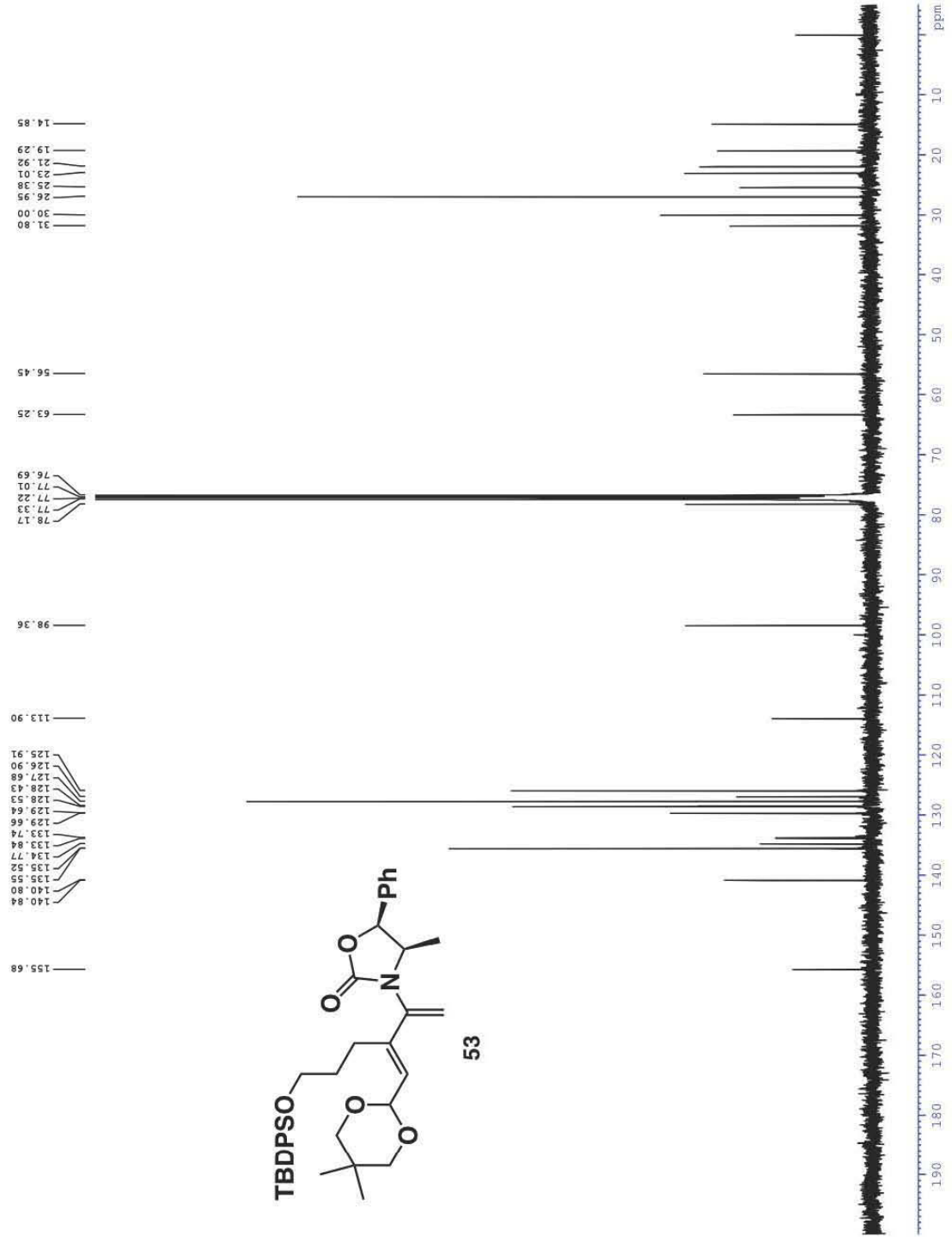
14.85
19.29
21.92
23.01
25.38
26.95
30.00
31.80
56.45
63.25
76.69
77.01
77.22
77.33
78.17
98.36
113.90
125.91
126.90
127.68
128.43
128.53
129.64
129.66
133.74
133.84
134.77
135.52
135.55
140.80
140.84
155.68
Ph
O
N
O
O
O
TBDPSO
53
ppm

TBDPSO
Ph
O
N
(CO)3Fe
54
ppm

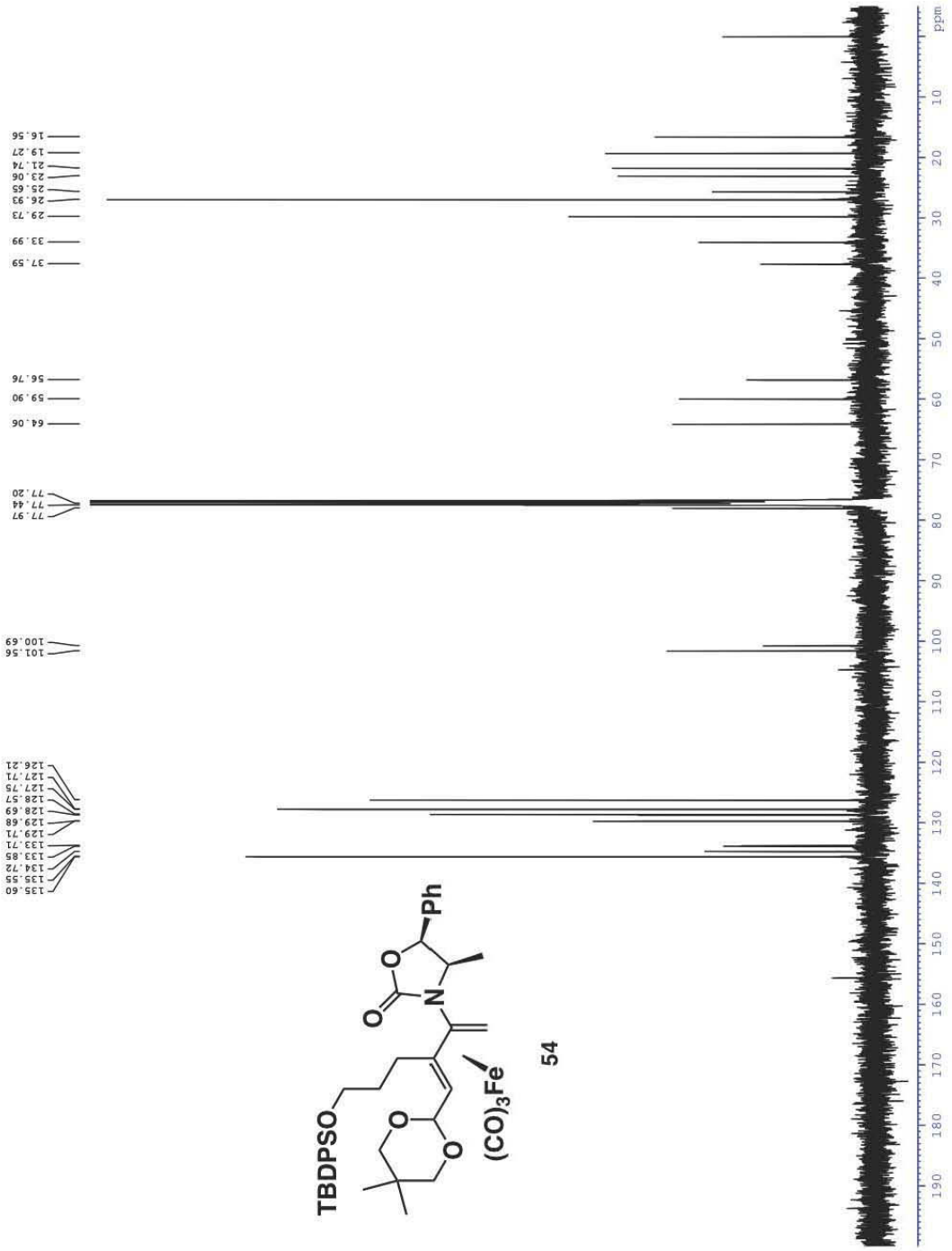
TBDPSO
Ph
O
N
O
O
O
(CO)3Fe
54
16.56
19.27
21.74
23.06
25.65
26.93
29.73
33.99
37.59
56.76
59.90
64.06
77.97
77.44
77.20
100.69
101.56
126.21
127.71
127.75
128.57
128.69
129.68
129.71
133.71
133.85
134.72
135.55
135.60
ppm

TBDPSO
Ph
O
N
O
O
O
55

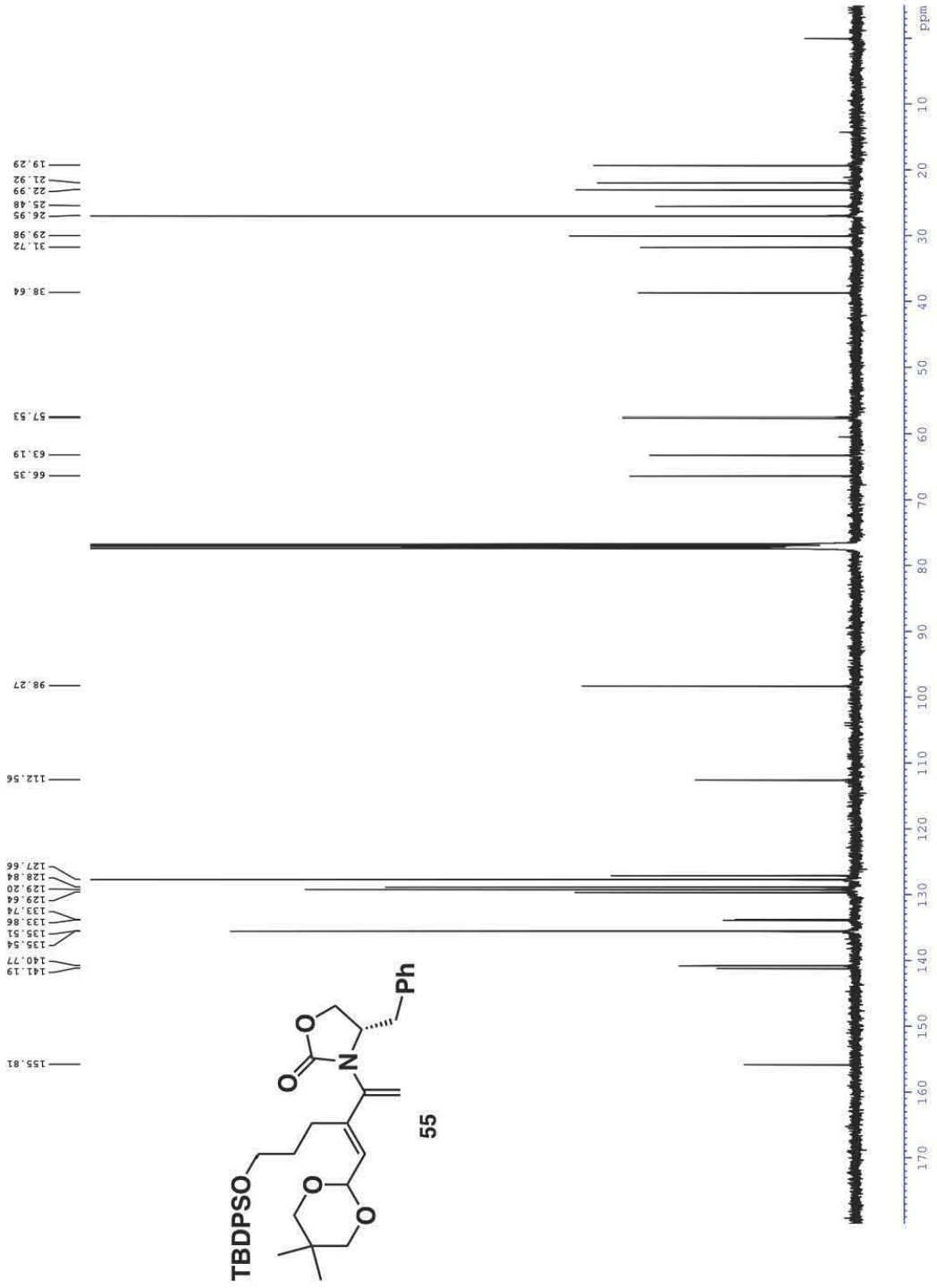
155.81
141.19
140.77
135.54
135.51
133.86
133.74
129.64
129.20
128.84
127.66
112.56
98.27
66.35
63.19
57.53
38.64
31.72
29.98
26.95
25.48
22.99
21.92
19.29
ppm
TBDPSO
Ph
55

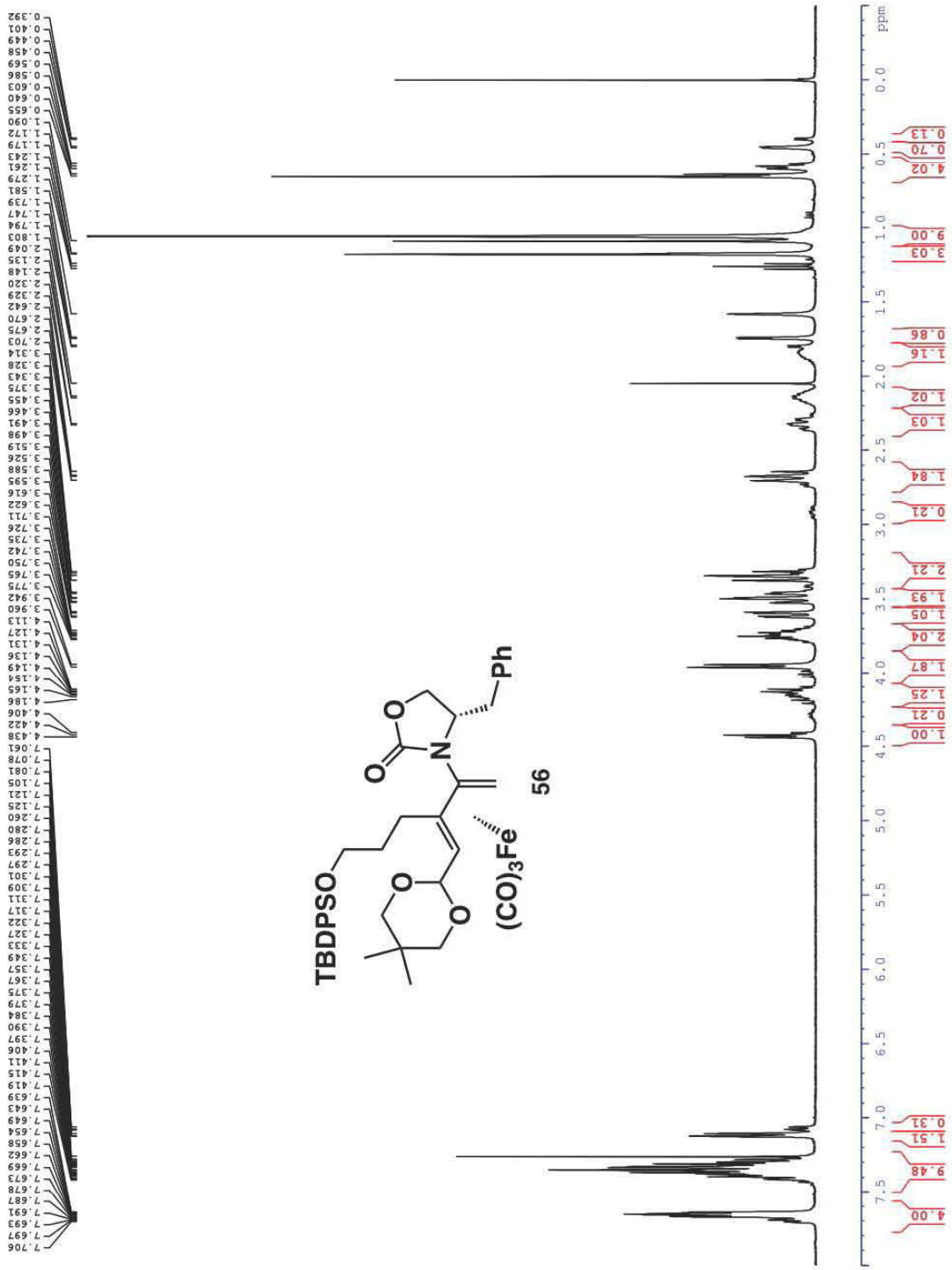
TBDPSO
O
O
N
O
O
Ph
(CO)3Fe
56
ppm

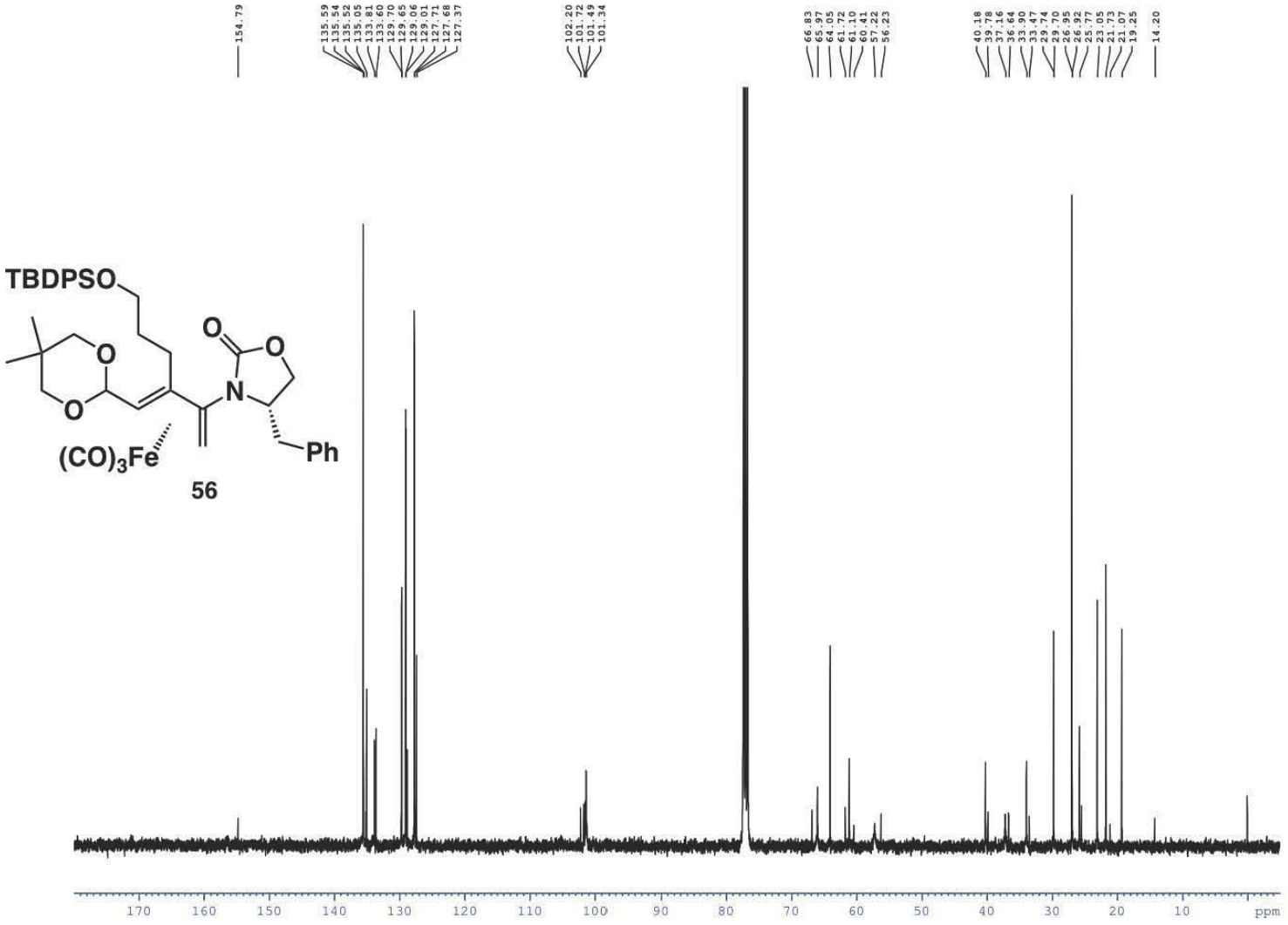
154.79
135.59
135.54
135.52
135.05
133.81
133.60
129.70
129.65
129.06
129.01
127.71
127.68
127.37
102.20
101.72
101.49
101.34
66.83
65.97
64.05
61.72
61.10
60.41
57.22
56.23
40.18
39.78
37.16
36.64
33.90
33.37
33.14
29.70
26.95
26.92
25.77
23.05
21.73
21.07
19.25
14.20
TBDPSO
O
O
O
O
N
(CO)3Fe
Ph
56
170
160
150
140
130
120
110
100
90
80
70
60
50
40
30
20
10
ppm

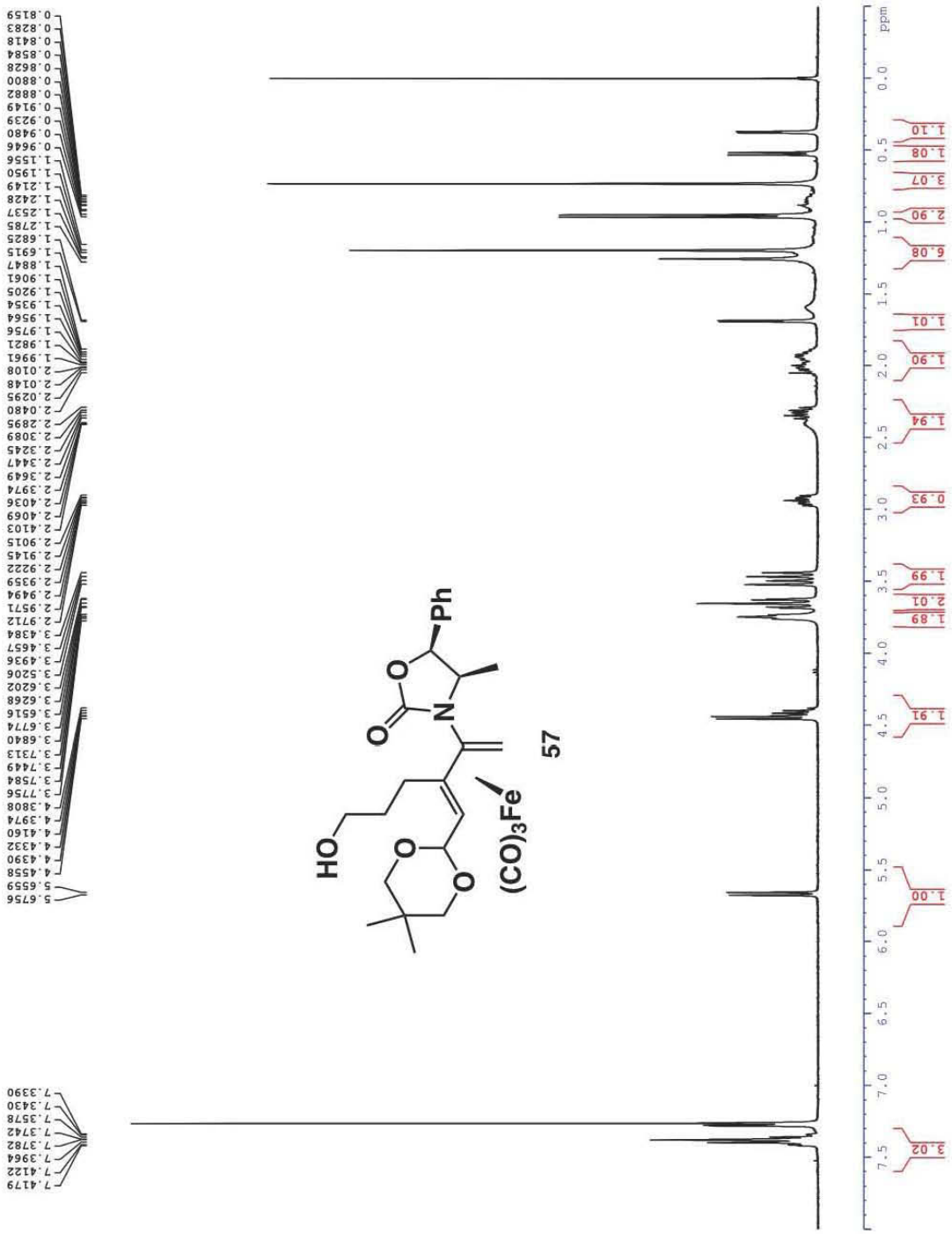
7.4179
7.4122
7.3964
7.3782
7.3742
7.3578
7.3430
7.3390
5.6756
5.6559
4.4558
4.4390
4.4332
4.4160
4.3974
4.3808
3.7756
3.7584
3.7449
3.7313
3.6840
3.6774
3.6516
3.6268
3.6202
3.5206
3.4936
3.4657
3.4384
2.9712
2.9571
2.9494
2.9359
2.9222
2.9145
2.9015
2.4103
2.4069
2.4036
2.3974
2.3649
2.3447
2.3245
2.3089
2.2895
2.0480
2.0295
2.0148
2.0108
1.9961
1.9821
1.9756
1.9564
1.9354
1.9205
1.9061
1.8847
1.6915
1.6825
1.2785
1.2537
1.2428
1.2149
1.1950
1.1556
0.9646
0.9480
0.9239
0.9149
0.8882
0.8800
0.8628
0.8584
0.8418
0.8283
0.8159
HO
O
O
O
N
O
Ph
(CO)3Fe
57
ppm
3.02
1.00
1.91
1.89
2.01
1.99
0.93
1.94
1.90
1.01
6.08
2.90
3.07
1.08
1.10

16.88
21.78
23.07
24.97
29.71
29.85
33.39
38.00
56.29
60.03
61.94
77.61
78.25
100.98
102.14
103.99
126.24
128.64
128.75
134.71
Ph
O
O
N
HO
O
O
(CO)3Fe
57
ppm

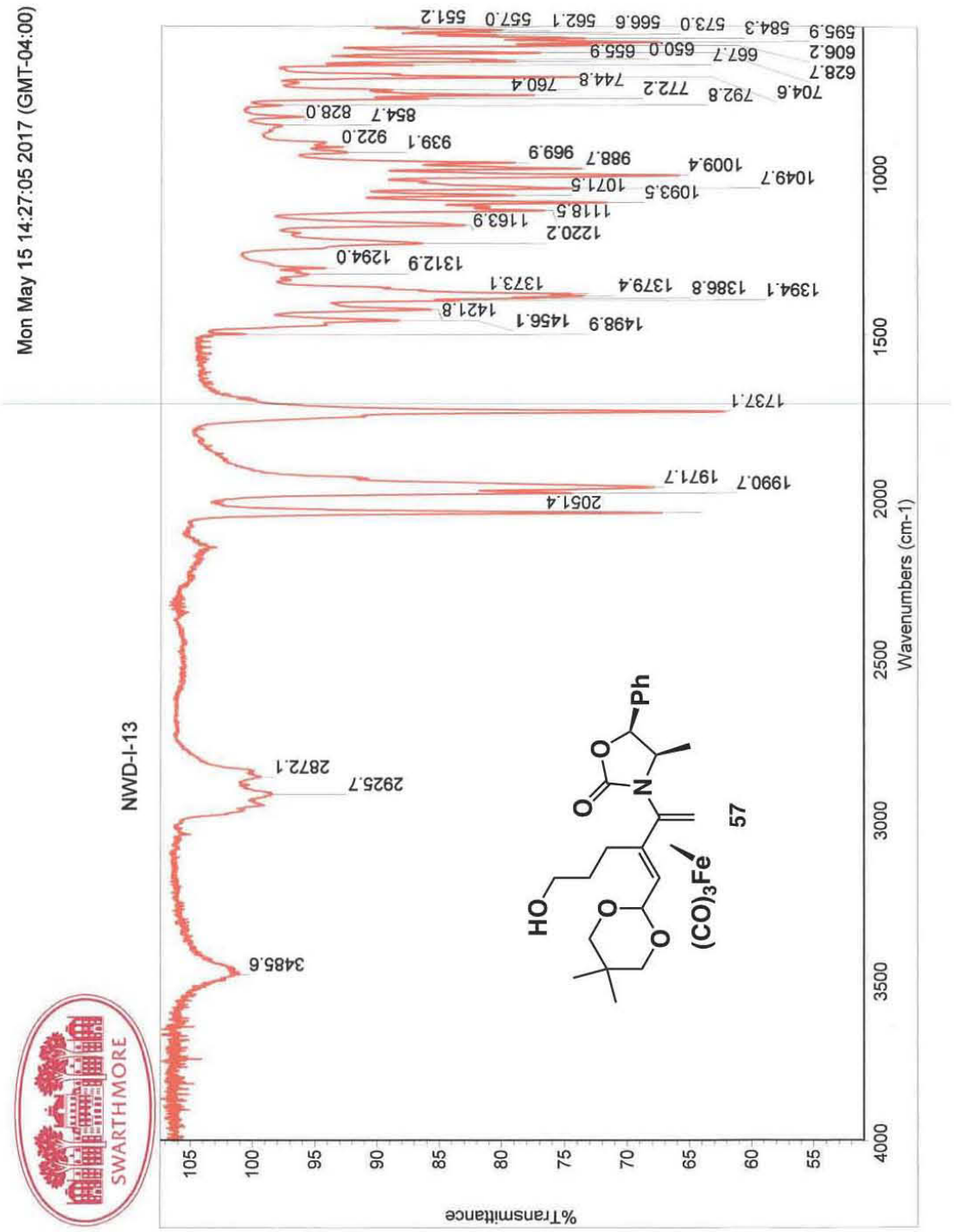
Mon May 15 14:27:05 2017 (GMT-04:00)
NWD-I-13
%Transmittance
Wavenumbers (cm-1)
4000
3500
3000
2500
2000
1500
1000
105
100
95
90
85
80
75
70
65
60
55
3485.6
2925.7
2872.1
2051.4
1990.7
1971.7
1737.1
1498.9
1456.1
1421.8
1394.1
1386.8
1379.4
1373.1
1312.9
1294.0
1220.2
1163.9
1118.5
1093.5
1071.5
1049.7
1009.4
988.7
969.9
939.1
922.0
854.7
828.0
792.8
772.2
744.8
760.4
704.6
667.7
650.0
655.9
628.7
606.2
595.9
584.3
573.0
566.6
562.1
557.0
551.2
Ph
O
O
N
HO
O
O
(CO)3Fe
57

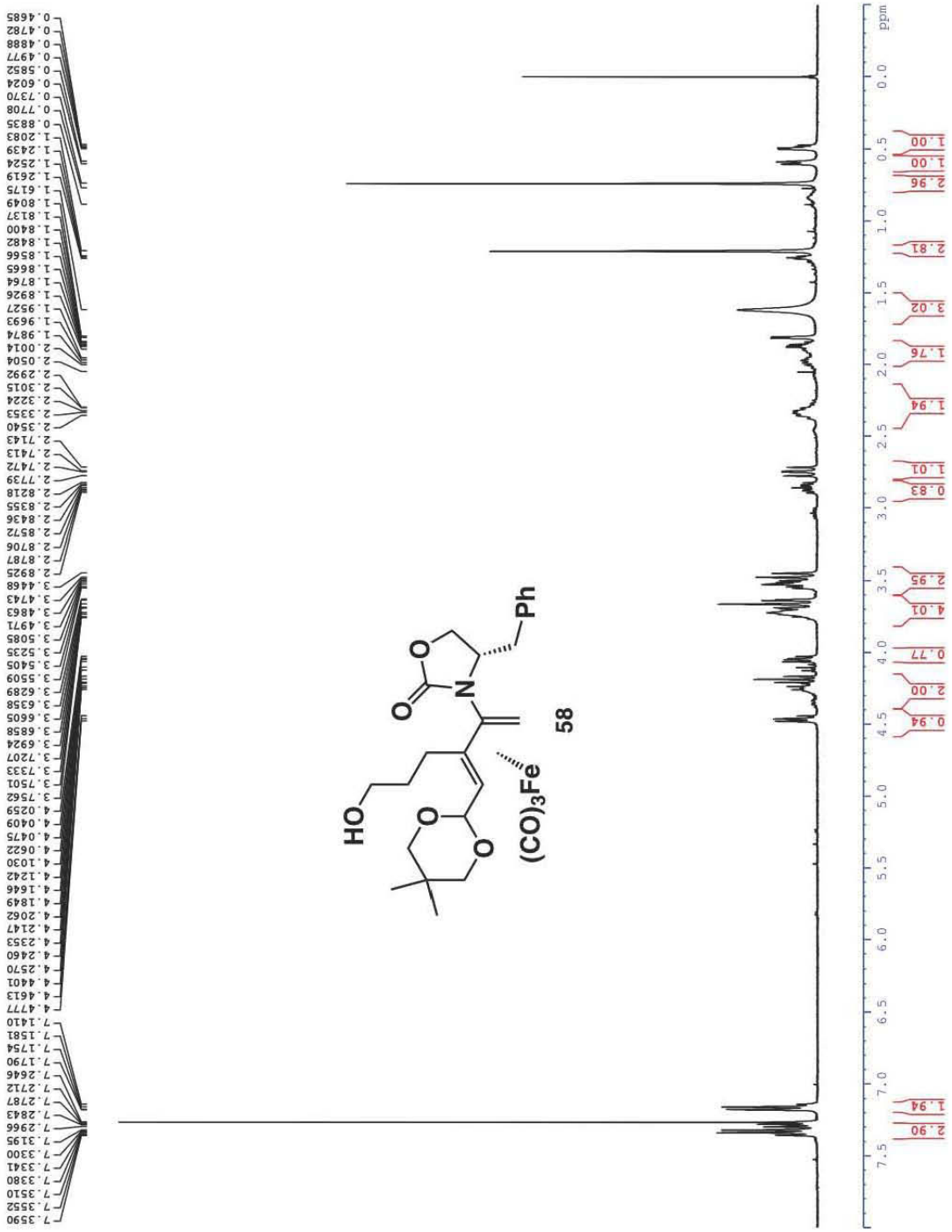
HO
O
O
N
O
O
Ph
(CO)3Fe
58
ppm

9.3608
9.3442
7.6601
7.6564
7.6482
7.6445
7.6409
7.6367
7.6287
7.6248
7.4559
7.4474
7.4371
7.4303
7.4194
7.4038
7.4011
7.3853
7.3691
7.3647
4.0587
4.0549
4.0406
3.9155
3.9073
3.9018
3.8933
3.8892
3.8830
3.7668
3.7555
3.7410
3.7337
3.7262
3.7175
3.7025
2.7849
2.7693
2.7622
2.7521
2.7465
2.7349
2.7291
2.7124
2.3319
2.3236
2.3146
2.1581
2.1488
1.8271
1.8126
1.8042
1.7985
1.7902
1.7752
1.6699
1.4424
1.0582
0.9100
0.9065
0.9002
0.8931
0.8889
0.8835
0.8660
0.7767
0.7674
0.7103
0.6936
TBDPSO
O
O
N
O
H
(CO)3Fe
60
ppm
9.5
9.0
8.5
8.0
7.5
7.0
6.5
6.0
5.5
5.0
4.5
4.0
3.5
3.0
2.5
2.0
1.5
1.0
0.5
0.0
1.00
4.04
6.07
1.95
1.01
2.09
2.02
1.04
1.03
2.06
9.16
11.96
1.11
1.10

TBDPSO
O
O
N
Ph
O
H
(CO)3Fe
61
ppm

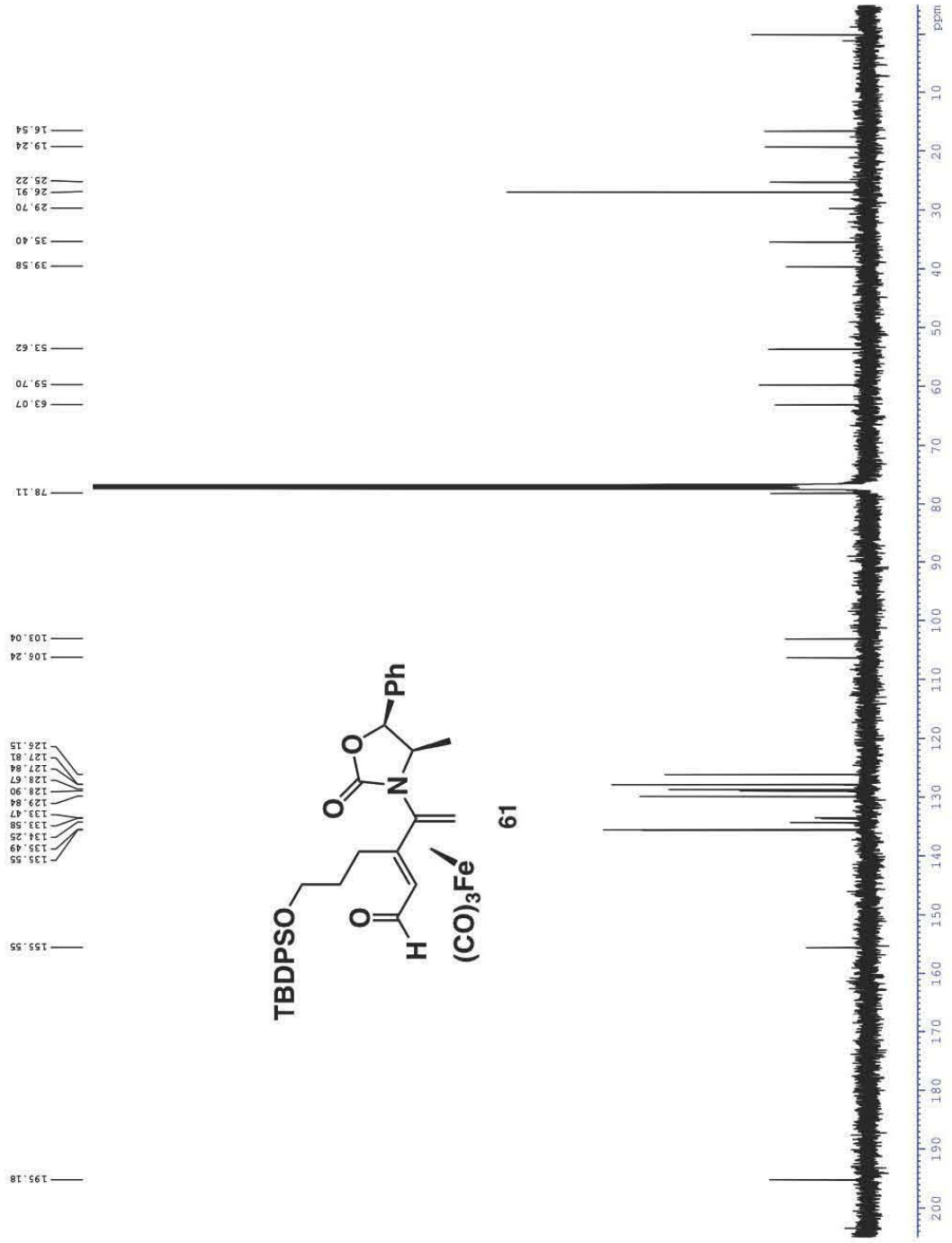
TBDPSO
O
O
N
Ph
O
H
(CO)3Fe
61
195.18
155.55
135.55
135.49
134.25
133.58
133.47
129.84
128.90
128.67
127.84
127.81
126.15
106.24
103.04
78.11
63.07
59.70
53.62
39.58
35.40
29.70
26.91
25.22
19.24
16.54
ppm

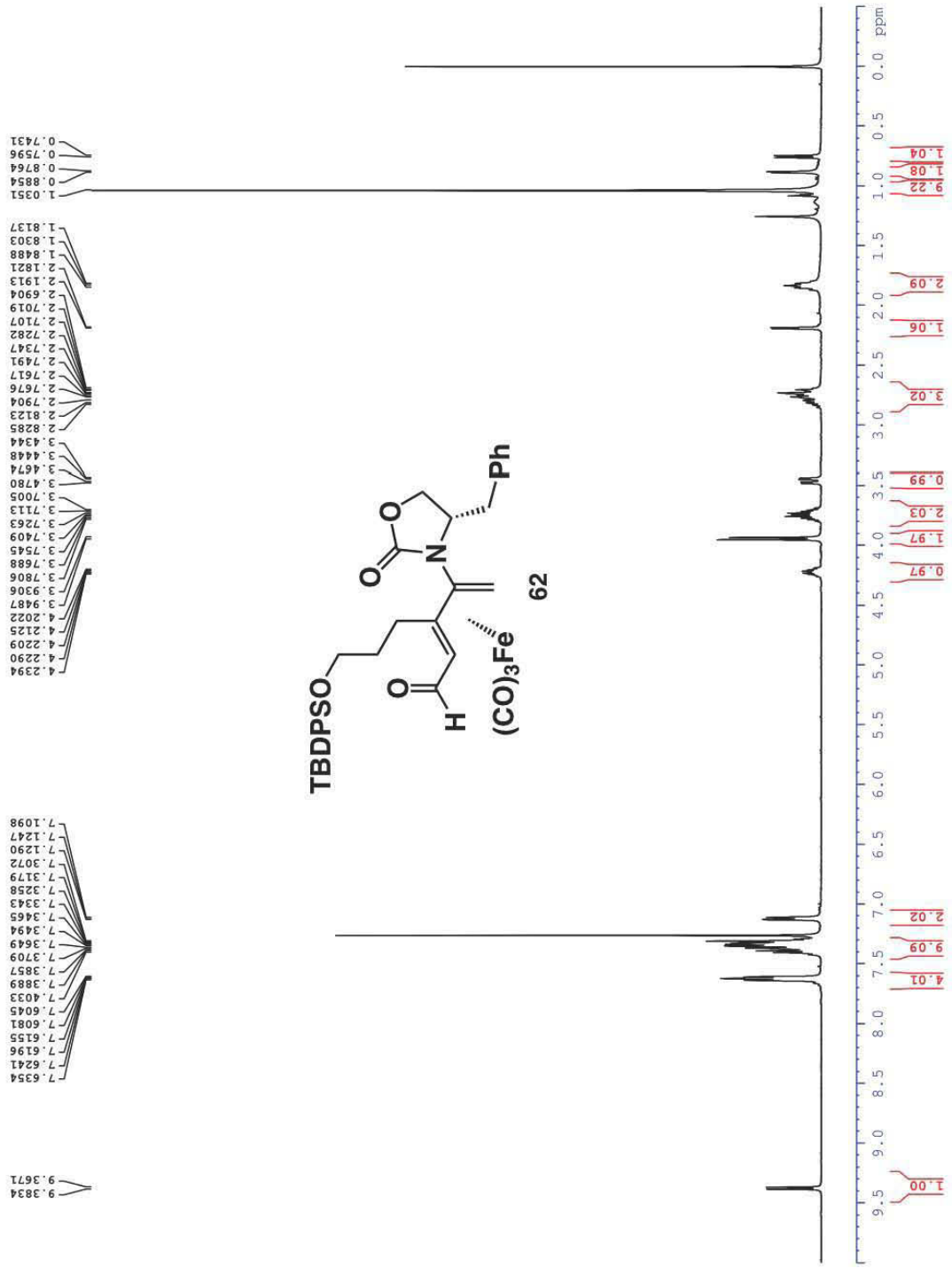
TBDPSO
O
O
N
Ph
O
H
(CO)3Fe
62
ppm

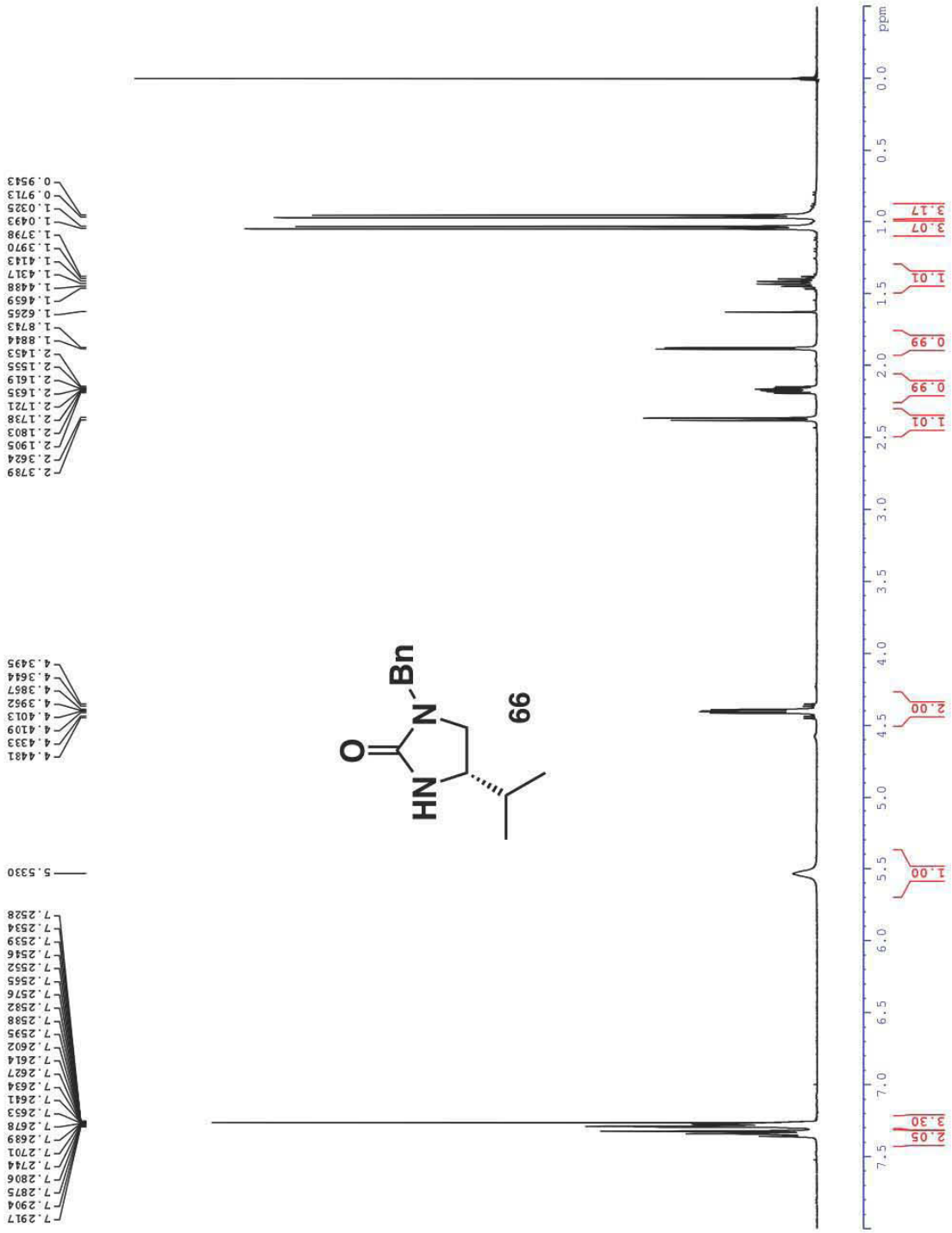
66
Bn
N
HN
O
ppm
0.0
0.5
1.0
1.5
2.0
2.5
3.0
3.5
4.0
4.5
5.0
5.5
6.0
6.5
7.0
7.5
3.17
3.07
1.01
0.99
0.99
1.01
2.00
1.00
3.30
2.05
0.9543
0.9713
1.0325
1.0493
1.3798
1.3970
1.4143
1.4317
1.4488
1.4659
1.6265
1.8743
1.8844
2.1453
2.1555
2.1619
2.1635
2.1721
2.1738
2.1803
2.1905
2.3624
2.3789
4.3435
4.3614
4.3867
4.3962
4.4013
4.4109
4.4333
4.4481
5.5330
7.2528
7.2534
7.2539
7.2546
7.2552
7.2555
7.2576
7.2582
7.2588
7.2595
7.2602
7.2614
7.2627
7.2634
7.2641
7.2653
7.2678
7.2689
7.2701
7.2744
7.2806
7.2875
7.2904
7.2917

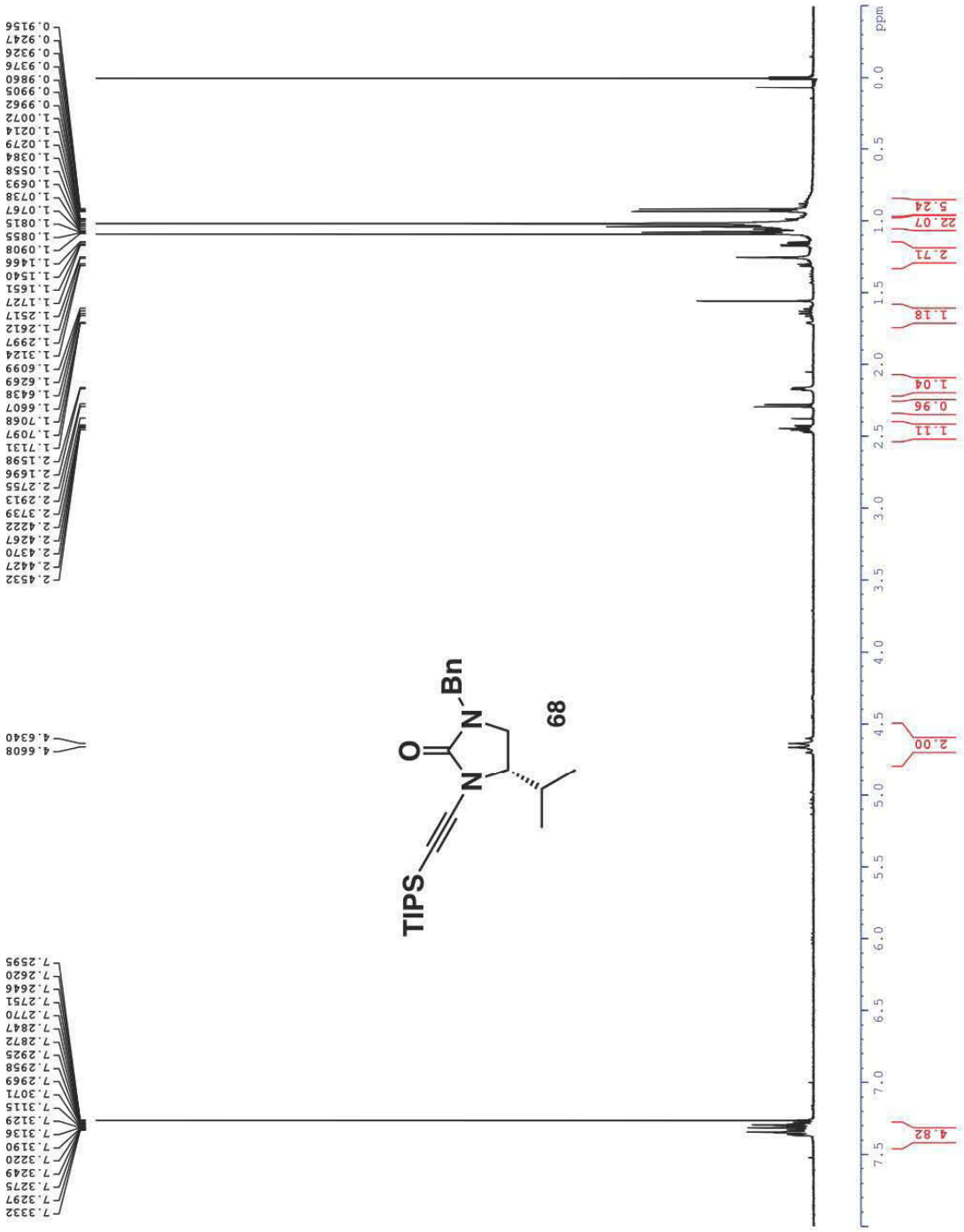
7.3332
7.3297
7.3275
7.3249
7.3220
7.3190
7.3136
7.3129
7.3115
7.3071
7.2969
7.2958
7.2925
7.2872
7.2847
7.2770
7.2751
7.2646
7.2620
7.2595
4.6608
4.6340
2.4532
2.4427
2.4370
2.4267
2.4222
2.3739
2.2913
2.2755
2.1696
2.1598
1.7131
1.7097
1.7068
1.6607
1.6438
1.6269
1.6099
1.3124
1.2997
1.2612
1.2517
1.1727
1.1651
1.1540
1.1466
1.0908
1.0855
1.0815
1.0767
1.0738
1.0693
1.0558
1.0384
1.0279
1.0214
1.0072
0.9962
0.9905
0.9860
0.9376
0.9326
0.9247
0.9156
O
N
Bn
N
TIPS
68
ppm
0.0
0.5
1.0
1.5
2.0
2.5
3.0
3.5
4.0
4.5
5.0
5.5
6.0
6.5
7.0
7.5
4.82
2.00
1.04
0.96
1.11
1.18
2.71
22.07
5.24

7.3312
7.3278
7.3227
7.3195
7.3134
7.3065
7.3044
7.3018
7.2951
7.2914
7.2858
7.2830
7.2803
7.2626
4.6727
4.6676
4.6538
3.0869
2.9699
2.5647
2.4854
2.4561
2.4457
2.4399
2.4294
2.4234
2.4131
2.3543
2.3354
2.3195
2.2358
2.1711
2.1608
2.1373
1.7348
1.7319
1.7152
1.6982
1.6814
1.6646
1.6477
1.5823
1.5778
1.5760
1.1542
1.1154
1.0851
1.0796
1.0555
1.0525
1.0406
1.0335
1.0150
0.9986
0.9817
0.9788
0.9655
0.9618
0.9526
0.9487
0.9441
0.9297
0.9236
0.9199
0.9126
0.9064
0.8959
0.8897
0.8834
0.8800
0.8726
0.8627
0.8520
0.8433
0.8276
0.8069
5.076
2.000
0.957
1.089
1.082
1.089
1.084
9.011
4.533
H
N
O
N
Bn
69
6
4
2
0
[ppm]
0
5
10
[*1e6]

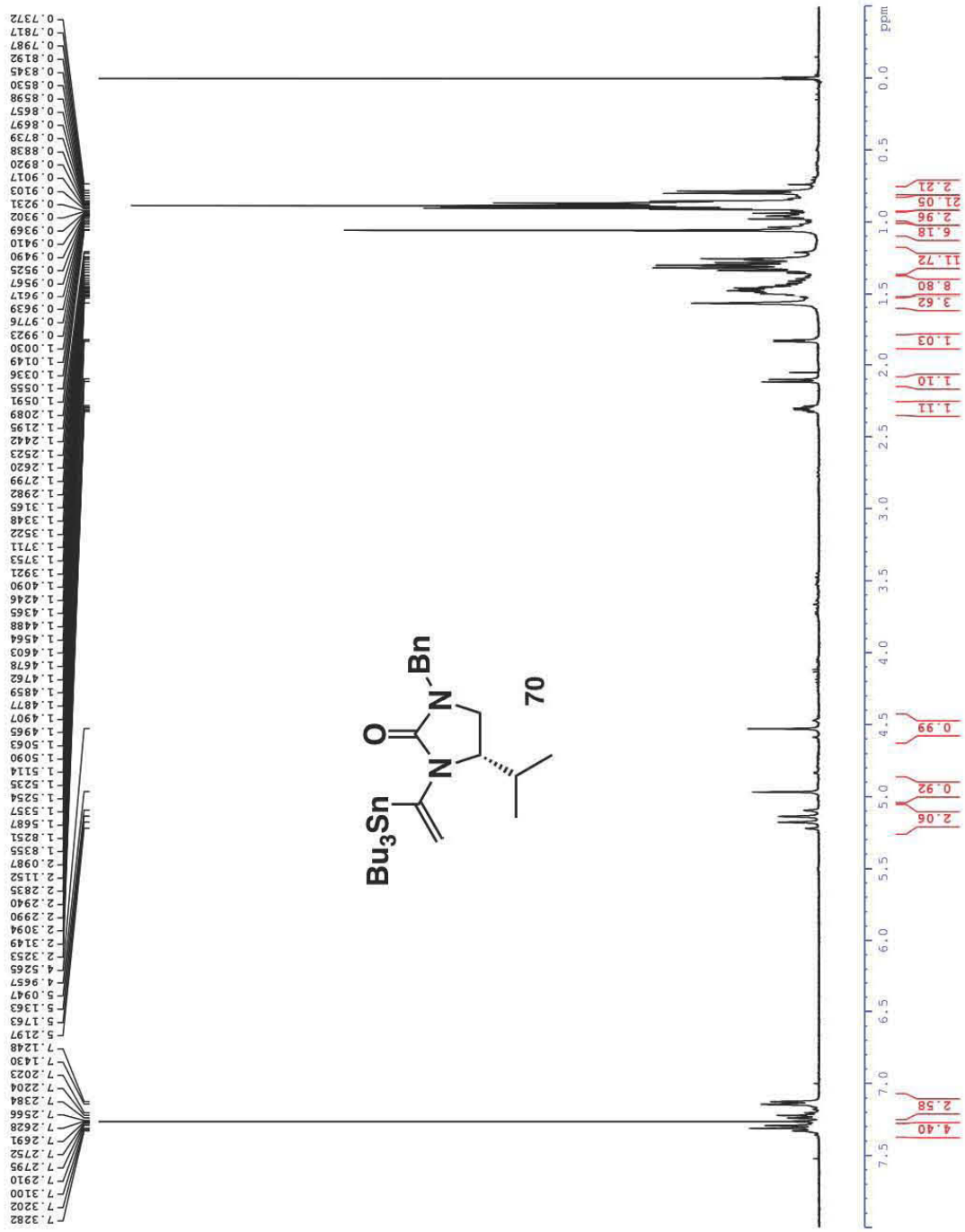
Bu3Sn
O
N
N
Bn
70
ppm

4.9059
4.8397
3.7284
3.7217
3.7159
3.7074
3.6969
3.6827
3.6793
3.6168
3.6024
3.5911
3.5857
3.5787
3.5746
3.5669
3.5609
3.5496
3.5375
3.5293
3.5198
3.5133
3.5028
3.1790
3.1616
3.1470
3.1295
1.8633
1.8465
1.8380
1.8296
1.8129
1.5136
1.4967
1.4893
1.4772
1.4709
1.4593
1.4406
1.3932
1.3754
1.3568
1.3367
1.3190
1.3013
0.9619
0.9456
0.9400
0.9291
0.9215
0.9034
OH
HN
O
H
N
Bu
71a
9.06
2.06
1.99
1.21
2.01
3.03
0.98
2.00
ppm

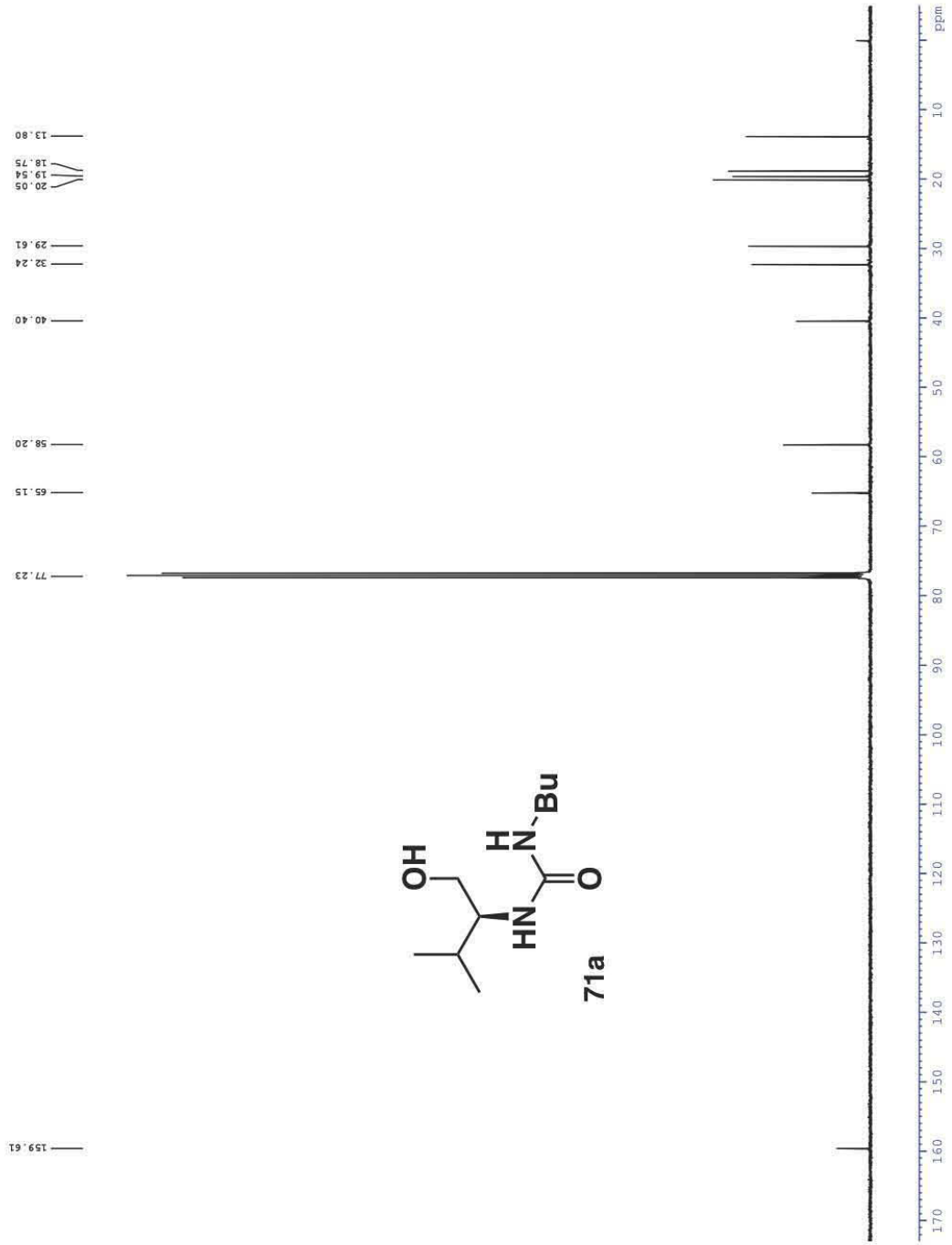
13.80
18.75
19.54
20.05
29.61
32.24
40.40
58.20
65.15
77.23
159.61
ppm
10
20
30
40
50
60
70
80
90
100
110
120
130
140
150
160
170
OH
HN
O
H
N
Bu
71a

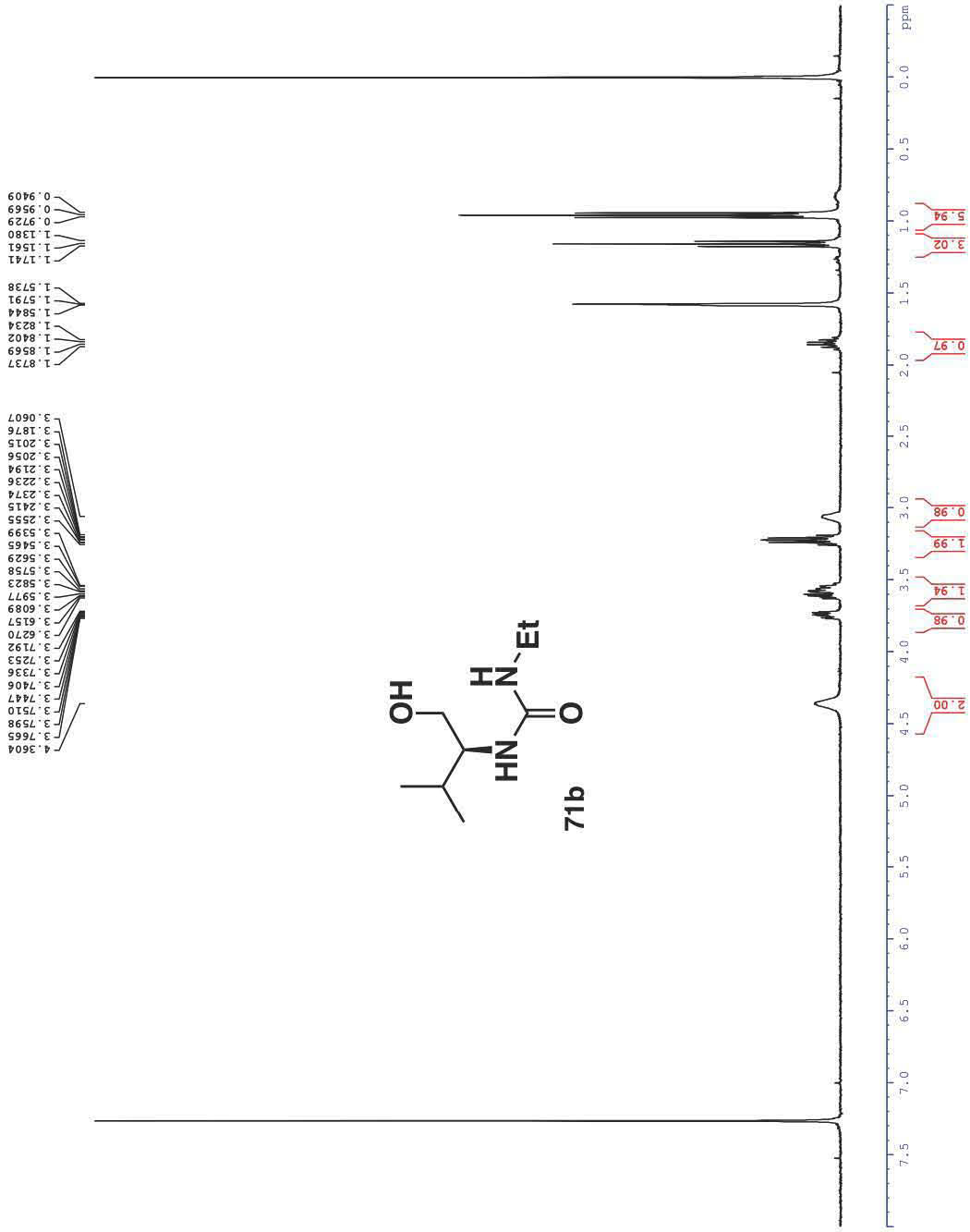
0.9409
0.9569
0.9729
1.1380
1.1561
1.1741
1.5738
1.5791
1.5844
1.8234
1.8402
1.8569
1.8737
3.0607
3.1876
3.2015
3.2056
3.2194
3.2236
3.2374
3.2415
3.2555
3.5399
3.5465
3.5629
3.5758
3.5823
3.5977
3.6089
3.6157
3.6270
3.7192
3.7253
3.7336
3.7406
3.7447
3.7510
3.7598
3.7665
4.3604
OH
HN
O
H
N
Et
71b
5.94
3.02
0.97
0.98
1.99
1.94
0.98
2.00
ppm

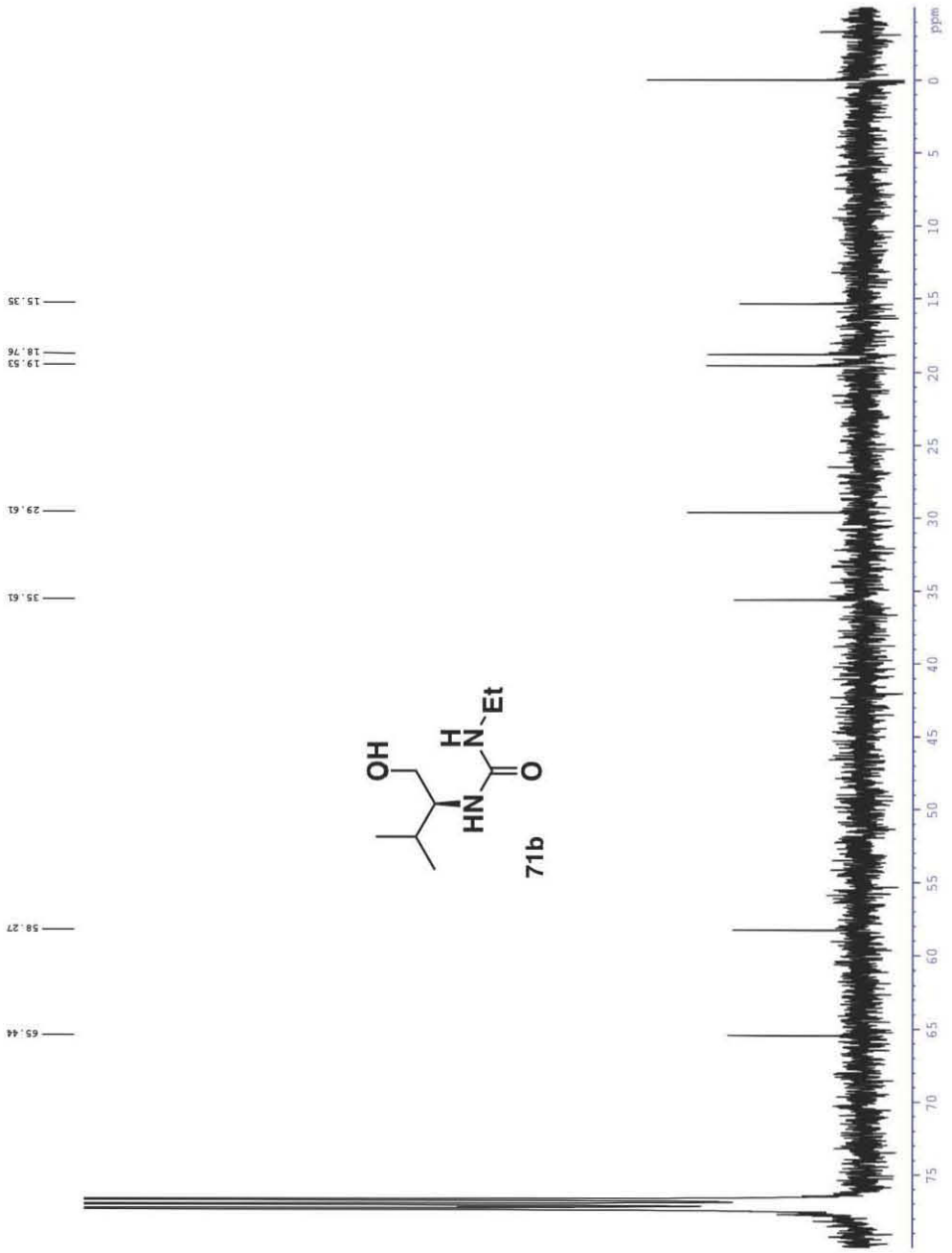
15.35
18.76
19.53
29.61
35.61
58.27
65.44
OH
HN
H
N
Et
O
71b
ppm

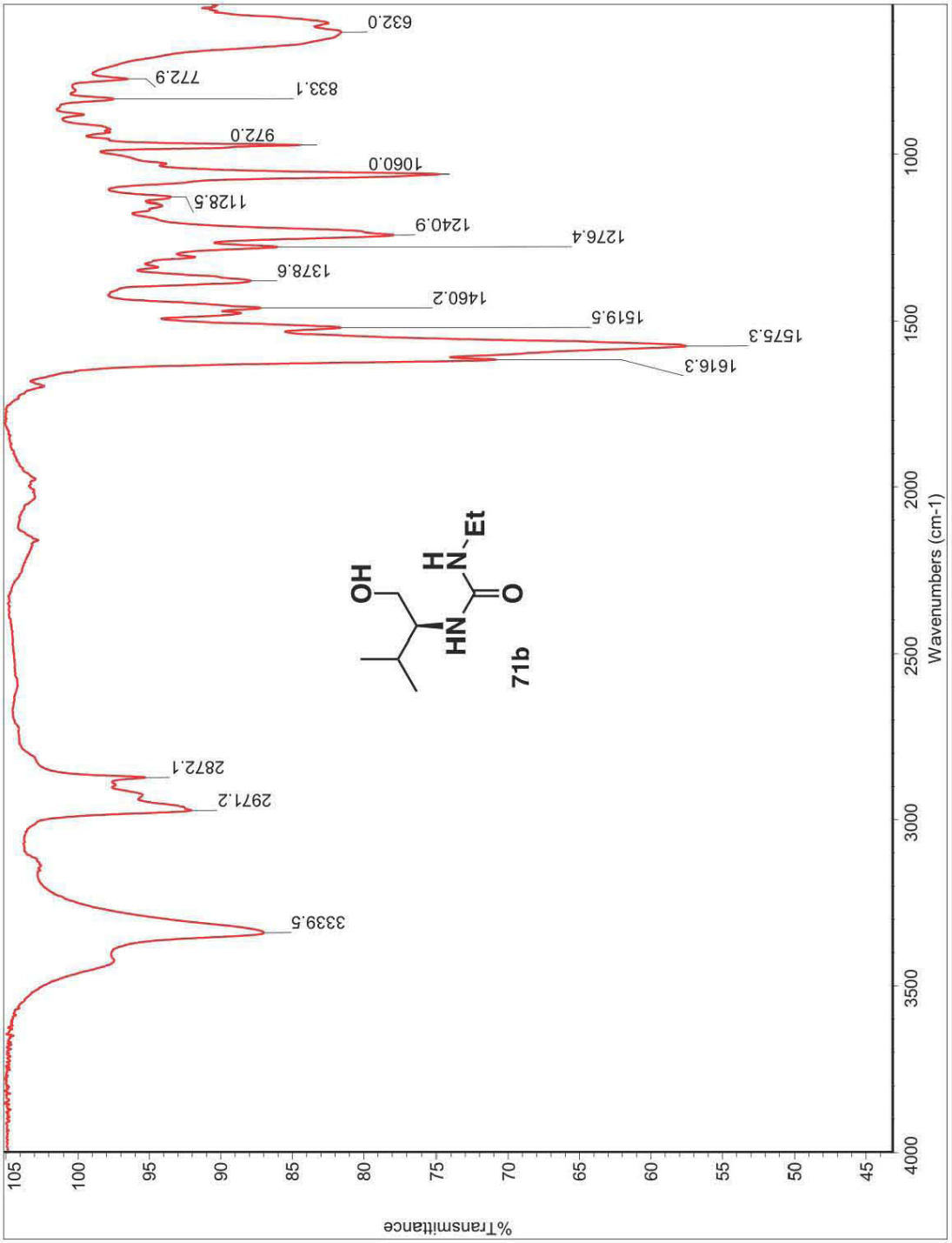
%Transmittance
Wavenumbers (cm-1)
4000
3500
3000
2500
2000
1500
1000
105
100
95
90
85
80
75
70
65
60
55
50
45
3339.5
2971.2
2872.1
1616.3
1575.3
1519.5
1460.2
1378.6
1276.4
1240.9
1128.5
1060.0
972.0
833.1
772.9
632.0
OH
HN
O
H
N
Et
71b

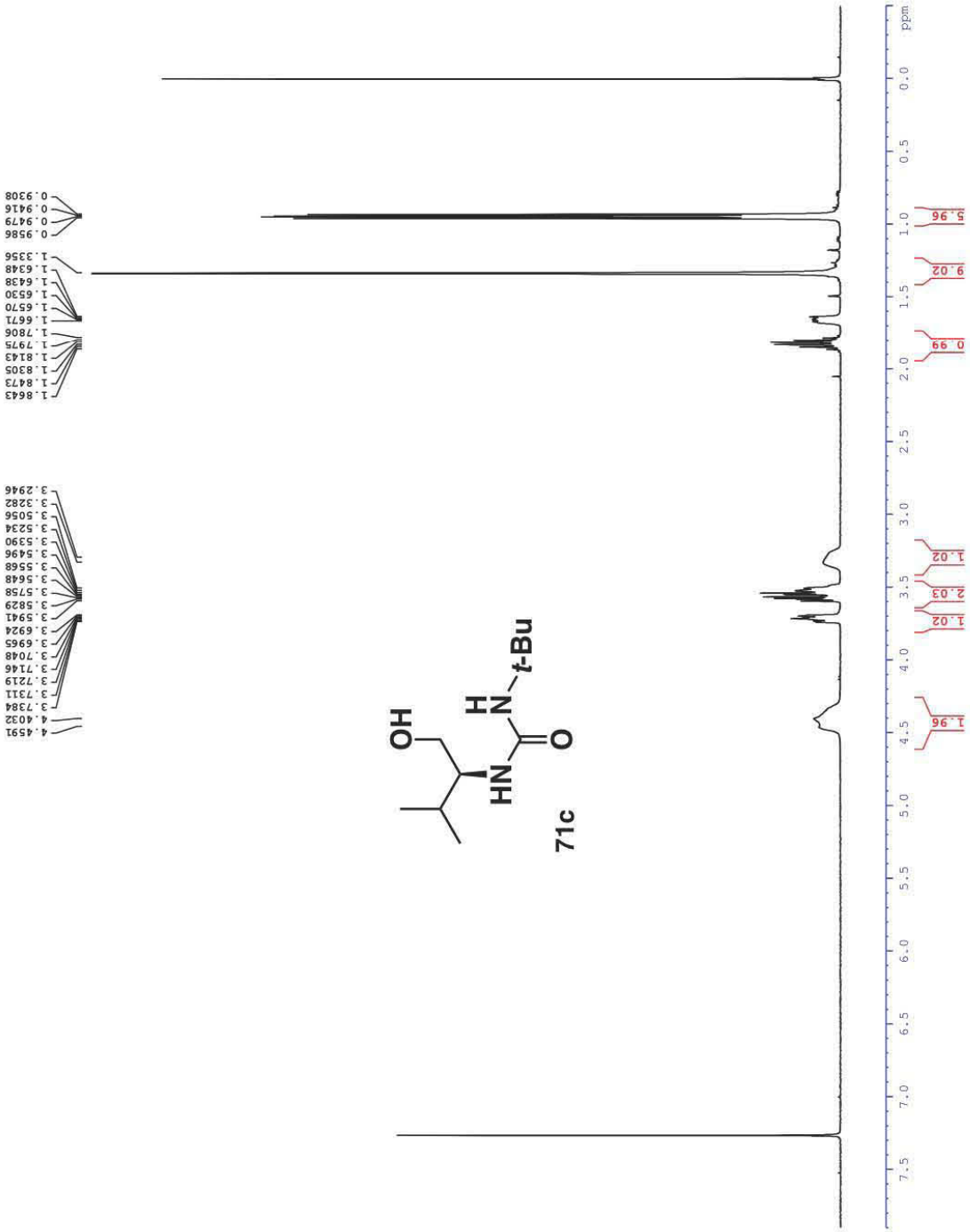
0.9308
0.9416
0.9479
0.9586
1.3356
1.6348
1.6438
1.6530
1.6570
1.6671
1.7806
1.7975
1.8143
1.8305
1.8473
1.8643
3.2946
3.3282
3.5056
3.5234
3.5390
3.5496
3.5568
3.5648
3.5758
3.5829
3.5941
3.6924
3.6965
3.7048
3.7146
3.7219
3.7311
3.7384
4.4032
4.4591
OH
HN
O
H
N
t-Bu
71c
ppm
0.0
0.5
1.0
1.5
2.0
2.5
3.0
3.5
4.0
4.5
5.0
5.5
6.0
6.5
7.0
7.5
5.96
9.02
0.99
1.02
2.03
1.02
1.96

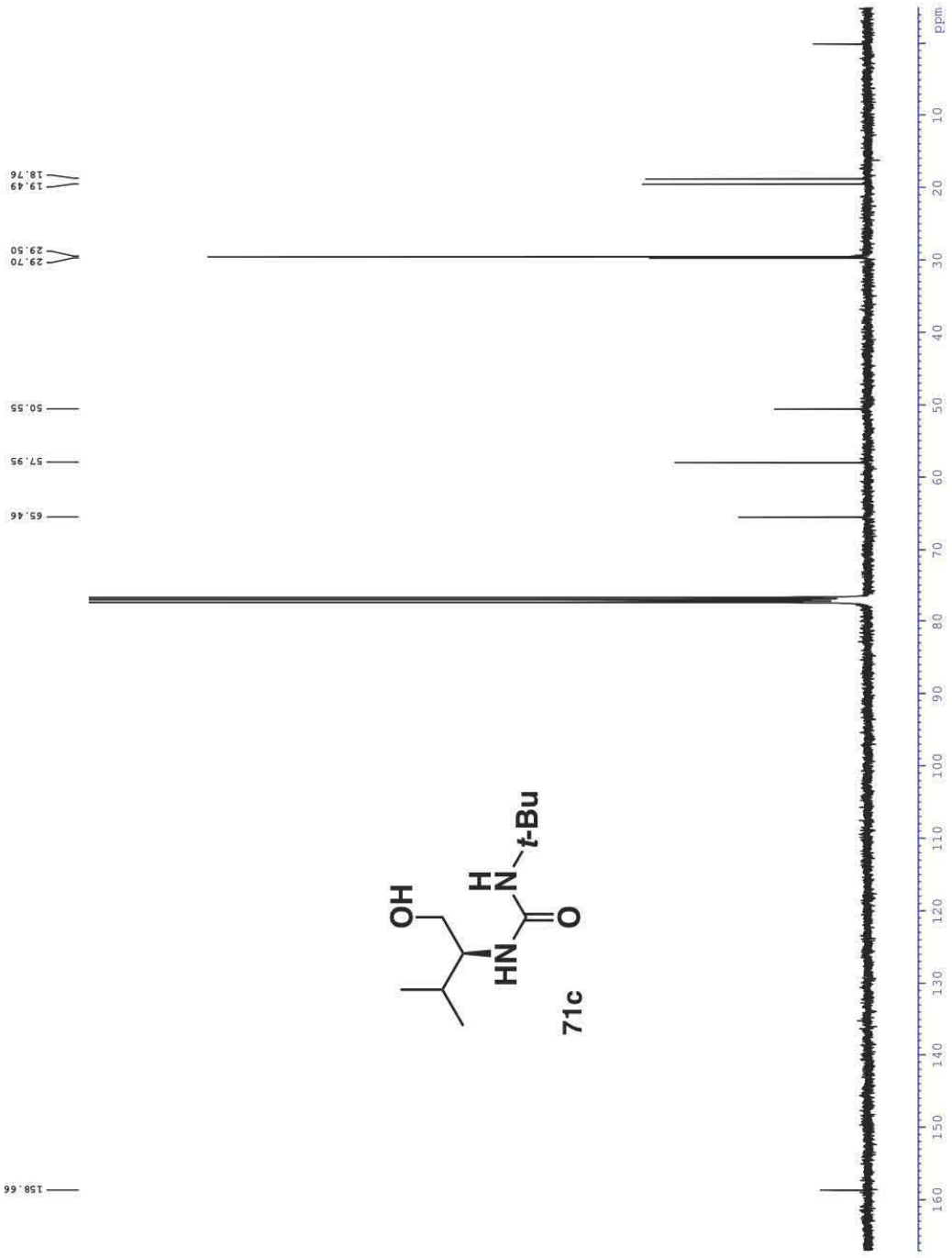
158.66
65.46
57.95
50.55
29.70
29.50
19.49
18.76
ppm
10
20
30
40
50
60
70
80
90
100
110
120
130
140
150
160
OH
HN
O
H
N
t-Bu

71c

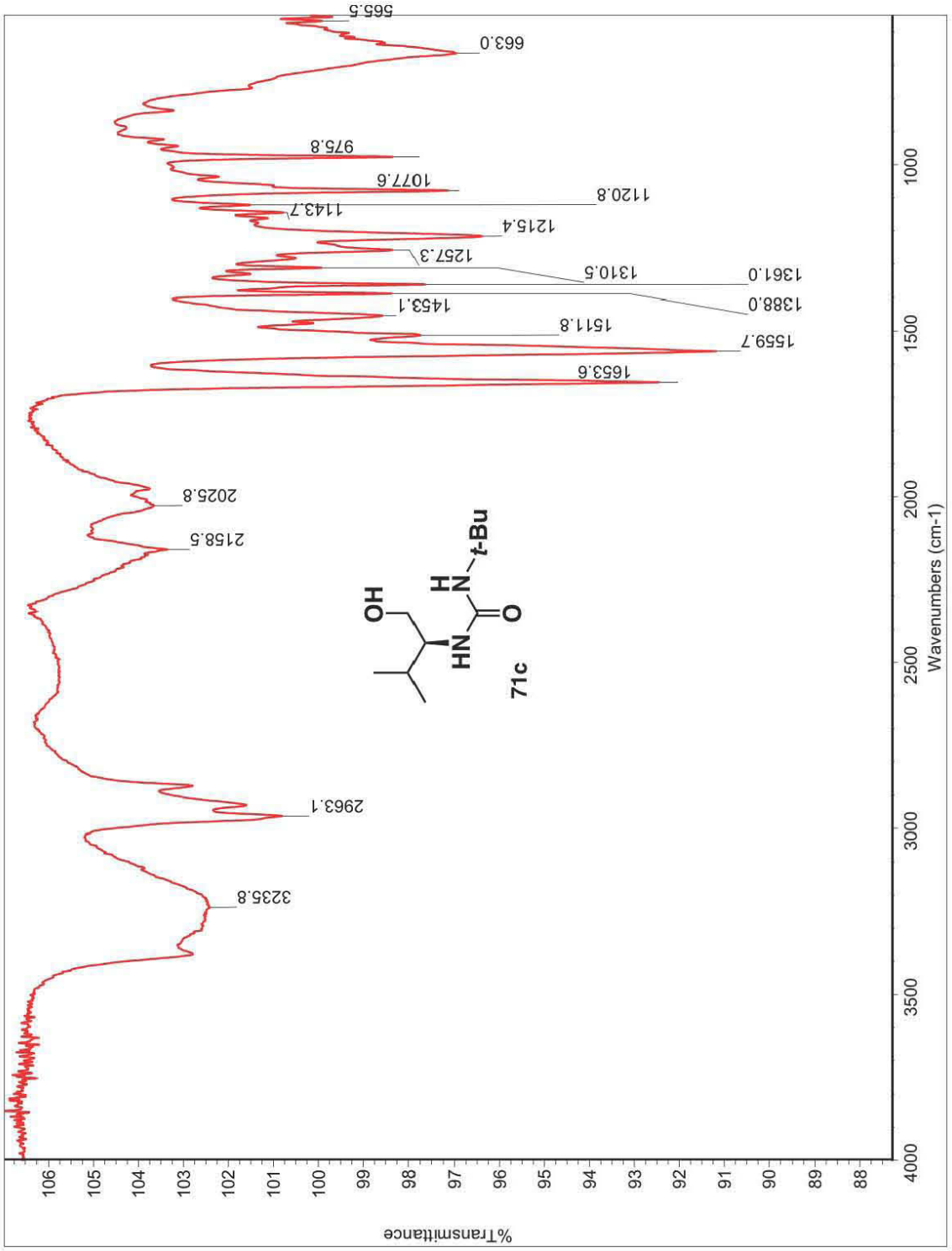
%Transmittance
Wavenumbers (cm-1)
4000
3500
3000
2500
2000
1500
1000
106
105
104
103
102
101
100
99
98
97
96
95
94
93
92
91
90
89
88
3235.8
2963.1
2158.5
2025.8
1653.6
1559.7
1511.8
1453.1
1388.0
1361.0
1310.5
1257.3
1215.4
1143.7
1120.8
1077.6
975.8
663.0
565.5
OH
HN
H
N
t-Bu
O
71c

0.9573
0.9743
1.0412
1.0579
1.3154
1.3330
1.3508
1.3546
1.3726
1.3903
1.4079
1.4461
1.4642
1.4671
1.4762
1.4818
1.4848
1.4997
1.5026
1.8356
1.8457
2.0760
2.0764
2.0863
2.0924
2.0929
2.0943
2.0948
2.1028
2.1039
2.1047
2.1052
2.1113
2.1118
2.1212
2.1217
2.1698
2.1712
2.1718
2.1725
2.1731
2.1737
2.1743
2.1750
2.1776
2.1809
2.1843
2.2207
2.3371
3.1709
3.1858
3.1885
3.2034
3.2210
5.2336
Bu
N
O
HN
72a
ppm
0.0
0.5
1.0
1.5
2.0
2.5
3.0
3.5
4.0
4.5
5.0
5.5
6.0
6.5
7.0
7.5
6.02
2.99
4.91
0.98
1.00
0.99
1.95
0.96

13.76
19.16
19.95
20.02
30.81
30.95
31.04
31.87
40.47
45.25
165.41
207.02
ppm
10
20
30
40
50
60
70
80
90
100
110
120
130
140
150
160
170
180
190
200
210
O
HN
N
Bu
72a

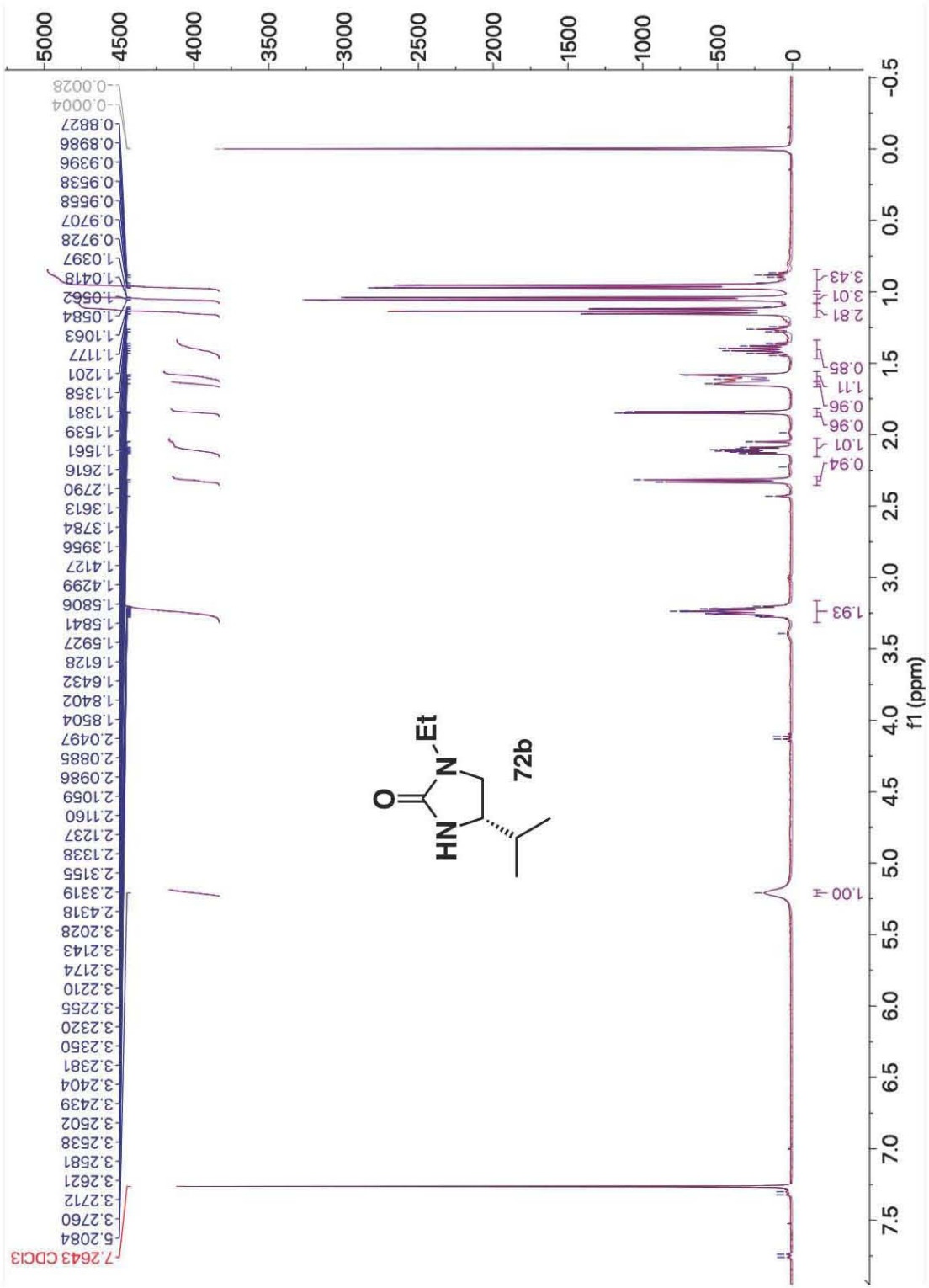
72b
Et
N
O
HN
f1 (ppm)
7.2643 CDCl3

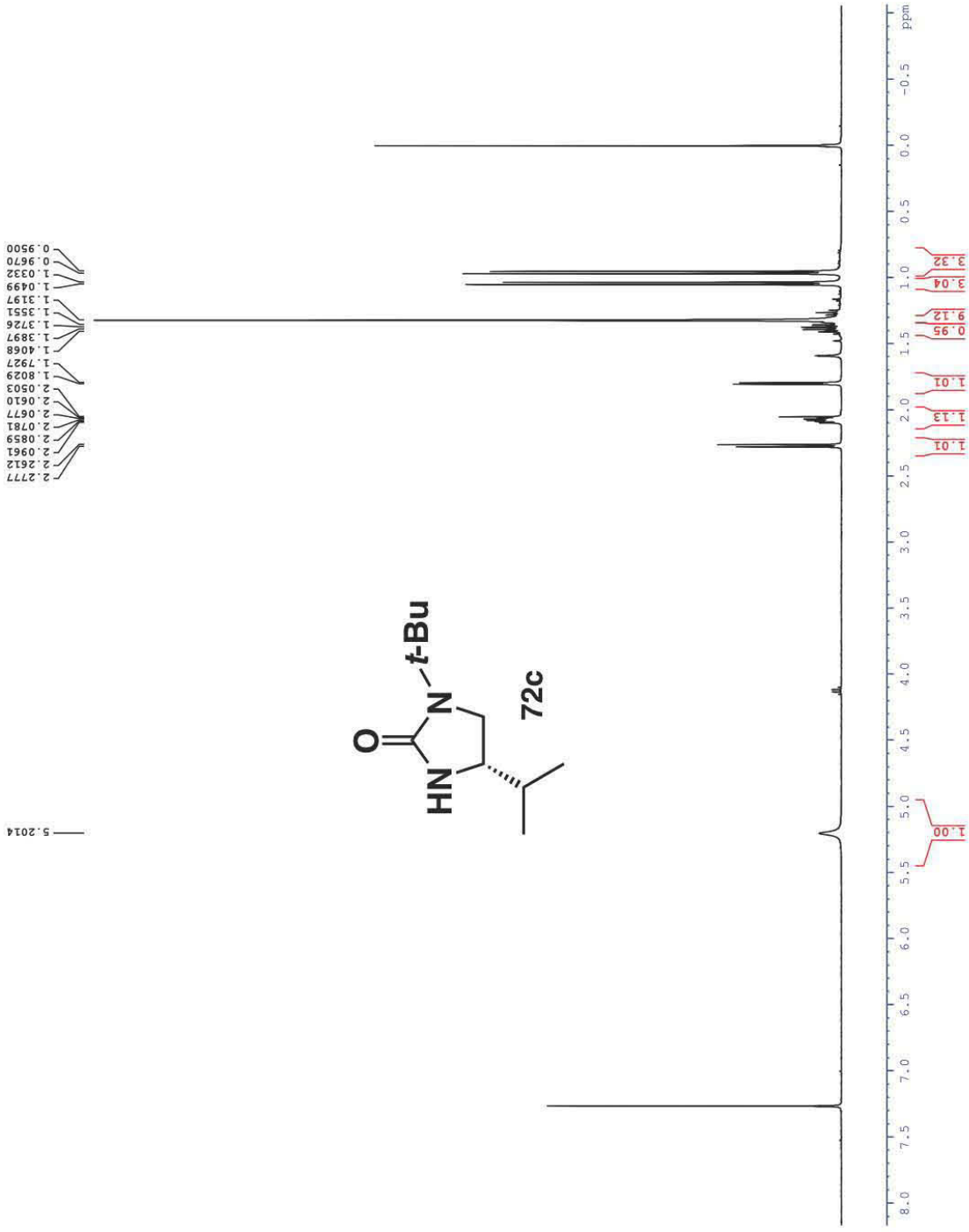
72c
t-Bu
N
HN
O
ppm
8.0
7.5
7.0
6.5
6.0
5.5
5.0
4.5
4.0
3.5
3.0
2.5
2.0
1.5
1.0
0.5
0.0
-0.5
5.2014
2.2777
2.2612
2.0961
2.0859
2.0781
2.0677
2.0610
2.0503
1.8029
1.7927
1.4068
1.3897
1.3726
1.3551
1.3197
1.0499
1.0332
0.9670
0.9500
1.00
1.01
1.13
1.01
0.95
9.12
3.04
3.32

6.2893
3.5137
3.4734
3.4933
3.4555
2.4451
2.4307
2.4193
2.4048
2.3928
2.3885
2.3223
2.3121
2.3064
2.2960
2.2806
1.9917
1.9820
1.6342
1.6205
1.6153
1.6033
1.3937
1.3754
1.3576
1.3398
1.3349
1.3303
1.0692
1.0523
1.0147
0.9979
0.9813
0.9516
0.9329
0.9151
0.8996
0.8828
0.8654
0.8520
0.8334
Bu
N
O
N
Cl
Cl
73
ppm
8.07
3.04
2.96
1.05
1.10
1.05
2.07
1.00

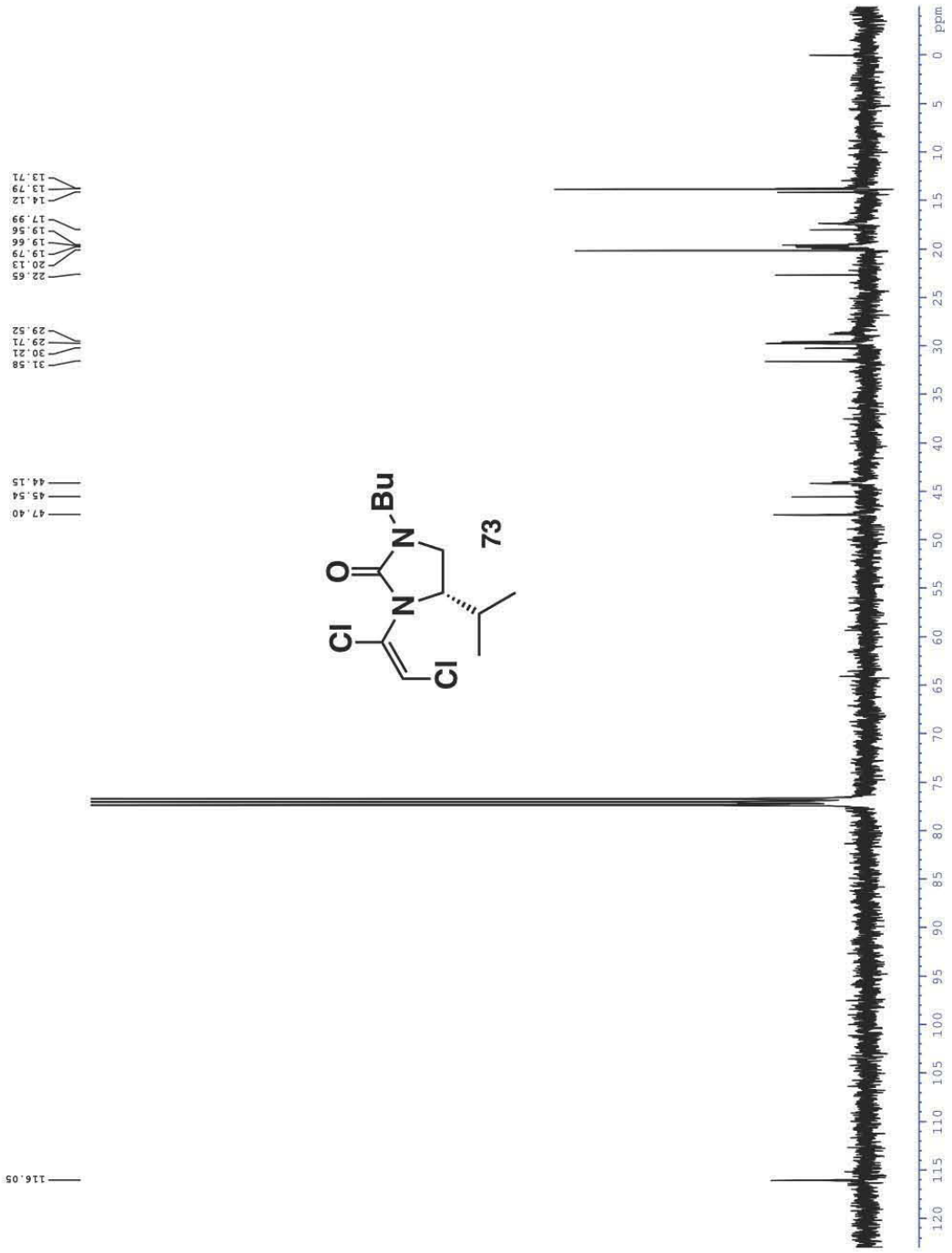
116.05
47.40
45.54
44.15
31.58
30.21
29.71
29.52
22.65
20.13
19.79
19.66
19.56
17.99
14.12
13.79
13.71
Bu
N
O
N
Cl
Cl
73
ppm

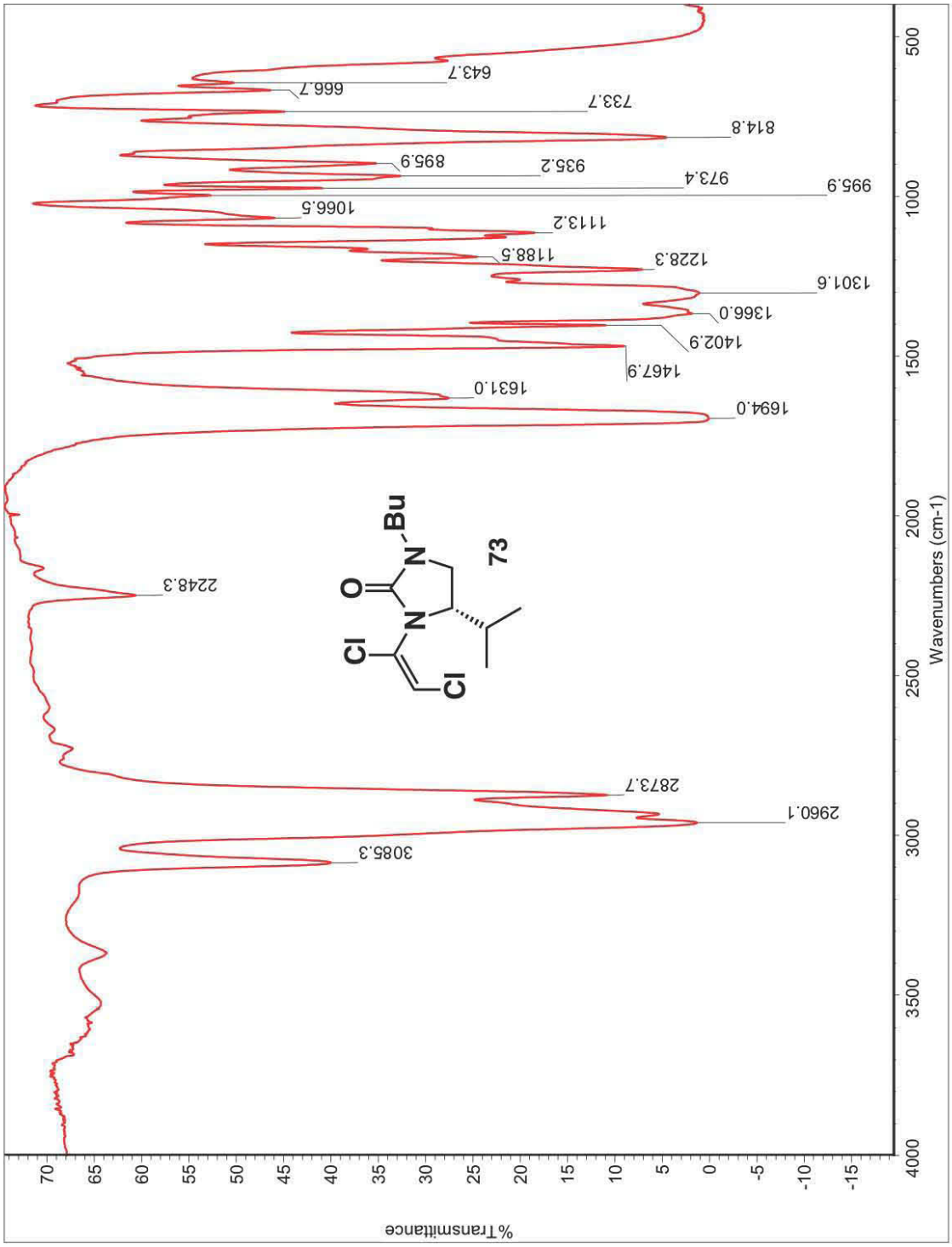
%Transmittance
Wavenumbers (cm-1)
73
2248.3
3085.3
2873.7
2960.1
1694.0
1631.0
1467.9
1402.9
1366.0
1301.6
1228.3
1188.5
1113.2
1066.5
995.9
973.4
935.2
895.9
814.8
733.7
666.7
643.7

7.8234
7.8207
7.8032
7.7997
7.5989
7.5804
7.5098
7.4905
7.4720
3.4986
3.4937
3.4799
2.9816
2.4082
2.3978
2.3193
2.3033
2.1588
2.1486
1.6950
1.6780
1.6684
1.6614
1.6496
1.6308
1.5916
1.3784
1.3595
1.3406
1.3221
1.0947
1.0777
1.0695
1.0526
0.9638
0.9514
0.9471
0.9387
0.9231
0.9216
0.9147
0.9064
0.8100
Ph
O
N
Bu
N
Ph
ppm
0.0
0.5
1.0
1.5
2.0
2.5
3.0
3.5
4.0
4.5
5.0
5.5
6.0
6.5
7.0
7.5
8.0
3.66
1.42
1.38
1.45
0.51
0.51
0.51
0.38
0.93
2.05
1.00
2.08

Ms
N
77
3.0625
2.5846
2.5668
2.5554
2.5530
2.5377
2.5490
2.5200
2.1580
2.1474
1.5583
1.5413
1.5243
1.5074
1.0660
1.0493
1.0223
1.0052
6.06
1.04
1.02
1.96
3.00
ppm

OTBDPS
1.0621
1.0550
1.0479
1.9546
1.9479
1.9413
2.4724
2.4657
2.4547
2.4480
2.4370
2.4303
3.7992
3.7815
3.7638
7.6914
7.6876
7.6841
7.6718
7.6677
7.4337
7.4164
7.4034
7.4000
7.3888
7.3853
8.96
0.96
1.94
2.00
5.56
3.75
ppm

1.1913
1.2090
1.2267
2.4974
2.5015
2.5151
2.5192
2.5327
2.5368
3.5281
3.5457
3.5517
3.5694
3.7006
3.7183
3.7242
3.7419
3.7571
3.7748
3.7925
5.2318
5.2359
5.2399
7.3621
7.3670
7.3820
7.3835
7.3848
7.3868
7.3880
7.3979
7.4001
7.4014
7.4031
7.4104
7.4147
7.4188
7.4322
7.6588
7.6614
7.6631
EtO
EtO
OTBDPS
9.06
6.05
2.05
2.05
4.03
1.00
6.01
4.04
ppm

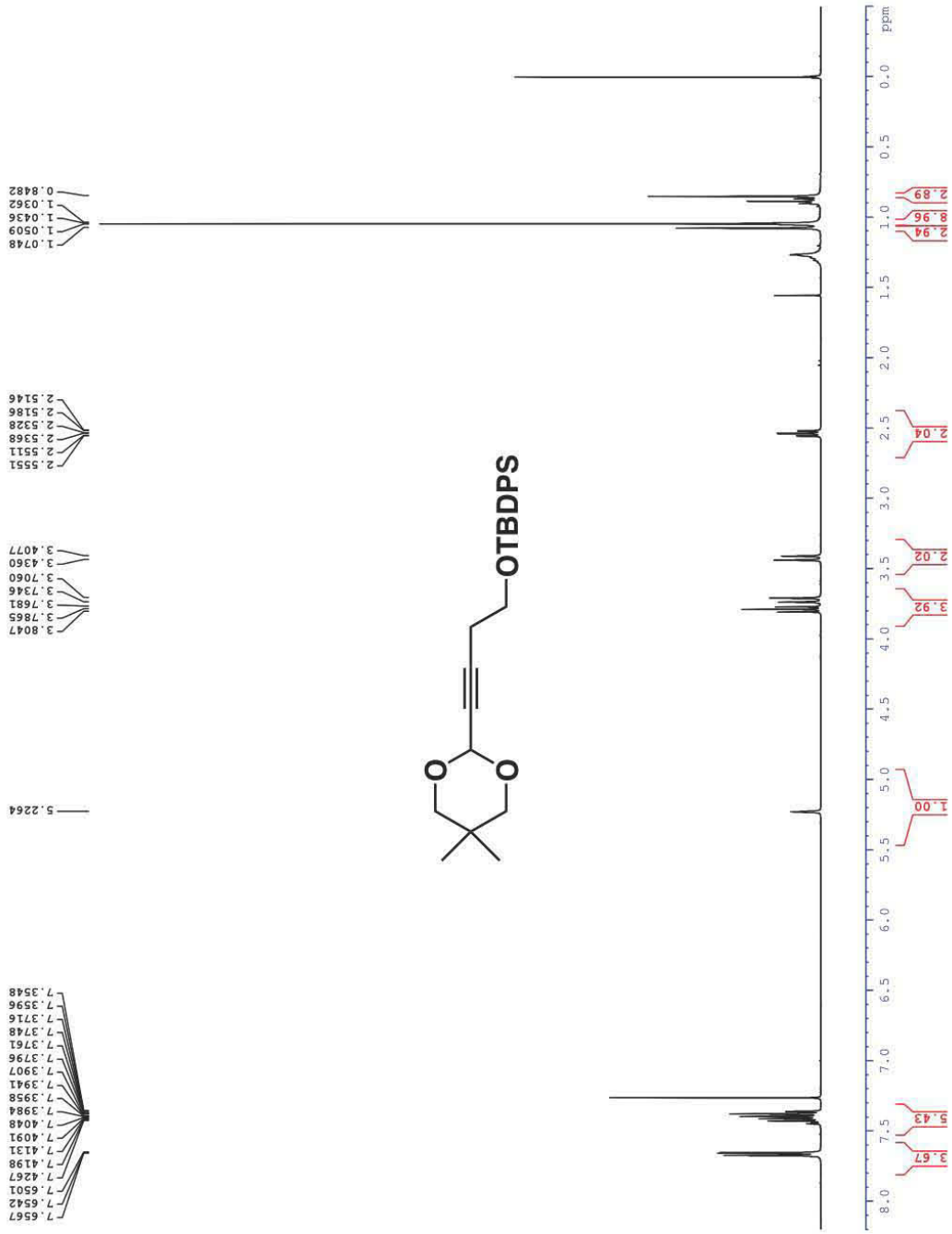
OTBDPS
O
O
7.6567
7.6542
7.6501
7.4267
7.4198
7.4131
7.4091
7.4048
7.3984
7.3958
7.3941
7.3907
7.3796
7.3761
7.3748
7.3716
7.3596
7.3548
5.2264
3.8047
3.7865
3.7681
3.7346
3.7060
3.4360
3.4077
2.5551
2.5511
2.5368
2.5328
2.5186
2.5146
1.0748
1.0509
1.0436
1.0362
0.8482
ppm
2.89
8.96
2.94
2.04
2.02
3.92
1.00
5.43
3.67

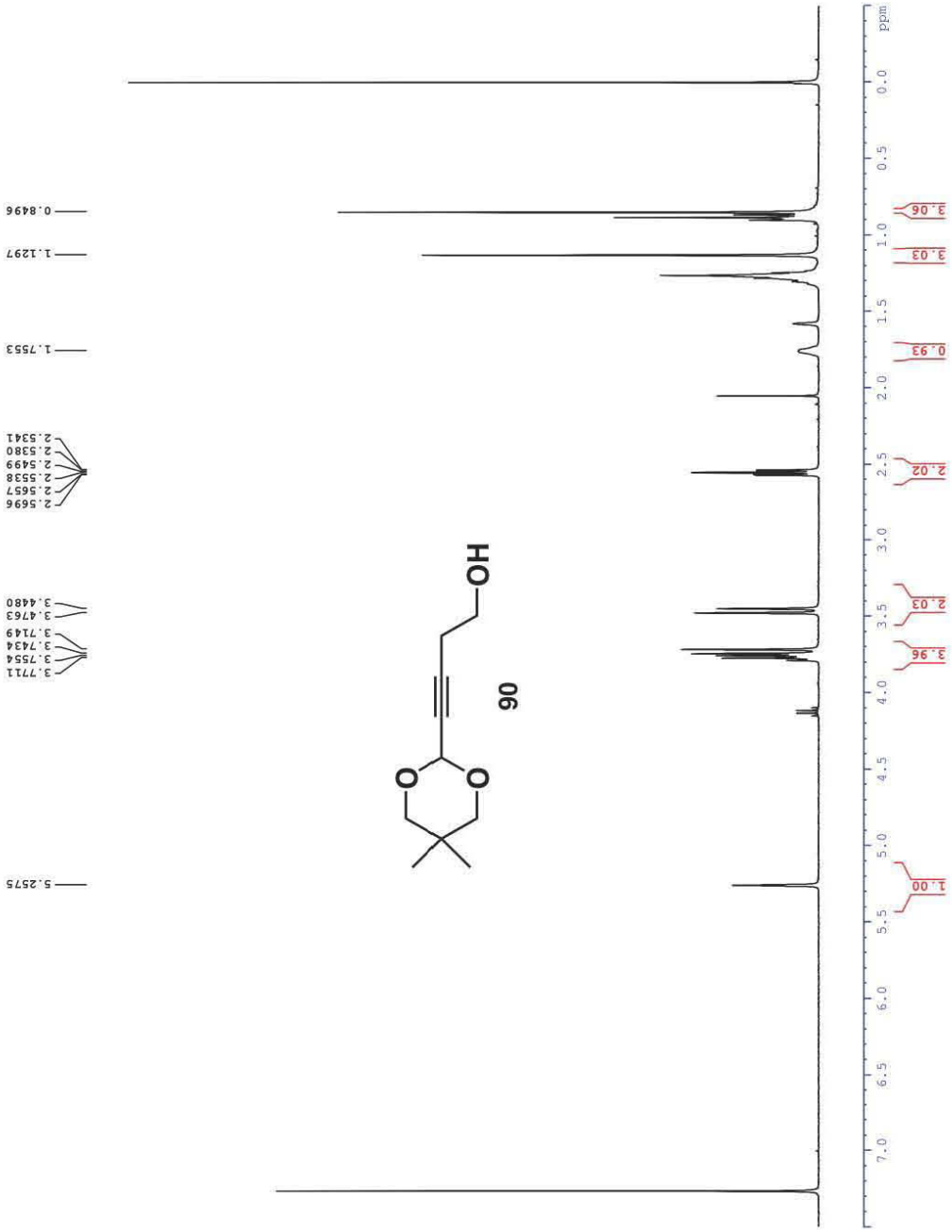
OH
O
O
90
ppm
0.0
0.5
1.0
1.5
2.0
2.5
3.0
3.5
4.0
4.5
5.0
5.5
6.0
6.5
7.0
3.06
3.03
0.93
2.02
2.03
3.96
1.00
0.8496
1.1297
1.7553
2.5341
2.5380
2.5499
2.5538
2.5657
2.5696
3.4480
3.4763
3.7149
3.7434
3.7554
3.7711
5.2575

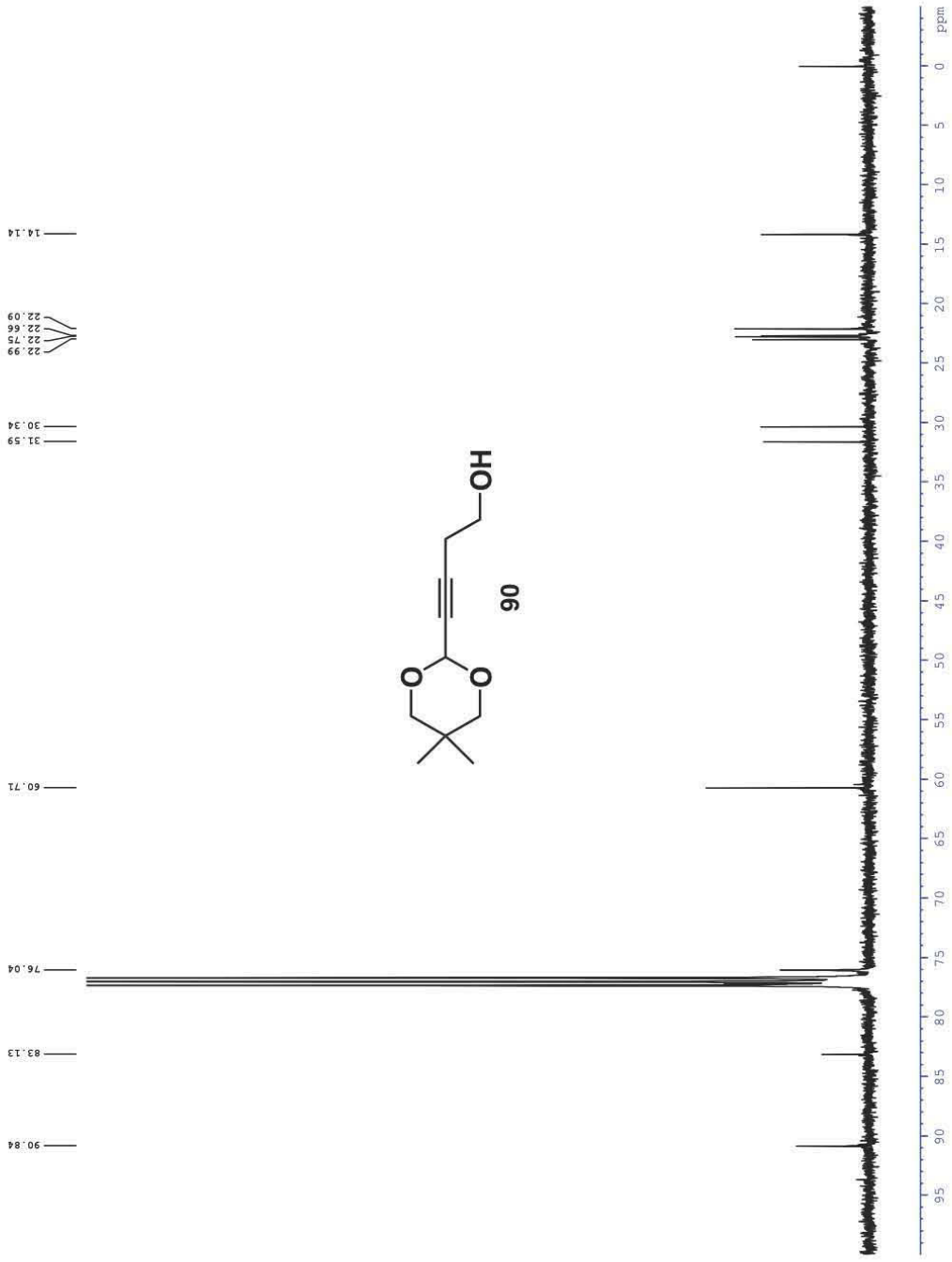
14.14
22.09
22.66
22.75
22.99
30.34
31.59
60.71
76.04
83.13
90.84
OH
O
O
90
ppm
0
5
10
15
20
25
30
35
40
45
50
55
60
65
70
75
80
85
90
95

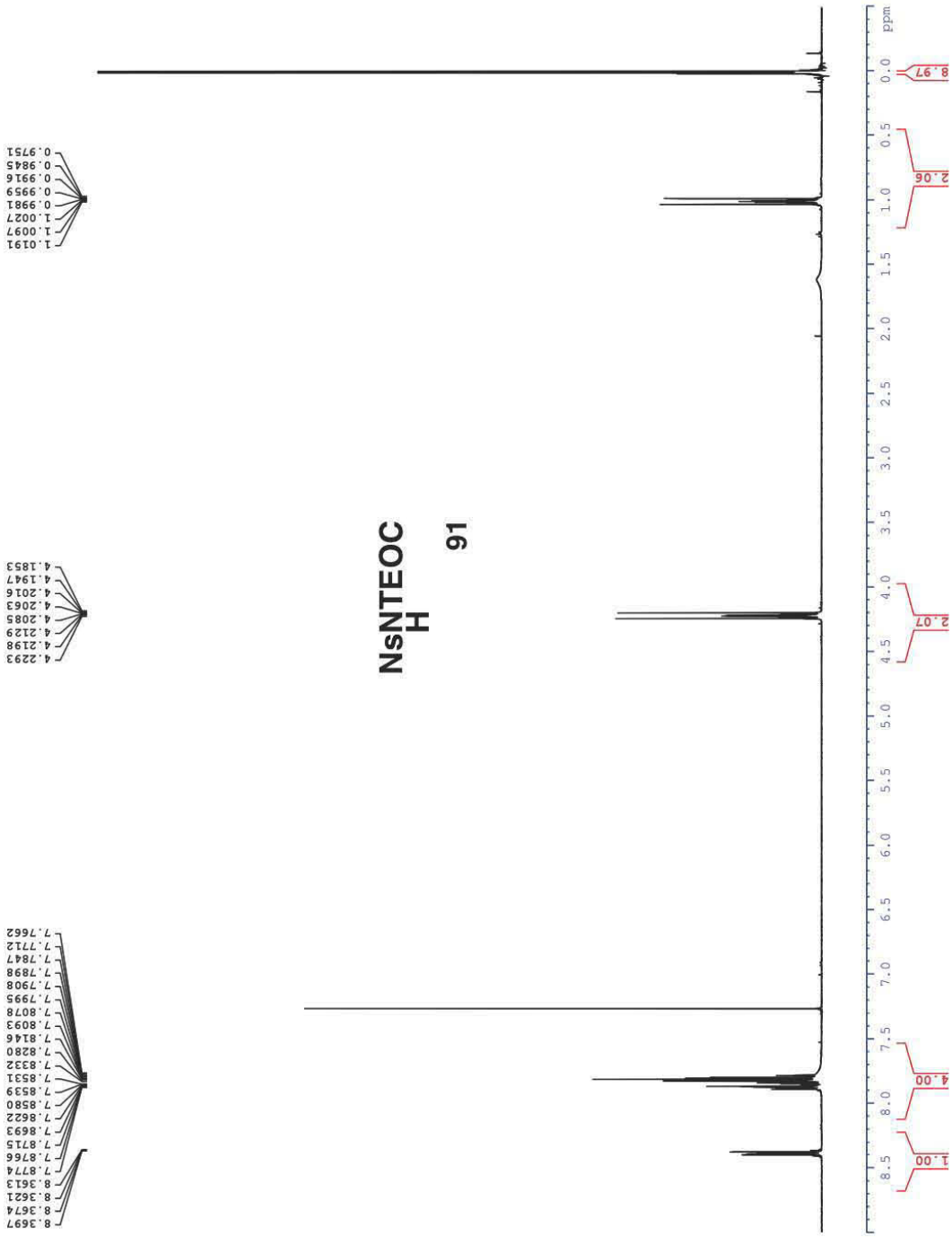
NsNTEOC
H
91
1.0191
1.0097
1.0027
0.9981
0.9959
0.9916
0.9845
0.9751
4.2293
4.2198
4.2129
4.2085
4.2063
4.2016
4.1947
4.1853
7.7662
7.7712
7.7847
7.7898
7.7908
7.7995
7.8078
7.8093
7.8146
7.8280
7.8332
7.8531
7.8539
7.8580
7.8622
7.8693
7.8715
7.8766
7.8774
8.3613
8.3621
8.3674
8.3697
ppm
8.97
2.06
2.07
4.00
1.00

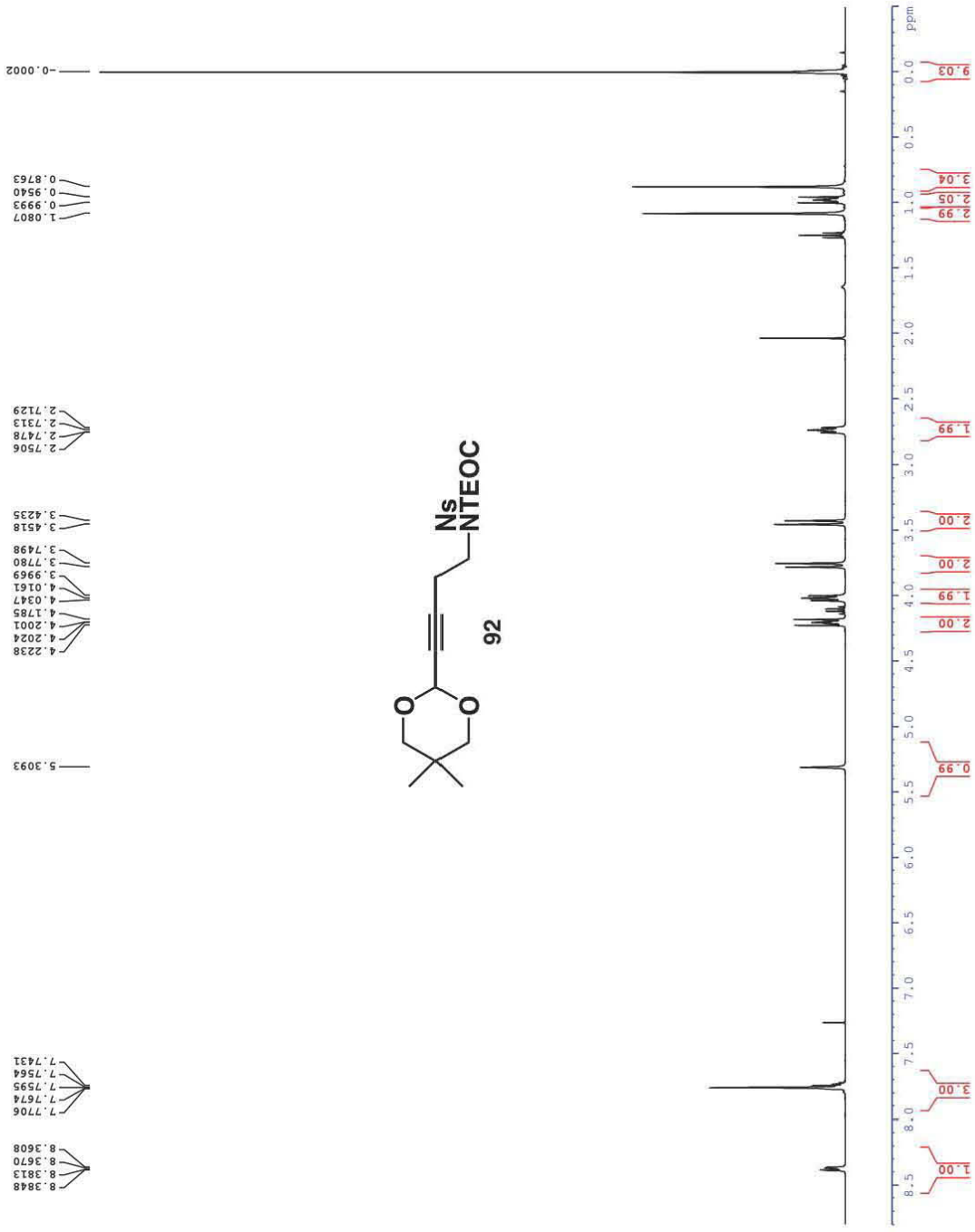
Ns
NTEOC
92

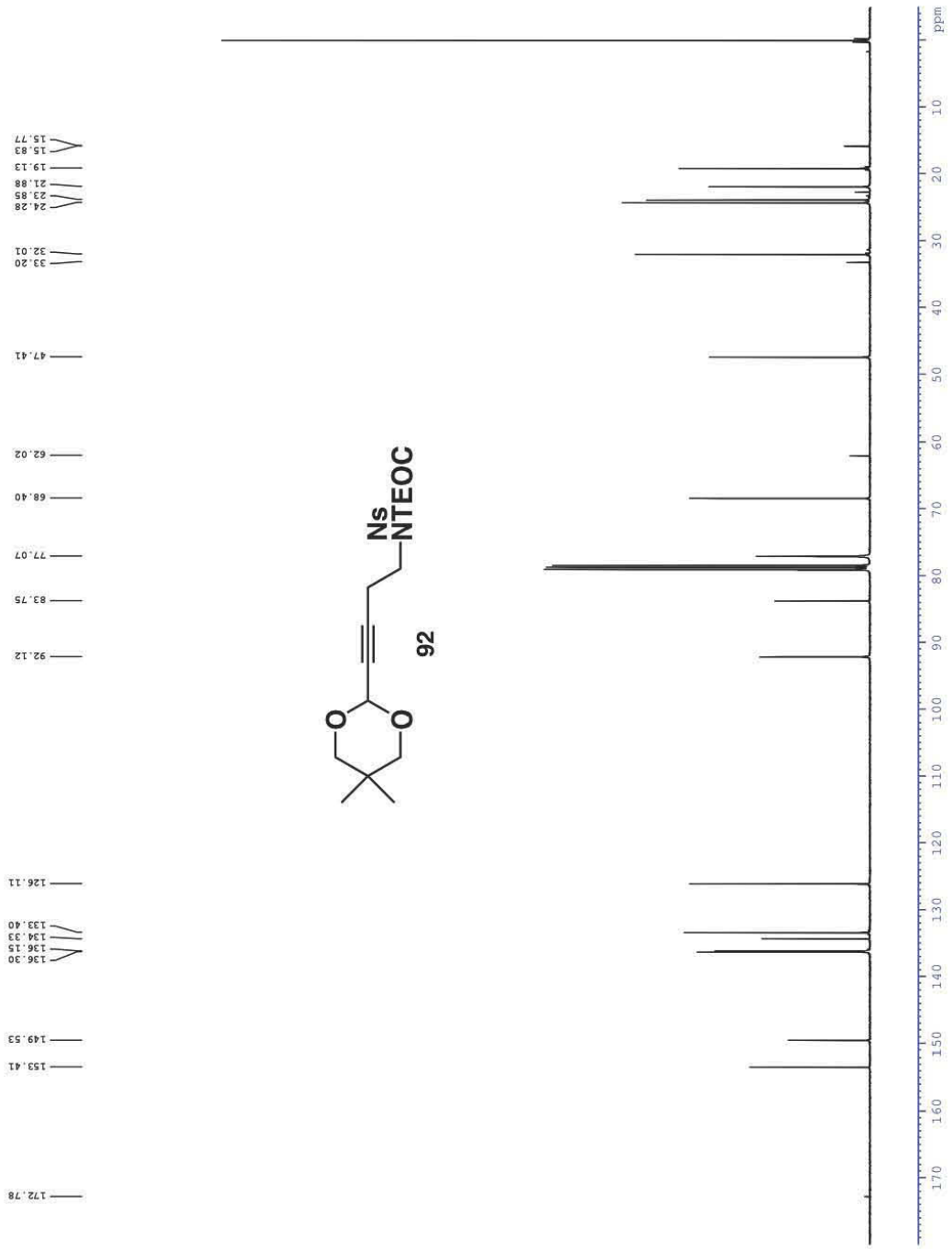
Ns
NTEOC
92
O
O
172.78
153.41
149.53
136.30
136.15
134.33
133.40
126.11
92.12
83.75
77.07
68.40
62.02
47.41
33.20
32.01
24.28
23.85
21.88
19.13
15.83
15.77
ppm
10
20
30
40
50
60
70
80
90
100
110
120
130
140
150
160
170

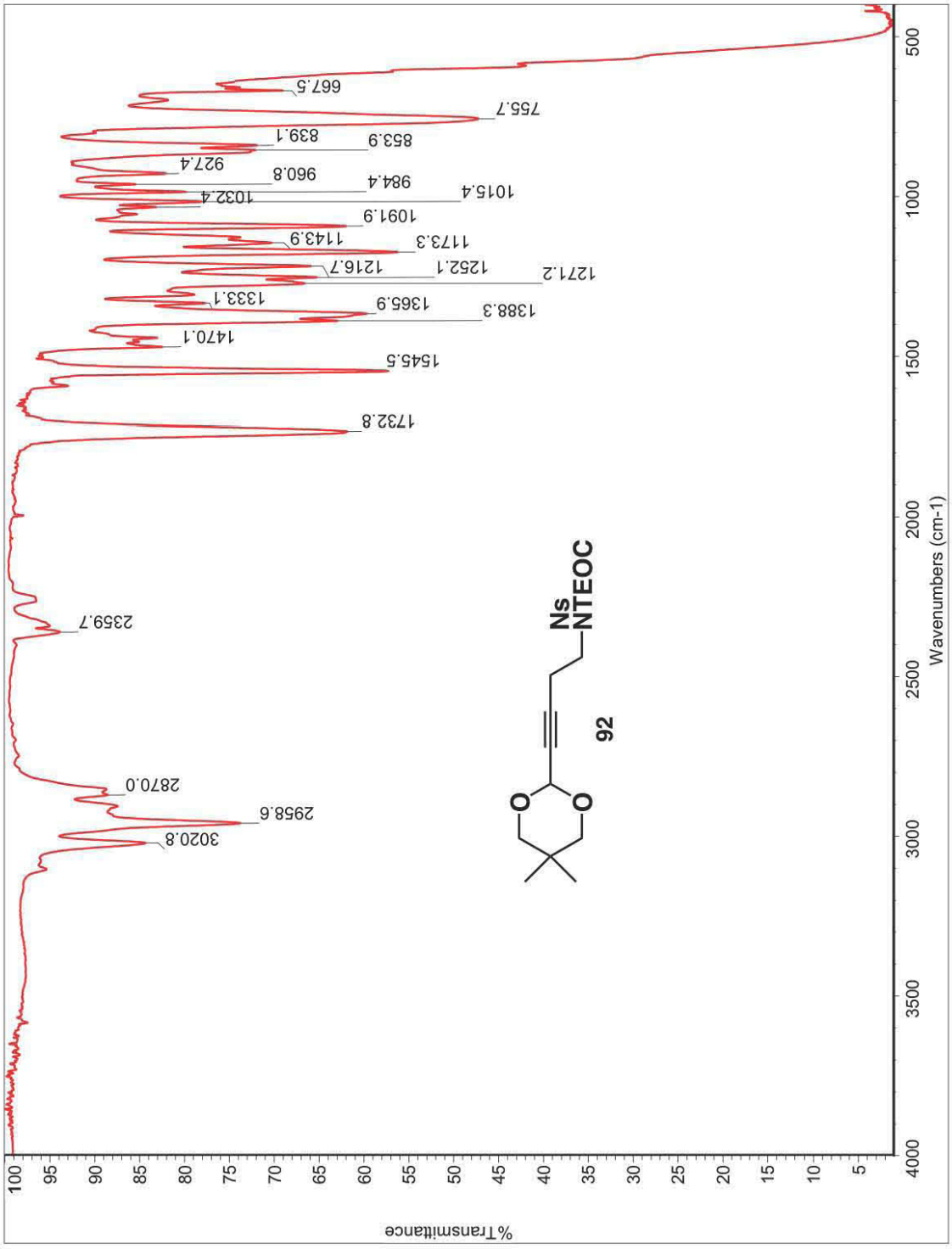
%Transmittance
Wavenumbers (cm-1)
4000
3500
3000
2500
2000
1500
1000
500
100
95
90
85
80
75
70
65
60
55
50
45
40
35
30
25
20
15
10
5
3020.8
2958.6
2870.0
2359.7
1732.8
1545.5
1470.1
1388.3
1365.9
1333.1
1271.2
1252.1
1216.7
1173.3
1143.9
1091.9
1032.4
1015.4
984.4
960.8
927.4
853.9
839.1
755.7
667.5
Ns
NTEOC
O
O
92

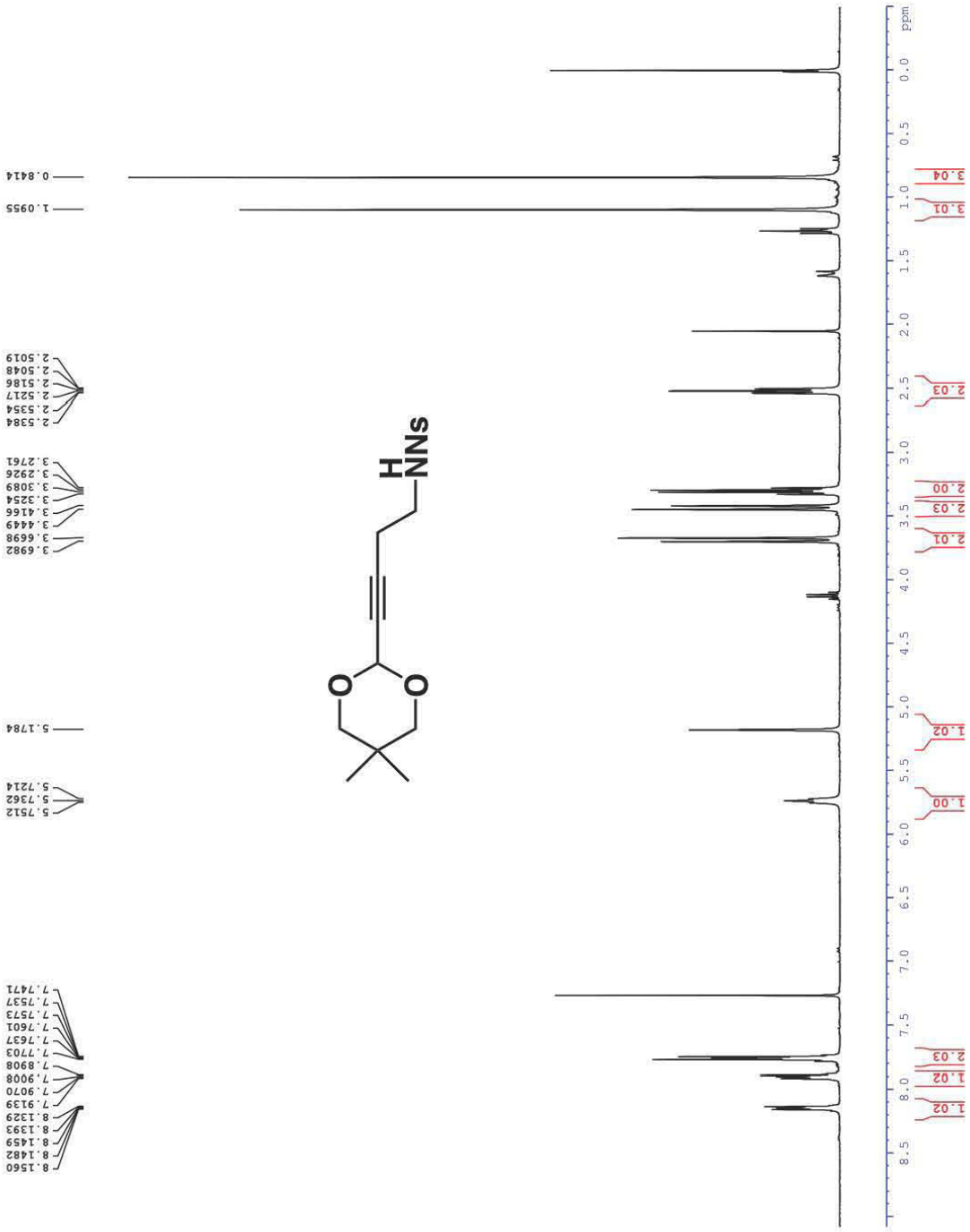
0.8414
1.0955
2.5384
2.5354
2.5217
2.5186
2.5048
2.5019
3.2761
3.2926
3.3089
3.3254
3.4166
3.4449
3.6698
3.6982
5.1784
5.7512
5.7362
5.7214
7.7471
7.7537
7.7573
7.7601
7.7637
7.7703
7.8908
7.9008
7.9070
7.9139
8.1329
8.1393
8.1459
8.1482
8.1560
3.04
3.01
2.03
2.00
2.03
2.01
1.02
1.00
2.03
1.02
1.02
ppm

20.04
22.05
22.66
30.32
42.17
75.93
77.88
81.65
90.54
125.72
130.88
132.98
133.66
133.86
H
NNs
O
O
0 ppm

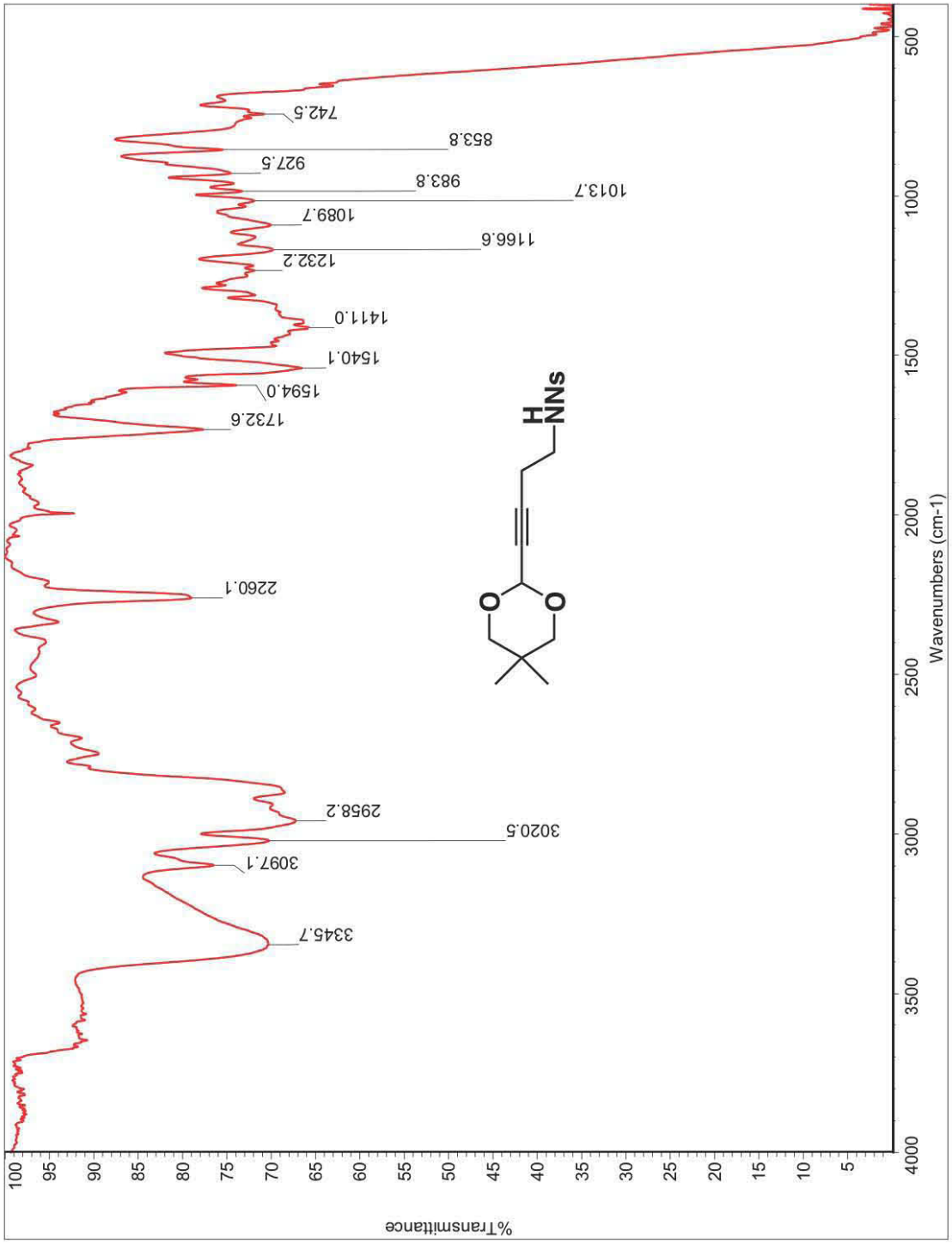
%Transmittance
Wavenumbers (cm-1)
4000
3500
3000
2500
2000
1500
1000
500
100
95
90
85
80
75
70
65
60
55
50
45
40
35
30
25
20
15
10
5
3345.7
3097.1
3020.5
2958.2
2260.1
1732.6
1594.0
1540.1
1411.0
1232.2
1166.6
1089.7
1013.7
983.8
927.5
853.8
742.5
H
N
Ns
O
O

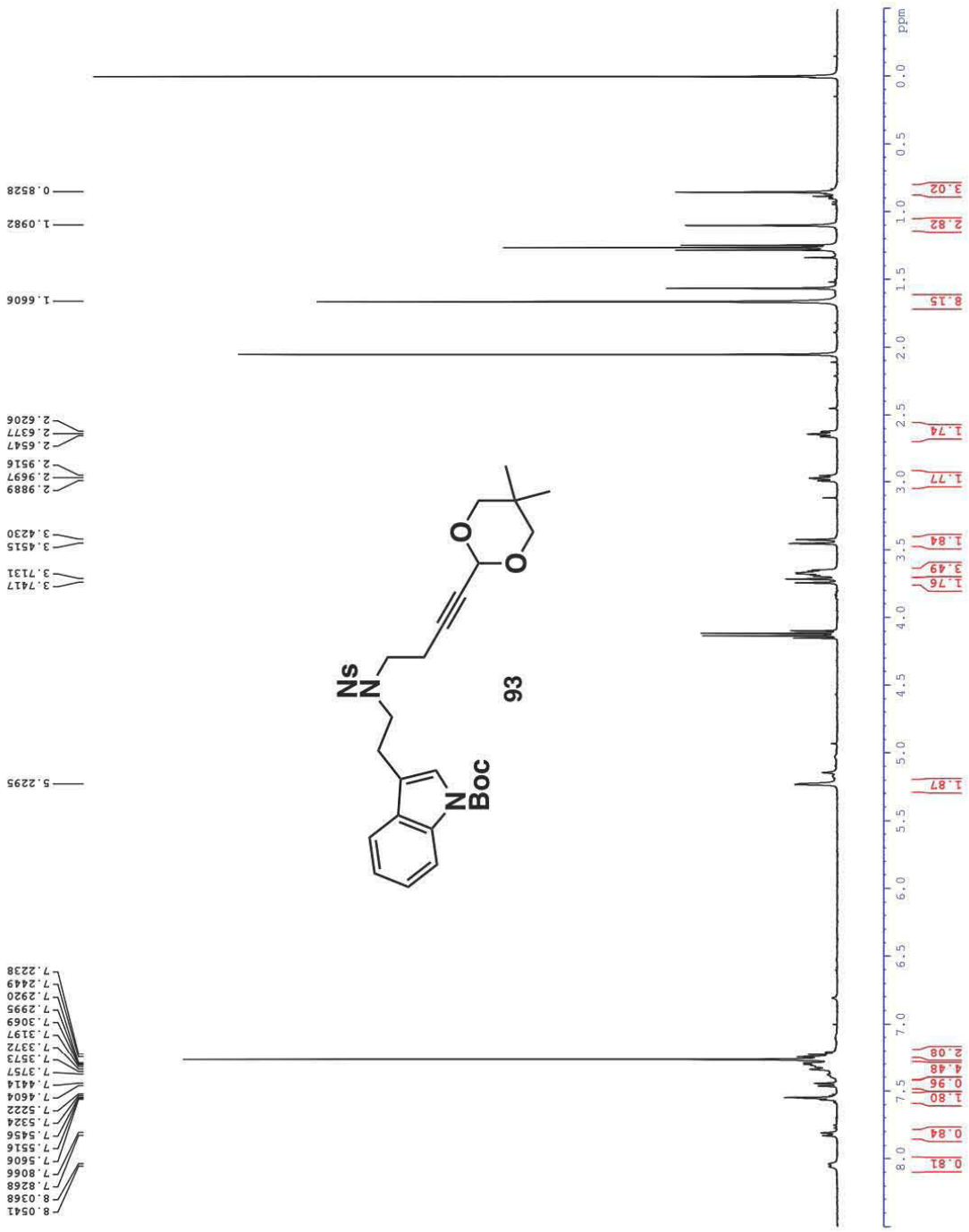
93
Ns
N
Boc
O
O
ppm
0.0
0.5
1.0
1.5
2.0
2.5
3.0
3.5
4.0
4.5
5.0
5.5
6.0
6.5
7.0
7.5
8.0
3.02
2.82
8.15
1.74
1.77
1.84
3.49
1.76
1.87
2.08
4.48
0.96
1.80
0.84
0.81
0.8528
1.0982
1.6606
2.6206
2.6377
2.6547
2.9516
2.9697
2.9889
3.4230
3.4515
3.7131
3.7417
5.2295
7.2238
7.2449
7.2920
7.2995
7.3069
7.3197
7.3372
7.3573
7.3757
7.4414
7.4604
7.5222
7.5324
7.5456
7.5516
7.5606
7.8066
7.8268
8.0368
8.0541

8.1262
8.1185
7.5542
7.5351
7.4131
7.3339
7.3160
7.2394
7.2218
5.1676
3.7138
3.6852
3.4405
3.4121
2.9681
2.9534
2.9100
2.8935
2.8689
2.8515
2.8344
2.4865
2.4829
2.4694
2.4658
2.4521
2.4485
1.6782
1.6178
1.0963
0.8441
O
O
H
N
N
Boc
94
ppm
0.0
0.5
1.0
1.5
2.0
2.5
3.0
3.5
4.0
4.5
5.0
5.5
6.0
6.5
7.0
7.5
8.0
0.92
1.04
0.93
1.05
0.72
1.00
1.98
1.99
1.94
3.94
1.95
8.91
1.98
2.99
3.08

179.16
142.74
124.36
123.04
122.41
119.00
115.29
90.93
48.64
47.71
30.33
28.24
25.71
22.76
22.14
19.76
O
O
H
N
N
Boc
94
210
200
190
180
170
160
150
140
130
120
110
100
90
80
70
60
50
40
30
20
10
0
-10 ppm

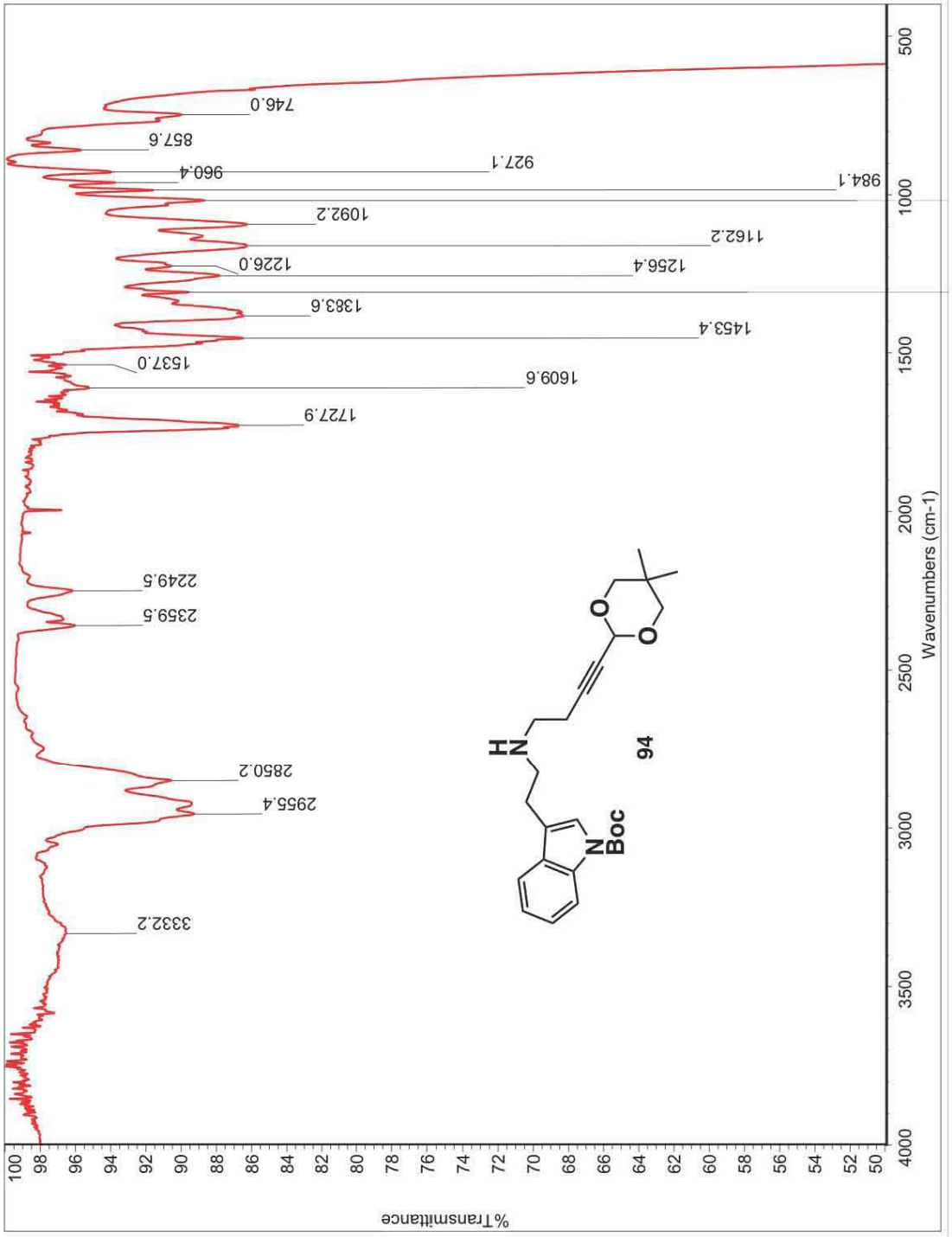
%Transmittance
Wavenumbers (cm-1)
3332.2
2955.4
2850.2
2359.5
2249.5
1727.9
1609.6
1537.0
1453.4
1383.6
1256.4
1226.0
1162.2
1092.2
984.1
960.4
927.1
857.6
746.0
94
Boc
N
H
O
O

8.1312
7.6437
7.6246
7.5767
7.5575
7.4274
7.4130
7.3497
7.3474
7.3294
7.3177
7.3117
7.3089
7.2996
7.2971
7.2474
7.2290
5.2257
5.2056
3.7087
3.6985
3.6803
3.6700
3.6279
3.6118
3.6073
3.5913
3.4694
3.4519
3.4431
3.4289
3.4146
3.4006
3.3881
3.3693
3.0510
3.0307
3.0119
3.0050
2.9843
2.9659
2.6117
2.5971
2.5942
2.5796
2.5332
2.5161
2.4986
1.6764
1.6699
1.5613
1.5436
1.0966
1.0624
0.8407
0.8243
Boc
N
Boc
N
O
O
95
ppm
8.0
7.5
7.0
6.5
6.0
5.5
5.0
4.5
4.0
3.5
3.0
2.5
2.0
1.5
1.0
0.5
0.0
1.00
1.06
1.08
0.92
1.05
1.06
1.03
2.09
1.96
4.06
2.00
2.04
9.06
8.85
3.03
3.06

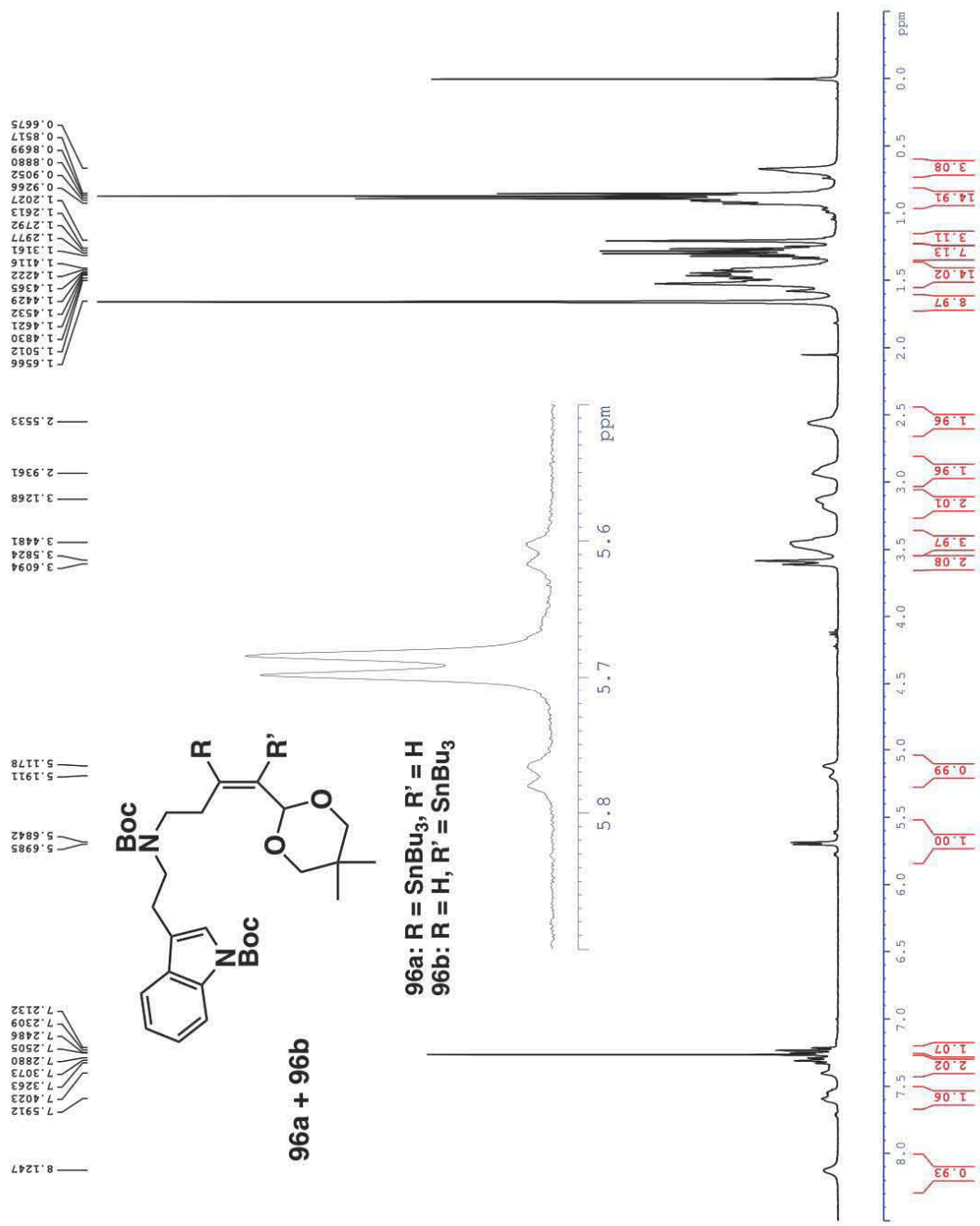
96a + 96b
96a: R = SnBu3, R' = H
96b: R = H, R' = SnBu3
Boc
N
Boc
R
R'
O
O
ppm

79
Boc
N
I
O
O
N
Boc
ppm

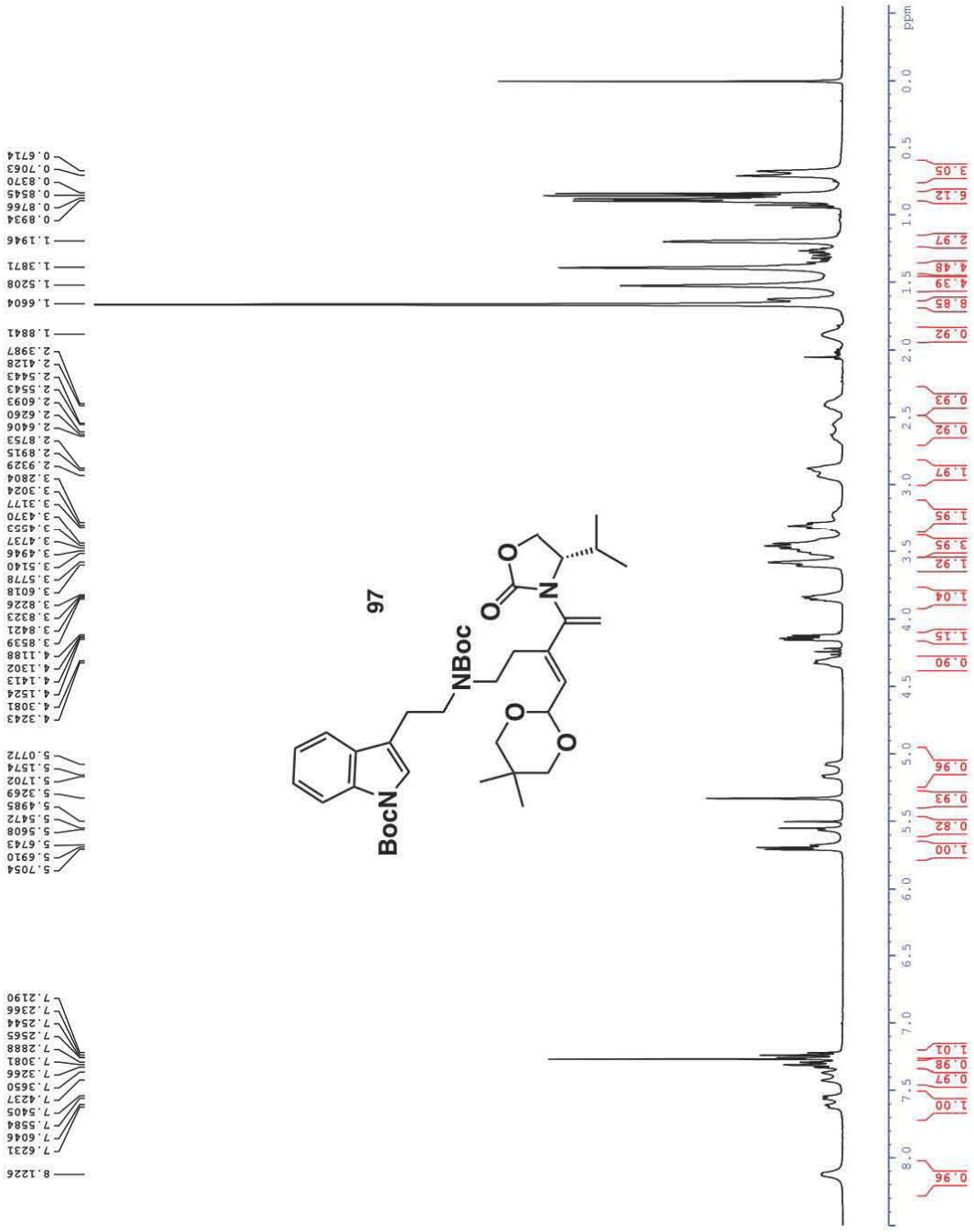
97
NBoc
BocN
O
N
O
O
O
O
O
ppm
0.0
0.5
1.0
1.5
2.0
2.5
3.0
3.5
4.0
4.5
5.0
5.5
6.0
6.5
7.0
7.5
8.0
3.05
6.12
2.97
4.48
4.39
8.85
0.92
0.93
0.92
1.97
1.95
3.95
1.92
1.04
1.15
0.90
0.96
0.93
0.82
1.00
1.01
0.98
0.97
1.00
0.96
8.1226
7.6231
7.6046
7.5584
7.5405
7.4237
7.3650
7.3266
7.3081
7.2888
7.2565
7.2544
7.2366
7.2190
5.7054
5.6910
5.6743
5.5608
5.5472
5.4985
5.3269
5.1702
5.1574
5.0772
4.3243
4.3081
4.1524
4.1413
4.1302
4.1188
3.8539
3.8421
3.8323
3.8226
3.6018
3.5778
3.5140
3.4946
3.4737
3.4553
3.4370
3.3177
3.3024
3.2804
2.9329
2.8915
2.8753
2.6606
2.6260
2.6093
2.5543
2.5443
2.4128
2.3987
1.8841
1.6604
1.5208
1.3871
1.1946
0.8934
0.8766
0.8545
0.8370
0.7063
0.6714

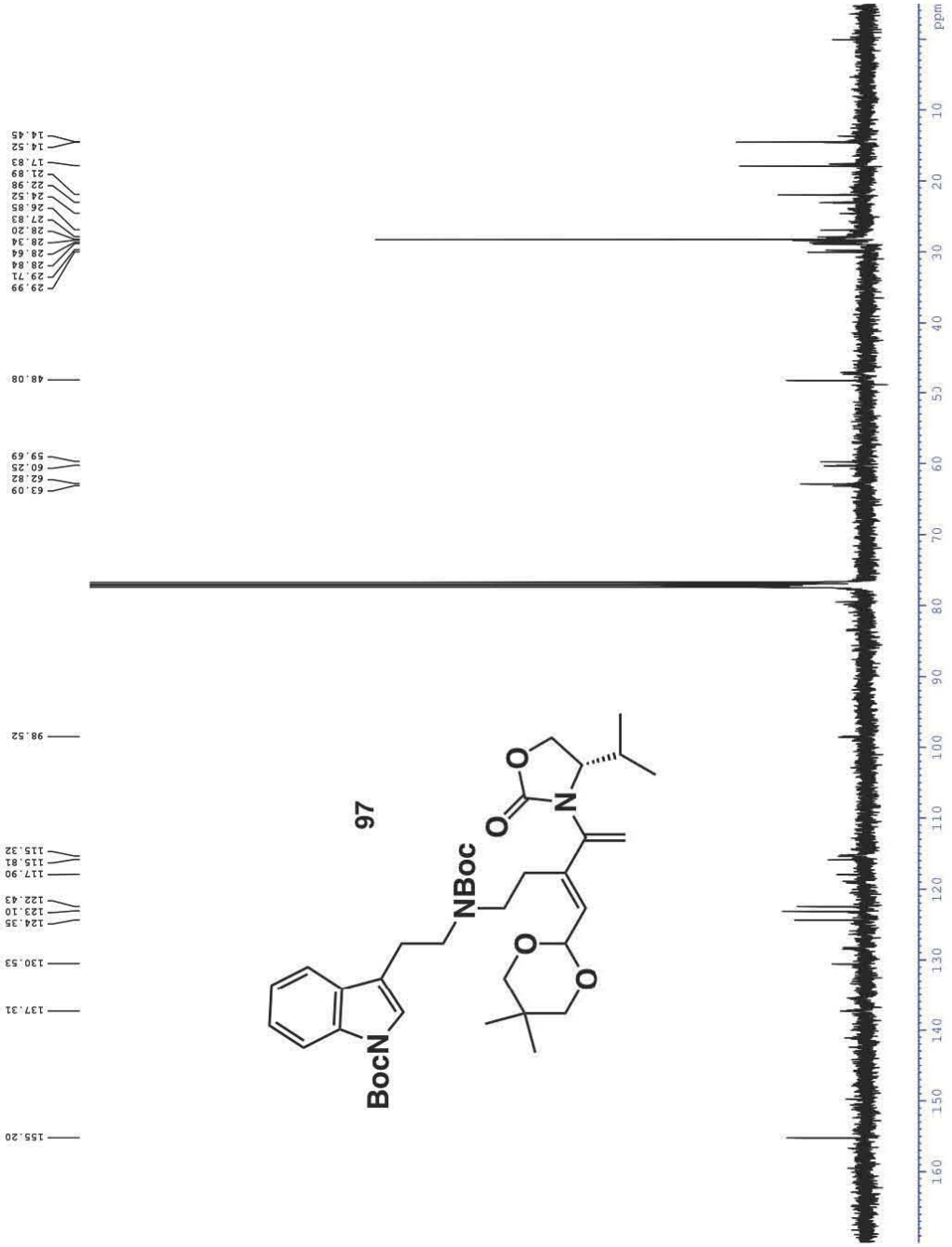
155.20
137.31
130.53
124.35
123.10
122.43
117.90
115.81
115.32
98.52
63.09
62.82
60.25
59.69
48.08
29.99
29.71
28.84
28.64
28.34
28.20
27.83
26.85
24.52
22.98
21.89
17.83
14.52
14.45
97
BocN
NBoc
O
O
N
O
O
O
ppm

98
BocN
NBoc
O
O
N
O
O
O
(CO)3Fe
8.1133
7.5500
7.5301
7.3541
7.3371
7.3171
7.2985
7.2355
7.2172
4.6996
4.6800
4.6595
4.3529
4.3377
4.1316
4.1134
4.1013
4.0805
3.6970
3.6744
3.6619
3.6341
3.6280
3.6046
3.6011
3.4635
3.4382
3.3887
3.3601
3.3356
3.3084
2.9188
2.9012
2.8832
2.7739
2.7663
2.7410
2.7152
2.3644
2.3468
2.3347
1.7422
1.6630
1.4969
1.3944
1.1598
0.9430
0.9259
0.9080
0.8912
0.6422
0.4499
0.4334
0.3106
0.3045
ppm
0.93
1.04
1.92
1.01
7.5
7.0
6.5
6.0
5.5
5.0
4.5
4.0
3.5
3.0
2.5
2.0
1.5
1.0
0.5
0.0
0.92
1.00
1.90
2.96
1.10
3.95
2.04
0.93
1.97
0.93
8.96
1.92
7.05
2.98
5.95
2.95
0.96
0.94

78
BocN
NBoc
O
N
O
O
H
(CO)3Fe
ppm

Conformation and Directionality of the Influenza A M2 Protein Domain Essential to Viral Replication

Hayley Raymond
Department of Chemistry and Biochemistry
Swarthmore College
May 14, 2018
Advisor: Kathleen P. Howard

Table of Contents

List of Figures and Tables

Abstract

Influenza A causes seasonal epidemics, and the possibility of another worldwide influenza A pandemic remains a public health concern. The influenza A M2 protein is implicated in the virus's ability to bud and create new infectious virus particles. Specifically, the C-terminal region of the virus is required for viral budding, and this protein domain binds another influenza protein, M1. M2-M1 binding is critical to packaging the viral genome into new virions. To probe the region of M2 involved in viral budding and genome packing, this thesis studied the conformation of residues 60-70 of the C-terminus via site-directed spin label electron paramagnetic resonance (SDSL-EPR) spectroscopy. SDSL-EPR spectroscopy provided structural information about M2 reconstituted into 1-palmitoyl-2-oleoyl-sn-glycero-3-phosphocholine : 1-palmitoyl-2-oleoyl-sn-glycero-3-phospho-1-rac-glycerol (POPC:POPG) 4:1 lipid bilayers, a physiologically relevant environment. Mobility and membrane accessibility data revealed that residues 60-64 are associated with the membrane and are less mobile than residues 65-70. Residues 65-70 form a region with some periodic secondary structure, extending into the aqueous phase. A unique contribution of this thesis was the determination of the directionality of M2 insertion into the membrane via trypsin fragmentation and matrix-assisted laser desorption ionization-mass spectrometry (MALDI-MS). According to current reconstitution protocols, M2 inserts into the membrane with no directionality, and both the N- and C-termini lie at the liposome exterior.

Chapter 1: Introduction to Influenza A and M2

Influenza, a contagious virus that infects the nose, throat, and lungs, causes illness that ranges in severity from mild to fatal.[1] Two types of influenza, A and B, cause seasonal epidemics each year.[2] The Centers for Disease Control and Prevention (CDC) estimates the number of annual influenza-related deaths since 2010 to range from 12,000 (2011-2012) to 56,000 (2012-2013).[3] The highly virulent influenza A has been responsible for four epidemics throughout world history, in 1918, 1957, 1968, and 2009.[4] The Spanish Flu epidemic of 1918, caused an estimated 50 million deaths worldwide, while estimates for fatalities of the Asian Flu of 1957 and the 1968 pandemic tallied at approximately one million each.[4] The Swine Flu outbreak of 2009, caused by a novel influenza strain named H1N1, caused as many as 575,400 deaths worldwide.[4] The high number of annual deaths[3] and threat of another pandemic caused by influenza A[5] make the virus a serious public health concern and provide the motivation for our work on an influenza protein.

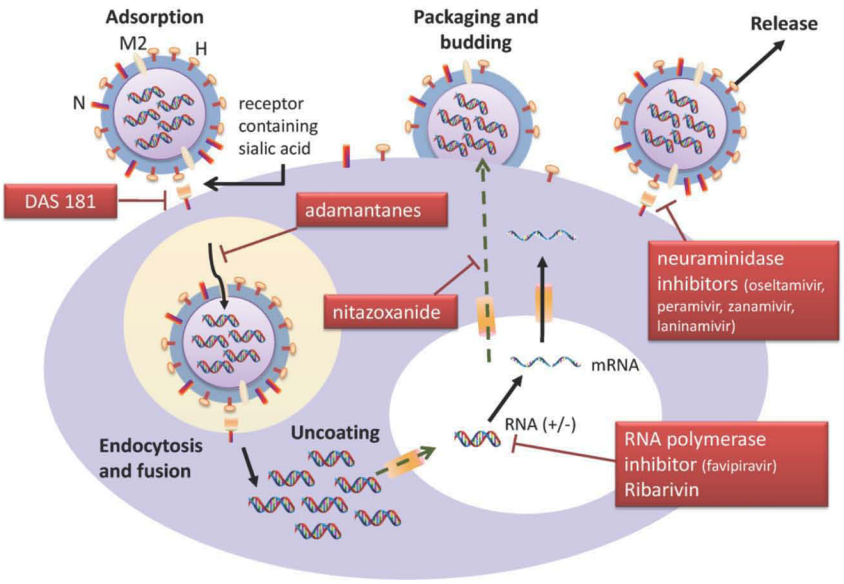

Fig 1. Viral replication cycle of influenza A. From [7].

Influenza A's replication cycle (Fig 1) begins with entry to the host cell, release of the viral genome into the nucleus, reverse transcription of the negative sense RNA and

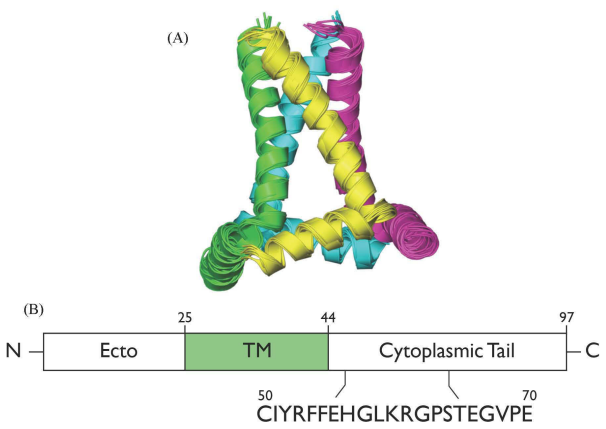

Fig 2. A) Ribbon diagram of residues 22-62 of M2. (Protein Data Bank (PDB) 2l0J). (B) Domain structure of influenza A's M2. Amino acid sequence of residues 50-70 is listed.

subsequent replication of RNA.[6] Then, this genetic material, also referred to as viral ribonucleoproteins (vRNPs) is exported from the nucleus packaged into new virions that bud from the host cell.[6] Influenza's genome contains genes that code for eleven proteins.[6] We are interested in the membrane-bound matrix 2 (M2) protein. One of these proteins is matrix 1 (M1), which is located just under the viral lipid membrane and binds the vRNPs .[6] Within the viral replication cycle, a crucial step is the release of vRNPs

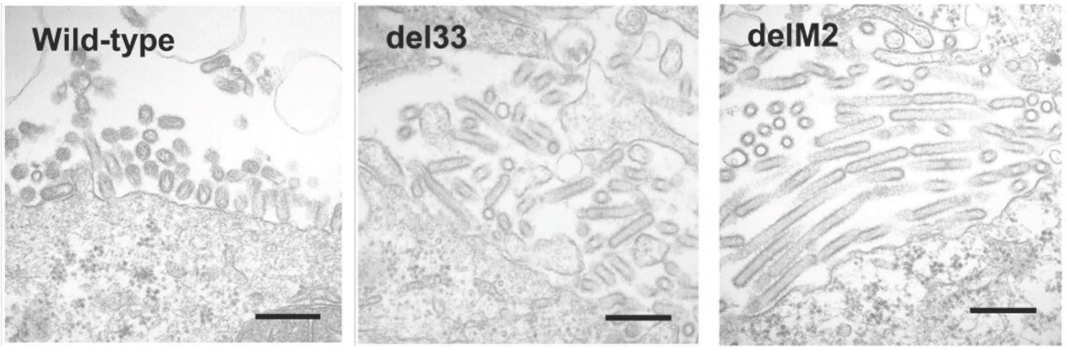

Fig 3. (A) A deletion of 33 residues from the C-terminal tail resulting in a truncation ending at residue S64, or removal of M2 altogether, results in viral buds with improper shape. Black bar is 500 nm. From [7].

from the endosome formed during viral entry into the cytoplasm to allow entry into the nucleus.[6] This endosome is acidic, and the low pH opens M2, an ion channel, allowing for acidification of the viral interior that leads to M1 to release the vRNPs.[6] M2 also plays crucial roles in generating membrane curvature in the viral budding process that releases new virions from the host.[6]

There are multiple antiviral targets at various points in the influenza A life cycle (Fig 1).[7] Previously, antivirals targeted the ion channel activity of M2 via the drug amantadine, which blocked the channel and prevented the viral replication cycle from proceeding.[7,8] However, influenza strains developed resistance to amantadine between 2002 and 2008,[7,8] leaving other regions of the influenza A M2 membrane protein to be explored as antiviral targets.

M2 has 97 residues and functions as a homotetramer (Fig 2). The protein consists of three domains (Fig 2). The C-terminal region consisting of residues 47-97 (Fig 2) has been implicated in a number of viral functions. For example, residue deletions from the C-terminal region result in viral buds with improper shape and lower amounts of viral vRNPs (Fig 3).[9] Specifically, mutations in sites 70-77 result in faulty viral genome packing.[10–13] M2 interacts with another matrix protein, M1, to pull vRNPs towards the cell membrane during the formation of new virus particles.[12] An M2 truncation consisting of residues 1-69 binds M1

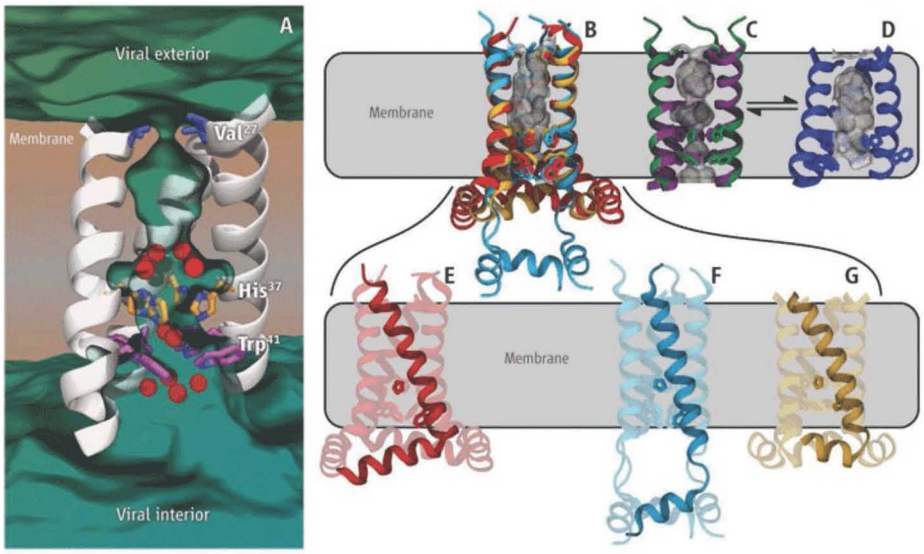

Fig 4. Previously published structures of influenza A M2. (A) X-ray crystallography structure of an M2 truncation. (B) Overlay of solid-state NMR (red), solution NMR (light blue), and EPR (yellow), respectively expanded in (E), (F), and (G) to portray differences in amphipathic helix (bottom region of protein on figure). (C) and (D) respectively portray high-pH and low-pH conformations determined by solid-state NMR (purple: PDB 3LBW) and X-ray crystallography (green: PDB 2KQT and dark blue: PDB 3BKD). From [17].

and produces new virions in this vRNP packaging mechanism, but the M2 truncation does not produce as many virions as the wild-type M2 produces during M1 binding.[11] On the other hand, the M2 truncation including only sites 70-97 alone does not bind M1.[11,12] When M2 is mutated at sites 71 to 73 or 74 to 76, M2-to-M1 binding is decreased.[12] These results indicate that *both* regions of M2, the region before residue 70 and the region between 71-76, are necessary for M1 incorporation. Residues in the 60-70 region are not only functionally important, but also conserved.[14] Notably, residues S64 and T65 are 98.4% and 99.4% conserved across influenza strains, respectively.[14]

M2 is a homotetramer with an ecto domain at its N-terminus, a transmembrane (TM) domain consisting of a helical bundle,[15] and a cytoplasmic tail at the C-terminus (Fig 2). Previously, the Howard Lab demonstrated that residues 50 to 60 of this functionally relevant C-terminal region form an amphipathic helix that lies along the membrane surface.[16] Many structural studies of M2 incorporating techniques such as X-ray crystallography, solid-state nuclear magnetic resonance (NMR), solution NMR, and electron paramagnetic resonance (EPR) display structural differences that arise from the choice of membrane mimic and M2 construct.[17] Additionally, these studies have focused on the TM region relevant for ion channel activity and the C-terminal region up to residue 60 (Fig 4).[17] Many of the differences in structure depicted in Figure 4 arise from choice of membrane mimic and the M2 construct studied. However, no published structural data exists for residues beyond 60. Predictions based off amino acid sequence indicate that M2 displays increasing disorder from residues 60-70. Additionally, much of the published structural data of C-terminal M2 was derived from M2 truncations,[18,19] which present the potential for artifacts. These M2 truncations do not include some C-

terminal residues that are the focus of this thesis, which exclusively studies full-length M2 (M2FL), the physiologically relevant form of the protein. M2FL was reconstituted into liposomes and site-directed spin label electron paramagnetic resonance (SDSL-EPR) data was collected for residues 60-70 to determine the conformation of this uncharacterized region, critical to viral budding and binding with M1 to facilitate genome packing (Chapter 3). SDSL-EPR is a powerful tool to study membrane proteins because the data can be collected on proteins reconstituted into lipid bilayers, at room temperature, a more physiologically relevant environment than the detergent micelles used in many other studies of membrane proteins.[20] A unique contribution of this thesis was determining whether the C-terminal domain of M2 faces either the inside or outside of our liposomes (Chapter 4), a key finding necessary for future studies regarding the interaction of M2 with the M1 protein.

Chapter 2: Experimental Methods

2.1. Overexpression and Purification of M2FL: Site-directed mutagenesis was used to remove native cysteine residues from the A/Udorn/M2 SGC DNA sequence. A C-terminal His_6-tag was added to aid in purification. For SDSL-EPR samples, cysteine residues were introduced one-at-a-time to residues 60-70, creating 11 unique protein constructs (Table S3). For directionality studies, cysteine-less (cysless) M2FL was expressed. Overexpression was completed as previously described.[21,22] Briefly, each construct was overexpressed in 1 L sterilized LB growth medium and aliquotted into ¼ L pellets, and stored at -80°C. Yield for protein expression ranged from 1.1×10^{-7} to 7.9×10^{-7} moles of M2 (Table S4).

Purification was done as previously described,[21,22] with some modifications introduced to prevent aggregation during purification and improve yield. Briefly, for each protein construct, ¼ L pellet was incubated in Lysis Buffer (50 mM TRIS pH 8, 30 mM octyl β-D-glucopyranoside (OG), 150 mM NaCl, 0.2 mg/mL DNase, 0.25 mg/mL lysozyme, 50 mM 4-(2-aminoethyl)benzenesulfonyl fluoride hydrochloride (AEBSF)) on ice for 30 minutes. The pellet was resuspended by vortexing and cells were lysed via sonication in an ice bath for a total of 40 minutes, corresponding to 20 minutes one second on / one second off, 20% amplitude. To remove cellular debris, the cell pellet lysate was centrifuged at 16,000 rpm 9 accel / 5 decel for 30 minutes at 4°C. The supernatant containing M2FL was decanted. To reduce disulfides between M2FL monomers, β-mercaptoethanol was added to a concentration of 7 mM and imidazole was added to a concentration of 20 mM. A 10 mL Bio-Rad chromatography column containing 0.5 mL of nickel (II) iminodiacetic acid (Ni-IDA) resin (Gold Biotechnology)

was rinsed in 10 column volumes Millipore water. The column was rinsed with 10 column volumes Standard Buffer (50 mM TRIS pH 8, 150 mM NaCl, 30 mM OG) and 20 mM imidazole.

The supernatant containing 7 mM β-mercaptoethanol and 20 mM imidazole was added to the column. The column was nutated at room temperature for 30 minutes for the His-tagged M2FL to bind to the Ni-IDA column. After this 30 minute nutation, insoluble protein aggregates sometimes formed. For solubilization of aggregation protocol, refer to Appendix 2. Protein impurities not bound to the Ni-IDA resin flowed through the column. To remove other protein impurities, the column was washed with 10 column volumes each of Wash I (50 mM TRIS pH 8, 150 mM NaCl, 30 mM OG, 20% v/vglyerol), Wash II (50 mM TRIS pH 8, 30 mM OG, 20% v/v glycerol), and Wash III (50 mM TRIS pH 8, 30 mM OG, 20% v/v glycerol, 20 mM imidazole). The higher concentration of imidazole in Wash III washed away any nonspecific proteins that may bind to the Ni-IDA resin.

For SDSL-EPR samples, a 1-oxyl-2,2,5,5-tetramethyl-Δ3-pyrroline-3-methyl methanethiosulfonate (MTSL) stock solution was prepared to a final concentration of 118 mM in acetonitrile. For more information on the spin label MTSL, refer to Chapter 2.2. A 16 μL aliquot of MTSL in acetonitrile, containing a 10:1 MTSL:M2FL molar ratio, was diluted into 1 mL of Wash III. The MTSL/Wash III solution was applied to the M2FL bound to the Ni-IDA column. The protein and spin label were nutated at room temperature for 24-36 hours. The Ni-IDA column was removed from the nutator and the excess MTSL/Wash III solution flowed through the column. To remove unreacted MTSL, the column was nutated at room temperature in the presence of 10 column

volumes of Wash III, and the column was washed with an additional 20 column volumes of Wash III. The presence of unreacted free spin label in the final sample had to be minimized for accurate analysis of EPR data.

For all samples, M2FL was eluted from the column in two 2.5 mL aliquots of Elution Buffer with a high concentration of imidazole to displace the His_6-tagged M2 protein (50 mM TRIS pH 8, 30 mM OG, 300 mM imidazole, 20% v/v glycerol). Additional 1-mL elutions were collected in Elution Buffer until the column contained no protein, as determined from the UV-Vis absorbance of 2 µL sample aliquots of the fractions at 280 nm, collected on a NanoDrop 2000 Spectrophotometer (Thermo Scientific). Between samples, the NanoDrop was cleaned with 5 µL Millipore water, 5 µL 0.5 M HCl, and 5 µL Millipore water. Elutions were concentrated to a volume of 2.5 mL in a 10K molecular weight cut-off concentrator (Amicon). The 2.5 mL sample was applied to a PD-10 desalting column (GE Healthcare) to remove any remaining free spin. PD-10 deslating columns were used to buffer swap M2FL into Desalting Buffer (50 mM TRIS pH 8, 30 mM OG). As determined by UV-Vis absorbance at 280 nm, fractions that contained M2FL were pooled (Appendix 1). Aliquots were removed after each major purification step for later analysis of purity via SDS-PAGE (Appendix 1). In order to check for presence of free spin label and to probe the percent completion of the spin label reaction, spin label efficiency was calculated (refer to Chapter 2.2 and Appendix 3).

2.2. EPR Spectroscopy of M2FL: Site-directed spin label electron

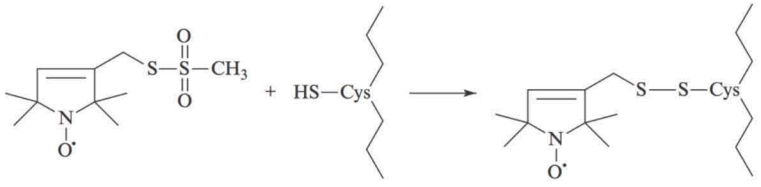

Figure 5. Attachment of MTSL free radical to cysteine residue via a disulfide bond in SDSL-EPR spectroscopy. From [20].

paramagnetic resonance (SDSL-EPR) is a powerful tool for studying proteins in physiologically relevant membrane systems. Introduction of cysteine residues at the site of interest allows the attachment of the MTSL label with a stabilized unpaired electron (Figure 5). In EPR spectroscopy, as the magnetic field increases, the energy between the two possible spin states of the unpaired electron increases.[20] When the energy between these two spin states equals the energy applied by the magnetic field ($\Delta E = h\nu$), a transition occurs and a peak appears on the EPR spectrum.[20] The number of spectral peaks is determined by the equation $2NI + 1$, where N is the number of nuclei with which the unpaired electron interacts, and I is an intrinsic value of these nuclei, specific to the

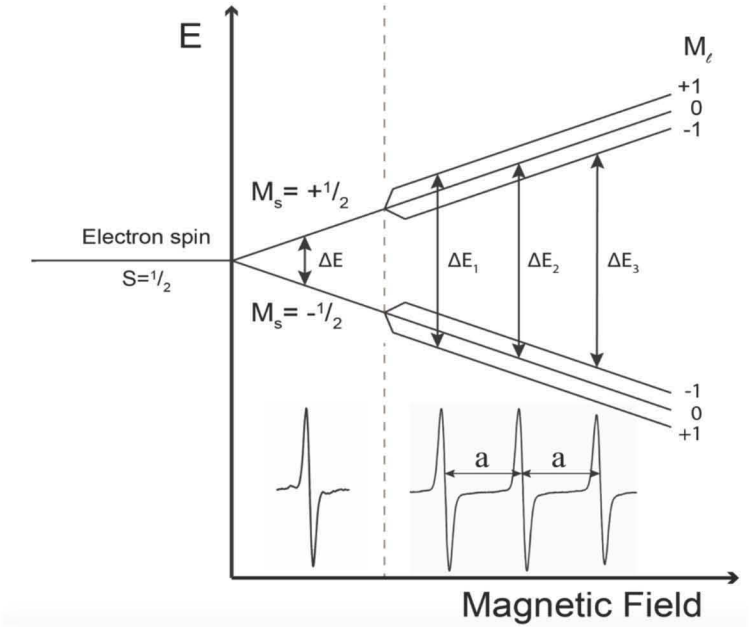

Fig 6. Origin of three EPR peaks in spectra of MTSL. From [23].

atom's identity. For MTSL, the unpaired electron is localized near a nitrogen. The most abundant isotope of nitrogen is ^{14}N. The ^{14}N nucleus has a nuclear spin of $I = 1$, and thus MTSL gives rise to three spectral peaks, represented as first-derivatives, a convention of EPR (Fig 6).[20]

Comparison of line shapes in continuous wavelength (CW) EPR spectra gives valuable information about residue dynamics and mobility.[20] Specifically, spectral broadening results from decreased spin label mobility.[20] The mobility parameter, ΔH_0^{-1}, is calculated from the inverse central linewidth of CW spectra (Appendix 4, Equation S3 & S4).[20]

Access of spin labels to relaxation agents with different membrane solubilities provides information on how a protein penetrates into a membrane bilayer. Accessibility to relaxation agents is measured using an EPR technique called power saturation. Power saturation data reflect residues' environments and a given region's secondary structure if different sides of a secondary structure are more or less embedded in the membrane.[20] In power saturation, the sample is equilibrated with a paramagnetic reagent, which alters the relaxation rate of the spin label.[20] As data are collected at increasing microwave powers in nonsaturating conditions, the central line height increases proportional to the square root of the microwave power.[20] However, at high enough powers, the relaxation rate is not high enough and the sample cannot absorb more energy.[20] As a result, the central line height decreases, and the signal is saturated.[20] Paramagnetic relaxation reagents increase the rate at which the sample relaxes.[20] Increased interaction of the spin label with these relaxation reagents gives rise to higher powers at which the signal is saturated.[20]

The two paramagnetic relaxation reagents used in this study were oxygen (O_2) and nickel (II) ethylenediaminediacetate (NiEDDA). In oxygen power saturation experiments, samples are equilibrated in air containing 20% oxygen, a sufficient level to interact with the spin label.[20] Oxygen is a small, hydrophobic molecule that preferentially partitions to the center of lipid bilayers.[20] Therefore, a residue that is more deeply buried

in the hydrophobic core of the cell membrane will interact more with oxygen.[20] This increased interaction with the paramagnetic reagent oxygen will lead to a higher power at which the signal is saturated and a higher oxygen power saturation parameter ($P_{1/2}$) for a more deeply buried residue (Appendix 4, Equation S5).[20] In NiEDDA power saturation experiments, data are collected in the presence of 50 mM NiEDDA. Unlike oxygen, NiEDDA is highly water-soluble and partitions into hydrophobic regions much less.[20] Therefore, a residue that is less deeply buried in the hydrophobic cell membrane will interact more with NiEDDA, leading to a higher NiEDDA $P_{1/2}$.[20] To standardize $P_{1/2}$ values, samples are then equilibrated with nitrogen, and data are collected at varying microwave powers, yielding a baseline $P_{1/2}$.[20] Subtracting the $P_{1/2}$ for nitrogen from the $P_{1/2}$ for oxygen or NiEDDA gives $\Delta P_{1/2}(O_2)$ or $\Delta P_{1/2}$(NiEDDA), respectively (Appendix 4, Equation S6).[20]

2.3. Reconstitution of M2FL into Lipsosomes: Previously, the Howard Lab conducted structural data for M2 reconstituted into POPC:POPG 4:1 membrane system,[16,18,19,23] chosen for its similarity to physiological membranes and reproducibility in sample preparation. This membrane system is also functionally relevant for M2's ability to induce viral budding and create new virions.[24]

For each NiEDDA power saturation study, two reconstitutions were completed: one reconstitution into POPC:POPG 4:1 lipid bilayers in the absence of NiEDDA, for CW spectra and oxygen and nitrogen power saturations, and one reconstitution into POPC:POPG 4:1 lipid bilayers in the presence of 50 mM NiEDDA. Lipid films were prepared by solubilizing 6.6×10^{-6} moles of POPC:POPG 4:1 at 25 mg/mL in chloroform. Excess chloroform was removed via evaporation and lyophilization, and

films were stored at -20°C. For samples without and with NiEDDA, a POPC:POPG 4:1 lipid film was resuspended in 500 µL of Extruder Buffer (50 mM TRIS, 100 mM KCl, 1 mM EDTA, pH 7.8) or NiEDDA Buffer (53.52 mM NiEDDA, 50 mM TRIS, 100 mM KCl, pH 7.8), respectively and extruded 15 times through a 0.2 µM polycarbonate nuclepore track-etch membrane filter (Whatman). To bring the concentration of OG to 30 mM, a value above the critical micelle concentration (CMC) of 25 mM, OG Detergent Buffer (25 mg/mL = 86 mM OG, 50 mM TRIS, 100 mM KCl, 1 mM EDTA, pH 7.8) or NiEDDA OG Detergent Buffer (25 mg/mL = 86 mM OG, 50 mM TRIS, 100 mM KCl, 1 mM EDTA, 53.52 mM NiEDDA, pH 7.8) were added to extruded lipids in the absence or presence of NiEDDA, respectively, in a 55:100 volumetric ratio. Each lipid sample equilibrated for 30 minutes. Increasing the OG concentration above the CMC and allowing the sample to equilibrate allowed micelles to form, a critical step in detergent-mediated reconstitution.

Pure, post-PD-10 protein sample was concentrated to the appropriate volume to add to extruded lipids in a 73:1000 volumetric ratio, in order to dilute the NiEDDA concentration to 50 mM required for EPR samples. For consistency, this ratio was also used for protein additions in the absence of NiEDDA. For each reconstitution, 1.312×10^{-8} moles of M2FL were added to the extruded lipids to achieve a 1:500 peptide:lipid molar ratio. The number of moles of M2FL was determined from the UV-Vis absorbance at 280 nm using the extinction coefficient 8480 mol^{-1} cm^{-1}.

Each protein/lipid sample was diluted two-fold with Extruder Buffer or NiEDDA Buffer to bring the OG concentration to 15 mM, a value below the critical micelle concentration, allowing for detergent to be removed. To remove detergent, a 10% slurry

of hydrophobic polystyrene Bio-Beads™ SM-2 Adsorbent Media (Bio-Rad Laboratories, Inc.) in TRIS/KCl Buffer (50 mM TRIS, 100 mM KCl, pH 7.8) was added to each protein/lipid sample in six, 50 µL aliquots, every 15 minutes, at 4°C. Bio-Beads™ were removed from solution via centrifugation.

Each protein/lipid solution was separated into 200 µL aliquots, and proteoliposomes were pelleted out of solution via ultracentrifugation at 90,000 rpm for 60 minutes at 4°C. Supernatant was decanted from the pellets, and the pellets were resuspended in a total volume of 200 µL of supernatant for each reconstitution. Proteoliposomes were pelleted again via ultracentrifugation at 90,000 rpm for 60 minutes at 4°C. Supernatant was decanted and stored at -20°C, and pellets were stored at -20°C.

Two main factors important in proteoliposomes are the size of vesicles and directionality of protein insertion. Dynamic light scattering data suggests that proteoliposome size remains constant throughout our current reconstitution protocols.[25] A unique contribution of this thesis was determining the directionality of M2FL upon completion of the reconstitution protocol described above. Proteoliposomes reconstituted according to this protocol were digested via enzymatic trypsin, and the products were tested via MALDI-MS to determine if M2 inserted into liposome unidirectionally or without preference for direction. Refer to "Chapter 4: Directionality of M2FL Reconstituted into POPC:POPG 4:1 Lipid Bilayers" for methods and results of trypsin digestion and MALDI-MS.

2.4. EPR Data Collection: A spin-labeled proteoliposome pellet and its corresponding supernatant were thawed at room temperature. The pellet was resuspended in 20 µL supernatant and loaded into a TPX capillary tube sealed with wax. All EPR data

was collected on a Bruker EMX spectrometer with an ER 4123S resonator. For samples without NiEDDA, a CW spectrum was collected at 2 mW incident microwave power, 1G field modulation amplitude 100 kHz, and 150 G sweep width centered at 3480 G. For the same sample, equilibrated in air, oxygen power saturation spectra were collected at 1G field modulation amplitude 100 kHz, and 150 G sweep width centered at 3480 G, at 19 power levels (Table S5). The sample was equilibrated in nitrogen gas for 15 minutes, and nitrogen power saturation spectra were collected at 1G field modulation amplitude 100 kHz, and 150 G sweep width centered at 3480 G, at 8 power levels (Table S6). Samples with NiEDDA were equilibrated in nitrogen gas for 15 minutes. Power saturation spectra were collected at 1G field modulation amplitude 100 kHz, and 150 G sweep width centered at 3480 G, at 19 power levels (Table S1).

Power saturation data were fit in Igor Pro 7.05 to calculate the accessibility parameter, $\Delta P_{1/2}$, as described previously.[19] All linear and sinusoidal data fits were performed in Igor Pro 7.05. A representative example of power saturation data processing is included in Appendix 4, Equations S5 & S6.

Chapter 3: Structure of Residues 60-70 of Full-Length M2

In order to elucidate the structure of residues 60-70 involved with viral budding and genome packing, SDSL-EPR was used to probe local secondary structure and membrane topology. The CW and membrane accessibility data in this chapter analyze residue mobility and association with the membrane, along with possible helical secondary structures.

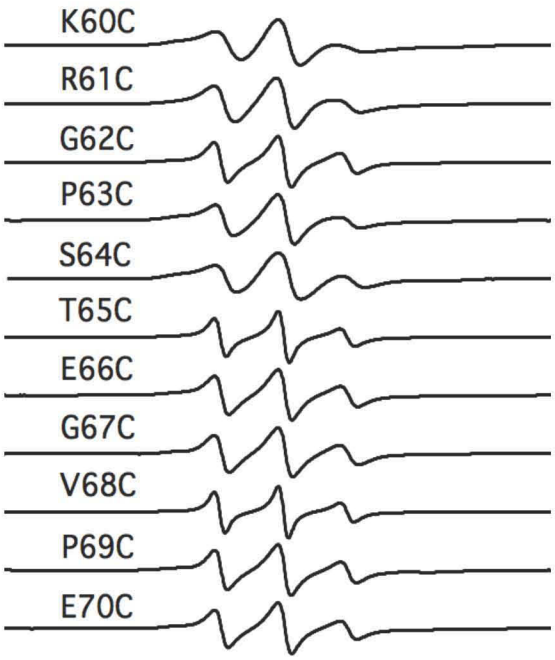

Fig 7. CW spectra of C-terminal M2FL, collected at 2 mW incident power, 1G field modulation, amplitude 100 kHz, and 150 G sweep width centered at 3480 G.

3.1. CW Spectra Show Increased Mobility of Residues 60-70: Moving from residue 60 to 70, CW spectra become sharper (Fig 7). Mobility parameters (ΔH_0^{-1}) from central linewidth indicate that overall, residues 60-70 are more mobile than residues 50-59 (Fig 8, Table S7). This trend is evident in a linear fit of mobility parameters, with a slope of (Fig 8, Table S7). CW lineshape features indicate that when moving towards the C-terminus of M2, there are increased residue mobility and dynamics, especially at residues 65-70.

Spin label mobility depends on restrictions from the environment, for example, packing against neighboring residues or association with the membrane. One possibility for the increase in mobility in residues 60-70 is that this region is not closely associated with the membrane surface as seen for 50-60. Thus, we measured the membrane depth for 60-70 to test this hypothesis.

3.2. Use of Two Complementary Paramagnetic Reagents in Membrane

Accessibility Measurements: Since a larger accessibility to the paramagnetic reagent oxygen, $\Delta P_{1/2}(O_2)$, indicates greater depth in the membrane and a larger accessibility to NiEDDA, $\Delta P_{1/2}$(NiEDDA), indicates greater extension into the aqueous phase, the $\Delta P_{1/2}(O_2)$ and $\Delta P_{1/2}$(NiEDDA) values should be out-of-phase, if in fact the helix is laying on the surface of the membrane. If the helix is completely buried, or completely in the water, there should be no periodic relationship between the two oxygen and nickel accessibilities.[20] For a region that has asymmetric accessibility to a hydrophobic

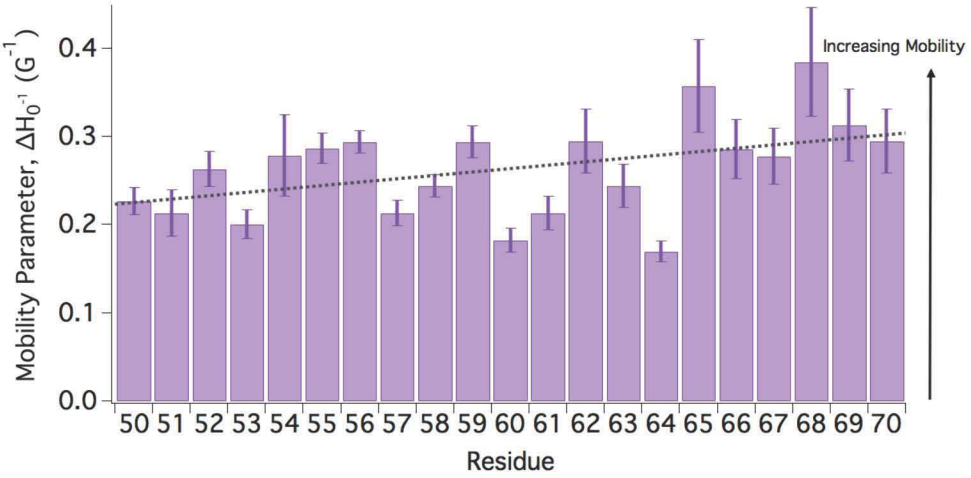

Fig 8. Mobility parameters calculated from CW spectra of C-terminal M2FL residues 50-60 (not shown, from [21]) and 60-70. Dotted line shows linear fit.

environment, a plot of $\Delta P_{1/2}$ values versus residue and the periodicity of these values when fit to a sine curve can then give information about a protein region's secondary structure.[20] The periodicity gives information about how many residue repeats there are per helical turn, e.g. 3.6 for an alpha helix (Fig 9).[26]

Another helical structure possibility is a left-handed poly-L-proline type II (PPII) helix (Fig 9).[27] PPII helices are more extended than alpha helices, measuring at 3.1 Å per residue, compared with 1.5 Å per residue for alpha helices (Fig 9).[27] As PPII helices lack

hydrogen bonding patterns present in other secondary structures, they are usually misidentified as "disordered" or "random" conformations.[28] Previous work with other disordered protein regions has demonstrated that secondary, helical protein structure is induced in the presence of a membrane.[29–31] Therefore, SDSL-EPR studies in this thesis aim to probe whether the 60-70 region is truly disordered, or if region adopts a secondary structure in the membrane environment. Appropriate for accessibility studies, PPII helices display 3 residues per helical turn, so when accessibility values of a PPII helix are fit to a sine curve, the periodicity equals 3.0 (Fig 9).[27] This study employs the curve given by equation (1):

$$\Delta P_{\frac{1}{2}}(O_2 \text{ or NiEDDA}) = A\sin\left(\frac{2\pi}{D} + \theta\right) + Bx + C \qquad (1)$$

where A is amplitude of the sine curve, B accounts for the helical tilt with respect to the membrane, C is the y-axis offset, and D is the periodicity. For a helical region not equally exposed to the hydrophobic membrane core and the aqueous cellular exterior, $\Delta P_{1/2}(O_2)$ and $\Delta P_{1/2}(\text{NiEDDA})$ values are out-of-phase, but ΔH_0^{-1} is approximately constant.[26] Accessibilities to oxygen and NiEDDA can also be combined in the contrast parameter, ϕ, given by equation (2):

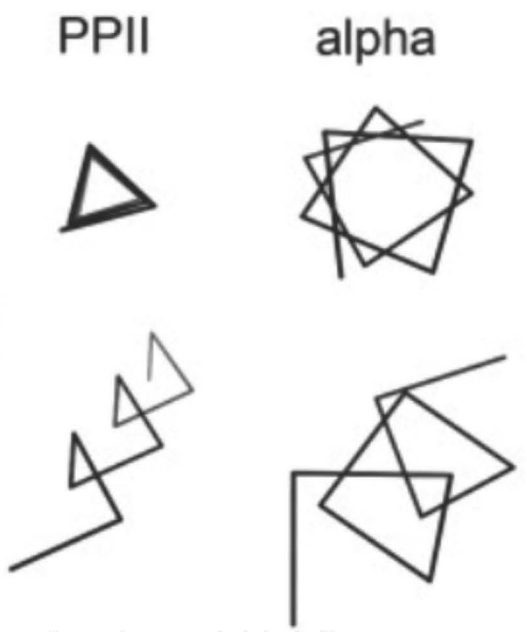

Fig 9. Comparison of PPII and alpha helix structures. From [27].

$$\phi = ln\left(\frac{\frac{\Delta P_1(\text{NiEDDA})}{2}}{\frac{\Delta P_1(O_2)}{2}}\right) \quad (2)$$

which gives information about residue depth.[32,33] Deeply buried residues will display sharp spikes in ϕ, while entire regions that are mostly aqueous exposed will exhibit relatively constant ϕ values.[32,33]

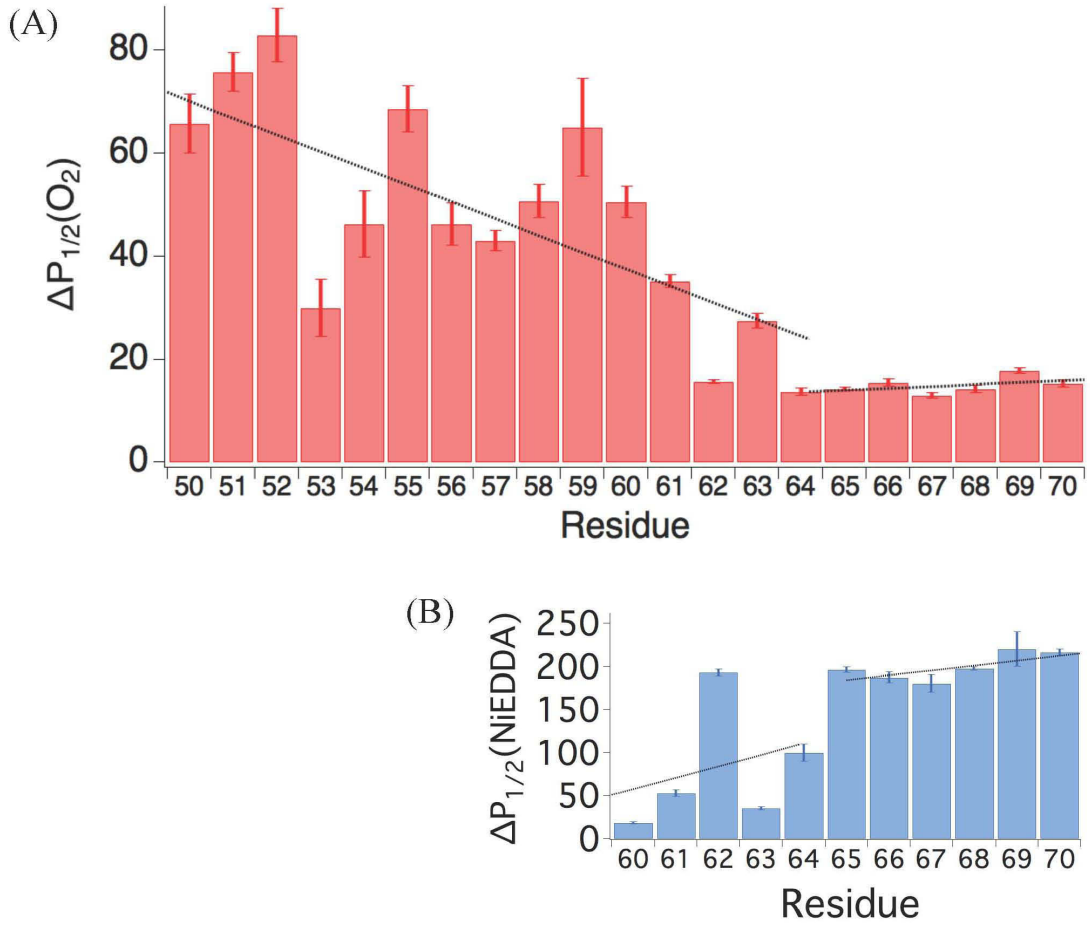

Fig 10. (A) $\Delta P_{1/2}(O_2)$ values and (B) $\Delta P_{1/2}$(NiEDDA) values for C-terminal residues. Error bars in both (A) and (B) represent the 95% confidence intervals from power saturation curve fits. Dotted lines show linear fits. Data for residues 50-59 from [21-22].

3.3. Membrane Accessibility Data Consistent With Extension Into the Aqueous Phase:

Moving from residue 60 to 70, $\Delta P_{1/2}(O_2)$ values decrease and

$\Delta P_{1/2}$(NiEDDA) values increase (Fig 10, Table S9). When fit with a linear equation, the negative slope -3.4 in oxygen accessibilities of residues 50-64 shows that residues are becoming less deeply buried (Fig 10A, Table S10). The small positive slope 0.4 for oxygen accessibilities in 64-70 demonstrates that the region is relatively constant in oxygen accessibility and not deeply embedded in the membrane (Fig 10A, Table S10). The positive slope 10 for NiEDDA accessibilities in 60-64 shows that these residues extend towards the aqueous phase (Fig 10B, Table S10). The large increase in NiEDDA accessibility at residue 65 and the

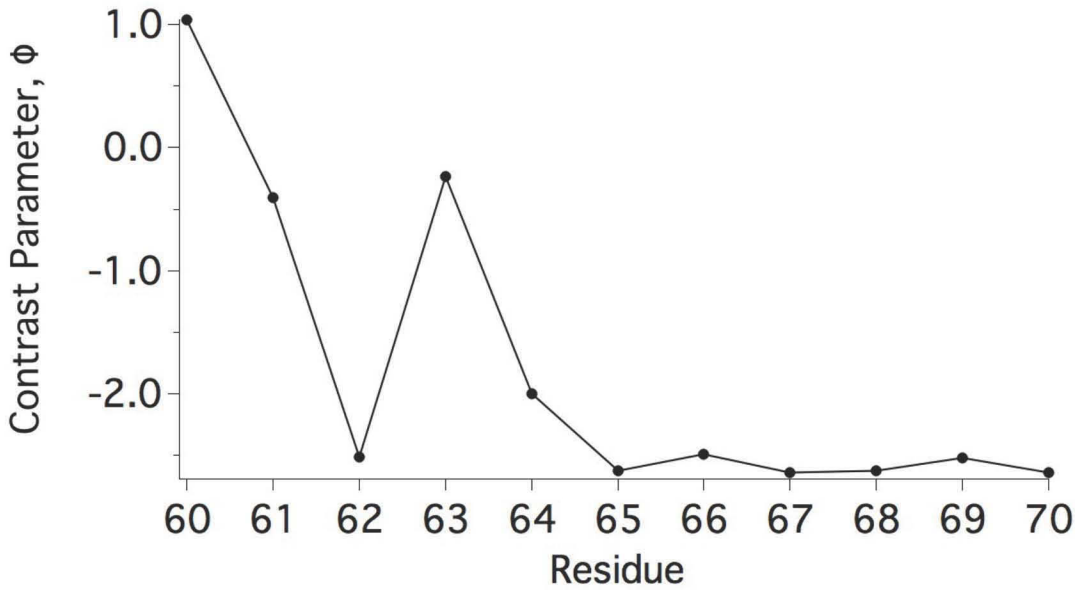

Fig 11. Contrast parameters of C-terminal residues 60-70.

small positive slope 6 for residues 65-70 indicates that these residues have similar accessibility to NiEDDA (Fig 10B, Table S10). These trends indicate that residues 65-70 of M2 extend into the aqueous phase more at sites further from the TM domain, but the region is still associated with the membrane (Fig 10, Table S9). The topology of the region can be described as extending along the membrane but angled towards the aqueous cellular exterior. The distinct decrease in $\Delta P_{1/2}(O_2)$ and increase in

$\Delta P_{1/2}$(NiEDDA) at residue 64 indicate that significant tilt towards the aqueous phase occurs at these residues (Fig 10, Table S9). Contrast parameter data calculated according to equation (2) also support this tilt model, as ϕ is approximately constant for residues 65-70, indicating that the region is solvent-exposed (Fig 11, Table S11). Since the accessibilities to oxygen are high when the accessibilities to NiEDDA are low (Fig 10, Table S9), a second condition for a helical region with unequal exposure to the aqueous phase and hydrophobic membrane core is fulfilled. Spikes in ϕ values for residues 60, 61, and 63 show that these residues are more accessible to membrane-solubilized oxygen than residues 65-70 (Fig 11, Table S11).

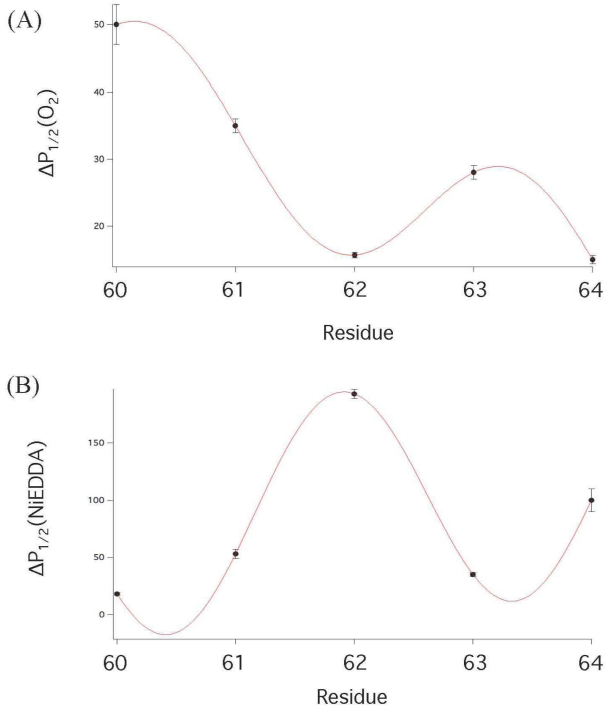

Fig 12. (A) Oxygen and (B) NiEDDA accessibilities with overlaid sine curve fit results of residues 60-64. Error bars represent 95% confidence intervals from power saturation curve fits.

To probe a possible helical structure this region, the oxygen and NiEDDA accessibilities of residues 60-64 and 64-70 were fit with equation (1). The periodicities of the sine curve fits to oxygen and NiEDDA accessibility data for 60-64 were 3.1 and 2.9

(Fig 12, Table S12). Periodicity values close to 3.0 indicate that the 60-64 region may form a PPII helix. The periodicities of the sine curve fits to oxygen and NiEDDA accessibility data for 64-70 were 3.1 and 3.4, respectively (Fig 13, Table S12). The periodicities for residues 64-70 indicate that there is some secondary structure in this region, which is membrane associated. However, a direct conclusion cannot be asserted regarding whether or not this region has a helical structure with a defined residue-per-turn periodicity. For sites 64-70, taking into account the out-of-phase NiEDDA and oxygen accessibility sine curve fits and the low and relatively constant contrast parameters, there is strong evidence that this region displays some membrane-associated secondary structure, with a slight tilt away from the membrane towards the aqueous phase.

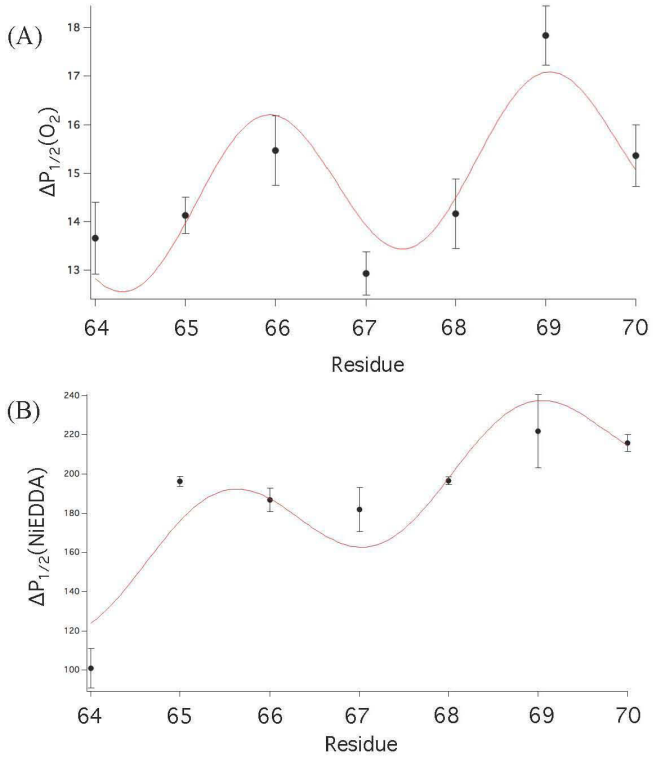

Fig 13. (A) Oxygen and (B) NiEDDA accessibilities with overlaid sine curve fit results of residues 64-70. Error bars represent 95% confidence intervals from power saturation curve fits.

method of preparation of proteoliposomes, membrane proteins can either be uniformly inserted in one orientation (either N-terminus or C-terminus inside the liposome) or prepared such that there is a mixture of two insertion orientations (Fig 14).

We studied the insertion of M2FL protein using our established reconstitution protocol to determine whether there was no directionality (a mix of N- and C- termini at the liposome exterior), unidirectional with the N-terminus at the liposome exterior, or unidirectional with the C-terminus at the liposome exterior. Regarding the conformational studies of the C-terminus, reversing the orientation of the C-terminus means that the curvature properties of the lipid bilayer are different. Therefore, the overall protein orientation has important conformational implications. There may be differences in membrane topology of C-terminal M2FL if the region lies along the concave liposome interior or the convex liposome exterior. In native M2FL, the N-terminal region is extracellular and the C-terminal region is cytoplasmic, while the protein acts as an ion channel.[34–37] In this orientation, the C-terminus would lie along a concave liposome interior. When M2 induces budding to generate new virions,[38] the C-terminus would lie along a convex liposome surface. Therefore, either M2 orientation can be physiologically relevant. If the C-terminus lies along the liposome exterior, the region is available to bind to M1 after the protein has been reconstituted. Therefore, a directionality with the C-terminus at the exterior would facilitate future studies where M2 can bind M1 in our current POPC:POPG 4:1 model membrane system.

In order to probe the directionality of M2FL in the current membrane system, M2FL samples in micelles or liposomes were digested with enzymatic trypsin. Trypsin cleaves at regions of accessible protein sites at the C-terminal side of lysine (K) and

arginine (R) residues. Previously, trypsin digestion of M2 solubilized in dodecylphosphocholine (DPC) detergent micelles produced fragments spanning residues 19-60 and 19-61 of M2, but no cleavage occurred at the possible trypsin targets R45, K49, and R53.[39]

Trypsin digested M2FL in OG detergent micelles and M2FL reconstituted into POPC:POPG 4:1 liposomes. Trypsin's cleavage at certain sites or lack of accessibility results from the directionality of M2FL reconstituted into liposomes, yielding different protein fragments dependent upon the three directionality schemes described above (Fig 14). If reconstituted M2FL inserted into the bilayer with no directionality, we expected to see MS fragments representative of cleavage at N-terminal and C-terminal residues for both the micelle and liposome samples. For insertion into the bilayer unidirectionally with the N-terminus at the liposome exterior, we expected to see only MS fragments for N-terminal cleavage. For M2FL sample solubilized in OG detergent micelles, we expected cleavage at N-terminal site residue R18 consistent with previous work.[39] For the unidirectional scheme with the N-terminus at the liposome exterior, some of these fragments representative of N-terminal cleavage fragments may have appeared on the liposome digestion mass spectrum. If insertion was unidirectional with the C-terminus at the lipsome exterior, the MS peaks representative of N-terminal cleavage at residue R18 for M2FL in micelles would not appear on the mass spectrum of digested M2FL in liposomes, and peaks representative of fragments from exclusively C-terminal cleavage sites would appear on the mass spectrum.

4.2. Trypsin Digestion Experimental Methods: Two samples were digested with enzymatic trypsin: cysteineless (cysless) M2FL solubilized in OG detergent micelles

and cysless M2FL reconstituted into POPC:POPG 4:1 lipid bilayers. (For purification of each sample and and reconstitution of proteoliposomes, see Chapter 2.) Lyophilized Sequencing Grade Modified Trypsin (Porcine, Promega) was thawed and resuspended in 50 mM acetic acid. Solubilized trypsin was incubated at 30°C for 15 minutes. A 1.312×10^{-8} mole M2FL sample was aliquoted out of the post-PD-10 cysless stock. Trypsin was added to the aliquot in a 1:20 (w/w) trypsin:M2FL ratio. A 1.312×10^{-8} mole M2FL sample reconstituted into POPC:POPG 4:1 lipid bilayers was resuspended as described in proteoliposome pellet resuspension procedure in Chapter 3.4. A 4.373×10^{-9} mole aliquot of resuspended proteoliposome was removed for analysis via MALDI-MS. Trypsin was added to the remaining resuspended proteoliposome in a 1:20 (w/w) trypsin:M2FL ratio. Both trypsin and M2FL samples were incubated at 37°C for 24 hours. Reaction aliquots were terminated at various time points, and these aliquots were analyzed via SDS-PAGE in order to optimize the time needed for digestion (Chapter 4.4). The final reaction used for MALDI-MS data collection was terminated after three hours. Trypsin digestion reactions were terminated by freezing at -20°C.

4.3. MALDI-MS Experimental Methods: Data was collected on a Bruker UltraFlex III TOF/TOF instrument located in the Biological Chemistry Resource Center located in the Department of Chemistry at the University of Pennsylvania. Assistance was provided from graduate student and facility technician Miklos Szantai-Kis.

For the first round of MALDI-MS data collection, two micelle samples were tested: M2 in micelles (90 μM M2) and M2 in micelles after trypsin digestion (60 μM M2). Three dilutions of each were prepared at 1:20, 1:100 and 1:500 in ddH_20 with 0.1% trifluoroacetic acid (TFA). TFA should deactivate trypsin. Each of the dilutions were

parts 1:1 with either of two matrices α-Cyano-4-hydroxycinnamic acid (CHCA) and sinapinic acid. Conditions that worked best for both micelle samples were the 1:20 dilution in the CHCA matrix. 0.5 μL of sample were added to the plate, followed by 0.5 μL of matrix which were mixed right on the MALDI plate by pulling sample up and down in a pipette tip.

Two liposome samples were tested: M2 in liposomes (440 μM M2) and M2 in liposomes after trypsin digestion (120 μM M2). Due to the high concentration of lipids, liposomes samples were prepared using Zip tips (Millipore reverse phase PRO 2358) to remove excess lipid and facilitate collection of MALDI data. Proteoliposome samples were pulled up into equilibrated Ziptips. Excess buffer and salt were removed from samples using ddH_2O. Lipids were eluted from Ziptips matrix using 50% water/50% acetonitrile and then 100% acetonitrile. Each of the samples were mixed with either of two matrices, CHCA and sinapinic acid. The matrix that worked best for the liposome samples was CHCA.

For the second round of MALDI-MS data collection, two micelle samples were tested: M2 in micelles (80 μM M2) and M2 in micelles after trypsin digestion (60 μM M2). Two liposome samples were tested: M2 in liposomes (440 μM M2) and M2 in liposomes after trypsin digestion (120 μM M2). the samples were eluted with a different solvent system. Instead of just 0.1% TFA/Acetonitrile the solvent included Isopropanol/Acetonitrile/Water/TFA so that M2FL could be knocked off the column instead of sticking. Two matrices were used: CHCA and 2,5-dihydroxybenzoic acid (DHB). Both CHCA and DHB worked, but DHB gave more sensitive data.

To identify MS peaks, an exhaustive list of all possible trypsin cleavage products was generated from the sequence of the M2FL cysless construct (Table 1, Table S3). The expected molecular weight of each fragment was calculated using the ExPASy ProtParam tool (Table 1).[40] Expected molecular weights were matched to experimental MS peaks with less than less than 2 Da difference (Table 1, Fig 15). Molecular weight of the cysless M2FL peak (Fig 10) corresponds to the molecular weight of the M2FL cysless construct (Table S3) without the first methionine residue, as this residue was cleaved during protein expression.

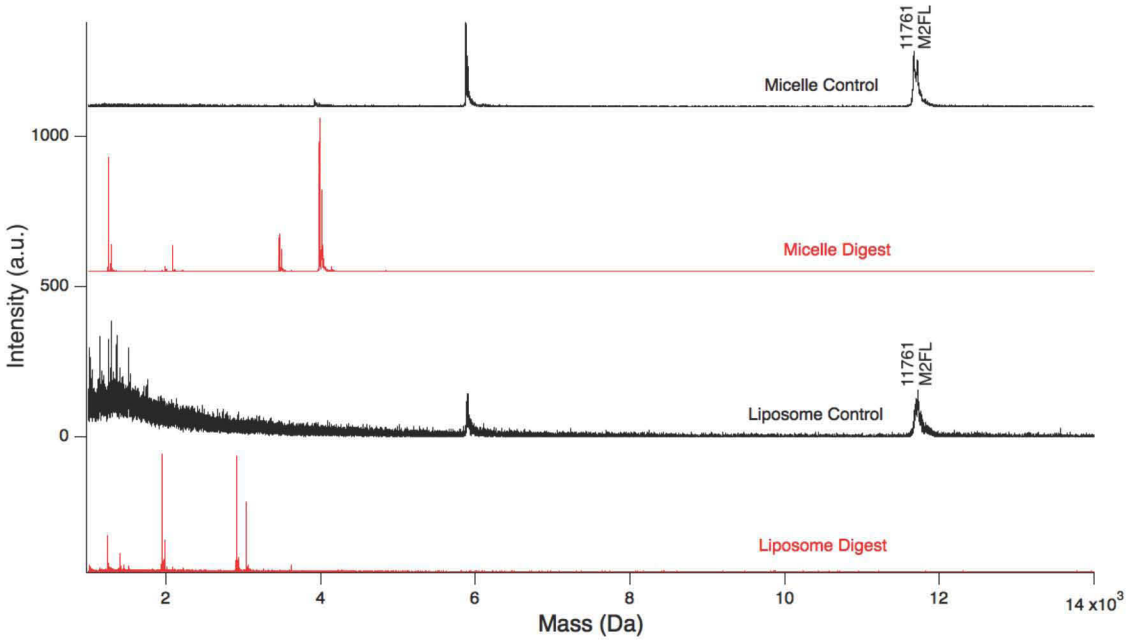

Fig 15. Mass spectra of undigested ("Control") and digested M2FL solubilized in OG detergent micelles ("Micelle") or reconstituted into POPC:POPG 4:1 lipid bilayers ("Liposome").

4.4. SDS-PAGE of Trypsin Digestion Products: SDS-PAGE was run to demonstrate that the trypsin digestion reaction of samples in micelles and liposomes did produce protein fragments smaller than M2FL. The first trypsin digestion reaction was run to demonstrate that the reaction did work for M2FL solubilized in micelles. The reaction worked, as demonstrated by the presence of bands smaller than 11.9 kDa (Fig

16). The length of time that the reaction ran did not produce any detectable difference in the length of fragments, indicating that nonspecific cleavage did not occur (Fig 16). A second reaction was run on micelles and liposomes to demonstrate that the reaction worked for M2FL reconstituted into lipid bilayers, and to compare the reaction products to those of micelles (Fig 17). Presence of liposomes created smears on the gel (Fig 17). Again, the reaction worked for micelles and liposomes and the length of time that the reaction ran did not produce any detectable difference in the length of fragments (Fig 17). Therefore, a three-hour reaction period was chosen for the final reaction. This reaction was completed for another set of micelle and liposome samples, producing fragments that could be analyzed via MALDI-MS (Fig 18). Samples for the gel in Fig 18 were aliquotted from the same reaction products used for MALDI-MS. This MALDI-MS data was inconclusive due to absence of M2FL peak on mass spectrum of undigested liposome (Fig S7 & S8). Purification, reconstitution, and trypsin digestion were repeated. Reaction products and control samples were analyzed via SDS-PAGE to demonstrate that trypsin produced M2 fragments (Fig 19). SDS-PAGE for proteoliposome samples still needs to be optimized; current progress on this protocol is detailed in Appendix 5.

4.5. M2FL Insertion Displays No Directionality: Digestion of M2FL solubilized in micelles produced N-to-C-terminus-spanning fragments S19-K60 and S19-R61 (Fig 20 & 21, Table 1) consistent with previous work.[39] Additionally, a fragment spanning the N-terminus to a residue previously protected from digestion,[39] S19-R53, was produced (Fig 20 & 21, Table 1). Other fragments generated from N-terminal, TM, and C-terminal cut sites were produced in the digestion of micelle samples (Fig 20 & 21, Table 1).

When M2FL reconstituted into POPC:POPG 4:1 liposomes was digested, trypsin made cuts at M2FL's N-terminus and C-terminus (Fig 20 & 21, Table 1). Both the micelle and liposome digestions revealed fragments S2-R12, S2-R18, K78-R97, and E79-R97 (Fig 20 & 21, Table 1) Some C-terminal fragments may have appeared on the liposome digestion but not on the micelle digestion because the OG detergent may have interfered with the enzymatic trypsin activity (Fig 20 & 21, Table 1). Micelle digestion peaks S19-K49, S19-R53, S19-K60, S19-R61, L46-K78, and G62-R77 did not appear on the liposome digestion spectrum (Fig 20, Table 1). Trypsin may not have been able to access the membrane-associated region at residues 40-62.

As trypsin was able to access both the N- and C-termini at the liposome exterior, M2FL does not show directionality upon reconstitution into the lipid bilayer. Both the N- and C-termini lie at the liposome exterior in proteoliposomes formed according to current reconstitution protocols.

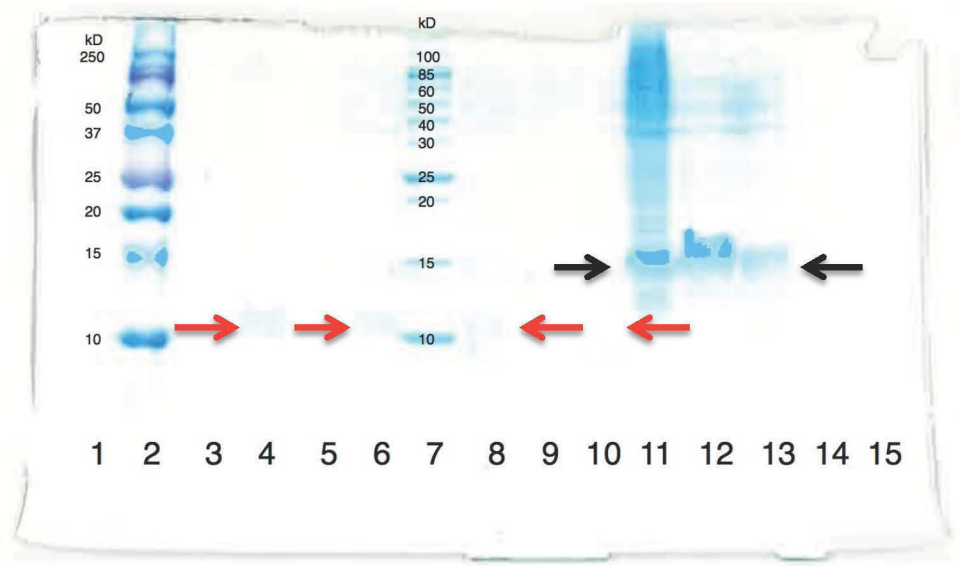

Fig 16. SDS-PAGE of trypsin digestion products. Red arrows point to digestion products. Black arrows point to undigested M2FL. Digestion reaction was terminated after one hour in lane 4, three hours in lane 6, 5 hours in lane 8, and 24 hours in lane 10.

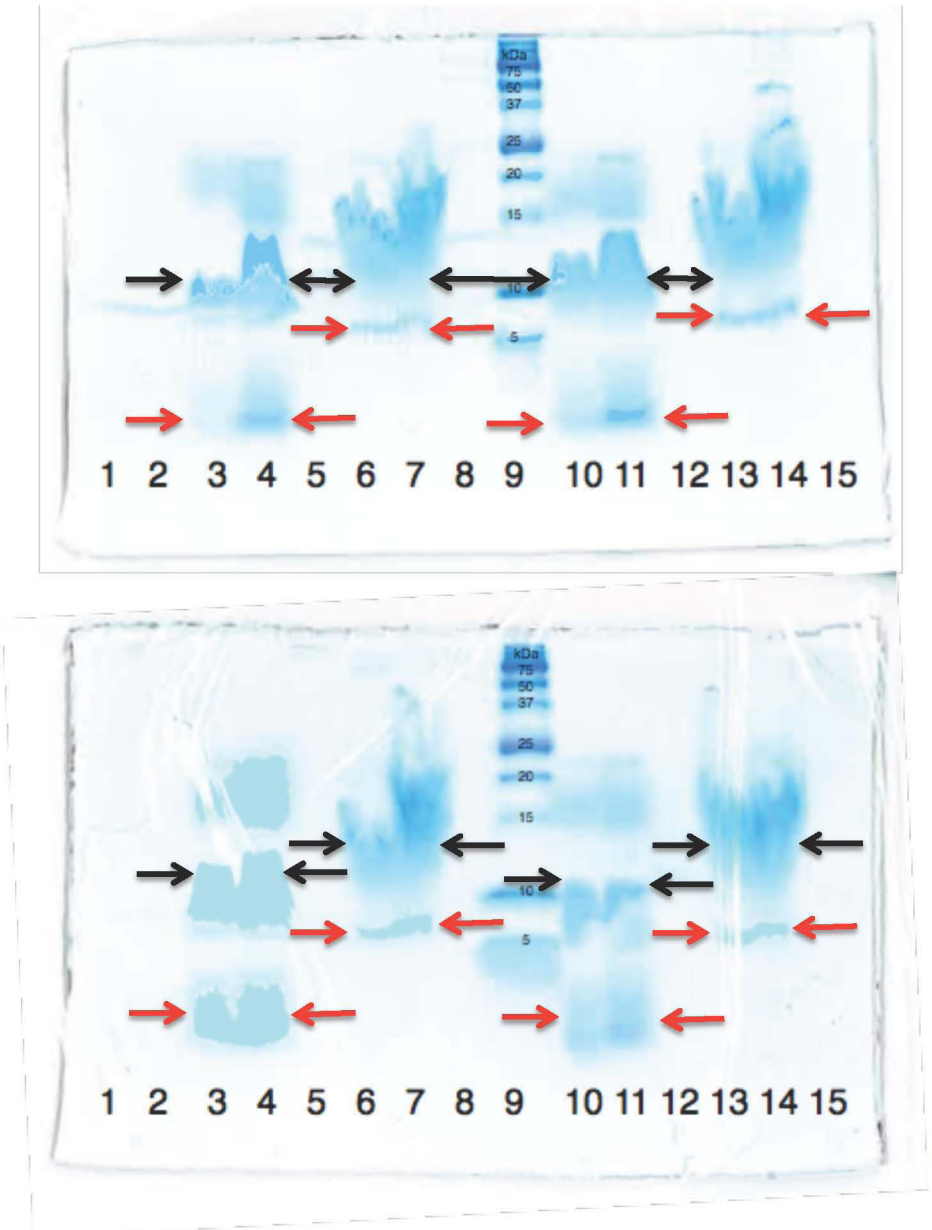

Fig 17. SDS-PAGE of trypsin digestion products. Red arrows point to digestion products. Black arrows point to undigested M2FL. Upper gel lanes 3 & 4: Micelle digestion terminated at one hour. Upper gel lanes 6 & 7: Liposome digestion terminated at one hour. Upper gel lanes 10 & 11: Micelle digestion terminated at two hours. Lanes 13 & 14: Liposome digestion terminated at two hours. Lower gel lanes 3 & 4: Micelle digestion terminated at 3 hours. Lower gel lanes 6 & 7: Liposome digestion terminated at 3 hours. Lower gel lanes 10 & 11: Micelle digestion terminated at 24 hours. Lower gel lanes 13 & 14: Liposome digestion terminated at 24 hours.

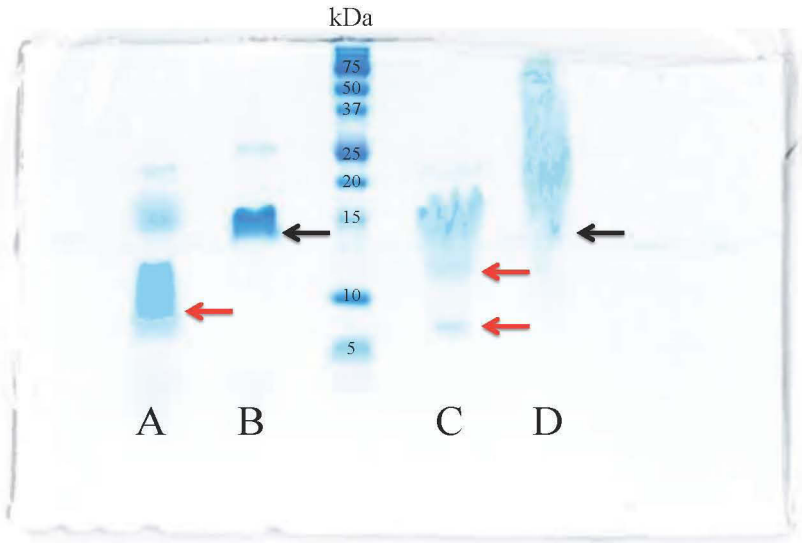

Fig 18. SDS-PAGE of trypsin digestion products. Red arrows point to digestion products. Black arrows point to undigested M2FL. Lane A: trypsin-digested M2FL solubilized in OG detergent micelles. Lane B: undigested M2FL solubilized in OG detergent micelles. Lane C: trypsin-digested M2FL reconstituted into POPC:POPG 4:1 liposomes. Lane D: undigested M2FL reconstituted into POPC:POPG 4:1 liposomes.

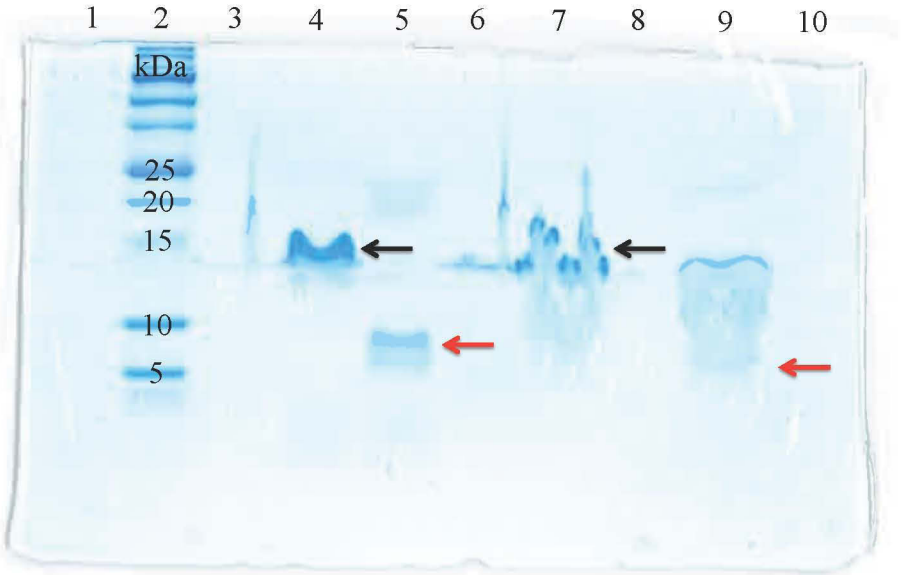

Fig 19. SDS-PAGE of trypsin digestion products. Red arrows point to digestion products. Black arrows point to undigested M2FL. Lane 2: Protein Ladder. Lane 4: undigested M2FL solubilized in OG detergent micelles. Lane 6: trypsin-digested M2FL solubilized in OG detergent micelles. Lane 7: undigested M2FL reconstituted into POPC:POPG 4:1 liposomes. Lane 9: trypsin-digested M2FL reconstituted into POPC:POPG 4:1 liposomes.

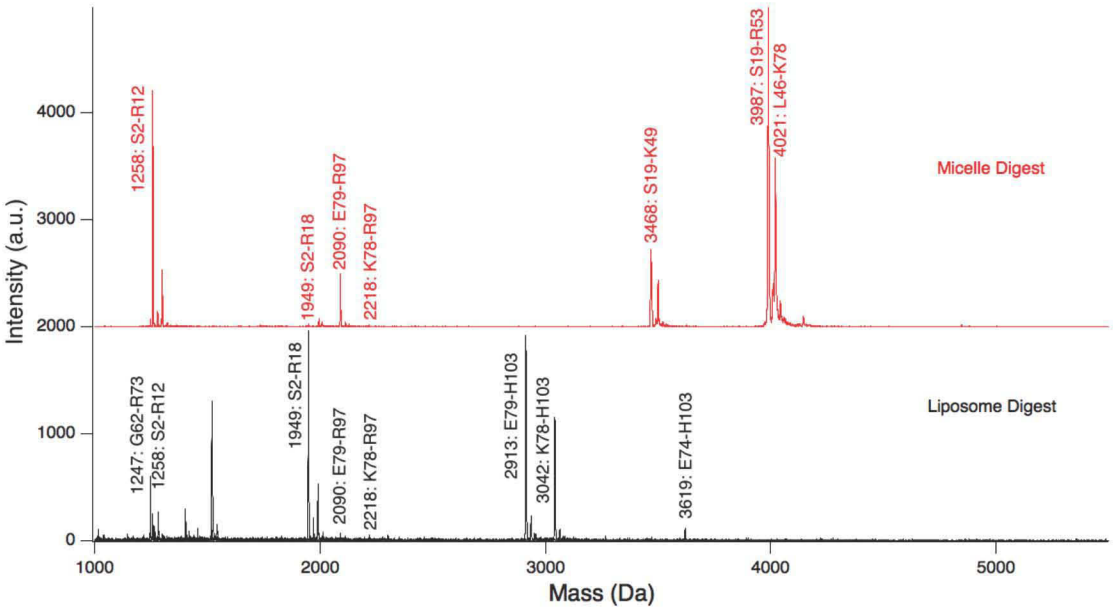

Fig 20. Mass spectra of digested M2FL solubilized in OG detergent micelles ("Micelle Digest") and M2FL reconstituted into POPC:POPG 4:1 lipid bilayers.

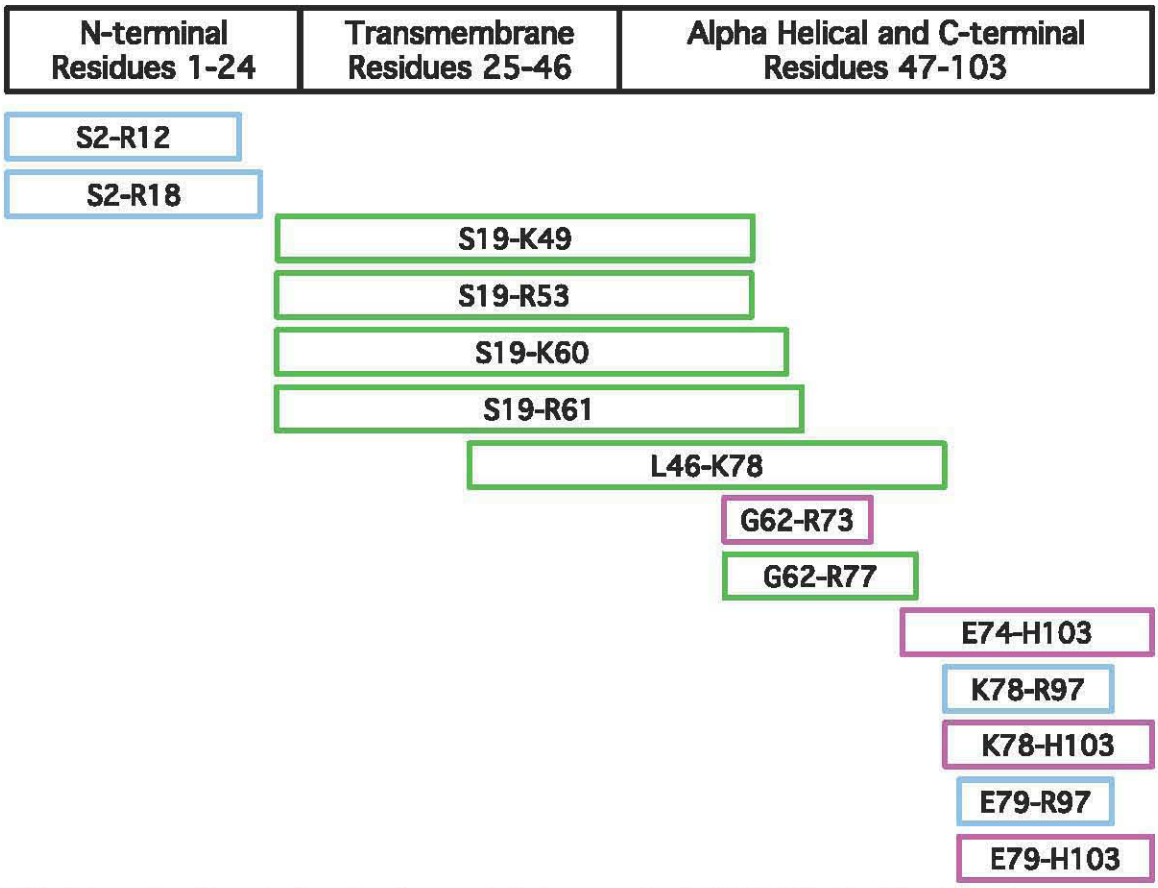

Fig 21. Schematic of trypsin digestion fragments that appeared in MALDI-MS data. Blue indicates fragments that appeared on micelle and liposome digestion spectra. Green indicates fragments that appeared only on micelle digestion spectrum. Pink indicates fragments that appeared only on liposome digestion spectrum. Molecular weights are listed in Table 1.

Table 1. All theoretical trypsin digestion fragments of M2FL. Fragments highlighted in blue correspond to peaks on both micelle and liposome digestion mass spectra. Fragments highlighted in green correspond to peaks only on micelle digestion mass spectrum. Fragments highlighted in pink correspond to peaks only on liposome digestion mass spectrum. Fragments larger than the maximum molecular weight on mass spectrum are not included.

Fragment	Expected Molecular Weight (Da)	Protein Domain
S2-R12	1257.45	N-terminus
S2-R18	1948.16	N-terminus
S2-R45	4861.57	N-terminus to TM
S2-R53	5916.86	N-terminus to TM
N13-R45	3622.14	N-terminus to TM
N13-R53	4677.43	N-terminus to C-terminus
N13-K60	5536.42	N-terminus to C-terminus
N13-R61	5692.61	N-terminus to C-terminus
S19-R45	2931.42	N-terminus to TM
S19-K49	3467.112	N-terminus to C-terminus
S19-R53	3986.71	N-terminus to C-terminus
S19-K60	4845.71	N-terminus to C-terminus
S19-R61	5001.90	N-terminus to C-terminus
S19-R73	6230.24	N-terminus to C-terminus
L46-R53	1073.3	TM to C-terminus
L46-K60	1932.30	TM to C-terminus
L46-R61	2088.49	TM to C-terminus
L46-R73	3316.83	TM to C-terminus
L46-R77	3894.42	TM to C-terminus
L46-K78	4022.60	TM to C-terminus
L46-R97	6094.73	TM to C-terminus
L46-H103	6917.58	TM to C-terminus
S50-K60	1396.61	C-terminus
S50-R61	1552.80	C-terminus
S50-R73	2781.14	C-terminus
S50-R77	3358.74	C-terminus
S50-K78	3486.91	C-terminus
S50-R97	5559.04	C-terminus
S50-H103	6381.89	C-terminus
F54-K60	877.01	C-terminus
F54-R61	1033.2	C-terminus
F54-R73	2261.54	C-terminus
F54-R77	2839.13	C-terminus
F54-K78	2967.31	C-terminus
F54-R97	5039.44	C-terminus
F54-H103	5862.29	C-terminus
R61-R73	1402.55	C-terminus

R61-R77	1980.14	C-terminus
R61-K78	2108.31	C-terminus
R61-R97	4180.45	C-terminus
R61-H103	5003.394	C-terminus
G62-R73	1246.755	C-terminus
G62-R77	1823.95	C-terminus
G62-K78	1952.13	C-terminus
G62-R97	4024.26	C-terminus
G62-H103	4847.125	C-terminus
E74-R77	595.60	C-terminus
E74-K78	723.78	C-terminus
E74-R97	2795.92	C-terminus
E74-H103	3618.76	C-terminus
K78-R97	2218.32	C-terminus
K78-H103	3041.17	C-terminus
E79-R97	2090.15	C-terminus
E79-H103	2912.99	C-terminus

Chapter 5: Summary and Future Directions

This thesis reported information on the conformation and dynamics of a previously uncharacterized region of the M2 protein that plays critical roles in the life cycle of the influenza virus. SDSL-EPR data on residues 60-70 within the C-terminal domain revealed that the region has accessibility to the lipid bilayer for residues 60-64 and high accessibility to the aqueous phase for residues 65-70. Residues 64-70 have periodic accessibilities to the lipid membrane and the aqueous phase, indicating some secondary structure. Further structural studies are required in order to determine if the region has a periodicity representative of a helix with a defined number of residues per turn. Two possibilities for more extensive structural studies of this region are to introduce cholesterol or M1 into the current system. Previously, the Howard Lab found that M2 conformation is sensitive to the presence of cholesterol.[18,23] The presence of cholesterol or M1 binding could induce a more defined secondary structure in residues 60-70 of the C-terminal region.

One possible future experiment could extend the membrane accessibility studies to residues 70-80. EPR power saturation techniques in the presence of oxygen or NiEDDA can be employed for residues 70-80, and accessibility values for residues 60-80 can be fit with equation (1). If periodicities of oxygen and NiEDDA accessibilities are closer for residues 60-80 than they are for residues 60-70, this data may further elucidate the presence of secondary structure. Constructing a conformational model of the C-terminal region in residues 60 through 80 would give more functional insight to the region that is implicated in genome packing through interaction with M1[10–13] and viral budding.[9]

Because of the work presented in this thesis, the Howard Lab can move forward with M1 binding assays. As MALDI-MS data revealed that, according to current reconstitution protocols into POPC:POPG 4:1 lipid bilayers, M2 inserts into the lipid bilayer with no directionality. In other words, both the N- and C-termini lie at the liposome exterior. Either orientation is physiologically relevant. When M2 functions as an ion channel, the C-terminus lies at the liposome interior and experiences concave curvature. When M2 induces membrane curvature, it experiences a convex membrane curvature. This orientation informs the design of future experiments because M1 can access C-terminal M2 at the membrane interface after M2 has been reconstituted into a model membrane system. Effects of M1 binding on M2 structure can be further probed via SDSL-EPR and compared to previous structural studies of M2.

Acknowledgements

First and foremost, I would like to thank my thesis advisor, Dr. Kathleen P. Howard, for her mentorship throughout the past two years of my research in her lab. Dr. Howard has been patient enough to let me make my own mistakes in lab, and has celebrated with me as I have learned from these mistakes. Without her guidance and constant positivity, none of the work in this thesis would have been possible. I would like to thank Abigail Wong-Rolle '19, for working by my side as the best teammate I could have imagined for the structural studies project. Having such a dedicated and adept lab partner made our project so fun to complete. With her broad knowledge of all skills required in our lab, I know she will have great success in completing her own future projects and in teaching new lab group members. Abigail Wong-Rolle '19 shared data on residues 61, 66, 69, and 70. I would like to thank my other lab partners, Aaron Holmes '18 and Ben Hsiung '18. While our projects may not have overlapped, both of you were such a positive presence in our lab every day. Working in a collaborative space with you made my Howard Lab experiences even more enjoyable.

I would like to thank previous Howard Lab members Grace Kim '17, D. Stuart Arbuckle '17, and Alice Herneisen '17. Stuart and Grace introduced me to all experimental techniques in my first summer in the Howard Lab. Alice has assisted me in lab and via email throughout the last year. Grace Kim '17 and Alice Herneisen '17 provided data for residues 50-59.

I would like to thank the University of Pennsylvania for providing the equipment used to collect MALDI-MS data. In particular, University of Pennsylvania's graduate

student and facility technician, Miklos Szantai-Kis, and Dr. Kathleen P. Howard collected MALDI-MS data.

Finally, I send my best wishes to Elizabeth Erler '20 and Reham Mahgoub '20, who are beginning work in the Howard Lab this spring. I am excited to see the great progress that they will surely make on influenza A proteins in the coming years. Thank you.

Appendix 1: Compound Verification Via SDS-PAGE and UV-Vis Spectroscopy

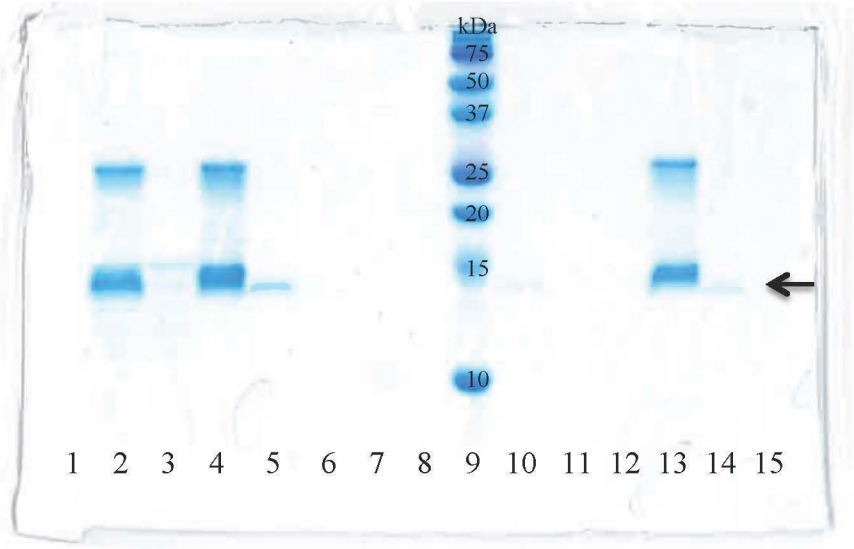

Figure S1. Representative results of SDS-PAGE for M2FL G67C purification. Star in lane 13 indicates pure, M2FL monomer band at 11.8 kDa. Band at 24 kDa in lane 13 is representative of M2FL dimer.

After each M2FL purification, a sodium dodecyl sulfate-polyacrylamide gel electrophoresis (SDS-PAGE) gel was run to determine the purity of the final protein stock after purification on the Nickel column and the PD-10 column. Aliquots were collected after various protein purification steps and then used to prepare the SDS-PAGE samples. The lanes numbered 1-15 on Figure S1 contain the following purification aliquots collected during the M2FL G67C purification:

1) Wash III Flow Through Column A: No visible bands.
2) Supernatant: Strong band for M2 at 12 kDa and M2 dimer at 24 kDa, along with bands for impurities on gel at 20 kDa and 10-15 kDa.
3) Aggregation flow through: Faint band for M2 at 12 kDa, along with various bands for

impurities from 10-15 kDa.

4) Aggregation Elution 1: Strong band for M2 at 12 kDa and M2 dimer at 24 kDa. Faint impurity band at 18 kDa.
5) Aggregation Elution 2: Faint band for M2 at 12 kDa.
6) Nickel Column Flow Through Column A: *Very* faint band for M2 at 12 kDa. No other bands visible.
7) Wash I Flow Through Column A: No visible bands.
8) Wash II Flow Through Column A: No visible bands.
9) Protein Ladder
10) Nickel Column Flow Through Column B: Faint band for M2 at 12 kDa. No other bands visible.
11) Wash I Flow Through Column B: No visible bands.
12) Wash II Flow Through Column B: No visible bands.
13) Post PD-10: Very concentrated bands for M2 at 12 kDa and M2 dimer at 24 kDa. No impurity bands visible.
14) Post PD-10 10x dilution: Faint band for M2 monomer at 12 kDa.
15) Wash III Flow Through Column B: No visible bands.

In order to determine the absorbance and 280 nm and the concentration of M2FL in solution, UV-Vis spectra were collected as described in Chapter 2. Figure S2 depicts the UV-Vis spectrum of cysless M2FL used in directionality studies, with an absorbance of 0.77 at 280 nm.

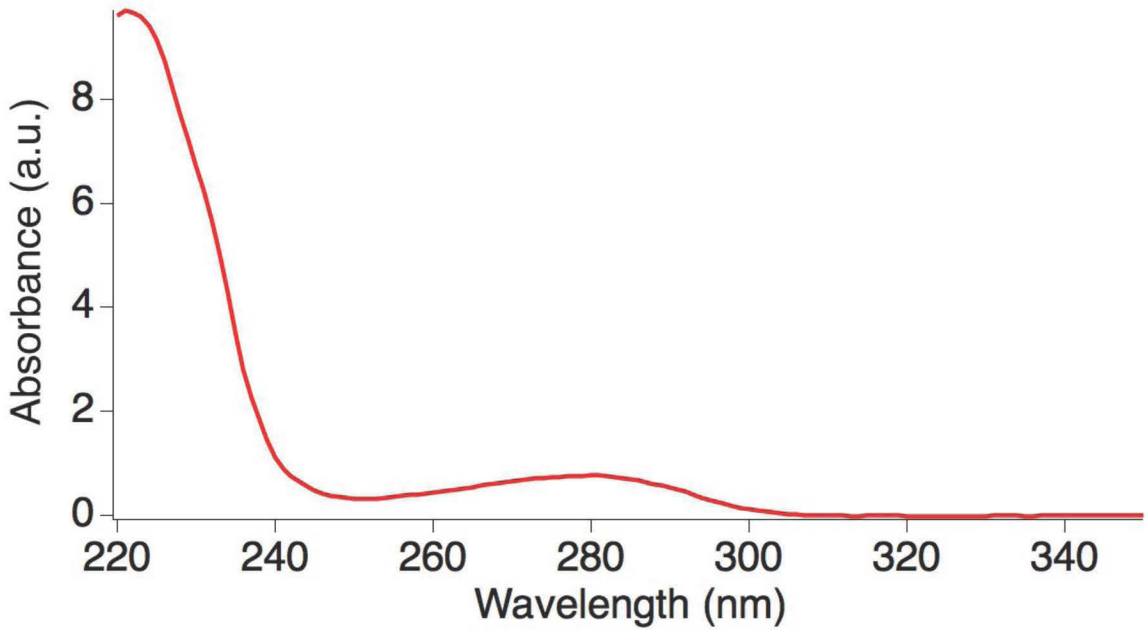

Fig S2. Representative UV-Vis spectrum of M2FL solubilized in Desalting Buffer (50 mM TRIS pH 8, 30 mM OG).

Appendix 2: Solubilization of M2FL Aggregation Upon Binding to Nickel Column Resin

Upon removal of nickel column from nutator, if insoluble aggregates formed, the aggregates were solubilized and eluted from the column in two 5-mL aliquots of Elution Buffer. If aggregation remained after these elutions, protein was solubilized and eluted with 1-mL aliquots of Elution Buffer until all was solubilized and eluted. All eluted fractions were pooled and buffer swapped to a final volume of 19 mL Standard Buffer in a 10K molecular weight cut-off concentrator (Amicon). The 19 mL M2FL in Standard Buffer was split into two 9.5-mL aliquots, and β-mercaptoethanol and imidazole were added to final concentrations of 7 mM and 20 mM, respectively.

The Ni-IDA column was re-equilibrated with 10 column volumes Millipore water followed by 10 column volumes Standard Buffer plus 20 mM imidazole. A second Ni-IDA column with 0.5 mL resin was prepared by washing with 10 column volumes Millipore water followed by 10 column volumes Standard Buffer plus 20 mM imidazole. Each 9.5 mL M2FL in Standard Buffer, 7 mM β-mercaptoethanol, and 20 mM imidazole was applied to each freshly prepared Ni-IDA column. The remaining purification and spin labeling protocol in chapter "3.1. Overexpression, Purification, and Spin Labeling of M2FL" was followed identically, except in duplicate.

Appendix 3: TEMPO Calibration Curve and Determination of Spin Labeling Efficiency

The spin labeling efficiency of the spin labeled protein was determined from the concentration of protein and the concentration of MTSL, as calculated from the TEMPO calibration curve.

The curve was prepared from four solutions of known concentrations of 4-hydroxy-2,2,6,6-tetramethylpiperidine 1-oxyl (TEMPO) in Desalting Buffer. TEMPO is a free radical, structurally similar to MTSL, so it can be used to accurately mimic the MTSL spin label in solution (Fig S3, Fig 5). A 4 µL sample of each of these solutions was loaded into a 25 µL capillary sealed at both ends with Crito-Seal wax. A CW spectrum of each solution was collected as described in 2.4. EPR Data Collection, except at 33 dB attenuation. Concentration of spin label was calculated in EPR Bruker Xenon software. Table S1 and Fig S4 show output spin label concentrations compared to actual TEMPO spin concentrations.

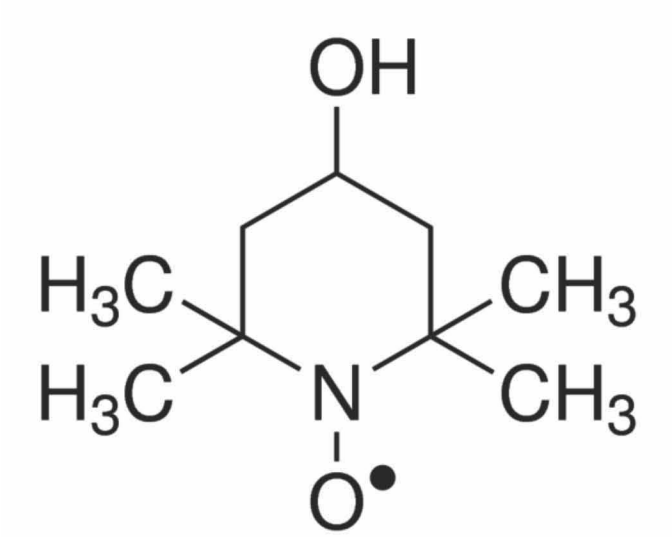

Fig S3. 4-Hydroxy-2,2,6,6-tetramethylpiperidine 1-oxyl (TEMPO).

Table S1. Actual spin concentrations of TEMPO free radical in Desalting Buffer and spin concentrations calculated in Bruker Xenon computer software.

Actual TEMPO Spin Concentration (µM)	Computer-Calculated TEMPO Spin Concentration (µM)
25	48.18
100	158.6
200	284.4
300	455.9

Computer-calculated spin concentrations versus actual spin concentrations were fit linearly in KaleidaGraph 4.1.3, yielding equation (1):

$$y = 9 + 1.46x \quad \text{(S1)}$$

where y is computer-calculated TEMPO spin concentration in μM and x is actual spin concentration in TEMPO solutions in μM.

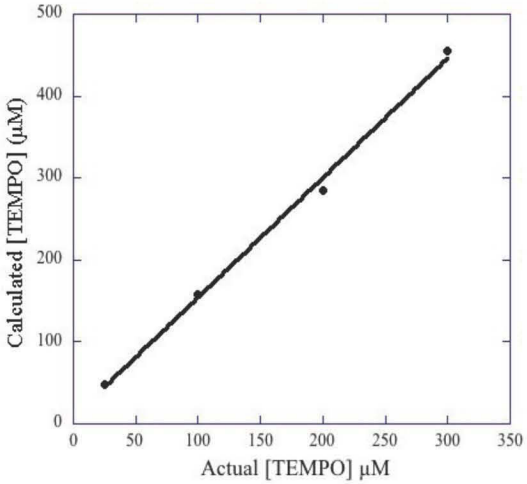

Figure S4. TEMPO calibration curve. Linear fit equation y = 9 + 1.46x used to determine actual concentration of spin label (x) from computer-calculated concentration of spin label (y).

To determine spin labeling efficiency of experimental samples, an aliquot of the pooled, post-PD-10 purification sample was concentrated to approximately 250 μM in a 10K molecular weight cut-off concentrator (Amicon). A 4 μL sample of each of the concentrated sample was loaded into a 25 μL capillary sealed at both ends with Crito-Seal wax. A CW spectrum of each solution was collected as previously described, in Chapter 2.4. EPR Data Collection, at 33 dB attenuation. Concentration of MTSL spin label was calculated in EPR Bruker Xenon software and converted to accurate spin concentration via equation (S1). Spin label efficiency was calculated according to equation (S2):

$$\text{Spin label efficiency} = \frac{[\text{MTSL}]}{[\text{M2FL}]} \times 100 \quad \text{(S2)}$$

Spin label efficiency values of all residues in the 60s are reported in Table S1.

Table S2. Spin label efficiencies of residues 60-70 EPR samples.

Residue	Spin Label Efficiency
K60C	71 %
R61C	56 %
G62C	86 %
P63C	65 %

S64C	11 %
T65C	92 %
E66C	1.0×10^2 %
G67C	28 %
V68C	1.0×10^2 %
P69C	47 %
E70C	34 %